MATERIALS FOR NEXT-GENERATION LITHOGRAPHY: CROSSLINKED MOLECULAR RESISTS AND PHOTO-PATTERNABLE UNDERLAYERS

A Dissertation
Presented to
The Academic Faculty

by

Brandon L. Sharp

In Partial Fulfillment
of the Requirements for the Degree
Doctor of Philosophy in the
School of Chemistry and Biochemistry

Georgia Institute of Technology
AUGUST 2018

MATERIALS FOR NEXT-GENERATION LITHOGRAPHY: CROSSLINKED MOLECULAR RESISTS AND PHOTO-PATTERNABLE UNDERLAYERS

Approved by:

Dr. Clifford L. Henderson, Advisor
School of Chemical & Biomolecular Engineering, School of Chemical & Biomedical Engineering
Georgia Institute of Technology, University of South Florida

Dr. Charles L. Liotta
School of Chemistry & Biochemistry
Georgia Institute of Technology

Dr. Laren M. Tolbert, Co-Advisor
School of Chemistry & Biochemistry
Georgia Institute of Technology

Dr. Pete J. Ludovice
School of Chemical & Biomolecular Engineering
Georgia Institute of Technology

Dr. David M. Collard
School of Chemistry & Biochemistry
Georgia Institute of Technology

Dr. David G. Bucknall
School of Engineering and Physical Sciences
Heriot-Watt University

Date Approved: [July 13, 2018]

ACKNOWLEDGEMENTS

I would like to thank my advisor, Cliff Henderson, for giving me many opportunities to present my research at conferences and share my research with the lithography community. I'd also like to thank Hannah Narcross for the many helpful and entertaining conversations we've had while sharing an office over the years and for her inspiring work ethic. Dr. Caleb Breaux and Dr. Benjamin Nation have also helped tremendously, especially those times when I waited until the last minute to finish a project before a conference deadline. Dr. Richard Lawson was a great help to me in the early years of my Ph.D. and taught me many useful skills that I carried with me throughout my graduate career. The friends that I've made here in Atlanta and Georgia Tech have also helped me get through some rough times both in and out of grad school. In particular, I'd like to thank Dr. Erin Gawron, one of the first friends I made at Tech, who was a constant source of advice throughout my degree. Dr. Nathan Jarnagin and Dr. Jing Cheng helped me tremendously when I first joined the lab and taught me so much before they left. Finally, I'd like to thank my mother for always believing in me and encouraging me throughout my life.

TABLE OF CONTENTS

LIST OF FIGURES

LIST OF SYMBOLS AND ABBREVIATIONS

^{1}H NMR	Proton-1 nuclear magnetic resonance
CAR	Chemically-amplified resist
DUV	Deep ultraviolet
E_0	Dose-to-clear
EUV	Extreme ultraviolet
IC	Integrated circuit
LER	Line-edge roughness
MIBK	Methyl isobutyl ketone
NBn	Nitrobenzyl
Non-CAR	Non-chemically-amplified resist
PAB	Post-apply bake
PAG	Photoacid generator
PEB	Post-exposure bake
PGMEA	Propylene glycol monomethyl ether acetate
PHOST	Poly(hydroxystyrene)
SEM	Scanning electron microscope
TMAH	Tetramethylammonium hydroxide
TPS-SbF_6	Triphenylsulphonium hexafluoro antimonate

SUMMARY

As feature sizes on integrated circuits (computer chips) continue to decrease in accordance with Moore's Law, new technologies are needed to maintain pace. Next-generation lithographic techniques, including extreme ultraviolet lithography (EUVL), are expected to replace current lithography processes in the coming years. This new technique will require new tools and materials in order to be realized. In particular, new photoresists will need to be developed that can be patterned at the small feature sizes expected to be used with these new techniques. This thesis will explore both negative and positive-tone crosslinked molecular resists as materials capable of sub-50nm imaging.

Block copolymers have also emerged as a means of extending the usefulness of current lithographic processes. The last portion of this thesis will explore underlayers designed to direct the self-assembly of block copolymers into lithographically-useful features. The underlayers presented can be directly patterned using various radiation sources, offering a more direct route to achieving self-assembly of block copolymers.

CHAPTER 1. INTRODUCTION

1.1 Photolithography techniques

Photolithography is one of the steps involved in the manufacture of integrated circuits (computer chips). Advancements in this technology have been one of the major driving forces for simultaneously obtaining faster computer chips and steadily decreasing the cost required to create each computer chip, a trend known as Moore's Law.[1] The lithography process is shown in Figure 1.1, and it involves growing a thin film of silicon dioxide on top of a silicon wafer, followed by coating a material known as a photoresist. The photoresist is either inherently sensitive to radiation or is formulated with a photosensitive compound that generates a reactive species (often an acid) upon irradiation. During the exposure step, selected areas of the photoresist are irradiated with ultraviolet light through a mask, which generates a reactive species, and then a post-exposure bake (PEB) is typically performed to allow reactions to occur that affect the solubility of the photoresist in the exposed regions. The wafer is then developed in a chosen solvent, and one of two patterning "tones" is achieved. In a positive tone material, the exposed regions become soluble in the developer, while the unexposed regions remain insoluble on the wafer. In a negative tone material, the exposed regions of the resist become insoluble in the developer solvent while the unexposed regions are washed away during development. After development and drying, an etch step is performed which transfers the pattern defined in the photoresist into the silicon substrate. It is the job of the photoresist to protect the silicon directly underneath it from the etch step so that only areas of the wafer that aren't covered

in photoresist are etched. After this etch step, the photoresist is removed and the litho-etch process is repeated as many times as necessary to build desired device architectures.

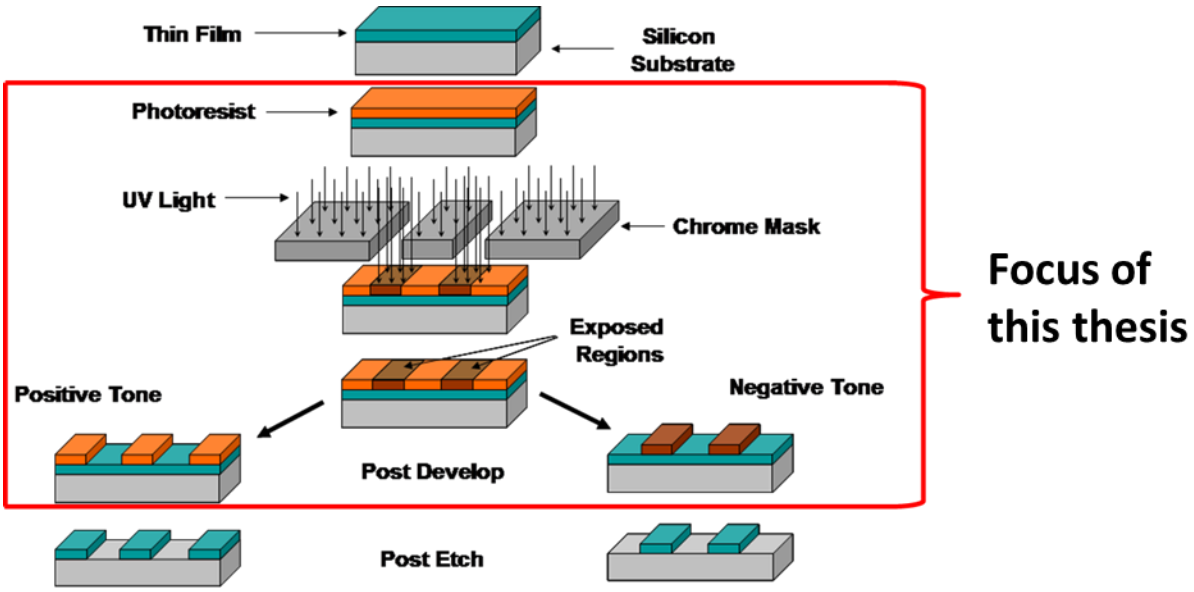

Figure 1.1 Overview of the photolithography process used to fabricate ICs.

The minimum feature size of the lithography process is governed by the resolution (R) formula in (Equation 1.1, where k is a process dependent constant, λ is the wavelength of light used, and NA is the numerical aperture of the system. In order to decrease the critical dimension of features, the wavelength of light used has decreased over the years. Lithography systems have evolved from 436 nm light to 193 nm. Eventually, 157 nm lithography was researched as a next-generation lithography technique, but it was difficult to find suitable materials for this process since many resists and lens materials strongly absorb this wavelength of light, and so it was abandoned. Thus, the industry extended the use of 193 nm lithography. In order to do this, the numerical aperture of the 193 nm systems was increased by using high-purity water, which increased the ultimate achievable

resolution in accordance with Equation 1.1. Water has a higher refractive index (n) than air, which leads to an increase in the numerical aperture (NA), as shown in Equation 1.2. The use of water as an immersion liquid has extended the use of 193nm immersion lithography to the 22nm node.[2]

$$\mathrm{R}(critical\ dimension) = k\frac{\lambda}{\mathrm{NA}} \quad \text{(Equation 1.1)}$$

$$\mathrm{NA} = \mathrm{n}\sin\theta \quad \text{(Equation 1.2)}$$

Eventually, without the use of toxic high refractive index materials, the resolution of 193 nm immersion lithography will be limited by diffraction, even when using double patterning techniques.[3] Electron beam lithography has demonstrated features as small as 2 nm, but in this technique, each feature must be written individually.[4] Thus, the time it takes to pattern features would be prohibitively slow on an industrial scale and use of e-beam lithography is generally restricted to the creation of the masks used for optical lithography. Efforts are currently underway to develop multi-beam electron lithography systems, but these are still in the early stages of development.[5]

Extreme ultraviolet lithography (EUVL) has been proposed as the next extension of optical lithography. This lithography technique uses a wavelength of 13.5 nm and is a significant departure from previous lithography approaches. Since all matter absorbs this wavelength of light, the optics must be enclosed in a vacuum. Due to the high energy of the photons (92 eV), the photon-resist interaction is much different in EUVL than in previous generations. In previous generations, such as 193 nm lithography, the ultraviolet light

caused excitation of electrons. In EUVL, photons have sufficient energy to directly break molecular bonds, which leads to ionization events that generate secondary electrons. These electrons then go on to generate additional ionization events and eventually generate photoacid.[6] Several groups are actively studying this phenomenon, and a complete discussion is beyond the scope of this thesis.

1.2 Chemically-amplified resists (CARs)

In order to realize EUVL in a high-volume manufacturing setting, new photoresists are needed to access the smaller feature sizes desired. Traditionally, a polymeric material has been used as the photoresist, which is typically a phenol protected with an acid-labile protecting group. In this imaging scheme, shown in Figure 1.2, the photoacid will deprotect the phenolic polymer, which is then capable of being deprotonated by 0.26N TMAH, the standard industry developer, transforming it into an aqueous-soluble salt. The advantage of this chemistry is that, at the end of each deprotection reaction, the photoacid is regenerated. In this manner, a single photoacid can catalyze many deprotection reactions, giving rise to the term "chemical amplification." The number of reactions catalyzed by each molecule of photoacid is termed the "catalytic chain length," and values between approximately 10 to 1,100 have been reported, though this number will vary for each unique set of processing conditions and materials.[7,8,9] By using such a chemistry paradigm, the doses required to pattern are usually much lower than non-chemically amplified resists (non-CARs), since non-CARs require a one photon for every deprotection reaction to occur.[10]

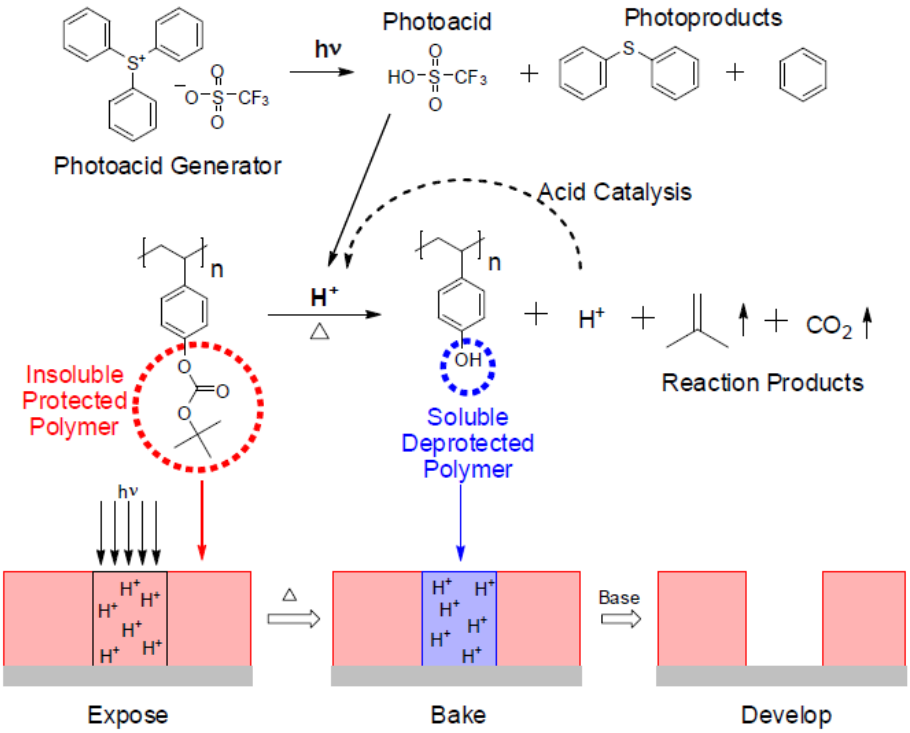

Figure 1.2 Overview of the imaging mechanism of an example chemically-amplified resist (CAR).

These so-called chemically-amplified resists (CARs) have been the dominant form of photoresists for many years.[11] However, as feature sizes continue to decrease, many problems will likely limit the usefulness of polymeric CARs. Several of these issues, including swelling, pattern collapse, and LER may be improved or eliminated by employing the use of smaller photoresist materials, called molecular resists.[12]

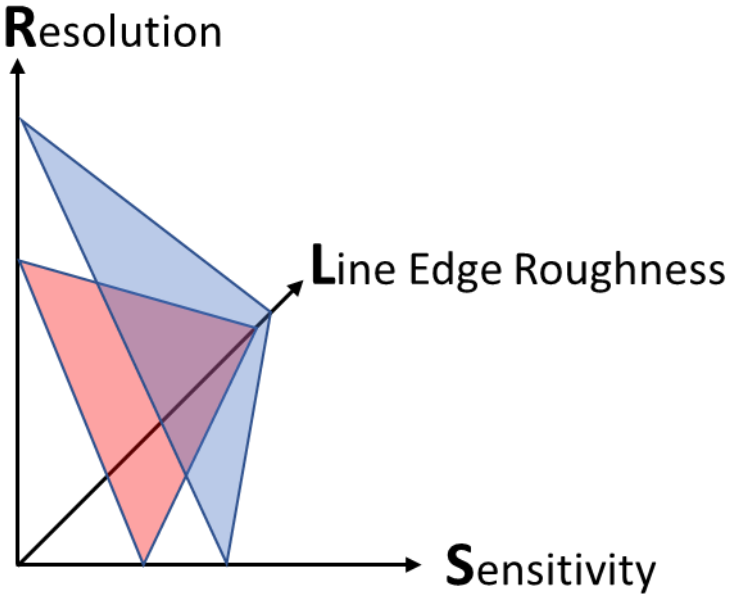

Figure 1.3 The RLS trade-off diagram.

In particular, the phenomenon known as the RLS-tradeoff has become increasingly problematic in recent years as feature sizes continue to scale well below 50nm. This is the interdependent relationship between three photoresist properties: resolution, sensitivity, and line edge roughness (LER).[13] At a basic level, the RLS trade-off states that one of the three properties can be improved at the expense of one or two of the other properties. For example, the sensitivity of a resist may be improved, but the resist may be limited in the ultimate resolution it achieves and its LER may increase. Various groups have researched methods to overcome this barrier to simultaneously improve all three properties, but little headway has been made.

1.2.1 Molecular Resists

Molecular resists offer many potential advantages over polymeric resists. Their smaller size will likely allow their use to be extended to smaller patterning nodes versus polymeric resists.[12] Synthesis of polymers always gives rise to a compositional dispersity, so it is quite difficult to produce the same composition from batch to batch. In contrast, molecular resists can be synthesized as truly monodisperse systems, such that each molecule in a resist film is structurally identical. Molecular resists were studied as early as the mid-1990s, based on calixarene cores and patterned with 365nm UV light.[14] Over the years, several additional groups began researching these materials for use in high-resolution lithography, and some of the resists that were developed are shown in Figure 1.4.[15]

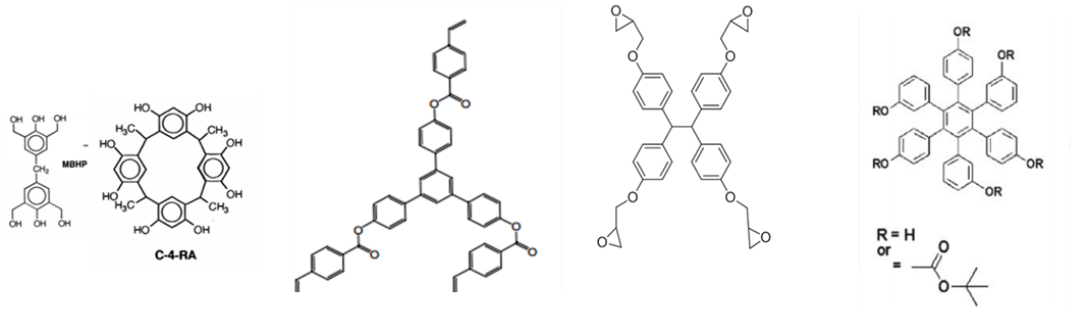

Figure 1.4 Examples of molecular resists reported in the literature.[14,16,17,18]

As feature sizes continue to decrease, pattern collapse during post-development drying becomes increasingly worse. Various methods have been explored by many academic and industry research groups, including supercritical CO_2 development, dry development rinse materials and processes (DDRM and DDRP), as well as surfactant-treated water, and reactive rinses.[19,20,21,22] Each of these materials and processes adds increased complexity

and cost to the nanofabrication process, which will drive up costs associated with fabricating computer chips.

A simpler method is to design a material that has some inherent resistance to pattern collapse, so that more expensive and time-consuming methods can be avoided. One such route is to use crosslinked resists. Polymeric versions of these resists have been reported in the literature, but these do not lend themselves to patterning at smaller feature sizes due to their tendency to swell during development. This is because the polymers reach a gelation point well before a high crosslink density is achieved, which results in a very loosely-crosslinked network, which imbibes developer. By using molecular resists, which require a much higher extent of conversion (crosslinking) before gelling, highly-crosslinked networks can be achieved. Thus, negative-tone crosslinked resists based on acid-catalyzed epoxide-homopolymerization were developed to provide some inherent resistance to pattern collapse in the photoresist itself.[23] Several negative-tone resists were developed, and it was demonstrated that one of them, TPOE-4Ep, was able to withstand roughly twice the capillary forces during post-development drying as a non-crosslinked positive tone resist.[24] Over the years, the patterning of TPOE-4Ep was optimized, and it eventually managed to resolve sub-20nm features in MIBK development when using EUVL.[23]

1.3 Block copolymers

Instead of developing new resists for EUV lithography, several groups have turned their attention to block copolymers (BCPs) as a means to further extend the usefulness of 193-immersion lithography. BCPs are materials where two individual homopolymers are

covalently linked to one another, as shown in Figure 1.5. Due to this covalent bond, the individual polymers cannot undergo complete macro-phase separation and instead undergo micro-phase separation where individual domains of each of the two blocks are formed. Depending on the relative volume fraction of the two blocks, a variety of morphologies is possible, including lamellae, cylinder, spheres, and gyroids.[25] Generally, lamellae are the most studied morphology for lithographic processes, except for cylinders, which are useful for printing bit-patterned media. The lamellar morphology is formed when the relative volume fraction between the two blocks is roughly 50:50.

Each of the two blocks in the BCP are referred to as domains, and the size of each of these domains is determined by the degree of polymerization of the block, N. BCPs are comprised of a non-polar block and a polar block, which can increase the thermodynamic driving force towards phase separation. The most commonly-researched BCP is poly(styrene)-*b*-poly(methyl methacrylate) (PS-*b*-PMMA) due to the ease of orienting the BCP perpendicular to the substrate. However, the thermodynamic driving force for phase separation of this BCP is quite low. In order to phase separate a BCP, the product of χN needs to be greater than 10.5, where χ is the Flory-Huggins interaction parameter. Due to the low χ of PS-*b*-PMMA, it is limited to a roughly 22 nm pitch.[26] In order to design BCPs that can achieve much smaller feature sizes and still phase separate them (i.e., have $XN>10.5$), χ must be increased. This has given rise to the pursuit of materials with much higher χ values than PS-*b*-PMMA, which has a χ value of approximates 0.037, in so-called high-χ BCPs. Several BCPs have been developed that can achieve sub-10nm lines.[27,28]

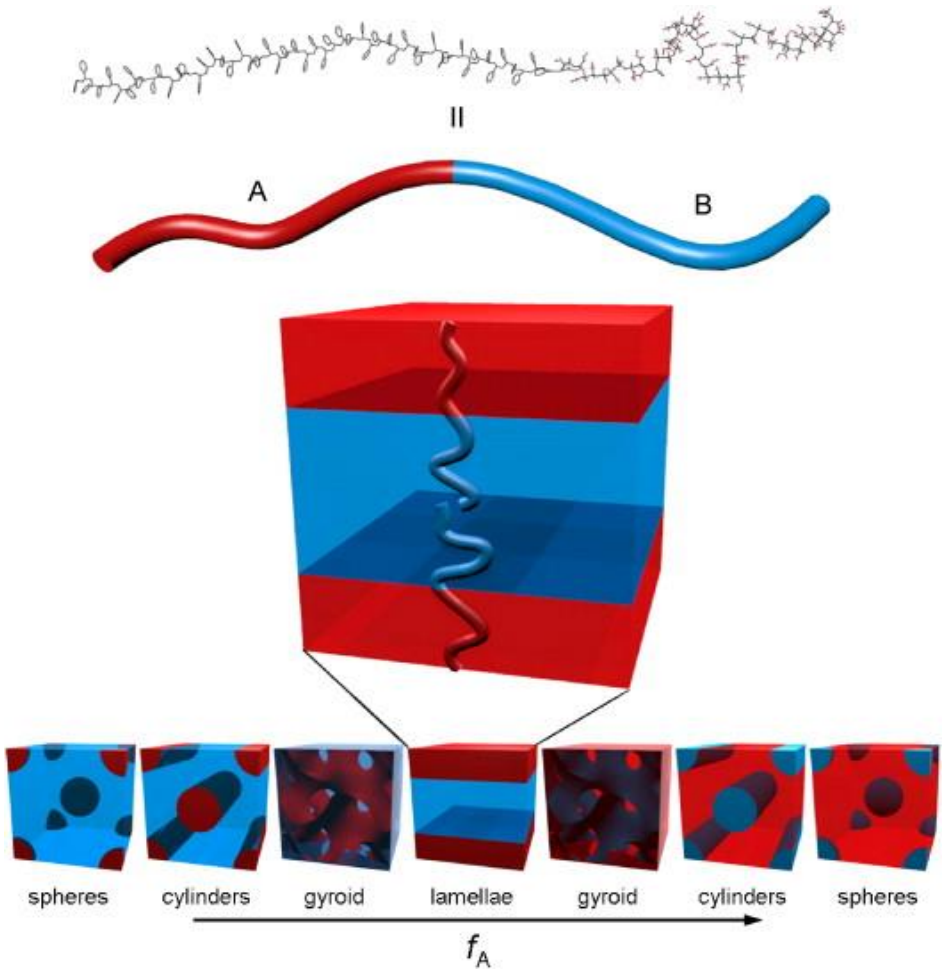

Figure 1.5. Diagram illustrating the variety of morphologies that BCPs can adopt, depending on their volume fraction.[29]

In order to phase separate BCPs, a driving force is necessary to perturb the BCP. There are multiple methods available to phase separate BCPs, including thermal annealing, solvent annealing, and electric fields.[30] Thermal annealing, where a film of the block copolymer is simply baked, is the most popular method employed to drive phase separation because it is the most feasible technique to be incorporated into a high-volume manufacturing setting.

By phase separating a BCP with this fraction on a neutral underlayer, a fingerprint pattern is formed, which is not lithographically-useful. In order to make a lithographically-useful BCP pattern, some form of guidance is needed. Directed self-assembly (DSA) is the means by which long-range order of BCPs is achieved. There are two very general methods to achieve such long-range order. The first is called graphoepitaxy, which uses traditional lithographic techniques to generate a relief pattern at a relaxed pitch in order to guide the self-assembly of a BCP. The second method is called chemoepitaxy, which uses chemical guiding patterns which preferentially wet one of the two blocks to direct the self-assembly of a BCP.

1.4 References

1. Moore, G. E., Cramming more components onto integrated circuits (Reprinted from Electronics, pg 114-117, April 19, 1965). *P Ieee* **1998,** *86* (1), 82-85.

2. LaPedus, M., IBM sees immersion at 22nm, pushes out EUV. *EE Times* **2007**.

3. Okazaki, S., Resolution Limits of Optical Lithography. *J Vac Sci Technol B* **1991,** *9* (6), 2829-2833.

4. Manfrinato, V. R.; Zhang, L. H.; Su, D.; Duan, H. G.; Hobbs, R. G.; Stach, E. A.; Berggren, K. K., Resolution Limits of Electron-Beam Lithography toward the Atomic Scale. *Nano Lett* **2013,** *13* (4), 1555-1558.

5. Platzgummer, E.; Klein, C.; Loeschner, H., Electron multibeam technology for mask and wafer writing at 0.1 nm address grid. *J Micro-Nanolith Mem* **2013,** *12* (3).

6. Narasimhan, A.; Grzeskowiak, S.; Ackerman, C.; Flynn, T.; Denbeaux, G.; Brainard, R. L., Mechanisms of EUV Exposure: Electrons and Holes. *Extreme Ultraviolet (Euv) Lithography Viii* **2017,** *10143*.

7. Schlegel, L.; Ueno, T.; Shiraishi, H.; Hayashi, N.; Iwayanagi, T., Acid Formation and Deprotection Reaction by Novel Sulfonates in a Chemical Amplification Positive Photoresist. *Chem Mater* **1990,** *2* (3), 299-305.

8. Frenette, M.; Ivan, M. G.; Scaiano, J. C., Use of fluorescent probes to determine catalytic chain length in chemically amplified resists. *Can J Chem* **2005,** *83* (6-7), 869-874.

9. Mckean, D. R.; Schaedeli, U.; Macdonald, S. A., Acid Photogeneration from Sulfonium Salts in Solid Polymer Matrices. *Abstr Pap Am Chem S* **1989,** *197*, 11-Pmse.

10. Ghosh, S.; Pradeep, C. P.; Sharma, S. K.; Reddy, P. G.; Pal, S. P.; Gonsalves, K. E., Recent advances in non-chemically amplified photoresists for next generation IC technology. *Rsc Adv* **2016,** *6* (78), 74462-74481.

11. Ito, H., Rise of chemical amplification resists from laboratory curiosity to paradigm enabling Moore's law - art. no. 692302. *Advances in Resist Materials and Processing Technology Xxv, Pts 1 and 2* **2008,** *6923*, 92302-92302.

12. Krysak, M.; De Silva, A.; Sha, J.; Lee, J. K.; Ober, C. K., Molecular Glass Resists for Next Generation Lithography. *Proc Spie* **2009,** *7273*.

13. Higgins, C. D.; Szmanda, C. R.; Antohe, A.; Denbeaux, G.; Georger, J.; Brainard, R. L., Resolution, Line-Edge Roughness, Sensitivity Tradeoff, and Quantum Yield of High Photo Acid Generator Resists for Extreme Ultraviolet Lithography. *Jpn J Appl Phys* **2011,** *50* (3).

14. Ueda, M.; Nakayama, T., A new negative-type photosensitive polyimide based on poly(hydroxyimide), a cross-linker, and a photoacid generator. *Macromolecules* **1996,** *29* (20), 6427-6431.

15. Li, L.; Liu, X.; Pal, S.; Wang, S. L.; Ober, C. K.; Giannelis, E. P., Extreme ultraviolet resist materials for sub-7 nm patterning. *Chem Soc Rev* **2017,** *46* (16), 4855-4866.

16. Lawson, R. A.; Lee, C. T.; Yueh, W.; Tolbert, L.; Henderson, C. L., Epoxide functionalized molecular resists for high resolution electron-beam lithography. *Microelectron Eng* **2008,** *85* (5-6), 959-962.

17. Chang, S. W.; Ayothi, R.; Bratton, D.; Yang, D.; Felix, N.; Cao, H. B.; Deng, H.; Ober, C. K., Sub-50 nm feature sizes using positive tone molecular glass resists for EUV lithography. *J Mater Chem* **2006,** *16* (15), 1470-1474.

18. Bratton, D.; Yang, D.; Dai, J. Y.; Ober, C. K., Recent progress in high resolution lithography. *Polym Advan Technol* **2006,** *17* (2), 94-103.

19. Sakamoto, R.; Shibayama, W.; Shigaki, S.; Nakajima, M., Dry Development Rinse Process (DDRP) and Material (DDRM) for Novel pattern collapse free process. *2016 China Semiconductor Technology International Conference (Cstic)* **2016**.

20. Yeh, W. M.; Lawson, R. A.; Tolbert, L. M.; Henderson, C. L., Resist Surface Crosslinking Using Amine-Based Reactive Rinses to Mitigate Pattern Collapse in Thin Film Lithography. *Advances in Resist Materials and Processing Technology Xxix* **2012,** *8325*.

21. Brakensiek, N. L.; Zhang, P.; King, D.; Ghelli, C., Advanced rinse process alternatives for reduction of photolithography development cycle defects. *Advances in Resist Technology and Processing XXII, Pt 1 and 2* **2005,** *5753*, 241-251.

22. Hoggan, E. N.; Wang, K.; Flowers, D.; DeSimone, J. M.; Carbonell, R. G., "dry" lithography using liquid and supercritical carbon dioxide based chemistries and processes. *Ieee T Semiconduct M* **2004,** *17* (4), 510-516.

23. Lawson, R. A.; Chun, J. S.; Neisser, M.; Tolbert, L. M.; Henderson, C. L., Methods of controlling cross-linking in negative-tone resists. *Advances in Patterning Materials and Processes Xxxi* **2014,** *9051*.

24. Yeh, W. M.; Noga, D. E.; Lawson, R. A.; Tolbert, L. M.; Henderson, C. L., Comparison of positive tone versus negative tone resist pattern collapse bahavior*. *J Vac Sci Technol B* **2010,** *28* (6), C6s6-C6s11.

25. Bates, F. S.; Fredrickson, G. H., Block copolymers - Designer soft materials. *Phys Today* **1999,** *52* (2), 32-38.

26. Durand, W. J.; Blachut, G.; Maher, M. J.; Sirard, S.; Tein, S.; Carlson, M. C.; Asano, Y.; Zhou, S. X.; Lane, A. P.; Bates, C. M.; Ellison, C. J.; Willson, C. G., Design of High-chi Block Copolymers for Lithography. *J Polym Sci Pol Chem* **2015,** *53* (2), 344-352.

27. Seshimo, T.; Maeda, R.; Odashima, R.; Takenaka, Y.; Kawana, D.; Ohmori, K.; Hayakawa, T., Perpendicularly oriented sub-10-nm block copolymer lamellae by atmospheric thermal annealing for one minute. *Sci Rep-Uk* **2016,** *6*.

28. Cheng, J.; Lawson, R. A.; Yeh, W. M.; Jarnagin, N. D.; Peters, A.; Tolbert, L. M.; Henderson, C. L., PS-b-PHEMA: Synthesis, Characterization, and Processing of a High chi Polymer for Directed Self-Assembly Lithography. *Alternative Lithographic Technologies V* **2013,** *8680*.

29. Darling, S. B., Directing the self-assembly of block copolymers. *Prog Polym Sci* **2007,** *32* (10), 1152-1204.

30. Olszowka, V.; Hund, M.; Kuntermann, V.; Scherdel, S.; Tsarkova, L.; Boker, A., Electric Field Alignment of a Block Copolymer Nanopattern: Direct Observation of the Microscopic Mechanism. *Acs Nano* **2009,** *3* (5), 1091-1096.

CHAPTER 2. AQUEOUS BASE SOLUBLE RESIST: TPOE-3EP

2.1 Introduction

As feature sizes of transistors continue to decrease according to Moore's Law, issues such as acid diffusion, line edge roughness (LER), and pattern collapse become increasingly problematic in conventional photoresists. Negative-tone, molecular glass resists offer potential solutions to these problems by crosslinking to form highly crosslinked networks, which have been shown to have superior resistance to collapse from capillary forces when compared to non-crosslinked polymeric resists.[1] Molecular resists are amorphous and do not crystallize, which allows them to form excellent films.[2] The negative-tone molecular glass resist presented here are designed to crosslink through acid-catalyzed cationic polymerization of epoxides. During the polymerization, the generated acid is attached to the growing polymer network, and this covalent attachment of photoacid could help reduce photoacid diffusion outside the exposed region of the resists, leading to a reduction in image blurring. Development of the resists in aqueous base is favored because of cost and environmental concerns with organic solvent development. This prompted the design of a molecular glass resist that can be developed in aqueous base.

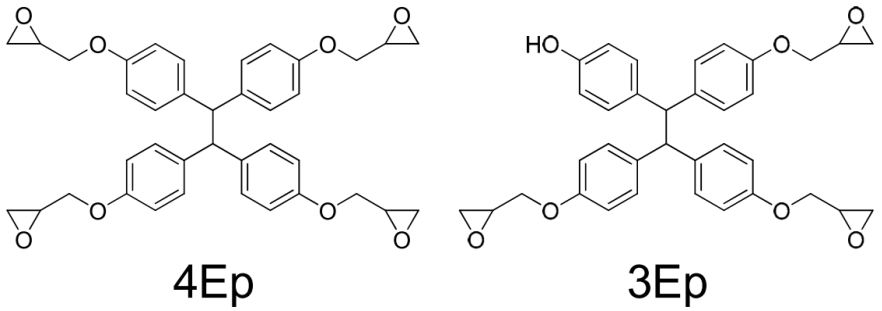

Figure 2.1 Structures of TPOE-4Ep and TPOE-3Ep.

TPOE-3Ep (or simply 3Ep) is an aqueous base developable negative tone resist that can be developed in both 0.26N TMAH and organic solvents. As shown in Figure 2.1, this molecule is designed to be a base-soluble analog to a previously-reported resist, 4Ep, and so the two will be compared.[3] The resist was designed to have a bulky core that provides etch resistance, to which crosslinkable epoxy groups are attached in order to provide negative tone behavior, and a base ionizable group, a phenol, to provide aqueous base solubility. 3Ep contains three glycidyl ether groups that can be protonated by a photoacid and crosslink during the post exposure bake (PEB). Crosslinking of the molecule provides a difference in molecular weight between exposed and unexposed regions of the resist, which allows it to be developed in organic solvents. It also contains a phenolic group, which renders the molecule soluble in standard aqueous base developers such 0.26 N tetramethylammonium hydroxide (TMAH). Thus, 3Ep allows for a direct comparison between the two development methods.

In previous work on aqueous-base developable molecular resists, DPA-2Ep, which contains an ionizable carboxylic acid group, was evaluated and showed significant amounts

of swelling after development that lead to pattern failure.[4] The swelling was likely a result of the formation of tetramethylammonium salts with un-reacted carboxylic acids inside the crosslinked network. Carboxylic acids are known to swell more than phenols in photoresists because carboxylic acids are more acidic than their phenolic counterparts and so will imbibe more of the basic developer.[5,6] Phenols can also react with the protonated epoxides during the PEB, which could, in principle, mask hydroxyl groups in the network, further prevent imbibing of the alkaline developer, leading to a reduction in swelling. For these reasons, the aqueous-base developable resist to be discussed includes an ionizable phenolic site.

2.2 Synthesis of TPOE-3Ep

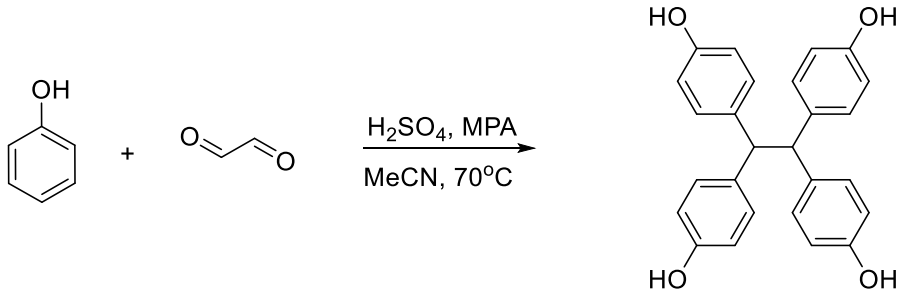

Figure 2.2 Synthesis of TPOE.

TPOE: All reagents were ordered from either TCI America or Sigma Aldrich and used without further purification. 1,1,2,2-tetrakis(*p*-hydroxyphenyl)ethane (TPOE) in Figure 2.2 was synthesized via the acid-catalyzed reaction between phenol and glyoxal, where 4 molar equivalents of phenol (58 g), 1 eq glyoxal (7.53 g of 40% solution in water), and 0.05 eq. (0.45 mL) 2-mercaptopriopionic acid (MPA) were added to 60 mL acetonitrile in

a 250-mL round bottom flask with stirring. 5.5 mL Concentrated sulfuric acid (H_2SO_4) was added dropwise to the solution. After addition, the flask was placed in an oil bath at 70ºC and stirred for 48 hours, during which time the solution turned a dark brown. After 48 hours, the solution was cooled to room temperature and precipitated into 500 mL cold acetone where a solid formed, which was vacuum filtered and washed with water and acetone to produce a white solid. ^{1}H NMR (300MHz, methanol-d_4, δ): 6.99 ppm (d,8H), 6.65 ppm (d, 8H), 4.55 ppm (s, 2H). MS (EI) m/z: [M]+: 199. Yield: 73%.

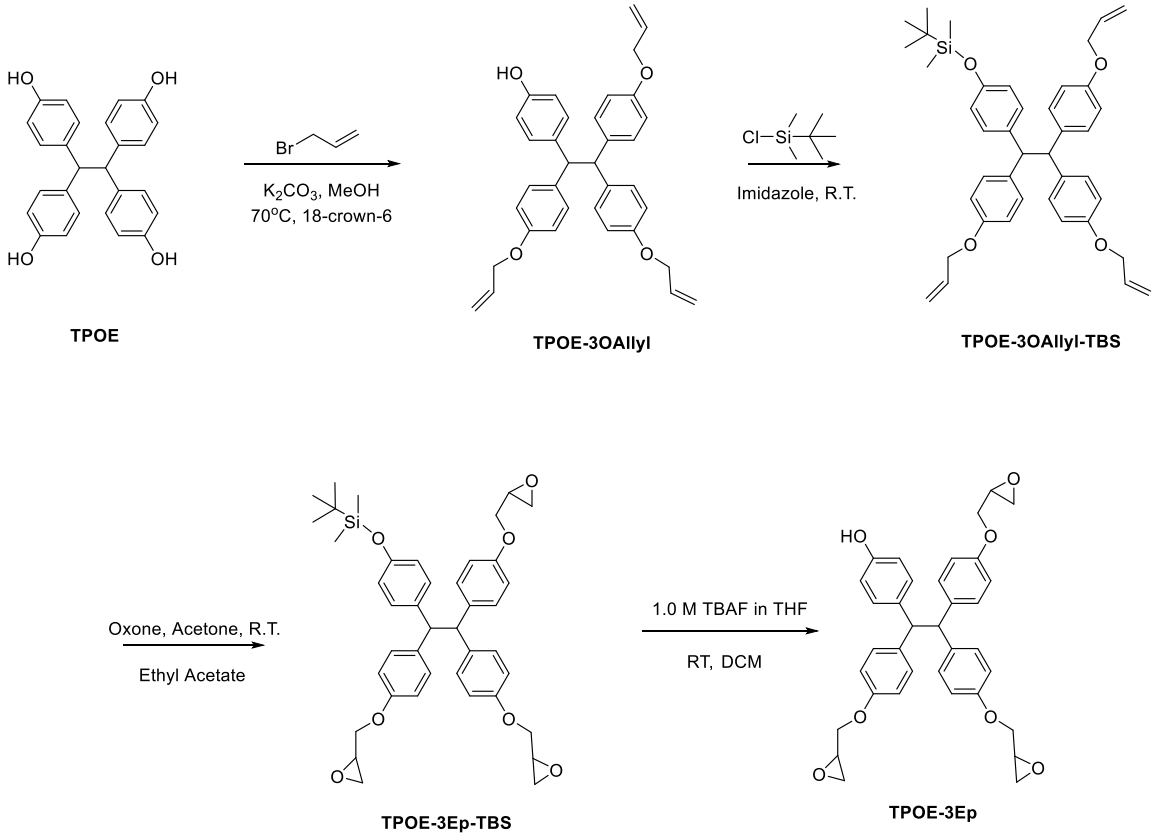

Figure 2.3 Synthesis scheme for TPOE-3Ep.

TPOE-3OAllyl: Allyl groups were then introduced onto the core by reacting TPOE (15.2 g) with 10.2 g (2.2 equivalents) of allyl bromide in the presence of 23.8 g (5 equivalents)

of potassium carbonate (K_2CO_3) and a catalytic amount (0.6 g) of 18-crown-6 ether in 750 mL of methanol in a 1L round bottom flask. The reaction was heated to reflux for 12 hours, after which it was cooled to room temperature, ethyl acetate added, and washed once with dilute HCl solution. The organic layer was washed twice with deionized water and then dried over $MgSO_4$. After concentrating solvents via rotary evaporator, the crude mixture was purified via silica gel chromatography to afford TPOE-3OAllyl (Figure 2.3). TPOE-2OAllyl and TPOE-1OAllyl were also isolated during this column, and they will be discussed in a later chapter. ^{1}H NMR (300MHz, acetone-d_6, δ): 7.25 ppm (d, 6H), 7.15 ppm (d, 2H), 6.65 ppm (d, 6H), 6.55 ppm (d, 2H), 5.97 ppm (m, 3H), 5.30 ppm (dd, 3H), 5.16 ppm (dd, 3H), 4.82 ppm (s, 1H), 4.78 ppm (s, 1H), 4.37 ppm (d, 6H). Yield: 17%.

TPOE-3OAllyl-TBS: The remaining phenol was protected by reacting 3.5 g of TPOE-3OAllyl with 1.5 equivalents (1.5 g) of tert-butyldimethylsilylchloride (TBS-Cl) in the presence of 1.5 equivalents (1.37 g) of imidazole in 100 mL chloroform at room temperature for 6 hours. Afterwards, the solution was washed once with dilute HCl solution and twice with deionized water. The organic layer was dried over $MgSO_4$ and solvents evaporated using a rotary evaporator. ^{1}H NMR (300MHz, $CDCl_3$, δ): 7.01 ppm (d, 6H), 6.84 ppm (d, 2H), 6.65 ppm (d, 6H), 6.51 ppm (d, 2H), 5.97 ppm (m, 3H), 5.30 ppm (dd, 3H), 5.20 ppm (dd, 3H), 4.50 ppm (s, 2H), 4.35 ppm (d, 6H), 0.88 ppm (s, 9H), 0.05 ppm (s, 6H). Yield: 95%.

TPOE-3Ep-TBS: Alkenes were converted to epoxides by reacting 4.5 g (1 equivalent) of TPOE-3OAllyl-TBS (dissolved in ethyl acetate) with 26 g (12 equivalents) of Oxone (dissolved in water) and 11.5 g (36 equivalents) of $NaHCO_3$ in the presence of a catalytic amount of acetone (10 mL). This procedure was repeated several times until conversion of alkenes to Oxone was complete, as monitored via ^{1}H NMR. After conversion was complete, deionized water was added until all solids dissolved and additional ethyl acetate

was added. The organic layer was then washed twice with deionized water and then solvents evaporated via rotary evaporator. ^{1}H NMR (300 MHz, $CDCl_3$, δ): 7.01 ppm (d, 6H), 6.84 ppm (d, 2H), 6.65 ppm (d, 6H), 6.52 ppm (d, 2H), 4.52 ppm (s, 2H), 4.09 ppm (dd, 3H), 3.75 (dd, 3H), 3.26 ppm (m, 3H), 2.80 ppm (dd, 3H), 2.68 ppm (dd, 3H), 0.88 ppm (s, 9H), 0.05 ppm (s, 6H). Yield: 83%.

TPOE-3Ep: Once conversion to epoxides was complete, the TBS group was removed by dissolving 1 equivalent of TPOE-3Ep-TBS in 50 mL DCM and adding 3 equivalents of tetrabutylammonium fluoride (TBAF) (1.0 M solution in THF), and stirring at room temperature for 4 hours. The solution was washed three times with water and the organic phase was dried over $MgSO_4$ and then concentrated via rotary evaporator. This crude product was then purified via silica gel column chromatography, eluting first with hexanes to remove residual TBS-F, and then hexanes:ethyl acetate (9:1) to remove TBAF, to give TPOE-3Ep as a yellow solid. ^{1}H NMR (300 MHz, $CDCl_3$, δ): 7.01 ppm (d, 6H), 6.84 ppm (d, 2H), 6.65 ppm (d, 6H), 6.52 ppm (d, 2H), 4.75 ppm (s, 1H), 4.52 ppm (s, 2H), 4.09 ppm (dd, 3H), 3.75 (dd, 3H), 3.26 ppm (m, 3H), 2.80 ppm (dd, 3H), 2.68 ppm (dd, 3H). Yield: 40%.

2.3 Lithographic Evaluation

Resists were dissolved in ethyl lactate with 5 mol% TPS-SbF_6 and coated onto a silicon wafer to produce 45 nm-thick films on O_2 plasma-cleaned silicon wafers. The films were subjected to a post-apply bake (PAB) of 90^{o}C for 2 minutes, patterned using 248 nm DUV light exposure using an Oriel Instruments 500 W Hg-Xe arc lamp with 248 nm band-pass filter, and then a PEB of 90^{o}C for 1 minute. For solvent development, the exposed resists were developed with MIBK for 30 sec., followed by a rinse with isopropyl alcohol.

For aqueous base development, the resists were developed with AZ300 for 30 sec., followed by a rinse with deionized water. Resist film thicknesses were measured using an M-2000 Woolam Ellipsometer. The patterned wafers were imaged using a Carl Zeiss Ultra 60 SEM with 2 keV accelerating voltage. EUV evaluation was performed using the Micro Exposure Tool (MET) at the Lawrence Berkeley National Lab Advanced Light Source.

2.4 Comparison to TPOE-4Ep

Although structurally similar to 4Ep, 3Ep has several differences that impact its patterning behavior. First, the phenol can be ionized, which renders the entire molecule soluble in TMAH during development. Secondly, replacement of a flexible glycidyl ether group with a phenol capable of hydrogen bonding has the effect of raising the glass transition temperature (T_g).[7,8] To measure glass transition temperature in these resists, films were coated and the thickness change with temperature was monitored using spectroscopic ellipsometry with a heated stage. When the system crosses the T_g, the slope changes as the coefficient of thermal expansion is different in the glass vs. the melt. As shown in Figure 2.4, the T_g changes from 48°C in 4Ep to 63°C in 3Ep. An increase in T_g would most likely reduce the mobility of the growing polymer chains, which would lead to a slower propagation rate.[9,10] In the imaging mechanism of epoxy-based negative- tone resists, it is theorized that a fast initiation and slow propagation is necessary for a polymerization to proceed in a controlled manner to produce networks with a high crosslink density.[11]

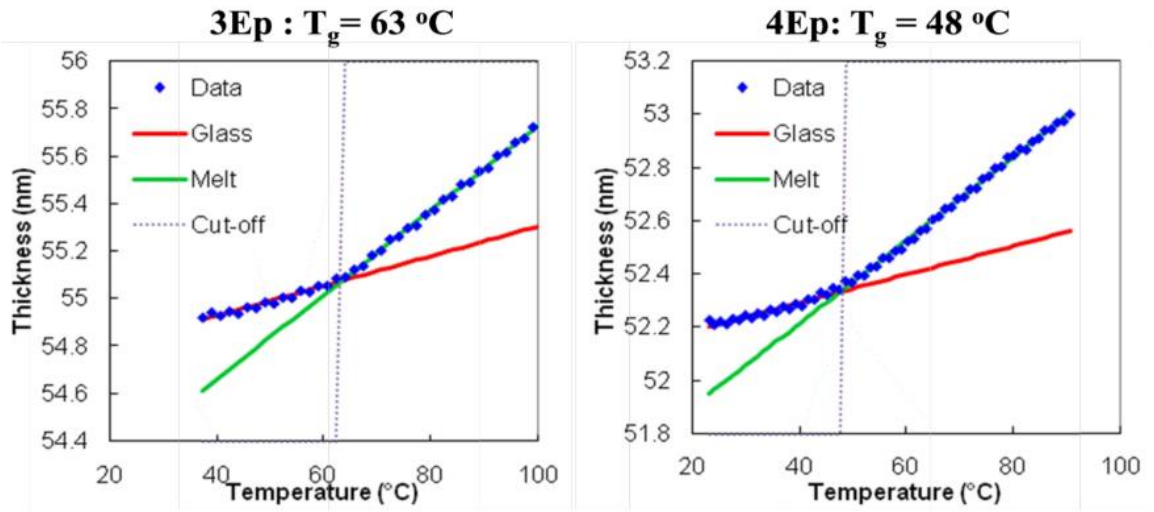

Figure 2.4 Ellipsometry data showing the differences in T_g values between TPOE-4Ep and TPOE-3Ep.

Another major difference between 4Ep and 3Ep is that polymerization of 3Ep can proceed in one of two ways, as shown in Figure 2.5. The top mechanism is common to both routes and involves generation of a photoacid which then protonates an epoxide, creating a highly electrophilic oxonium species. This molecule can then react via epoxide-epoxide crosslinking as shown in the middle route, which involves an unprotonated epoxide attack on the oxonium ion. It can also proceed via the bottom route, in which a phenol attacks the oxonium ion. It is likely that each reaction is occurring during the polymerization due to the high reactivity of the oxonium. Since the photoacid is only present in catalytic amounts, several steps are required for the oxonium to be regenerated after a successful phenol-epoxide reaction, and thus the rate of crosslinking is likely reduced. This reduction in rate could assist in reducing the amount of polymerization that occurs outside the exposed regions of the resist, reducing image blur and LER.

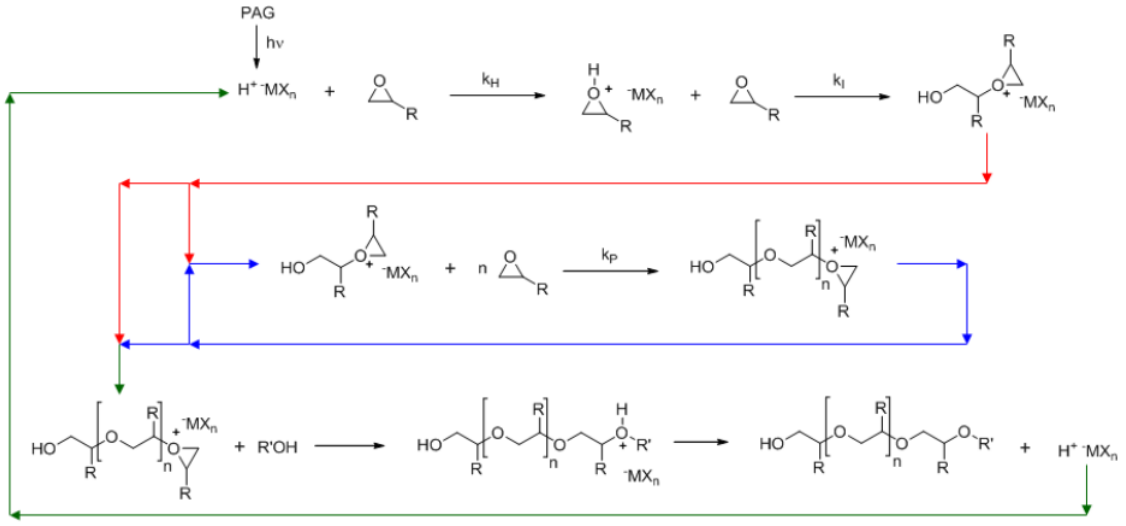

Figure 2.5 Potential crosslinking mechanisms that 3Ep can participate in. The bottom represents a new crosslinking route due to inclusion of a phenol.

Taken together, these three differences make it difficult to precisely identify the source of changes in the patterning behavior of the two molecules, but it is likely caused by some combination of them. The EUV contrast curve in

Figure 2.6 shows the impact of these differences on patterning. In MIBK development, 3Ep shows a much more gradual increase in NRT compared to 4Ep, attributed to the slower polymerization kinetics discussed previously. While 3Ep does have a lower contrast than 4Ep, it also exhibits a shift of E_0 away from zero dose, which should help prevent crosslinking in the unexposed regions of the resist due to flare and reduce issues such as bridging. In the same figure, development of 3Ep in 0.26 N TMAH shows a shift of E_0 away from zero dose as well, out to approximately 3 mJ/cm^2. After the delay in film thickness response, 3Ep then shows a rapid rise in NRT to produce an insoluble film.

In both MIBK and TMAH development, solubility switching occurs though the molecular weight increase and network formation that occurs as the system cross-links. The reason for the better contrast behavior in TMAH development is that it also has a solubility switching that occurs as the phenol group reacts with epoxides. Thus, even though a low amount of epoxide homopolymerization may occur at low doses, a small amount of epoxide-phenol crosslinking at low doses can mask the phenol, resulting in a large increase in NRT. It is possible that even a single epoxide-phenol crosslink could render a molecule insoluble in TMAH.

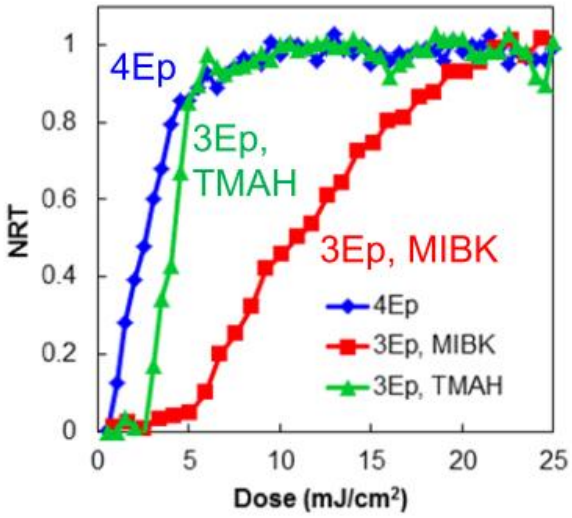

Figure 2.6 EUV contrast curves comparing TPOE-4Ep in MIBK development with TPOE-3Ep in 0.26N TMAH and MIBK development.

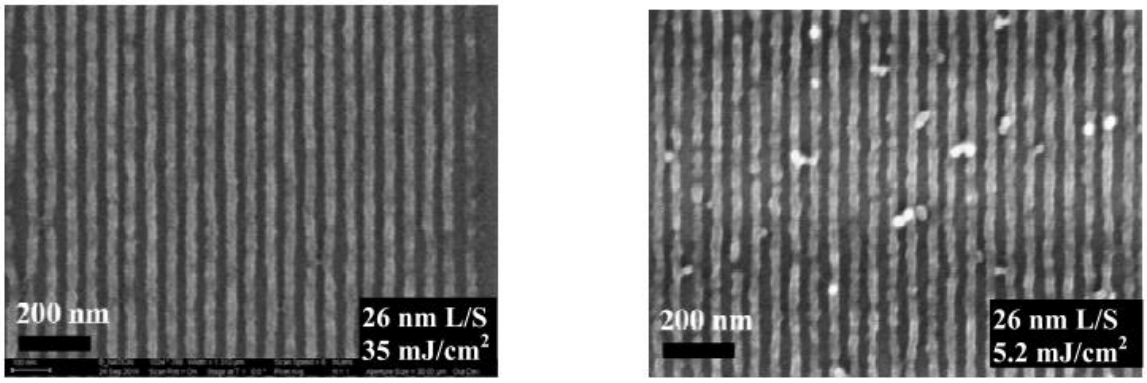

Figure 2.7 SEM images comparing TPOE-3Ep (left) and TPOE-4Ep (right) in MIBK development. E_{size} and resolution (1:1 line:space) is shown in bottom right.

Comparing SEM images of MIBK solvent developed 4Ep vs. 3Ep in Figure 2.7, 3Ep forms better lines than 4Ep and also exhibits fewer particle defects. The defects in 4Ep are likely an effect of how close E_0 is to zero dose, so that any flare can generate crosslinked species, leading to insoluble material. 3Ep also has a much higher E_{size} than 4Ep because of the different polymerization kinetics as discussed previously. Although higher-quality lines are formed in 3Ep, its higher E_{size} could be responsible for the better patterning performance due to reduction in LER with increasing dose.[12] At a given dose, the 4Ep polymerization likely proceeds at a faster rate than 3Ep because 4Ep is not impeded by the epoxide- phenol crosslinking that 3Ep participates in so a higher dose is required to pattern comparable features in 3Ep. Previous work with 4Ep used additives to help control the polymerization rate and showed higher-quality lines than 3Ep.[13] Thus, future work will be performed where these additives are included in 3Ep formulations.

2.5 Comparison Between 0.26 N TMAH and MIBK Development of TPOE-3Ep

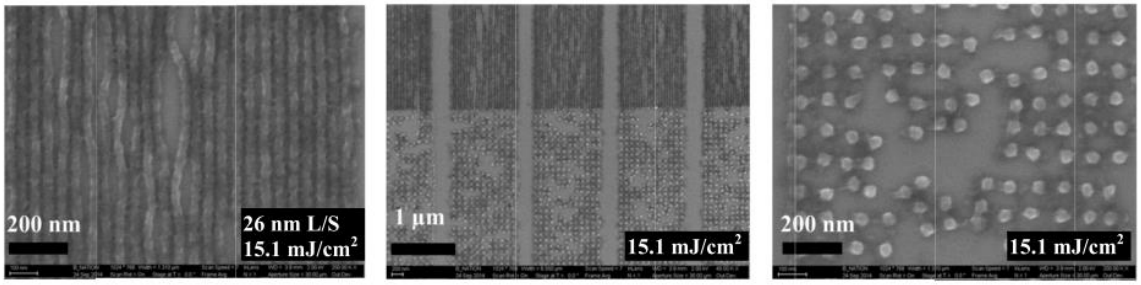

Figure 2.8 SEM images of TPOE-3Ep patterned on bare silicon wafers, showing lack of adhesion to the silicon substrate.

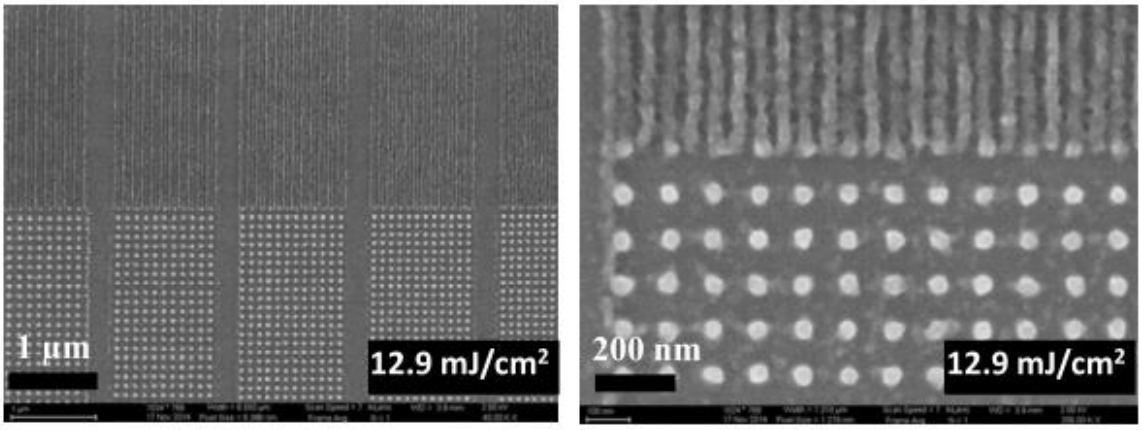

Figure 2.9 SEM images of TPOE-3Ep showing that use of an underlayer corrected the adhesion issue.

Although the contrast curve of TMAH-developed 3Ep shows a shift of E_0 away from zero dose, SEM images of EUV-exposed wafers in Figure 2.8 show a serious issue with lack of adhesion of the resist to the silicon substrate. This is indicated by shifted line patterns and dots missing or displaced from the dot arrays. At low doses, there is insufficient energy to promote significant amounts of polymerization, and the polar TMAH

will wet the surface of the wafer, causing the resist film to lose adhesion to the wafer. This results in entire regions of patterns to be missing from the wafer. This adhesion issue prompted the use of an underlayer, which the polar TMAH developer would not preferentially wet. An epoxide-containing underlayer (GT1) that can be thermally crosslinked was developed in-house to coat the silicon wafers. As shown in Figure 2.9, use of the underlayer corrected the adhesion issues in this resist.

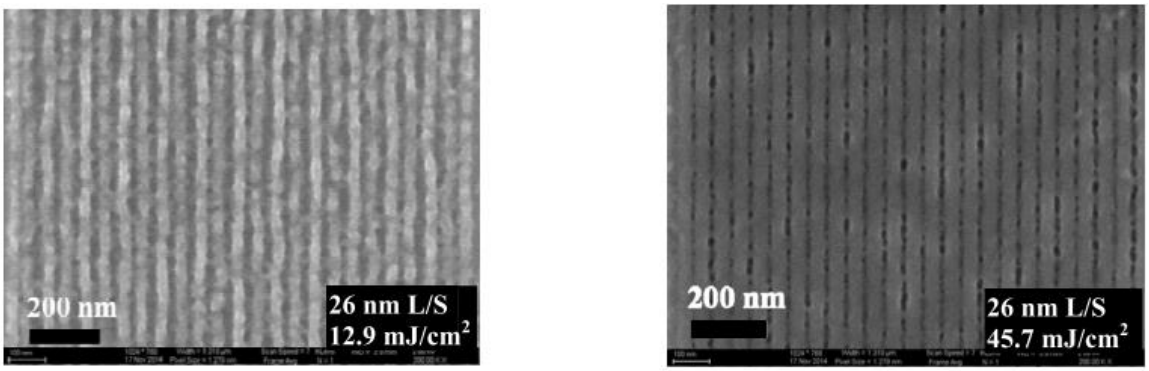

Figure 2.10 SEM images that show the bridging that occurs in TMAH development at both low doses (left) and high doses (right).

Although use of the underlayer improves the adhesion issue, TMAH development of 3Ep still has poorer performance than MIBK solvent development. Figure 2.10 shows that bridging occurs at low doses and that the formation of patterned lines is very poor because polymer networks are not yet fully-formed. The problem with bridging only becomes worse at high doses, as such significant bridging occurs that the unexposed regions are rendered almost completely filled-in. This behavior is attributed to the same polarity-switching chemistry that results in the high contrast that is seen with TMAH development.

Molecules of 3Ep that are rendered insoluble at low doses because of masking of the phenol through epoxide-phenol crosslinking have not reached the gel point. Even a single epoxide-phenol crosslink could potentially render the molecule insoluble in TMAH. This presents a serious problem in the dark regions of the photoresist, where flare can generate photoacid, which promotes epoxide-phenol crosslinking during the PEB, resulting in insolubilization of material in nominally unexposed regions. This insoluble material is likely the culprit behind the formation of bridges in the resist images. This result suggests that there is a balance between the number of ionizable -OH groups and epoxides that must be maintained to prevent phenol-epoxide insolubilization of the resist at low doses where a network has not been completely formed. A negative tone cross-linking resist that maintains basic solubility until network formation is almost complete (i.e. a high extent of conversion) is likely necessary to pattern high-quality features. The next chapter will discuss methods that were explored to attempt to create a resist that showed high network conversion at lower doses.

2.6 References

1. Yeh, W. M.; Noga, D. E.; Lawson, R. A.; Tolbert, L. M.; Henderson, C. L., Comparison of positive tone versus negative tone resist pattern collapse bahavior*. *J Vac Sci Technol B* **2010,** *28* (6), C6s6-C6s11.

2. Yang, D.; Chang, S. W.; Ober, C. K., Molecular glass photoresists for advanced lithography. *J Mater Chem* **2006,** *16* (18), 1693-1696.

3. Lawson, R. A.; Tolbert, L. M.; Younkin, T. R.; Henderson, C. L., Negative-Tone Molecular Resists Based on Cationic Polymerization. *Proc Spie* **2009,** *7273*.

4. Lawson, R. A.; Cheng, J.; Noga, D. E.; Younkin, T. R.; Tolbert, L. M.; Henderson, C. L., Aqueous and Solvent Developed Negative-Tone Molecular Resists. *P Soc Photo-Opt Ins* **2010,** *7639*.

5. Ito, H., Rise of chemical amplification resists from laboratory curiosity to paradigm enabling Moore's law - art. no. 692302. *Advances in Resist Materials and Processing Technology Xxv, Pts 1 and 2* **2008,** *6923*, 92302-92302.

6. Mark, H. F., *Encyclopedia of polymer science and technology*. Concise 3rd ed.; Wiley-Interscience: Hoboken, N.J., 2007; p xxv, 1462 p.

7. De Silva, A.; Lee, J. K.; Andre, X.; Felix, N. M.; Cao, H. B.; Deng, H.; Ober, C. K., Study of the structure-properties relationship of phenolic molecular glass resists for next generation photolithography. *Chem Mater* **2008,** *20* (4), 1606-1613.

8. Lawson, R. A.; Yeh, W. M.; Henderson, C. L., Bond contribution model for the prediction of glass transition temperature in polyphenol molecular glass resists. *J Vac Sci Technol B* **2009,** *27* (6), 3004-3009.

9. Dusek, K.; Havlicek, I., Diffusion-Controlled Kinetics of Cross-Linking. *Prog Org Coat* **1993,** *22* (1-4), 145-159.

10. Decker, C.; Viet, T. T. N.; Thi, H. P., Photoinitiated cationic polymerization of epoxides. *Polym Int* **2001,** *50* (9), 986-997.

11. Lawson, R. A.; Noga, D. E.; Younkin, T. R.; Tolbert, L. M.; Henderson, C. L., Negative tone molecular resists using cationic polymerization: Comparison of epoxide and oxetane functional groups. *J Vac Sci Technol B* **2009,** *27* (6), 2998-3003.

12. Brainard, R. L.; Trefonas, P.; Lammers, J. H.; Cutler, C. A.; Mackevich, J. F.; Trefonas, A.; Robertson, S. A., Shot noise, LER and quantum efficiency of EUV photoresists. *Emerging Lithographic Technologies Viii* **2004,** *5374*, 74-85.

13. Lawson, R. A.; Chun, J. S.; Neisser, M.; Tolbert, L. M.; Henderson, C. L., Methods of controlling cross-linking in negative-tone resists. *Advances in Patterning Materials and Processes Xxxi* **2014,** *9051*.

CHAPTER 3. STRUCTURAL EFFECTS ON THE PATTERNING PERFORMANCE OF AQUEOUS BASE SOLUBLE EPOXIDE MOLECULAR RESISTS

3.1 Introduction

As feature sizes of individual transistors continue to decrease on integrated circuits (ICs), issues such as pattern collapse and photoacid blur become increasingly problematic during the lithography step of IC fabrication. Typically, polymers are utilized as the photoresist, but they come with several drawbacks which can potentially be solved by molecular resists, which are much smaller and have a more well-defined composition than polymers.[1] Several years ago, it was demonstrated that a negative-tone, epoxy-based, crosslinked molecular resist exhibited increased resistance to pattern collapse compared to a non-crosslinked resist.[2] In epoxide-based resists, the photoacid is active for only a short time and is quickly consumed by epoxides, which then become the reactive centers as oxonium ions. This reactive center will eventually become diffusion-limited as the crosslinking proceeds, which can help control crosslinking outside of exposed regions.[3] Much of the work on epoxy-based negative-tone molecular glass resists has concentrated upon resists that were not soluble in 0.26N TMAH, as these molecules do not possess an ionizable functional group such as a phenol or carboxylic acid.[4,5,6] Thus, TPOE-3Ep was designed to contain a single phenol to provide an epoxy-based negative-tone molecular resist that is soluble in standard 0.26N TMAH developer.[7]

TPOE-3Ep exhibited good DUV and EUV sensitivity and contrast in TMAH development, however, when patterns were resolved, several problems emerged. The first issue observed was delamination of films during TMAH development which was not observed in MIBK development, and the material required an underlayer to eliminate delamination. At low doses, network formation was likely incomplete, which might have allowed the TMAH to wet and etch the resist/substrate interface. At these low doses, any formed network would have a very low crosslink density which would likely result in a material with very different mechanical properties than a fully crosslinked feature. Additionally, bridging occurred in the low-dose regions of the resist because the solubility transition for TMAH development occurs at lower doses than in MIBK.

Due to these issues, there is a need to understand how various structural features of a resist affect its lithographic properties to enable the rational design of negative-tone materials. Ideally, a resist would maintain TMAH solubility until network formation is complete. TMAH solubility is primarily driven by epoxide-phenol reactions that consume the phenol, while development in organic solvent is primarily driven by molecular weight increases as the resist crosslinks.

For TMAH development of aqueous soluble epoxide resists, ideally the solubility transition for TMAH would occur where network formation is almost complete, reducing the amount of microbridging observed, as well as potentially eliminating the delamination and need for an underlayer. Additionally, since highly-crosslinked features are desired, if lines are resolved in TMAH at doses well below doses where complete network formation occurs, the patterned features will likely not be as mechanically robust as those at higher doses.

Thus, it is important for us to identify a ratio of epoxides to phenols that results in similar solubility transitions in both organic solvent and in 0.26N TMAH developers.

Using the TPOE core, this ratio can be varied and expect that increasing the number of phenols relative to the number of epoxides will increase the shift in E_0 away from zero dose and reduce the amount of insoluble material in the low-dose regions of the resist, since increasing the number of phenols will likely increase the number of crosslinking events required to insolubilize the material in TMAH. Ideally, the insolubility transition in these materials will occur when network formation is almost complete, which would manifest itself with the TMAH and MIBK DUV contrast curves being similar. The proposed molecules to study are shown in Figure 3.1.

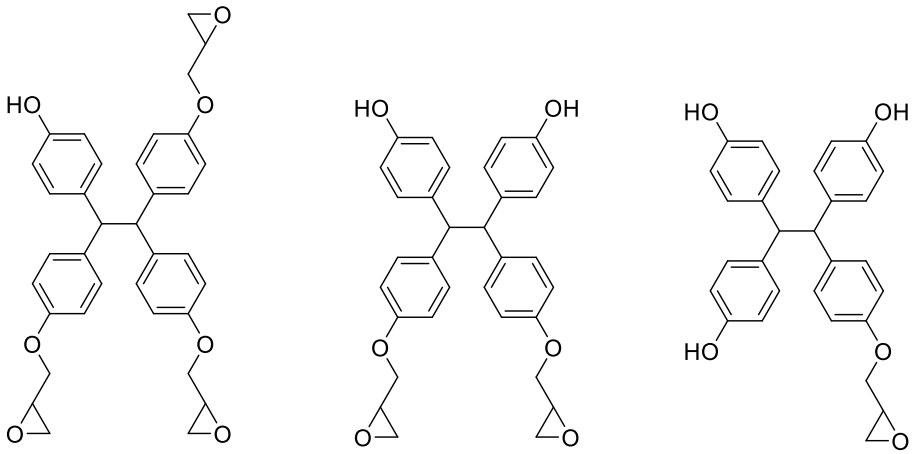

Figure 3.1 TPOE-Ep molecules to be synthesized and studied. Patterning data for TPOE-3Ep has already been obtained.

The molecules were chosen because data for TPOE-3Ep has already been gathered and this core allows us to study three different ratios: an excess number of phenols (TPOE-1Ep), a balanced ratio of phenols and epoxides (TPOE-2Ep), and a case where there are more epoxides than phenols (TPOE-3Ep). Calixarenes are also a potential candidate to use as cores for this process but it is extremely difficult to isolate individual functionalities due to the large number of hydroxyl groups on the core, as well as the numerous conformations these molecules can adopt, which further complicates isolation of individual functionalities.[8]

The goal is to design a molecule that has increased TMAH solubility at low extents of conversion, to avoid bridging in between patterned lines. To quickly screen molecules for their TMAH solubility, a calculation called logD is performed, the details of which are described elsewhere.[9] Briefly, if a compound with a functional group that can be deprotonated by TMAH (such as a phenol or carboxylic acid), has a logD value of less than 2, it is considered soluble in 0.26N TMAH. Figure 3.2 shows the logD values for the product of a single epoxide-phenol crosslink for TPOE-3Ep and TPOE-2Ep. After a single epoxide-phenol crosslinking reaction for TPOE-3Ep, the material becomes insoluble. For TPOE-2Ep, after a single epoxide-phenol crosslink, the product of that reaction is still quite soluble in 0.26N TMAH, and it would likely take several crosslinks to render insoluble. Thus, from a design standpoint, TPOE-2Ep and TPOE-1Ep are expected to have much

higher TMAH solubility than TPOE-3Ep, which should help reduce bridging in between patterned lines, assuming the materials are processed at identical conditions.

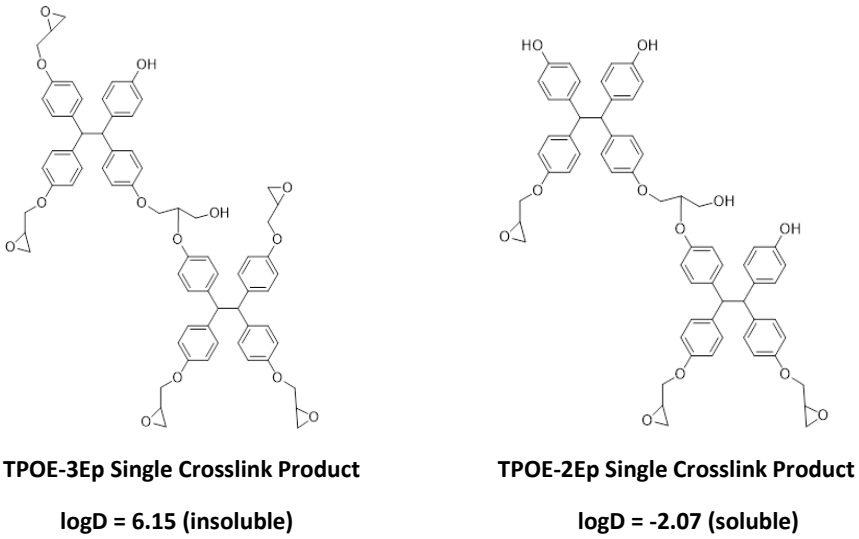

TPOE-3Ep Single Crosslink Product

logD = 6.15 (insoluble)

TPOE-2Ep Single Crosslink Product

logD = -2.07 (soluble)

Figure 3.2 Structures and logD values of products formed from a single epoxide-phenol reaction. The TPOE-3Ep is insoluble after only one crosslink, while the TPOE-2Ep remains soluble.

3.2 Experimental

3.2.1 Synthesis of resists

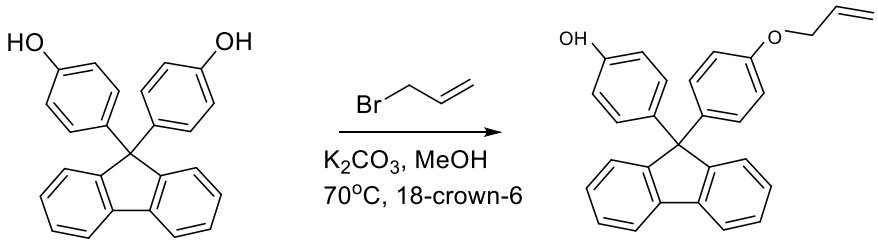

Figure 3.3 Synthesis scheme of BHPF-1OAllyl

BHPF-1OAllyl: 2g BHPF (TCI America) was dissolved in 50 mL methanol, and then 4 equivalents (2.36g) of potassium carbonate were added, along with a catalytic amount of 18-crown-6 ether. Then, 1 equivalent of allyl bromide was added dropwise, and the reaction mixture was allowed to stir in an oil bath set to 70°C for 18 hours. Afterwards, the solution was cooled to room temperature and then ethyl acetate was added and then washed once with dilute HCl solution and then twice with deionized water. The organic phase was then filtered/dried over $MgSO_4$ and solvents were evaporated. ^{1}H NMR (300 MHz, $CDCl_3$, δ): 7.80 ppm (d, 2H), 7.30 ppm (m, 6H), 7.11 ppm (d, 2H), 7.05 ppm (d, 2H), 6.70 ppm (d, 2H), 6.60 ppm (d, 2H), 6.01 ppm (m, 1H), 5.75 ppm (s, 1H, OH), 5.40 ppm (dd, 1H), 5.30 ppm (dd, 1H), 4.49 ppm (dd, 2H). Yield: 0.6961g.

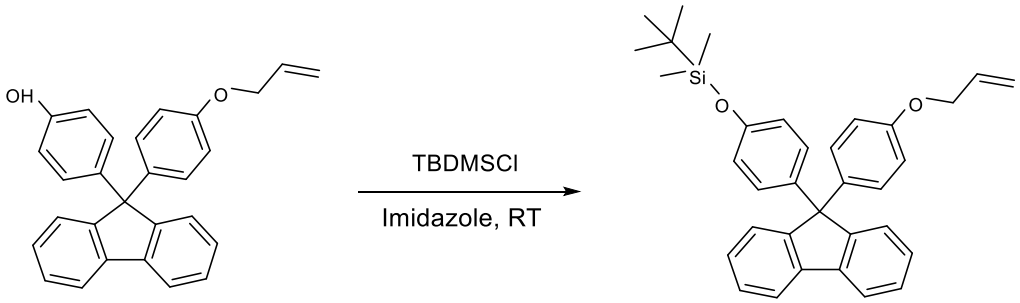

Figure 3.4 Synthesis scheme of BHPF-1OAllyl-TBS

BHPF-1OAllyl-TBS: 0.6961g BHPF-1OAllyl was dissolved in ethyl acetate, and 1.5 equivalents (0.4 g) of *tert*-butyldimethylsilylchloride (TBS-Cl) were added, along with 1.5 equivalents (0.36g) of imidazole and stirred at room temperature overnight. Afterwards, the solution was washed once with dilute HCl solution and twice with deionized water. The organic layer was dried over $MgSO_4$ and solvents evaporated using a rotary evaporator. The final product was isolated using silica gel chromatography, using hexanes:ethyl acetate (5:2) as the eluent. ^{1}H NMR (300 MHz, $CDCl_3$, δ): 7.80 ppm (d, 2H), 7.30 ppm (m, 6H), 7.11 ppm (d, 2H), 7.05 ppm (d, 2H), 6.70 ppm (d, 2H), 6.60 ppm (d, 2H), 6.01 ppm (m, 1H), 5.75 ppm (s, 1H, OH), 5.40 ppm (dd, 1H), 5.30 ppm (dd, 1H), 4.49 ppm (dd, 2H), 0.98 ppm (s, 9H), 0.11 ppm (s, 6H). Yield: 0.5404.

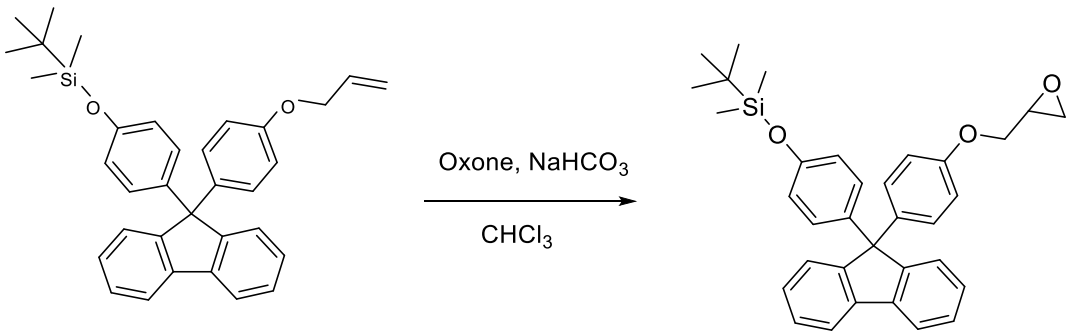

Figure 3.5 Synthesis scheme of BHPF-1Ep-TBS

BHPF-1Ep-TBS: Alkenes were converted to epoxides by reacting 0.5409g (1 equivalent) of BHPF-1OAllyl-TBS (dissolved in dichloromethane) with 2 equivalents (1.31g) of Oxone (dissolved in water) and 4 equivalents (1.08g) of $NaHCO_3$ in the presence of a catalytic amount of acetone (5 mL). This procedure was repeated several times until conversion of alkenes to Oxone was complete. After conversion was complete, deionized water was added until all solids dissolved and additional ethyl acetate was added. The organic layer was then washed twice with deionized water and then solvents evaporated via rotary evaporator. ^{1}H NMR (300 MHz, $CDCl_3$, δ): 7.80 ppm (d, 2H), 7.30 ppm (m, 6H), 7.11 ppm (d, 2H), 7.05 ppm (d, 2H), 6.70 ppm (d, 2H), 6.60 ppm (d, 2H), 4.12 ppm (m, 2H), 3.91 ppm (m, 1H), 3.32 ppm (m, 1H), 2.90 ppm (dd, 1H), 2.65 ppm (dd, 1H), 0.98 ppm (s, 9H), 0.11 ppm (s, 6H). Yield: 0.1759.

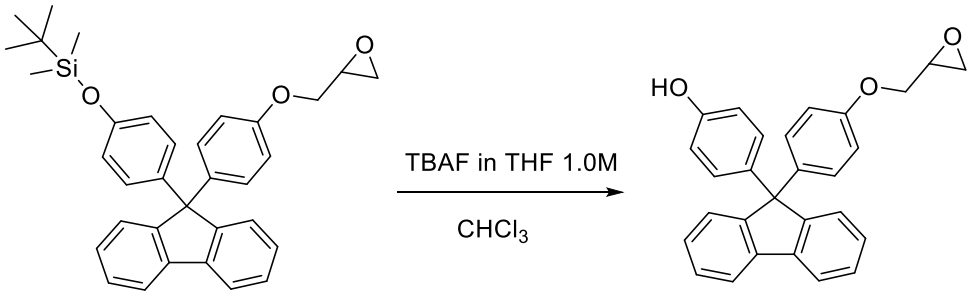

Figure 3.6 Synthesis scheme of BHPF-1Ep.

BHPF-1Ep: 0.1759g BHPF-1Ep-TBS was dissolved in chloroform and then 2 equivalents of TBAF (1.0 M in THF) were added. The solution was stirred at room temperature for 6 hours and then washed with water three times. The organic layer was then filtered/dried over $MgSO_4$ and purified vis silica gel chromatography, using hexanes and then ethyl acetate as eluents. ^1H NMR (300 MHz, $CDCl_3$, δ): 7.80 ppm (d, 2H), 7.30 ppm (m, 6H), 7.11 ppm (d, 2H), 7.05 ppm (d, 2H), 6.70 ppm (d, 2H), 6.60 ppm (d, 2H), 5.05 ppm (s, 1H, OH), 4.10 ppm (m, 2H), 3.90 ppm (m, 1H), 3.32 ppm (m, 1H), 2.90 ppm (dd, 1H), 2.65 ppm (dd, 1H). Yield: 94.1 mg.

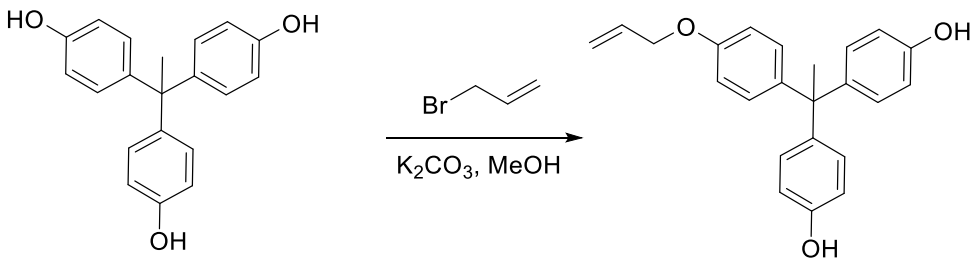

Figure 3.7 Synthesis scheme of THPE-1OAllyl.

THPE-1OAllyl: 4g THPE (TCI America) was dissolved in methanol, and then 6 equivalents (10.82 g) of potassium carbonate were added, along with a catalytic amount of 18-crown-6 ether. Then, 2 equivalents (2.36g) of allyl bromide was added dropwise, and the reaction mixture was allowed to stir in an oil bath set to 70^{o}C for 18 hours. Afterwards, the solution was cooled to room temperature and then ethyl acetate was added and then washed once with dilute HCl solution and then twice with deionized water. The organic phase was then filtered/dried over $MgSO_4$ and solvents were evaporated. The final product, along with TPOE-2OAllyl, was isolated using a silica gel column with hexanes:ethyl acetate (5:2) as the eluent. ^{1}H NMR (300 MHz, $CDCl_3$, δ, ppm): 6.98 (d, 2H), 6.92 (d, 4H), 6.81 (d, 2H), 6.71 (d, 4H), 6.05 (m, 1H), 5.79 (s, 2H, -OH), 5.41 (m, 1H), 5.27 (m, 1H), 4.51 (m, 2H), 2.08 (s, 3H). Yield: 1.21 g.

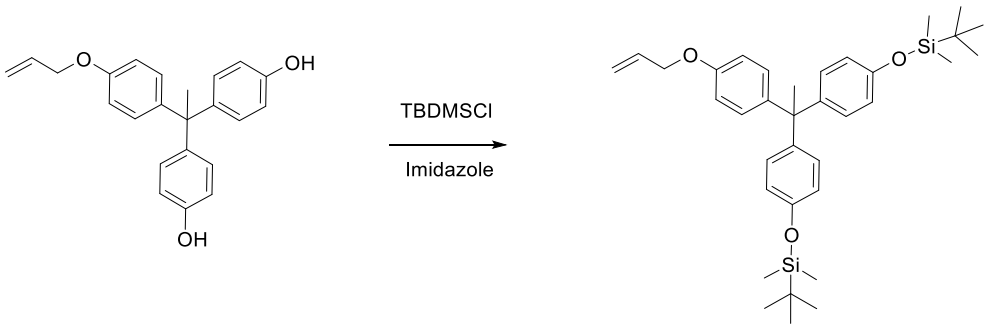

Figure 3.8 Synthesis scheme of THPE-1OAllyl-2TBS.

THPE-1OAllyl-2TBS: 1.20g THPE-1OAllyl was dissolved in ethyl acetate, and 3 equivalents (1.31g) of tert-butyldimethylsilylchloride (TBS-Cl) were added, along with 3 equivalents (1.42g) of imidazole and stirred at room temperature overnight. Afterwards, the solution was washed once with dilute HCl solution and twice with deionized water. The organic layer was dried over $MgSO_4$ and solvents evaporated using a rotary evaporator. ^1H NMR (300 MHz, $CDCl_3$, δ): 6.98 (d, 2H), 6.92 (d, 4H), 6.81 (d, 2H), 6.71 (d, 4H), 6.05 (m, 1H), 5.79 (s, 2H, -OH), 5.41 (m, 1H), 5.27 (m, 1H), 4.51 (m, 2H), 2.10 (s, 3H), 0.96 (s, 18H), 0.18 (s, 9H). Yield: 1.6017g.

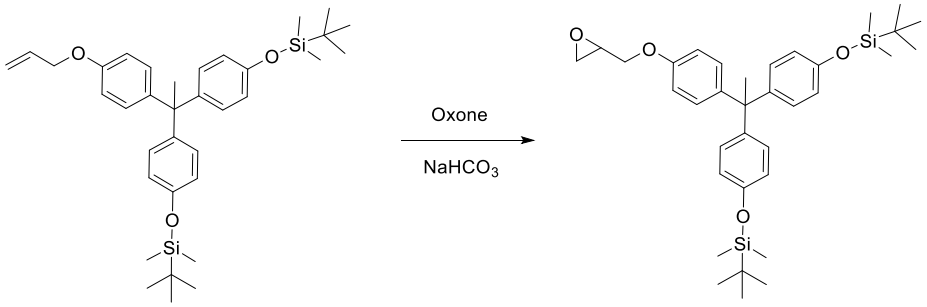

Figure 3.9 Synthesis scheme of THPE-1Ep-2TBS.

THPE-1Ep-2TBS: Alkenes were converted to epoxides by reacting 1 equivalent (1.60g) of THPE-2OAllyl-TBS (dissolved in dichloromethane) with 4 equivalents (3.42g) of Oxone (dissolved in water) and 6 equivalents (1.4g) of $NaHCO_3$ in the presence of a catalytic amount of acetone (5 mL). This procedure was repeated several times until conversion of alkenes to Oxone was complete. After conversion was complete, deionized water was added until all solids dissolved, and additional ethyl acetate was added. The organic layer was then washed twice with deionized water and then solvents evaporated via rotary evaporator. ^{1}H NMR (300 MHz, $CDCl_3$, δ): 6.94 (d,4H), 6.87 (d, 2H), 6.77 (d, 4H), 6.68 (d, 2H), 4.48 (dd, 2H), 4.15 (dd, 2H). 3.90 (dd, 2H), 3.31 (m, 2H), 2.86 (m, 2H), 2.72 (m, 2H), 2.07 (s, 3H), 0.89 (s, 9H), 0.13 (s, 6H). Yield: 0.5196g.

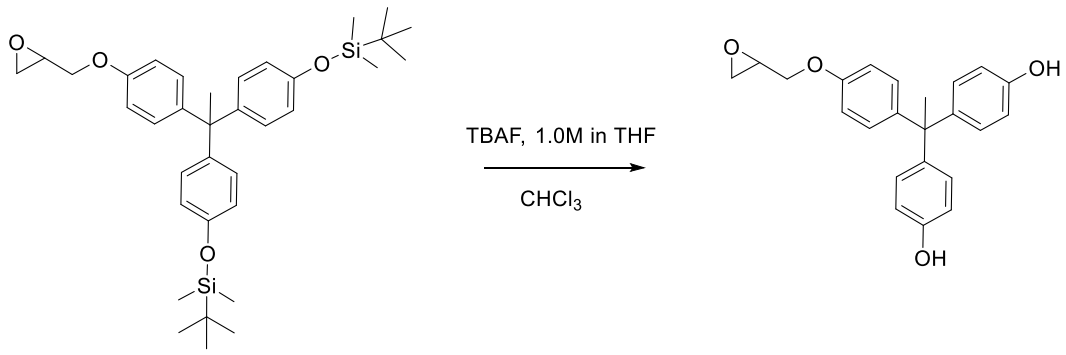

Figure 3.10 Synthesis scheme of THPE-1EP

THPE-1Ep: THPE-1Ep-2TBS was dissolved in chloroform and then 4 equivalents of TBAF (1.0 M in THF) was added. The solution was allowed to stir at room temperature for 6 hours and then washed with water three times. The organic layer was then filtered/dried over $MgSO_4$ and purified vis silica gel chromatography, using hexanes and then ethyl acetate as eluents. ^1H NMR (300 MHz, $CDCl_3$, δ, ppm): 6.98 (d, 2H), 6.89 (d, 4H), 6.70 (d, 2H), 6.61 (d, 4H), 5.30 (s, 2H, -OH), 3.93 (dd, 1H), 3.41 (m, 1H), 2.90 (t, 1H), 2.70 (m, 1H), 2.10 (s, 3H). HR MS (ESI) Calculated: 385.1410. Found: 385.1410. Yield: 0.1202g.

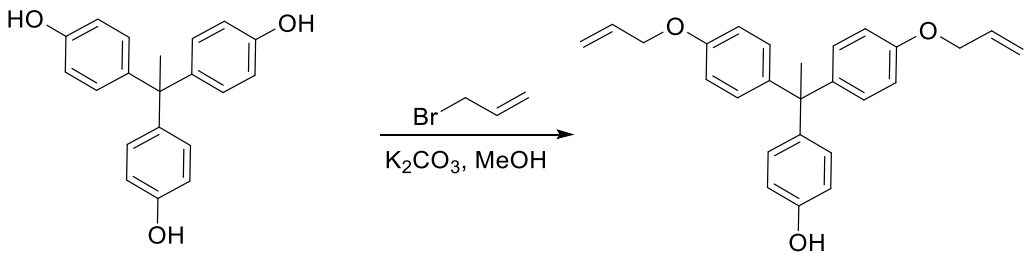

Figure 3.11 Synthesis scheme of THPE-2OAllyl.

THPE-2OAllyl: 4g THPE (TCI America) was dissolved in methanol, and then 4 equivalents (10.82g) of potassium carbonate and 2 equivalents (2.36g) of allyl bromide were added. This reaction mixture was placed in an oil bath set to 70^{o}C and allowed to stir for 18 hours. It was then cooled to room temperature, and ethyl acetate and dilute HCl solution were added. The organic phase was then washed an additional two times with deionized water and then filtered/dried over $MgSO_4$ and solvents evaporated. The final product, along with THPE-1OAllyl, was isolated using a silica gel column with hexanes:ethyl acetate (5:2) as the eluent. ^{1}H NMR (300 MHz, $CDCl_3$, δ, ppm): 6.98 (d, 4H), 6.94 (d, 2H), 6.80 (d, 4H), 6.72 (d, 2H), 6.06 (m, 2H), 5.53 (s, 1H, -OH), 5.41 (dd, 2H), 5.28 (dd, 2H), 4.15 (m, 4H), 2.10 (s, 3H). Yield: 0.8282.

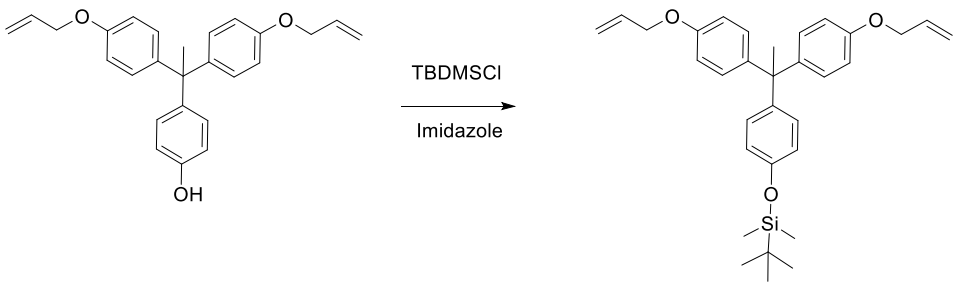

Figure 3.12 Synthesis scheme of THPE-2OAllyl-TBS.

THPE-2OAllyl-TBS: 0.8282g THPE-2OAllyl was dissolved in ethyl acetate, and 1.5 equivalents (0.48g) of tert-butyldimethylsilylchloride (TBS-Cl) were added, along with 2 equivalents (0.29g) of imidazole and allowed to stir at room temperature overnight. Afterwards, the solution was washed once with dilute HCl solution and twice with deionized water. The organic layer was dried over $MgSO_4$ and solvents evaporated using a rotary evaporator. ^{1}H NMR (300 MHz, $CDCl_3$, δ, ppm): 6.98 (d, 4H), 6.94 (d, 2H), 6.80 (d, 4H), 6.72 (d, 2H), 6.06 (m, 2H), 5.53 (s, 1H, -OH), 5.41 (dd, 2H), 5.28 (dd, 2H), 4.15 (m, 4H), 2.10 (s, 3H), 1.03 (s, 9H), 0.24 (s, 6H). Yield: 0.8891g.

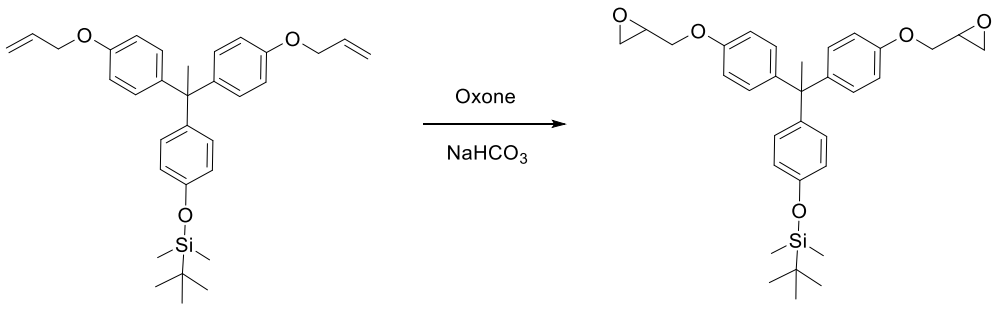

Figure 3.13 Synthesis scheme of THPE-2Ep-TBS

THPE-2Ep-TBS: Alkenes were converted to epoxides by reacting 1 equivalent (0.8891g) of THPE-2OAllyl-TBS in the presence of 8 equivalents (4.36g) of Oxone (dissolved in water) and 12 equivalents (1.78g) of $NaHCO_3$ in the presence of a catalytic amount of acetone (5 mL). This procedure was repeated several times until conversion of alkenes to Oxone was complete. After conversion was complete, deionized water was added until all solids dissolved and additional ethyl acetate was added. The organic layer was then washed twice with deionized water and then solvents evaporated via rotary evaporator. ^{1}H NMR (300 MHz, $CDCl_3$, δ, ppm): 6.98 (d, 4H), 6.94 (d, 2H), 6.80 (d, 4H), 6.72 (d, 2H), 6.06 (m, 2H), 4.13 (m, 2H), 3.93 (m, 2H), 3.32 (m, 2H), 2.88 (dd, 2H), 2.73 (dd, H), 2.10 (s, 3H), 1.03 (s, 9H), 0.24 (s, 6H). Yield: 0.8683g.

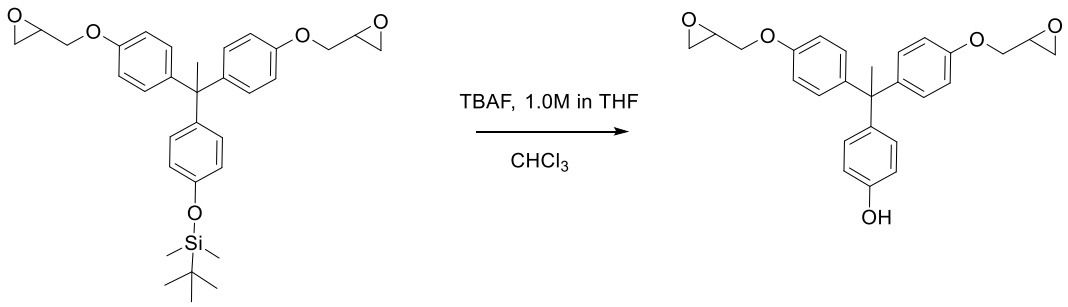

Figure 3.14 Synthesis scheme of THPE-2Ep.

THPE-2Ep: THPE-2Ep-TBS (1 eq) was dissolved in chloroform and then 2 equivalents of TBAF (1.0 M in THF) was added. The solution was allowed to stir at room temperature for 6 hours and then washed with water three times. The organic layer was then filtered/dried over $MgSO_4$ and purified vis silica gel chromatography, using hexanes and then ethyl acetate as eluents. ^{1}H NMR (300 MHz, $CDCl_3$, δ, ppm): 6.97 (d, 4H), 6.91 (d, 2H), 6.79 (d, 4H), 6.70 (d, 2H), 4.18 ppm (dd, 2H), 3.95 ppm (d, 1H), 3.90 (d, 1H), 3.35 (m, 2H), 2.90 (dd, 2H), 2.75 ppm (dd, 2H), 2.10 (s, 3H), 1.58 (s, 1H, -OH). HR MS (EI): Calculated: 418.1780 Found: 418.1781. Yield: 41%.

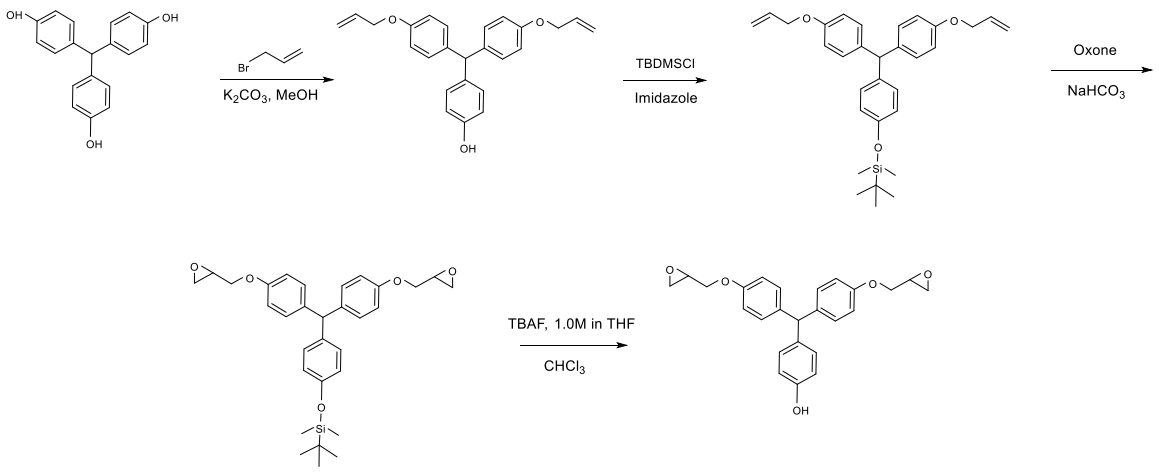

Figure 3.15 Synthesis scheme of THP-2Ep.

THP-2OAllyl: 5g THP (TCI America) was dissolved in methanol, and then 4 equivalents of potassium carbonate (7.1g) and 1.5 equivalents (3.10g) of allyl bromide were added. This reaction mixture was placed in an oil bath set to 70^{o}C and allowed to stir for 18 hours. It was then cooled to room temperature, and ethyl acetate and dilute HCl solution were added. The organic phase was then washed an additional two times with deionized water and then filtered/dried over $MgSO_4$ and solvents evaporated. The final product, along with THP-2OAllyl, was isolated using a silica gel column with hexanes:ethyl acetate (5:2) as the eluent. ^{1}H NMR (300 MHz, $CDCl_3$, δ, ppm): 6.99 (d,4H), 6.92 (d, 2H), 6.81 (d, 4H), 6.72 (d, 2H), 6.04 (m, 1H), 5.77 (s, 1H, -OH), 5.8 (m, 1H), 5.39 (m, 1H), 5.35 (s, 1H), 4.51 (m, 2H). Yield: 1.2234g.

THP-2OAllyl-TBS: 1.2234g THP-2OAllyl was dissolved in ethyl acetate, and 1.5 equivalents (0.74g) of tert-butyldimethylsilylchloride (TBS-Cl) were added, along with 2 equivalents (0.447g) of imidazole and allowed to stir at room temperature overnight.

Afterwards, the solution was washed once with dilute HCl solution and twice with deionized water. The organic layer was dried over $MgSO_4$ and solvents evaporated using a rotary evaporator. ^{1}H NMR (300 MHz, $CDCl_3$, δ ppm): 6.99 (d,4H), 6.92 (d, 2H), 6.81 (d, 4H), 6.72 (d, 2H), 6.04 (m, 1H), 5.39 (m, 1H), 5.35 (s, 1H), 5.82 (m, 1H), 4.51 (m, 2H), 0.95 (s, 9H), 0.16 (s, 6H). Yield: 1.3677g.

THP-2Ep-TBS: Alkenes were converted to epoxides by reacting 1 equivalent (0.8891g) of THP-2OAllyl-TBS in the presence of 8 equivalents (4.49g) of Oxone (dissolved in water) and 12 equivalents (1.84g) of $NaHCO_3$ in the presence of a catalytic amount of acetone. This procedure was repeated several times until conversion of alkenes to Oxone was complete. After conversion was complete (as tracked via ^{1}H NMR spectroscopy), deionized water was added until all solids dissolved, and additional ethyl acetate was added. The organic layer was then washed twice with deionized water and filtered/dried over $MgSO_4$, and then solvents evaporated via rotary evaporator. ^{1}H NMR (300 MHz, $CDCl_3$, δ(ppm)): 6.96 (d,4H), 6.92 (d, 2H), 6.81 (d, 4H), 6.72 (d, 2H), 5.27 (s, 1H), 4.12 (m, 2H), 3.95 (m, 2H), 3.32 (m, 2H), 2.87 (m, 2H), 2.73 (m, 2H), 0.95 (s, 9H), 0.16 (s, 6H). Yield: 0.6400g.

THP-2Ep: 0.64g THP-2Ep-TBS was dissolved in dichloromethane, and then 2.5 mL (2 equivalents) of TBAF (1.0 M in THF) was added. The solution was stirred at room temperature for 2 hours, and then water and additional DCM were added. The organic layer was washed with water three times. The organic layer was then filtered/dried over $MgSO_4$ and purified vis silica gel chromatography, using hexanes and then ethyl acetate as eluents. ^{1}H NMR (300 MHz, $CDCl_3$, δ, ppm): 6.96 (d,4H), 6.92 (d, 2H), 6.81 (d, 4H), 6.72 (d, 2H),

5.36 (s, 1H, -OH), 5.27 (s, 1H), 4.12 (m, 2H), 3.95 (m, 2H), 3.32 (m, 2H), 2.87 (m, 2H), 2.73 (m, 2H). Yield: 0.5984g.

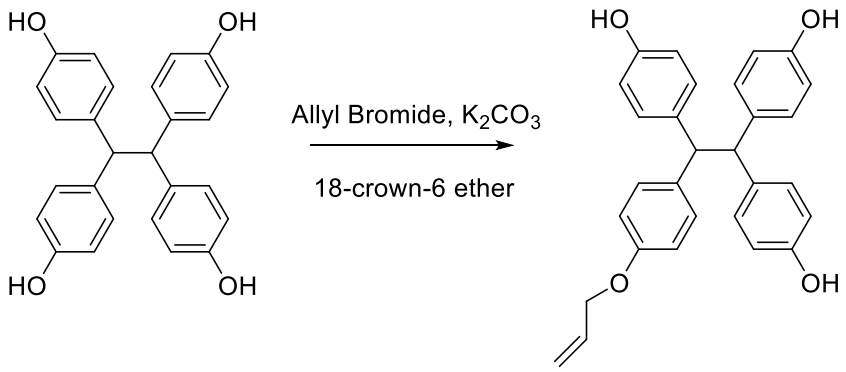

Figure 3.16 Synthesis scheme of TPOE-1OAllyl.

TPOE-1OAllyl synthesis is described in Chapter 2. ^{1}H NMR (300 MHz, $CDCl_3$, δ, ppm): 7.01 (d, 6H), 6.84 (d, 2H), 6.65 (d, 6H), 6.51 (d, 2H), 5. (m, 1H), 5.30 (dd, 1H), 5.20 (dd, 1H), 4.50 (s, 2H), 4.35 (d, 2H). Yield: 0.236g.

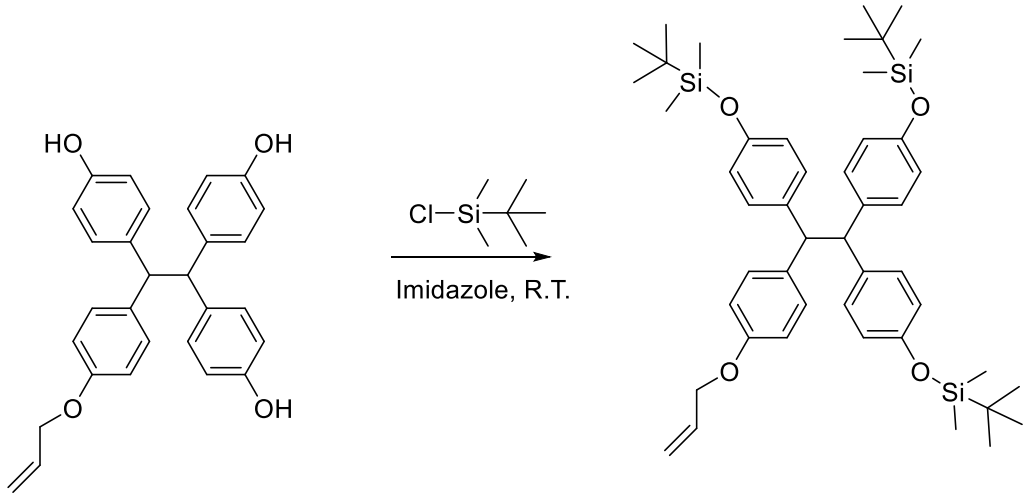

Figure 3.17 Synthesis scheme of TPOE-1OAllyl-3TBS.

TPOE-1OAllyl-3TBS: TPOE-1OAllyl (0.236g) was dissolved in ethyl acetate, and 4.5 equivalents (0.408g) of tert-butyldimethylsilylchloride (TBS-Cl) were added, along with 0.424g of imidazole and stirred at room temperature overnight. Afterwards, the solution was washed once with dilute HCl solution and twice with deionized water. The organic layer was dried over $MgSO_4$ and solvents evaporated using a rotary evaporator. ^{1}H NMR (300 MHz, $CDCl_3$, δ): 7.01 ppm (d, 6H), 6.84 ppm (d, 2H), 6.65 ppm (d, 6H), 6.51 ppm (d, 2H), 5.97 ppm (m, 1H), 5.30 ppm (dd, 1H), 5.20 ppm (dd, 1H), 4.50 ppm (s, 2H), 4.35 ppm (d, 2H), 0.88 ppm (s, 27H), 0.05 ppm (s, 18H). Yield: 0.423g.

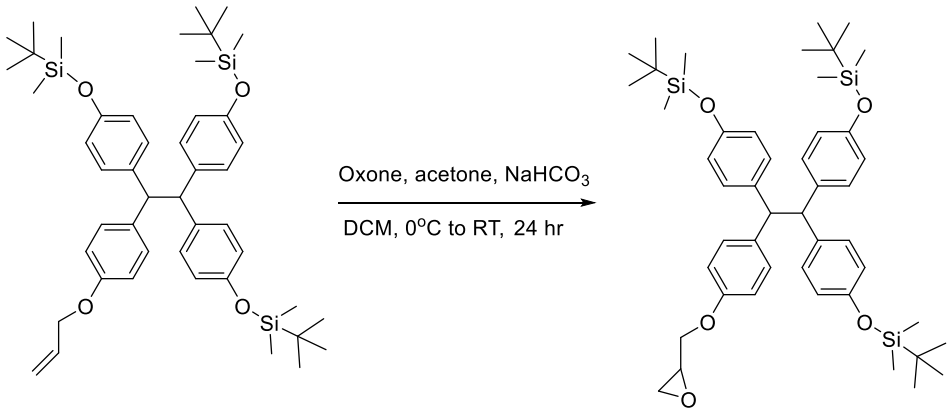

Figure 3.18 Synthesis scheme of TPOE-1Ep-3TBS.

TPOE-1Ep-3TBS: Alkenes were converted to epoxides by reacting (0.423g) 1 equivalent of TPOE-1OAllyl-3TBS (dissolved in ethyl acetate) with 4 equivalents (0.0668g) of Oxone (dissolved in water) and 12 equivalents of $NaHCO_3$ in the presence of a catalytic amount of acetone. This procedure was repeated several times until conversion of alkenes to Oxone was complete. After conversion was complete, deionized water was added until all solids dissolved and additional ethyl acetate was added. The organic layer was then washed twice with deionized water and then solvents evaporated via rotary evaporator. ^{1}H NMR (300 MHz, $CDCl_3$, δ): 7.01 ppm (d, 6H), 6.84 ppm (d, 2H), 6.65 ppm (d, 6H), 6.52 ppm (d, 2H), 4.52 ppm (s, 2H), 4.09 ppm (dd, 1H), 3.75 (dd, 1H), 3.26 ppm (m, 1H), 2.80 ppm (dd, 1H), 2.68 ppm (dd, 1H), 0.88 ppm (s, 27H), 0.05 ppm (s, 18H). Yield: 0.3886g.

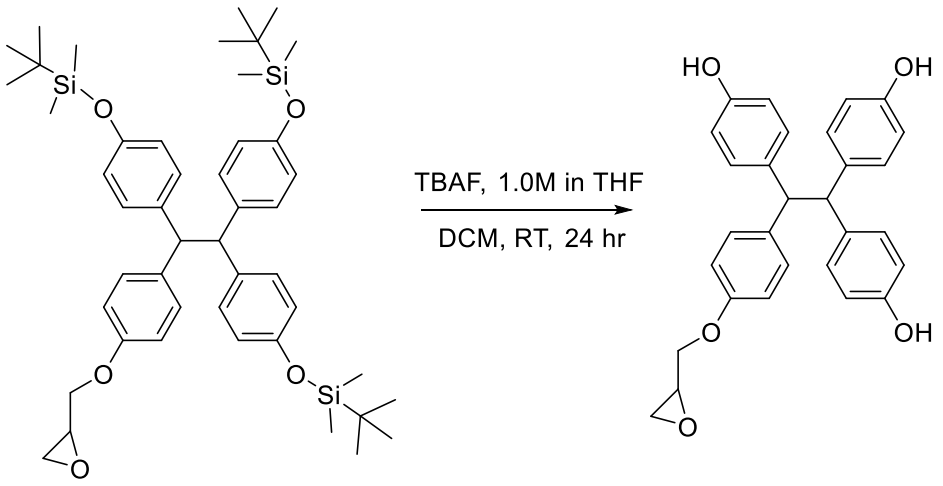

Figure 3.19 Synthesis scheme of TPOE-1Ep.

TPOE-1Ep: 0.3886g (1 equivalent) of TPOE-1Ep-3TBS was added to DCM, and 6 equivalents of TBAF (1.0 M in THF) were added. The solution turned dark brown upon addition of TBAF, and the solution was allowed to stir at room temperature for 4 hours before being washed with water 3 times. The organic phase was filtered/dried over $MgSO_4$ and then solvents were removed using rotary evaporator. The resulting crude material was then purified via a silica gel column, first eluting with hexanes and then with hexanes:ethyl acetated (9:1) to remove residual TBAF impurities. ^{1}H NMR (300 MHz, $CDCl_3$, δ, ppm): 7.01 ppm (d, 6H), 6.84 ppm (d, 2H), 6.65 ppm (d, 6H), 6.52 ppm (d, 2H), 4.52 ppm (s, 2H), 4.09 ppm (dd, 1H), 3.75 (dd, 1H), 3.26 ppm (m, 1H), 2.80 ppm (dd, 1H), 2.68 ppm (dd, 1H). Yield: 0.1259g.

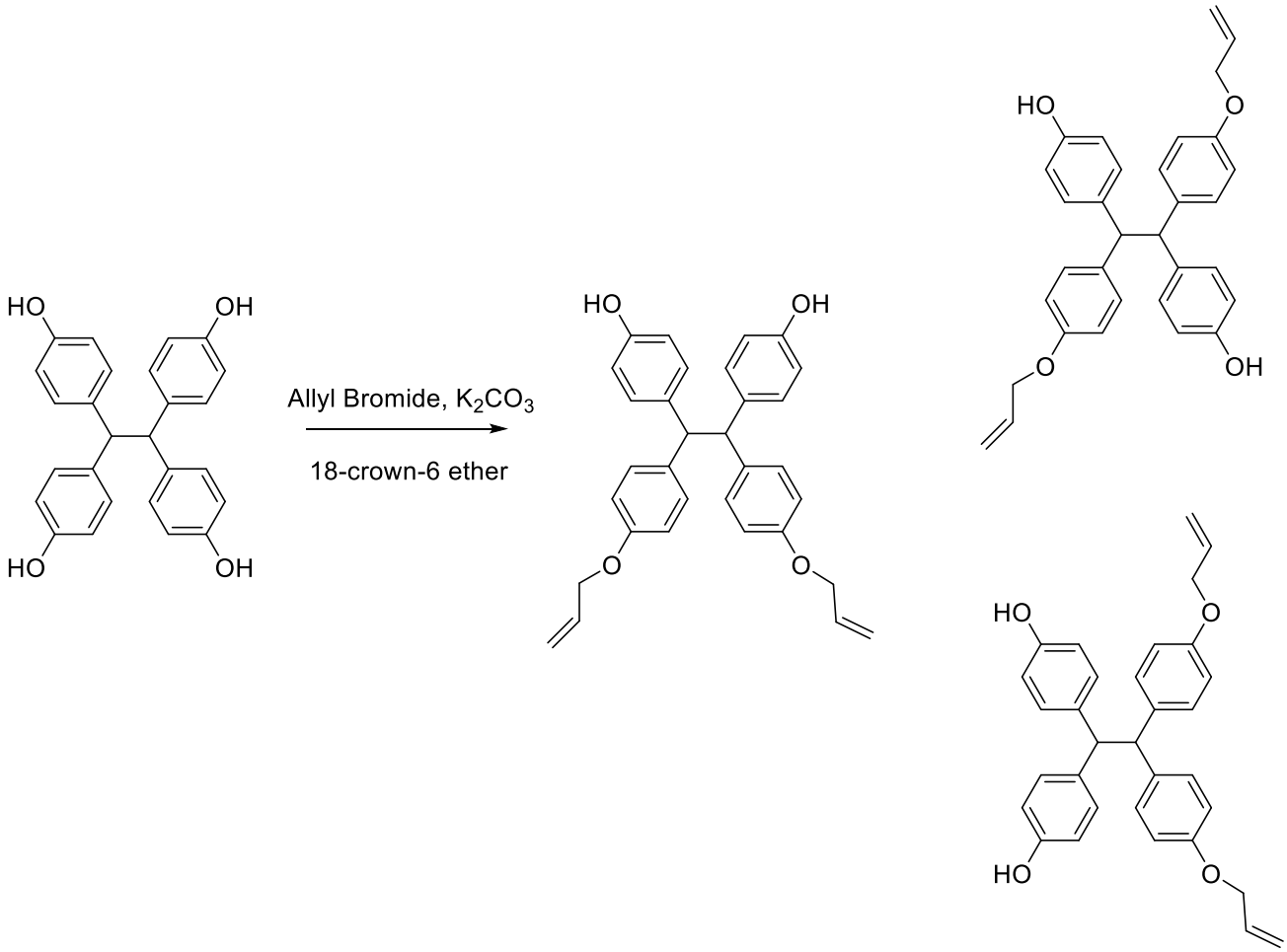

Figure 3.20 Synthesis scheme of TPOE-2OAllyl.

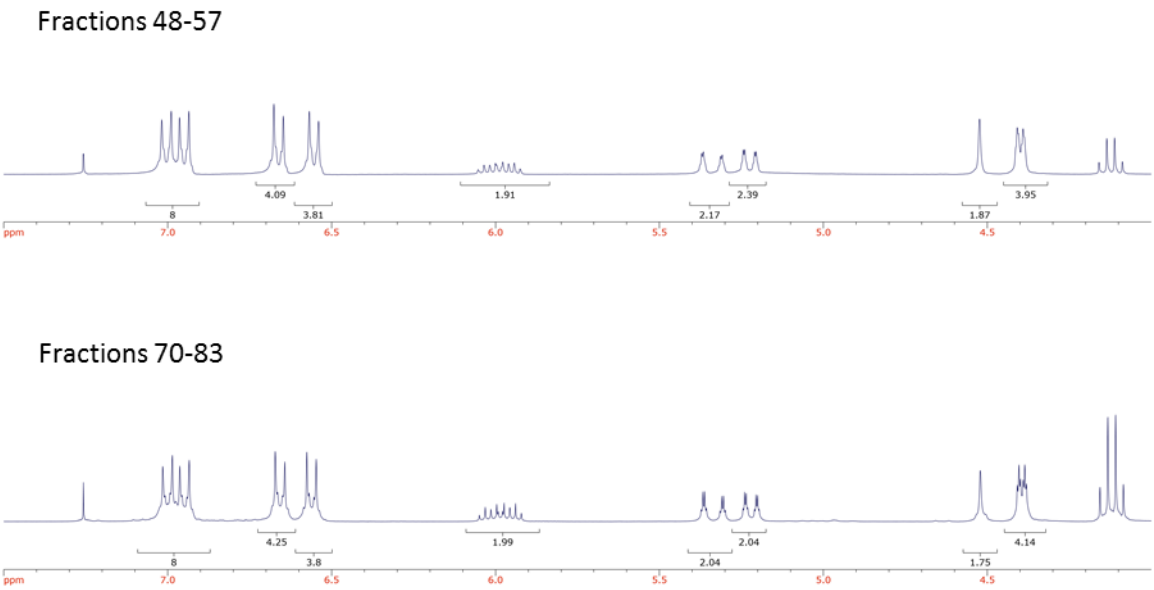

Figure 3.21. ^{1}H NMR spectra of TPOE-2OAllyl isomers in $CDCl_3$. The isomers elute with a different R_f, but have a near-identical ^{1}H NMR spectrum.

TPOE-2OAllyl synthesis is described in Chapter 2. The TPOE-2OAllyl product exists as a mixture of isomers, as shown in Figure 3.20, but no effort was made to isolate a single isomer, since the ^{1}H NMR spectra were nearly identical, as shown in Figure 3.21. For brevity, only a single isomer is shown in the synthetic schemes following this one. ^{1}H NMR (300 MHz, $CDCl_3$, δ, ppm): 7.00 (d, 4H), 6.95 (d, 4H), 6.65 (d, 4H), 6.55 (d, 4H), 5.98 (m, 2H), 5.34 (dd, 2H), 5.21 (dd, 2H), 4.87 (s, 1H, -OH), 4.51 (s, 2H), 4.39 (m, 4H). Yield: 0.475g.

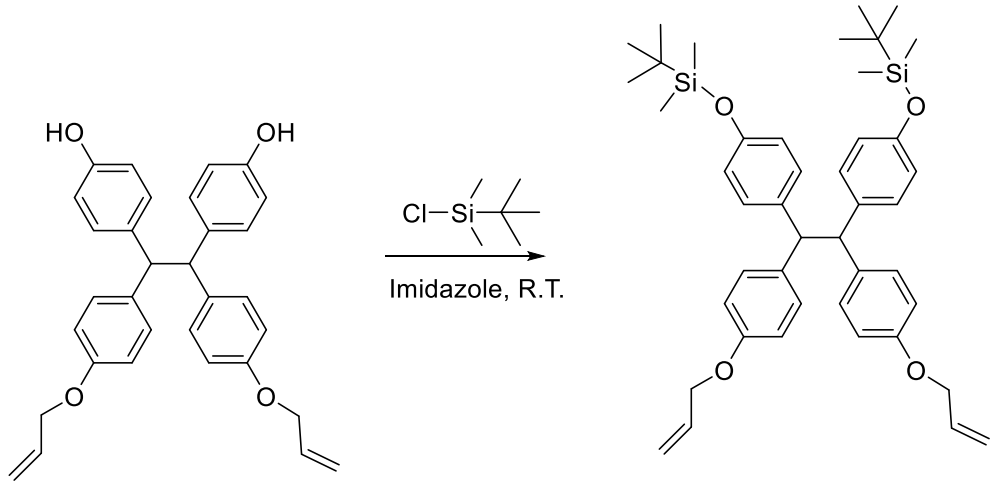

Figure 3.22 Synthesis scheme of TPOE-2OAllyl-2TBS.

TPOE-2OAllyl-2TBS: 0.475g TPOE-2OAllyl was dissolved in ethyl acetate, and 3 equivalents (0.44g) of tert-butyldimethylsilylchloride (TBS-Cl) were added, along with 3 equivalents (0.411g) of imidazole and stirred at room temperature overnight. Afterwards, the solution was washed once with dilute HCl solution and twice with deionized water. The organic layer was dried over $MgSO_4$ and solvents evaporated using a rotary evaporator. ^1H NMR (300 MHz, $CDCl_3$, δ): 7.01 ppm (d, 6H), 6.84 ppm (d, 2H), 6.65 ppm (d, 6H), 6.51 ppm (d, 2H), 5.97 ppm (m, 2H), 5.30 ppm (dd, 2H), 5.20 ppm (dd, 2H), 4.50 ppm (s, 2H), 4.35 ppm (d, 4H), 0.88 ppm (s, 18H), 0.05 ppm (s, 12H). Yield: 0.34g

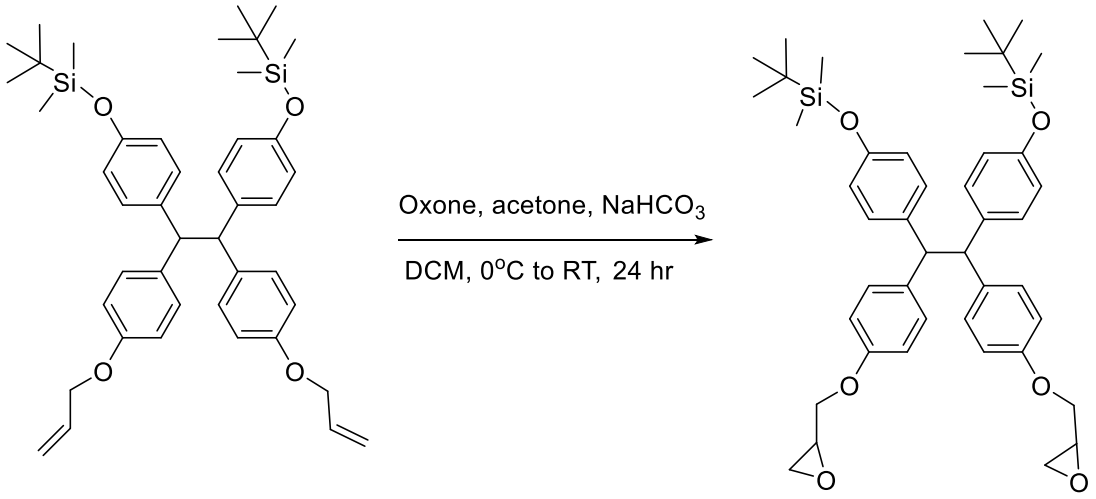

Figure 3.23 Synthesis scheme of TPOE-2Ep-2TBS.

TPOE-2Ep-2TBS: Alkenes were converted to epoxides by reacting 0.284g (1 equivalent) of TPOE-2OAllyl-2TBS (dissolved in dichloromethane) with (0.98g) 8 equivalents of Oxone (dissolved in water) and 12 equivalents (0.81g) of $NaHCO_3$ in the presence of a catalytic amount of acetone. This procedure was repeated several times until conversion of alkenes to Oxone was complete. After conversion was complete, deionized water was added until all solids dissolved and additional ethyl acetate was added. The organic layer was then washed twice with deionized water and then solvents evaporated via rotary evaporator. ^{1}H NMR (300 MHz, $CDCl_3$, δ): 6.97 ppm (d, 4H), 6.90 ppm (d, 4H), 6.62 ppm (d, 4H), 6.54 ppm (d, 4H), 4.47 ppm (s, 2H), 4.05 ppm (dd, 2H), 3.75 (dd, 2H), 3.23 ppm (m, 2H), 2.80 ppm (dd, 2H), 2.64 ppm (dd, 2H), 0.88 ppm (s, 18H), 0.05 ppm (s, 12H). Yield: 0.1923g.

TPOE-2Ep: 1 equivalent of TPOE-1Ep-3TBS was added to DCM, and 4 equivalents of TBAF (1.0 M in THF) were added. The solution was allowed to stir at room temperature

for 4 hours before being washed with water 3 times. The organic phase was filtered/dried over $MgSO_4$ and then solvents were removed using rotary evaporator. The resulting crude material was then purified via a silica gel column, first eluting with hexanes and then with hexanes:ethyl acetated (9:1) to remove residual TBAF impurities. ^{1}H NMR (300 MHz, $CDCl_3$, δ): 6.97 ppm (d, 4H), 6.90 ppm (d, 4H), 6.62 ppm (d, 4H), 6.54 ppm (d, 4H), 4.47 ppm (s, 2H), 4.05 ppm (dd, 2H), 3.75 (dd, 2H), 3.23 ppm (m, 2H), 2.80 ppm (dd, 2H), 2.64 ppm (dd, 2H). Yield: 64%.

TPOE-3Ep synthesis is detailed in Chapter 2.

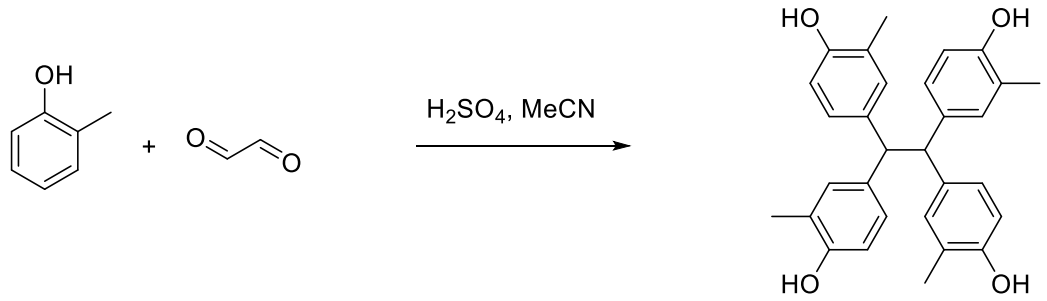

Figure 3.24 Synthesis scheme of TMPOE.

TMPOE: 25 g *o*-cresol and 5.8 g glyoxal (40 wt% solution in water) were added to 25 mL of acetone in a 100-mL round-bottom flask. 5 g concentrated sulfuric acid was added dropwise and the mixture was stirred at room temperature for 72 hours, and afterwards was poured into 250 mL acetone, where a white precipitate formed. This mixture was then filtered, and the solid was washed with acetone until white and then three times with deionized water. The solid was then boiled in approximately 50 mL acetone for 30 minutes, filtered, and then dried overnight to yield a white powder. Yield: 5.4 g. ^{1}H NMR (300 MHz,

methanol-d_4, δ): 6.89 ppm (s, 4H), 6.80 ppm (d, 4H), 6.47 ppm (d, 4H), 4.48 ppm (s, 2H), 2.01 ppm (s, 12H). MS (EI) m/z: [M]+: 227.1. Anal. Calcd for C30H30O4: C, 79.97; H, 7.50. Found: C, 79.95; H, 7.36.

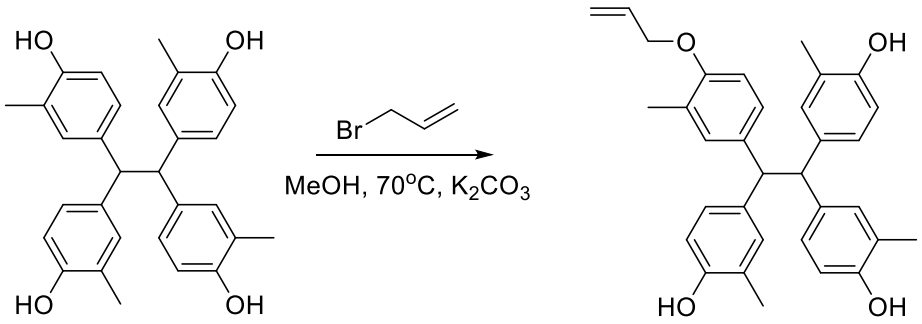

Figure 3.25 Synthesis scheme of TMPOE-1OAllyl.

TMPOE-1OAllyl: 3g (1 molar equivalent) of TMPOE and 3 molar equivalents (2.73g) of potassium carbonate were added to methanol in a round bottom flask in an oil bath set to 70°C. Then, 2.2 equivalents (1.6g) of allyl bromide were added dropwise, and the reaction mixture stirred in the oil bath at 70°C for 12 hours/overnight. The reaction mixture was cooled to room temperature, and then ethyl acetate and HCl were added. The organic phase was then washed once more with dilute HCl solution, and three times with deionized water. The organic phase was filtered/dried over $MgSO_4$ and then solvents were evaporated using a rotary evaporator. A mixture of products, which included TMPOE-1OAllyl, TMPOE-2OAllyl, and TMPOE-3OAllyl was produced. The individual molecules of interest were then isolated and purified from each other using silica gel chromatography with hexanes:ethyl acetate (5:2) used as the eluent. ^{1}H NMR (300 MHz, $CDCl_3$, δ, ppm):

6.83 (m, 8H), 6.52 (d, 2H), 6.47 (d, 2H), 6.00 (m, 1H), 5.35 (dd, 1H), 5.19 (dd, 1H), 4.63 (s, 3H, -OH), 4.43 (s, 2H), 4.38 (dd, 2H), 2.11 (s, 6H), 2.07 (s, 6H). Yield: 0.4984g.

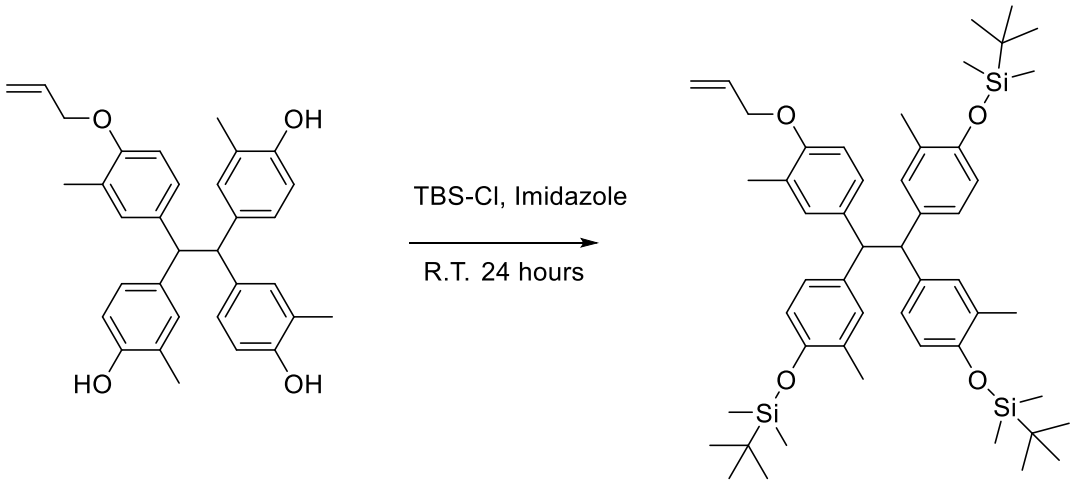

Figure 3.26 Synthesis scheme of TMPOE-1OAllyl-3TBS.

TMPOE-1OAllyl-3TBS: 0.4984g TMPOE-1OAllyl was dissolved in ethyl acetate, and 3.5 molar equivalents (0.531g) of *tert*-butyl dimethylsilylchloride and 6 equivalents (0.27g) of imidazole were added and then stirred at room temperature for 18 hours (overnight). Afterwards, the solution was washed once with dilute HCl solution and then twice with deionized water. The organic phase was then filtered/dried over $MgSO_4$ and solvents were removed using a rotary evaporator. ^1H NMR (300 MHz, $CDCl_3$, δ, ppm): 6.83 (m, 8H), 6.52 (d, 2H), 6.47 (d, 2H), 6.00 (m, 1H), 5.35 (dd, 1H), 5.19 (dd, 1H), 4.43

(s, 2H), 4.38 (dd, 2H), 2.11 (s, 6H), 2.07 (s, 6H). 0.9 ppm (s, 27H), 0.05 ppm (s, 18H). Yield: 0.5757g.

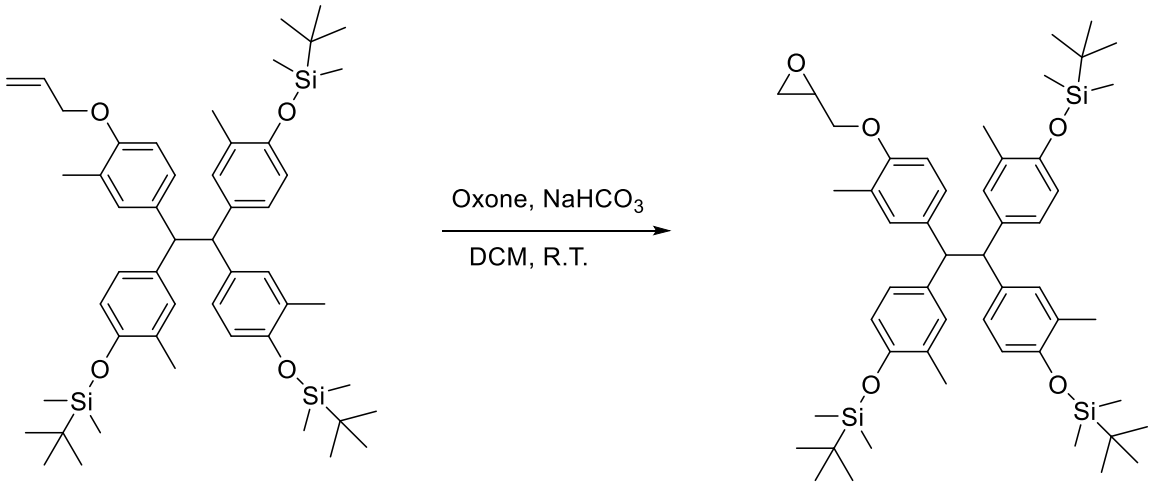

Figure 3.27 Synthesis scheme of TMPOE-1Ep-3TBS.

TMPOE-1Ep-3TBS: TMPOE-1OAllyl-3TBS was dissolved in DCM, and a catalytic amount of acetone was added. 4 equivalents of sodium bicarbonate were dissolved in water and added to the reaction mixture. 2 equivalents of Oxone were dissolved in water and then added dropwise the reaction mixture. This procedure was repeated multiple times until conversion of alkenes to epoxides was complete, as tracked with ^{1}H NMR. Once conversion was complete, the reaction mixture was washed with water and extracted with ethyl acetate, and then solvents were evaporated via rotary evaporator. ^{1}H NMR (300 MHz, $CDCl_3$, δ, ppm): 6.83 (m, 8H), 6.52 (d, 2H), 6.47 (d, 2H), 6.00 (m, 1H), 4.38 (m, 1H), 4.03

(m, 1H), 3.84 (m, 1H), 3.26 (m, 1H), 2.83 (m, 1H), 2.71 (m, 1H), 2.11 (s, 6H), 2.07 (s, 6H), 0.9 ppm (s, 27H), 0.05 ppm (s, 18H). Yield: 0.56g.

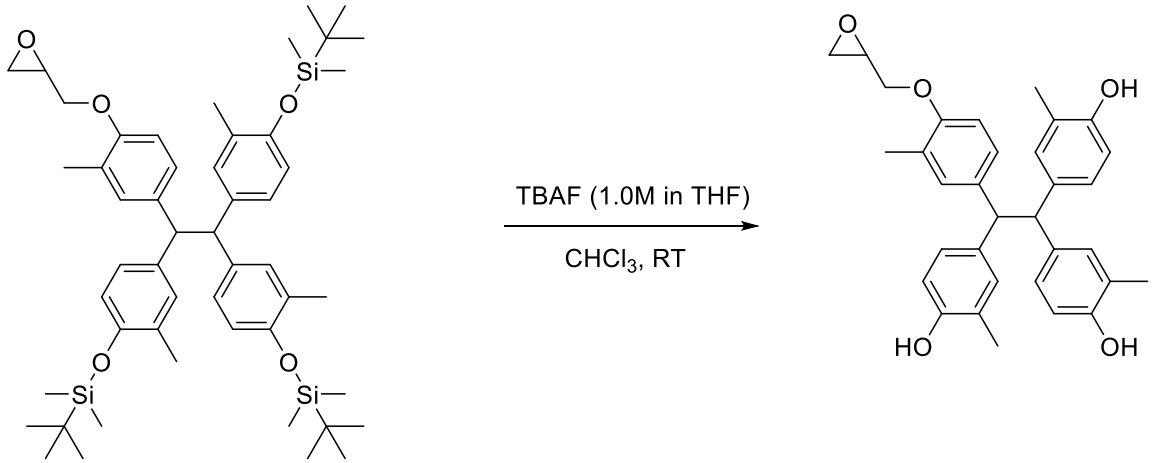

Figure 3.28 Synthesis scheme of TMPOE-1Ep.

TMPOE-1Ep: 1 equivalent (0.56 g) of TMPOE-1Ep-3TBS was added to CHCl3, and 6 equivalents of TBAF (1.0 M in THF) were added. The solution turned dark brown upon addition of TBAF, and the solution was allowed to stir at room temperature for 4 hours before being washed with water 3 times. The organic phase was filtered/dried over MgSO4 and then solvents were removed using rotary evaporator. The resulting crude material was then purified via a silica gel column, first eluting with hexanes and then with hexanes:ethyl acetated (9:1) to remove residual TBAF impurities. ^{1}H NMR (300 MHz, $CDCl_3$, δ, ppm): 6.83 (m, 8H), 6.52 (d, 2H), 6.47 (d, 2H), 6.00 (m, 1H), 5.26 (s, 3H, -OH), 4.38 (m, 1H), 4.03 (m, 1H), 3.84 (m, 1H), 3.26 (m, 1H), 2.83 (m, 1H), 2.71 (m, 1H), 2.11 (s, 6H), 2.07 (s, 6H). Yield: 67%.

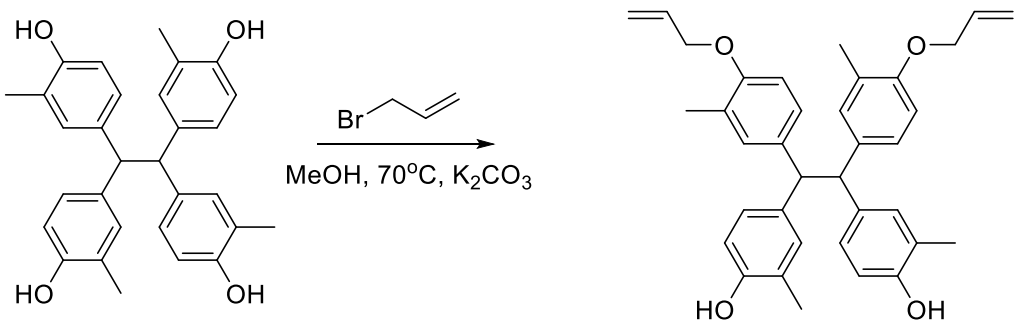

Figure 3.29 Synthesis scheme of TMPOE-2OAllyl.

TMPOE-2OAllyl synthesis is described in the synthesis for TMPOE-1OAllyl. ^{1}H NMR (300 MHz, $CDCl_3$, δ ppm): 6.86 (m, 8H), 6.54 (d, 2H), 6.47 (d, 2H), 5.97 (m, 2H), 5.35 (m, 2H), 5.20 (m, 2H), 4.58 (s, 2H), 4.4 (m, 4H), 2.10 (s, 6H), 2.07 (s, 6H). Yield: 0.7347g.

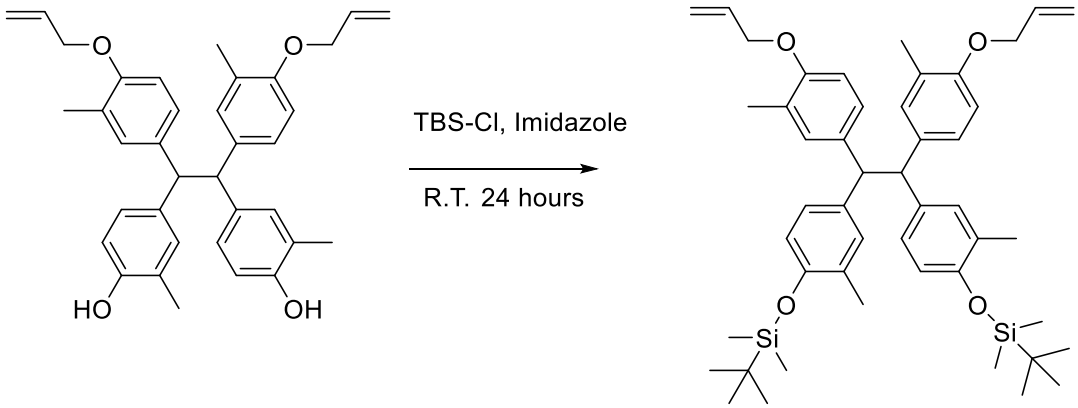

Figure 3.30 Synthesis scheme of TMPOE-2OAllyl-2TBS.

TMPOE-2OAllyl-2TBS: 0.4315g TMPOE-2OAllyl was dissolved in ethyl acetate, and 2.5 equivalents (0.30g) of TBS-Cl and 3 equivalents (0.164g) of imidazole were added. The solution was allowed to stir at room temperature for 24 hours, after which it was washed once with dilute HCl solution and twice with deionized water. The organic phase

was filtered/dried over $MgSO_4$ and then solvents were removed via rotary evaporator. ^1H NMR (300 MHz, $CDCl_3$, δ ppm): 6.86 (m, 8H), 6.54 (d, 2H), 6.47 (d, 2H), 5.97 (m, 2H), 5.35 (m, 2H), 5.20 (m, 2H), 4.58 (s, 2H), 4.4 (m, 4H), 2.10 (s, 6H), 2.07 (s, 6H), 0.95 (s, 18H), 0.09 (s, 12H). Yield: 0.3605g.

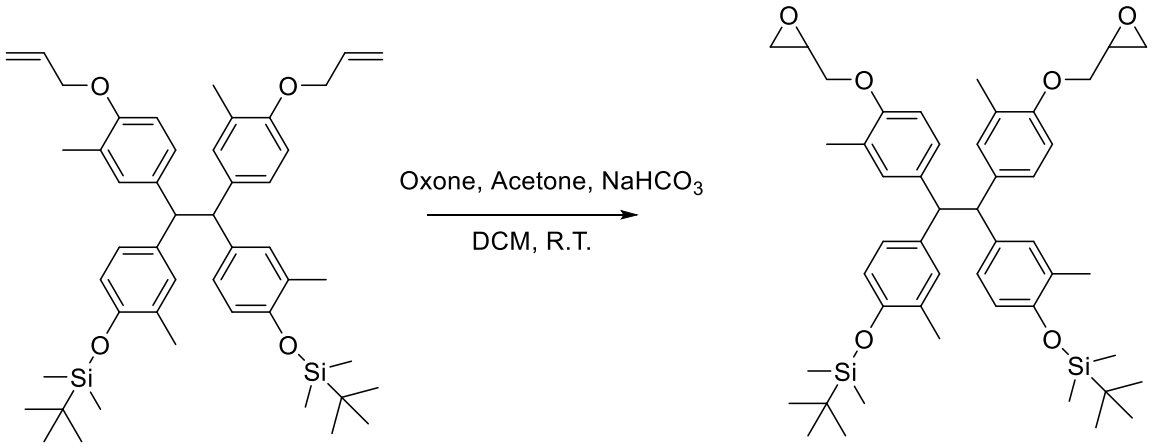

Figure 3.31 Synthesis scheme of TMPOE-2Ep-2TBS.

TMPOE-2Ep-2TBS: TMPOE-2OAllyl-2TBS was dissolved in DCM, and a catalytic amount of acetone was added. 8 equivalents of sodium bicarbonate were dissolved in water and added to the reaction mixture. 4 equivalents of Oxone were dissolved in water and then added dropwise the reaction mixture. This procedure was repeated multiple times until conversion of alkenes to epoxides was complete, as tracked with ^1H NMR. Once conversion was complete, the reaction mixture was washed with water and extracted with ethyl acetate, and then solvents were evaporated via rotary evaporator. ^1H NMR (300 MHz, $CDCl_3$, δ ppm): 6.86 (m, 8H), 6.54 (d, 2H), 6.47 (d, 2H), 4.38 (s, 2H), 4.06 (m, 2H), 3.74

(m, 2H), 3.29 (m, 2H), 2.82 (dd, 2H), 2.70 (dd, 2H), 2.10 (s, 6H), 2.07 (s, 6H), 0.95 (s, 18H), 0.09 (s, 12H). Yield: 0.20g.

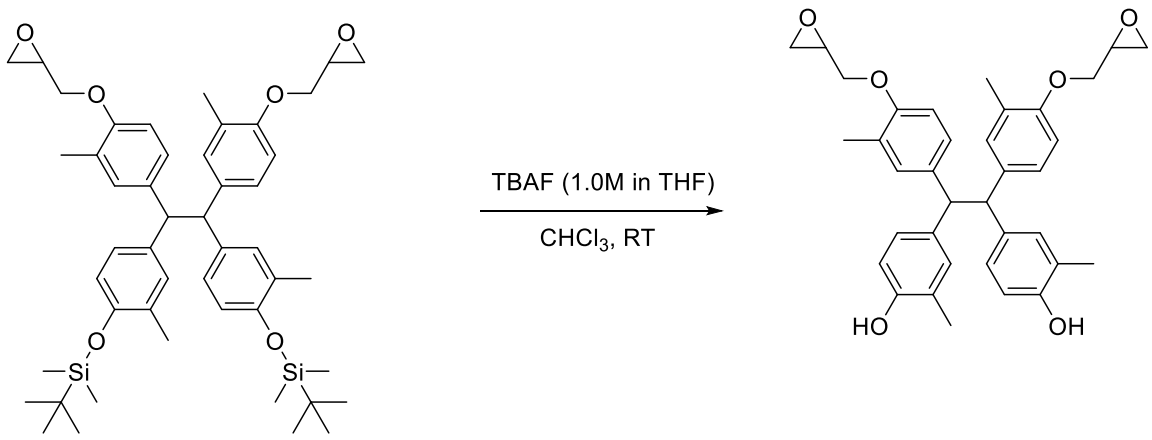

Figure 3.32 Synthesis scheme of TMPOE-2Ep.

TMPOE-2Ep: 0.25g TMPOE-2Ep-2TBS was dissolved in CHCl3 and then 4 equivalents of TBAF (0.63mL) (1.0 M in THF) were added. The solution was allowed to stir at room temperature overnight and was then washed 3 times with deionized water. The organic phase was then filtered/dried over $MgSO_4$ and then solvents were removed via rotary evaporator. The resulting crude material was then purified via silica gel column, eluting first with hexanes and then with ethyl acetate to remove impurities. ^{1}H NMR (300 MHz, $CDCl_3$, δ ppm): 6.86 (m, 8H), 6.54 (d, 2H), 6.47 (d, 2H), 4.38 (s, 2H), 4.06 (m, 2H), 3.74 (m, 2H), 3.29 (m, 2H), 2.82 (dd, 2H), 2.70 (dd, 2H), 2.10 (s, 6H), 2.07 (s, 6H). Yield: 22%.

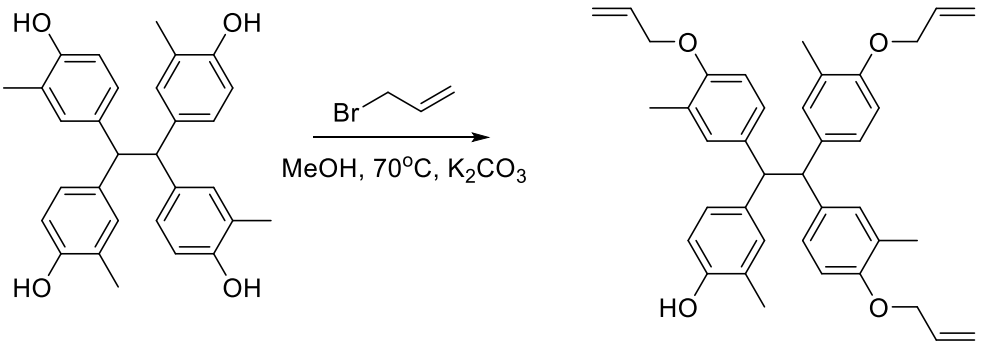

Figure 3.33 Synthesis scheme of TMPOE-3OAllyl.

TMPOE-3OAllyl synthesis is described in the synthesis for TMPOE-1OAllyl. ^{1}H NMR (300 MHz, $CDCl_3$, δ (ppm)): 6.90 (d, 6H), 6.87 (d, 2H), 6.56 (s, 2H), 6.53 (s, 2H), 6.01 (m, 3H), 5.37 (m, 3H), 5.22 (m, 3H), 4.49 (s, 3H, -OH), 4.40 (m, 6H), 2.12 (s, 6H), 2.10 (s, 6H). Yield: 0.7578g.

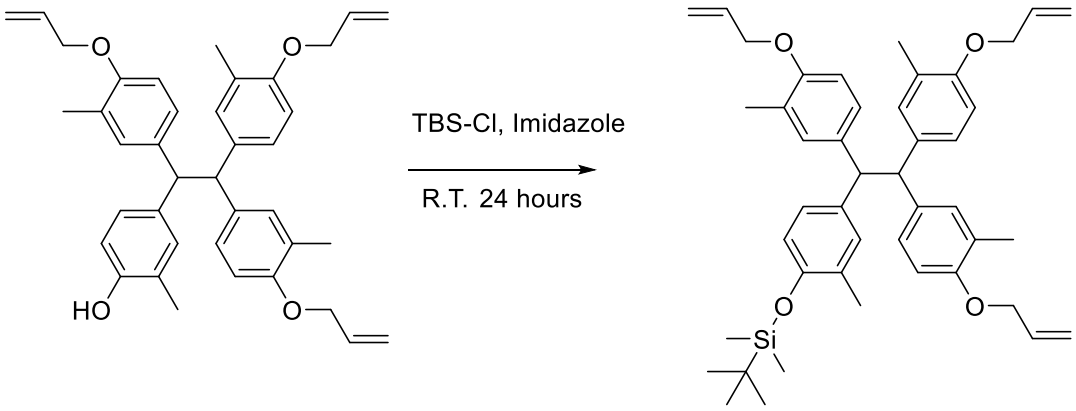

Figure 3.34 Synthesis scheme of TMPOE-3OAllyl-TBS.

TMPOE-3OAllyl-TBS: 0.7578g TMPOE-3OAllyl was dissolved in ethyl acetate and 1.5 equivalents (0.298g) of TBS-Cl and 2 equivalents (0.179g) of imidazole were added. The solution was stirred at room temperature for 24 hours and then washed once with dilute

HCl solution and twice with deionized water. The organic phase was filtered/dried over $MgSO_4$ and then solvents were removed with rotary evaporator. ^{1}H NMR (300 MHz, $CDCl_3$, δ (ppm)): 6.90 (d, 6H), 6.87 (d, 2H), 6.56 (s, 2H), 6.53 (s, 2H), 6.01 (m, 3H), 5.37 (m, 3H), 5.22 (m, 3H), 4.49 (s, 3H, -OH), 4.40 (m, 6H), 2.12 (s, 6H), 2.10 (s, 6H), 0.92 (s, 18H), 0.11 (s, 9H). Yield: 0.7406g.

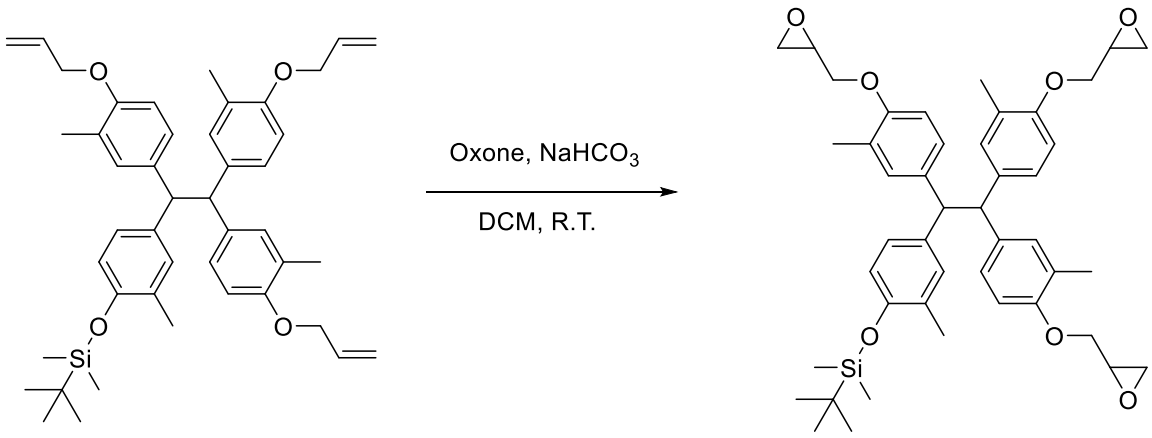

Figure 3.35 Synthesis scheme of TMPOE-3Ep-TBS.

TMPOE-3Ep-TBS: TMPOE-3OAllyl-TBS was dissolved in DCM, and a catalytic amount of acetone was added. 9 equivalents of sodium bicarbonate were dissolved in water and added to the reaction mixture. 6 equivalents of Oxone were dissolved in water and then added dropwise the reaction mixture. This procedure was repeated multiple times until conversion of alkenes to epoxides was complete, as tracked with ^{1}H NMR. Once conversion was complete, the reaction mixture was washed with water and extracted with ethyl acetate, and then solvents were evaporated via rotary evaporator. ^{1}H NMR (300 MHz, $CDCl_3$, δ (ppm)): 6.90 (d, 6H), 6.87 (d, 2H), 6.56 (s, 2H), 6.53 (s, 2H), 4.06 (m, 2H), 3.74

(m, 2H), 3.31 (m, 2H), 2.80 (dd, 2H), 2.67 (dd, 2H), 2.12 (s, 6H), 2.10 (s, 6H), 0.92 (s, 18H), 0.11 (s, 9H). Yield: 0.5646g.

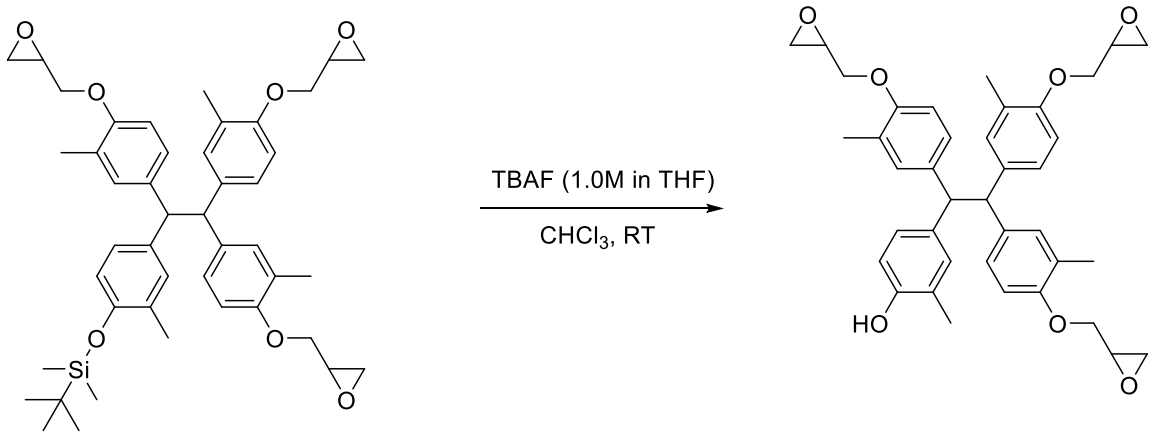

Figure 3.36 Synthesis scheme of TMPOE-3Ep.

TMPOE-3Ep: 0.5646g TMPOE-3Ep-TBS was dissolved in $CHCl_3$ and then 2 equivalents of TBAF (1.52mL) (1.0 M in THF) were added. The solution was allowed to stir at room temperature overnight and was then washed 3 times with deionized water. The organic phase was then filtered/dried over $MgSO_4$ and then solvents were removed via rotary evaporator. The resulting crude material was then purified via silica gel column, eluting first with hexanes and then with ethyl acetate to remove impurities. ^{1}H NMR (300 MHz, $CDCl_3$, δ (ppm)): 6.90 (d, 6H), 6.87 (d, 2H), 6.56 (s, 2H), 6.53 (s, 2H), 4.06 (m, 2H), 3.74 (m, 2H), 3.31 (m, 2H), 2.80 (dd, 2H), 2.67 (dd, 2H), 2.12 (s, 6H), 2.10 (s, 6H). Yield: 0.0922g.

3.3 Lithographic evaluation

3.3.1 DUV Contrast Curves

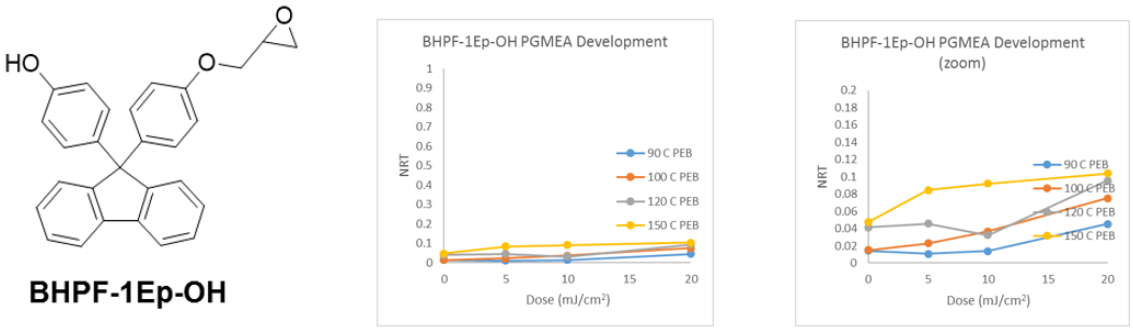

Figure 3.37 Structure of BHPF-1Ep and 248nm DUV contrast curves in PGMEA development.

In the contrast curves of BHPF-1Ep in Figure 3.37, very little conversion is seen, based on the low NRT values. Even at a PEB temperature of 150°C, only 10% of the original film thickness remains. A compound with only 1 epoxide appears to be insufficient to form an insoluble network.

Surprisingly, even though the logD value of this material was calculated to be 1.83, a film of the material was not soluble in 0.26N TMAH developer (a logD value lower than 2 generally indicates that the resist will be soluble in 0.26 N TMAH developer). The material was placed in 0.26N TMAH developer with no PAB to discount the possibility of thermal reactions between epoxides and phenols leading to insoluble films. Still, the film remained insoluble. The ^{1}H NMR spectrum of BHPF-1Ep in Figure 3.38 confirms that there are both epoxides and phenols present on the molecule. Because of these issues, no further data was gathered on this material.

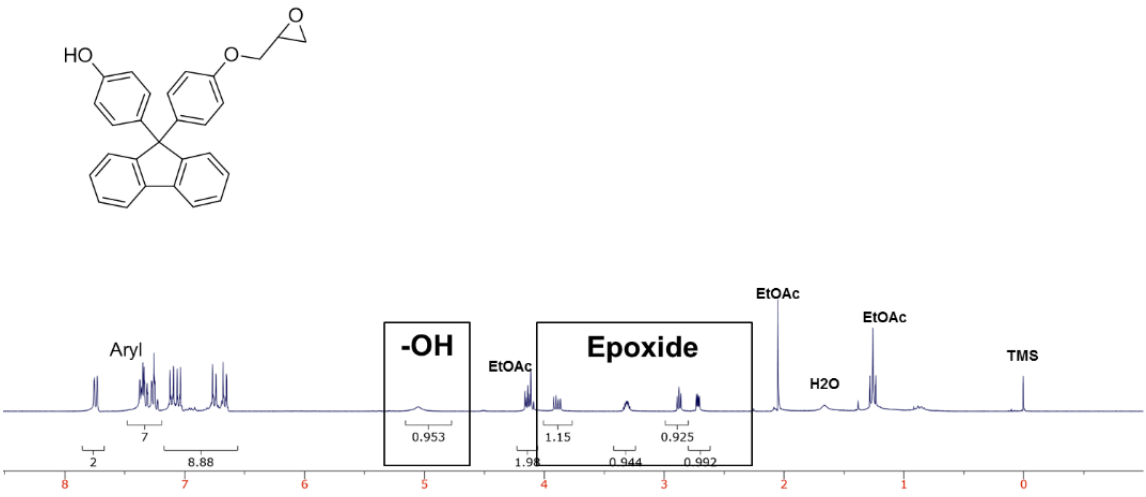

Figure 3.38 ^{1}H NMR spectrum of BHPF-1Ep in $CDCl_3$, showing the presence of epoxides.

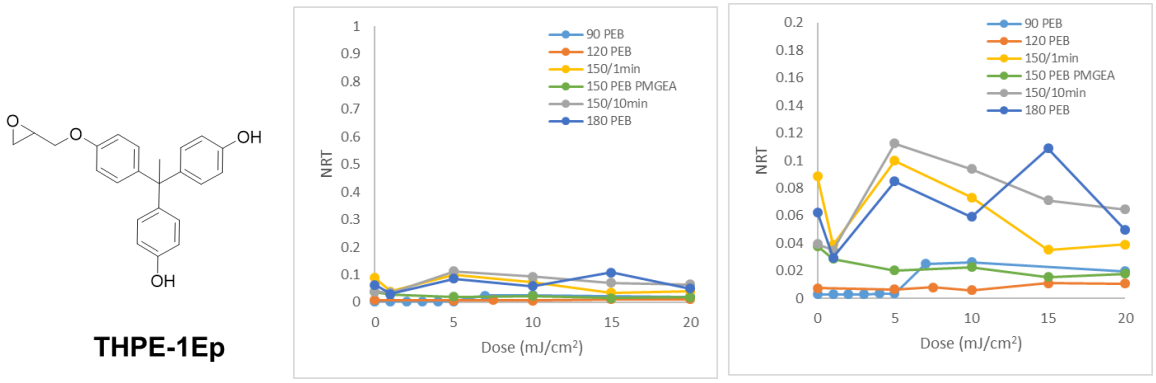

Figure 3.39 Structure and 248nm DUV contrast curve of THPE-1Ep showing the low NRT of this material. The right graph is a zoom of the left graph.

A similar situation is seen in THPE-1Ep contrast curves (Figure 3.39) in both PGMEA and 0.26N TMAH development. A maximum of approximately 10% remaining film thickness is seen in each development solvent. Various temperatures, PEB times, and development solvents were explored, but none of them produced enough insoluble material to warrant further investigation of this resist.

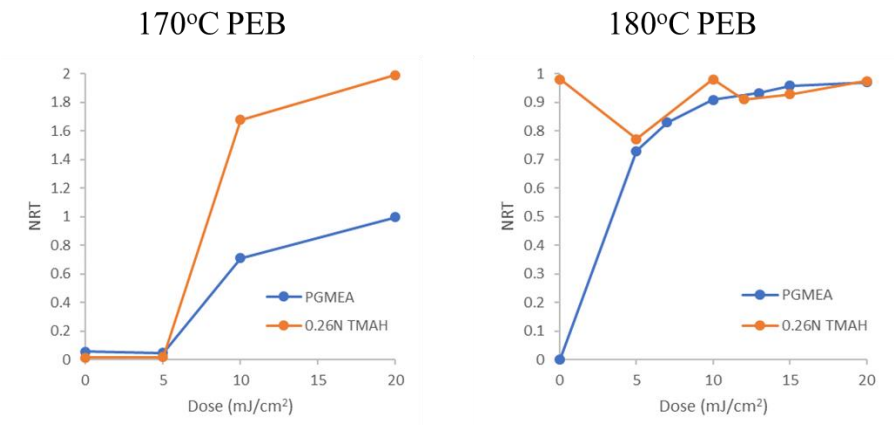

Figure 3.40 DUV contrast curves for TPOE-1Ep showing the effect of increasing the PEB temperature.

Unlike the other 1Ep compounds, TPOE-1Ep showed an increase in NRT with dose in its contrast curves in Figure 3.40 and appears to have a sufficient number of functional groups to achieve an insoluble network. An extraordinarily high PEB of 170°C is required to reach an NRT of 1 in PGMEA development. Unfortunately, the material swells to an NRT value of 2 when developed in 0.26N TMAH. This enormous swelling is likely due to the large number of phenols present on the core, which are likely not being completely consumed through epoxide-phenol reactions. To increase consumption of phenols, the PEB was raised 10 degrees to 180°C. While the swelling was eliminated, crosslinked material remained on the wafer, even at a dose of 0 mJ/cm^2. At this temperature, there is apparently sufficient energy to allow epoxide-phenol crosslinking to occur in the absence of photoacid to generate insoluble material in unexposed regions.

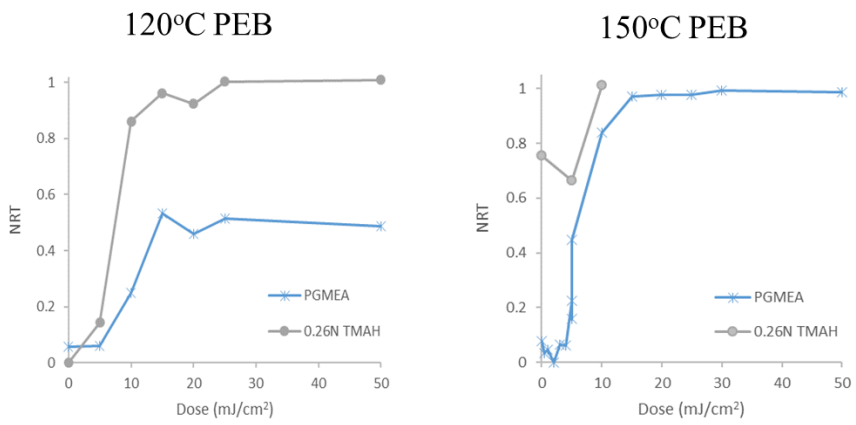

Figure 3.41 DUV contrast curves of TPOE-2Ep at two different PEB temperatures.

For TPOE-2Ep in Figure 3.41, a similar situation is seen where increasing the PEB from 120°C to 150°C causes thermal crosslinking in unexposed regions of the resist film. At a PEB of 120°C, there is insufficient material remaining to reach an NRT of 1 in PGMEA development. While increasing the PEB to 150°C does increase the NRT to 1 in PGMEA development, thermal crosslinking appears in 0.26N TMAH development at a dose of 0 mJ/cm^2.

An increase in glass transition temperature (T_g) is seen with increasing the number of phenols, which requires much higher PEBs to be used as the number of phenols is increased. To achieve good contrast behavior in these materials, there appears to be a need to balance the increase in phenols with a decrease in their glass transition temperature. Literature reports show that for small phenolic molecules, inclusion of a methyl or methoxy group adjacent to a phenol decreases melting points, possibly due to hydrogen-bond disruption.[10] Incorporating methyl groups in the ortho position in TPOE resists may also

lead to a reduction in T_g so that the resists can be crosslinked at temperatures much lower than where epoxide-phenol thermal crosslinking occurs. To that end, several new molecules were synthesized, based on the TMPOE core and are shown in Figure 3.42

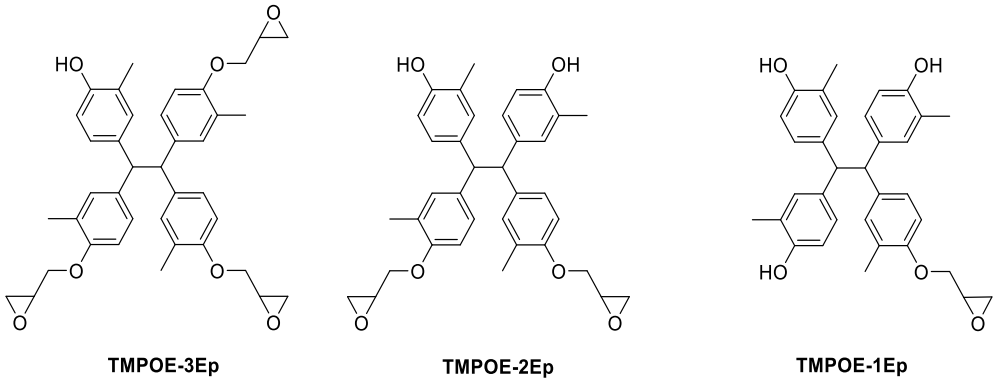

Figure 3.42 Structures of new TMPOE resists that were designed with methyl groups adjacent to phenols to reduce glass transition temperatures.

TMPOE-3Ep has an identical T_g to TPOE-3Ep, which could possibly be due to opposing effects of mass increase and disruption of hydrogen bonding. TMPOE-2Ep and TMPOE-1Ep both show a slight decrease in glass transition temperature due to the inclusion of the methyl groups.

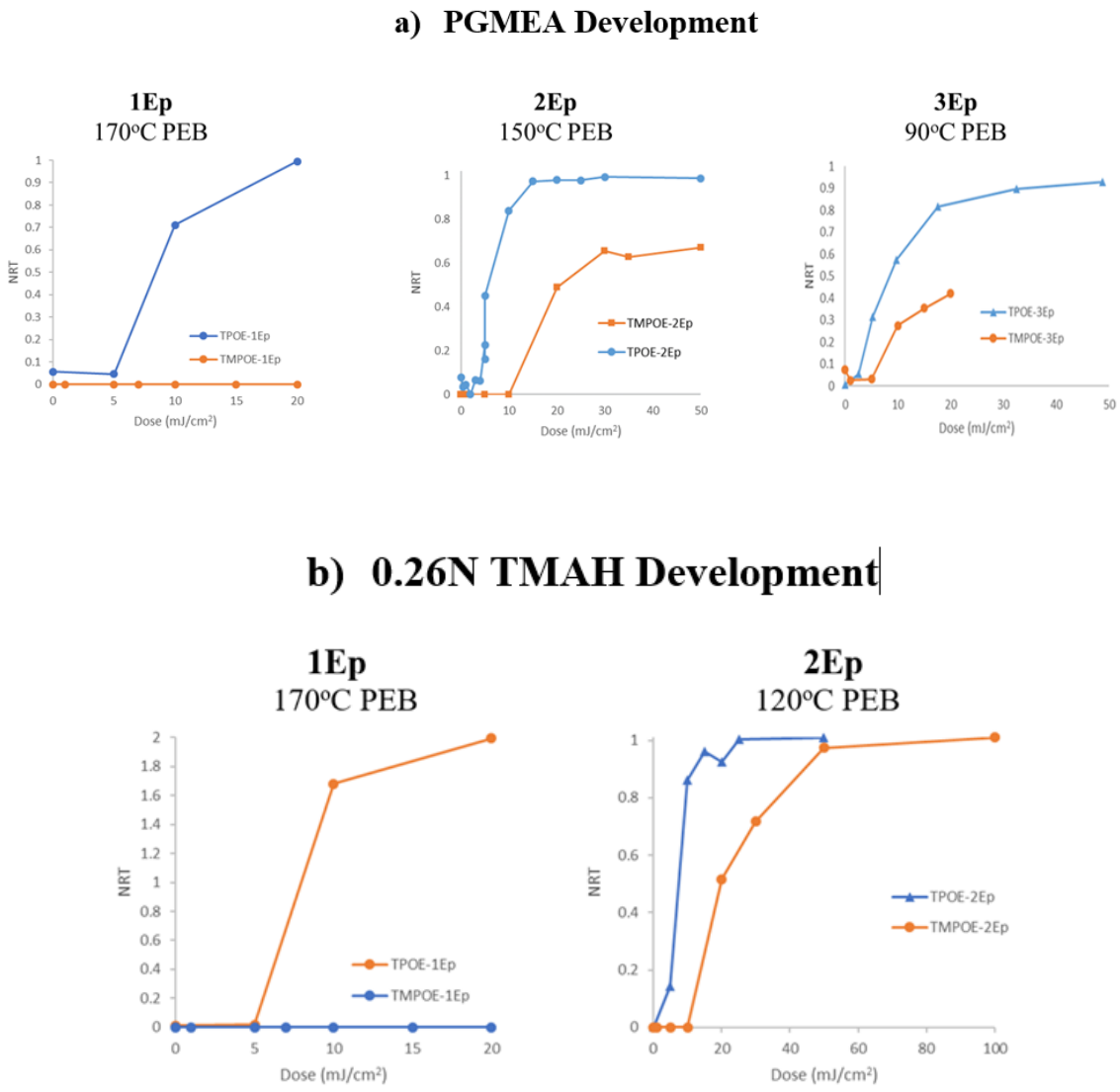

Figure 3.43 DUV contrast curves comparing TMPOE and TPOE resists, developed in PGMEA and 0.26N TMAH. No TMAH curve is shown for TMPOE-3Ep, as it is insoluble in 0.26N TMAH.

In Figure 3.43 the DUV contrast curves of the new methylated TMPOE resists are compared to their predecessors, which lack a methyl group. As a whole, the new methylated materials achieve much lower ultimate NRT than their TPOE counterparts in

both PGMEA and 0.26 N TMAH development. The methyl groups can cause a reduction in one of two possible ways. Placement of the methyl group adjacent to the phenol likely provides steric hindrance to the phenol such that it is prevented from crosslinking with protonated epoxides, reducing the overall amount of crosslinking in the exposed films. If the phenols cannot crosslink into the network, phenols will be present in the final crosslinked film, which will likely increase the T_g of the growing network. Such an increase in T_g can cause the film to become vitrified more quickly at a similar PEB, which limits the diffusion of the growing network, reducing the final NRT value.[3] An attempt was made to gather e-beam patters for these molecules, but the materials do not appear to resolve high-resolution pattern at doses below the highest doses probed, up to 120 $\mu C/cm^2$. The material does appear to pattern large squares used to obtain the e-beam contrast curves, but there was not enough material remaining to locate the squares using a profilometer, and so no contrast curves were obtained. Future work should focus on identifying the correct doses required to resolve patterns in these materials.

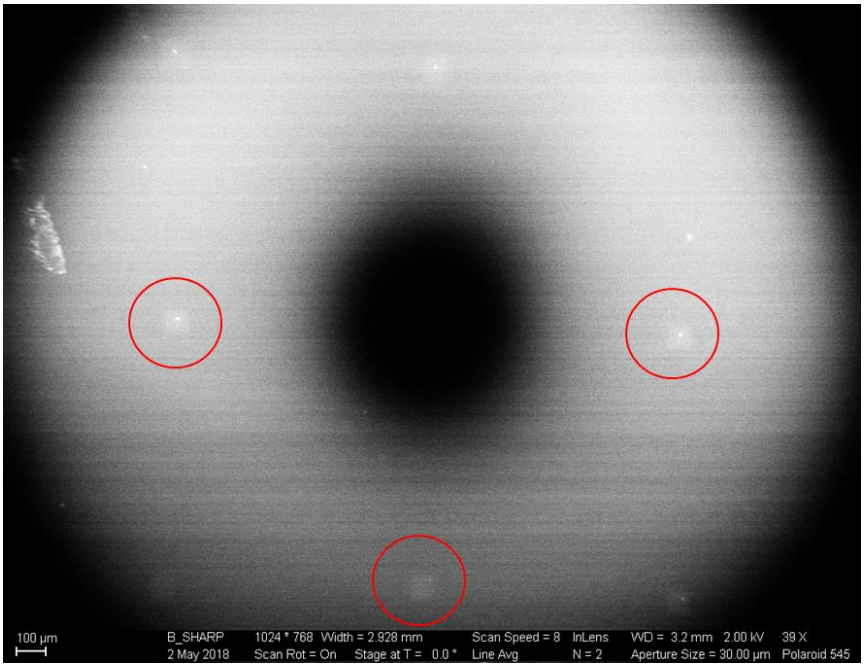

Figure 3.44. SEM image of squares formed from TMPOE-2Ep using e-beam patterning. Squares are circled in red.

3.4 Glass Transition Temperature

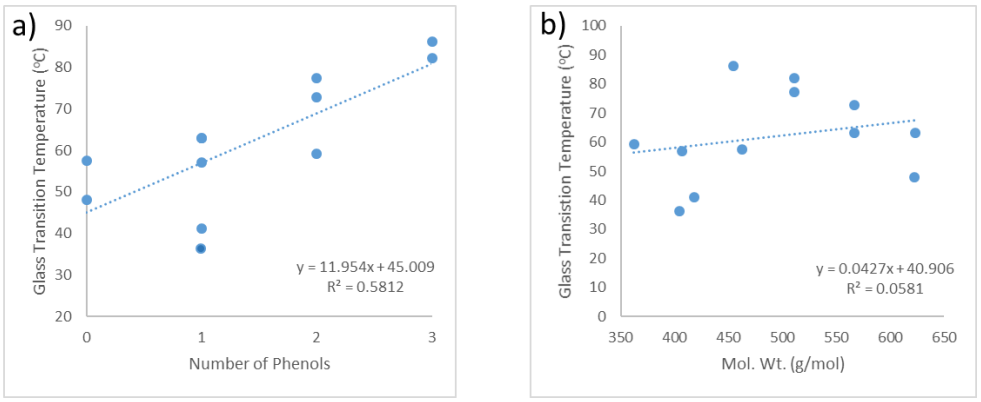

Figure 3.45 a) Plot of the T_g of selected compounds versus the number of phenols on the resist. b) A plot of the glass transition temperature versus molecular weight of the resists.

These results suggest that, in order to successfully design a TMAH-developable epoxide resist, there are two resist parameters that must be carefully balanced: base solubility and T_g. The first is influenced by the number of ionizable phenols vs. non-ionizable portions of the resist (such as epoxides and other structural features which lack an ionizable phenol). Glass transition temperature is influenced by a variety of factors, but in epoxide materials, we have seen that many of our smaller resists tend to have a lower T_g than those based on the TPOE core.[11] Figure 3.45a plots the glass transition temperature of the molecules synthesized in this chapter as a function of the number of phenols they contain. (Figure 3.46 contains the structures of the molecules, along with their T_gs, as measured via spectroscopic ellipsometry). We chose to measure the resists via ellipsometry instead of a traditional DSC for two reasons: 1) the T_g often produces a vanishingly weak signal for small molecules in a DSC, and 2) thin-film confinement effects can drastically alter the T_g of a compound, due to substrate-material interactions and the presence of a free surface at

the top of a film.[12] For example, it has been shown that for thin films of PMMA, the T_g increases as the film thickness decreases due to the hydrogen-bonding interactions between the silicon substrate and the methacrylate-containing polymer.[13] In contrast, poly(α-methylstyrene) was shown to have a lower T_g as its film thickness decreased due to the absence of preferential substrate interactions and the presence of a free surface.[12]

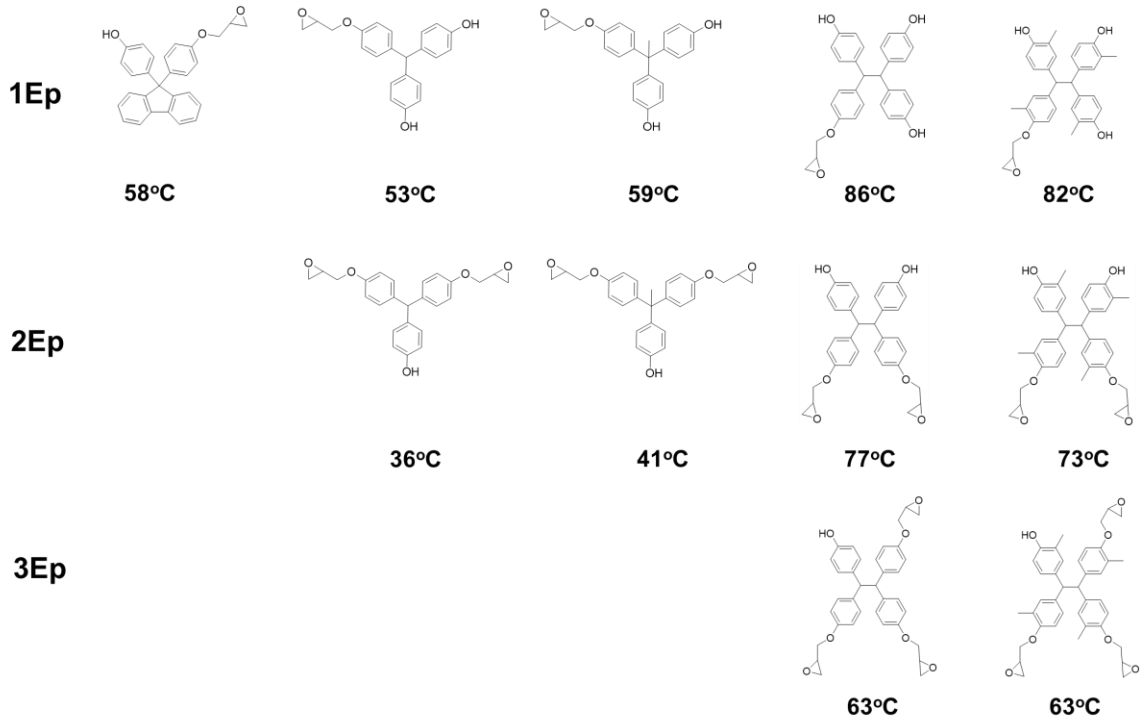

Figure 3.46 Base-soluble molecular resists synthesized in this study to examine the effect of phenol:epoxide ratio on glass transition temperature.

A general increase in T_g is seen in these resists across all cores as the number of phenols is increased. The only molecule to defy this trend is BHPF-1Ep, which has a near-identical T_g (58°C) to BHPF-2Ep (57°C).[11] There is only a very weak correlation between molecular

weight and T_g, likely because in these molecules, a decrease in molecular weight is often the result of removal of epoxide groups, which introduces phenols, which raise the T_g by increasing the amount of hydrogen bonding in the resist films.[14,15] Inclusion of methyl groups adjacent to the phenol in the TMPOE molecules appears to lead to a very slight reduction of the T_g of the resists, possibly through disruption of hydrogen bonding.[16] However, in TMPOE-3Ep, an identical T_g was observed compared to TPOE-3Ep, and this is potentially due to competing effects between disruption of hydrogen bonding and restriction the rotational freedom of the molecules.[17] As more phenols are introduced into the molecule, the degree of hydrogen bonding would also increase, so the effect of T_g reduction due to hydrogen-bond disruption is more pronounced in TMPOE-2Ep and TMPOE-1Ep.

By designing a material with both increased base solubility and a lower T_g, it might be possible to design a resist with increased base solubility while increasing network conversion at low doses. Such a molecule, called THPE-2Ep, is shown in Figure 3.47

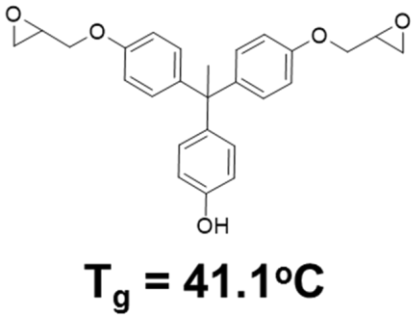

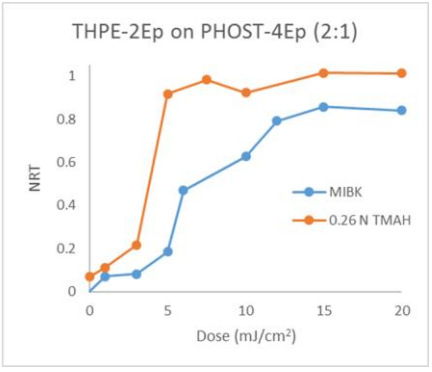

Figure 3.47 Structure of low-T_g, base-soluble resist, THPE-2Ep and its 248nm DUV contrast curve on an underlayer.

The T_g of THPE-2Ep is 41.1°C, which is much lower than the T_g of any of the base-soluble materials reported here. The exception is THP-2Ep, which is structurally identical to THPE-2Ep, but THP-2Ep lacks a methyl group in the center of the resist. THP-2Ep de-wet from both unprimed silicon wafers and wafers treated with an underlayer, and such a low T_g has been problematic in the past with resists.[11] The 248nm DUV contrast curve in Figure 3.47 shows that THPE-2Ep achieves an NRT of 1 in 0.26N TMAH at a dose of 7 mJ/cm^2, while in PGMEA development, it achieves an NRT of 0.8 at a dose of 15 mJ/cm^2 at the same PEB.

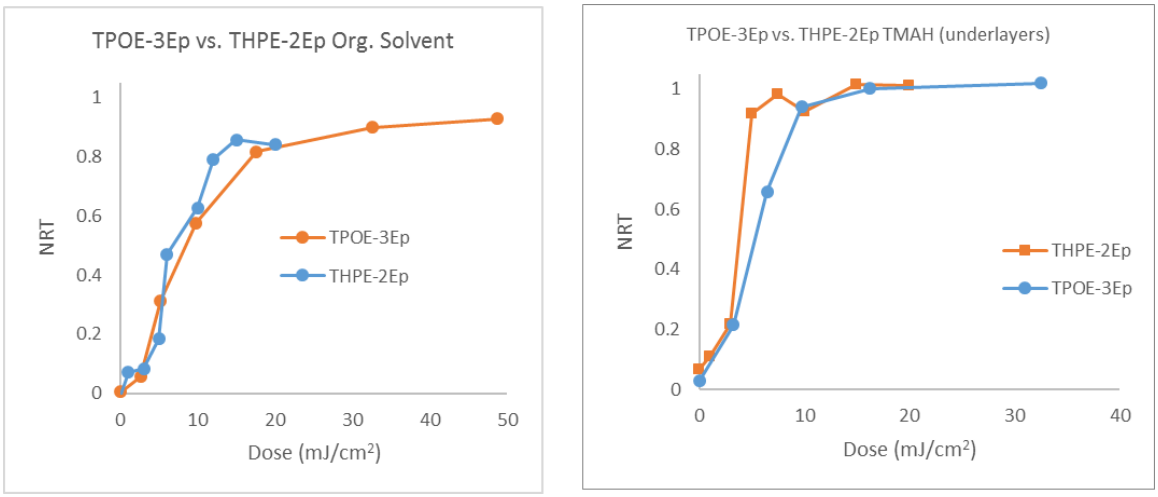

Figure 3.48 Contrast curve comparison between THPE-2Ep and TPOE-3Ep.

Figure 3.48 compares the contrast curve of THPE-2Ep to TPOE-3Ep where each is formulated with 5 mol% TPS-SbF_6 and baked at a 90°C PEB. Even though THPE-2Ep has a lower functionality than TPOE-3Ep, it achieves a remarkably similar NRT in both MIBK and TMAH development. Previous results have shown that lower-functionality resists tend to require higher doses since more crosslinking needs to occur in order to insolubilize the

films.[4] However, THPE-2Ep has a lower T_g, which gives its growing chain ends more mobility compared to TPOE-3Ep, and so the resist can match the NRT of TPOE-3Ep.[4]

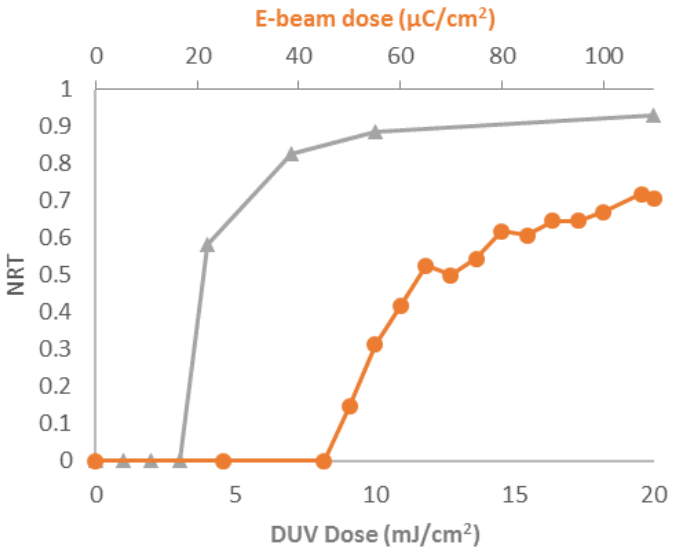

Figure 3.49 100keV e-beam contrast curve with the 248nm DUV contrast curve of THPE-2Ep in MIBK development. (PAB = 60°C/2 min; PEB = 100°C/60s; 5 mol% TPS-SbF_6).

The e beam contrast curve of THPE-2Ep is shown in Figure 3.6 for MIBK development. The material reaches a maximum NRT of approximately 0.7 at a dose of 100 µC/cm^2. Figure 3.50 shows the resulting e-beam patterns of THPE-2Ep when developed in MIBK and 0.26N TMAH. The material appears capable of resolving 30 nm (1:1 line:space) patterns. Similar to TPOE-3Ep without an underlayer, no patterns were resolved in TMAH development due to severe delamination.

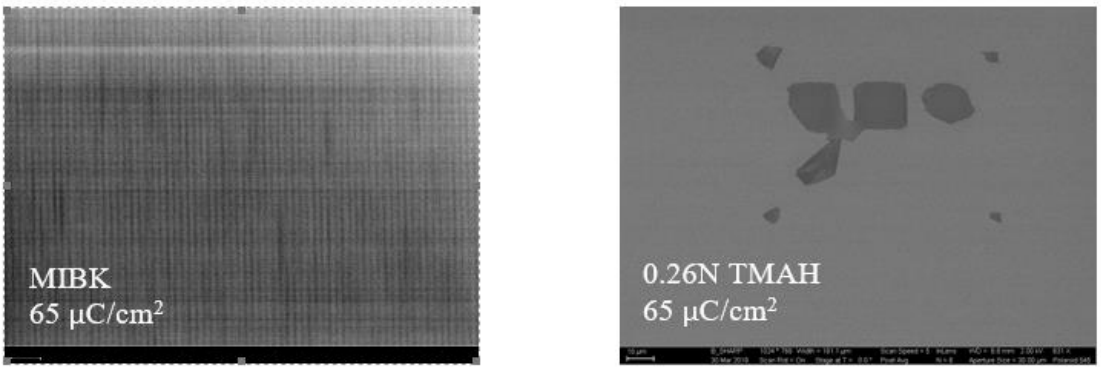

Figure 3.50 (left) E-beam patterns of THPE-2Ep using MIBK development showing 30nm lines and spaces. (right) development in 0.26N TMAH showing delamination.

An underlayer based on poly(hydroxy styrene) and 4Ep was developed to combat this issue. After a series of bake tests, it was determined that a molar ratio of phenol to epoxide of 2:1 provided the best resistance to de-wetting. The PEB temperature was also lowered, since the SEM images of TMAH development in Figure 3.50 showed only large swaths of polymerized resist. The resulting e-beam patterns are shown in Figure 3.51.

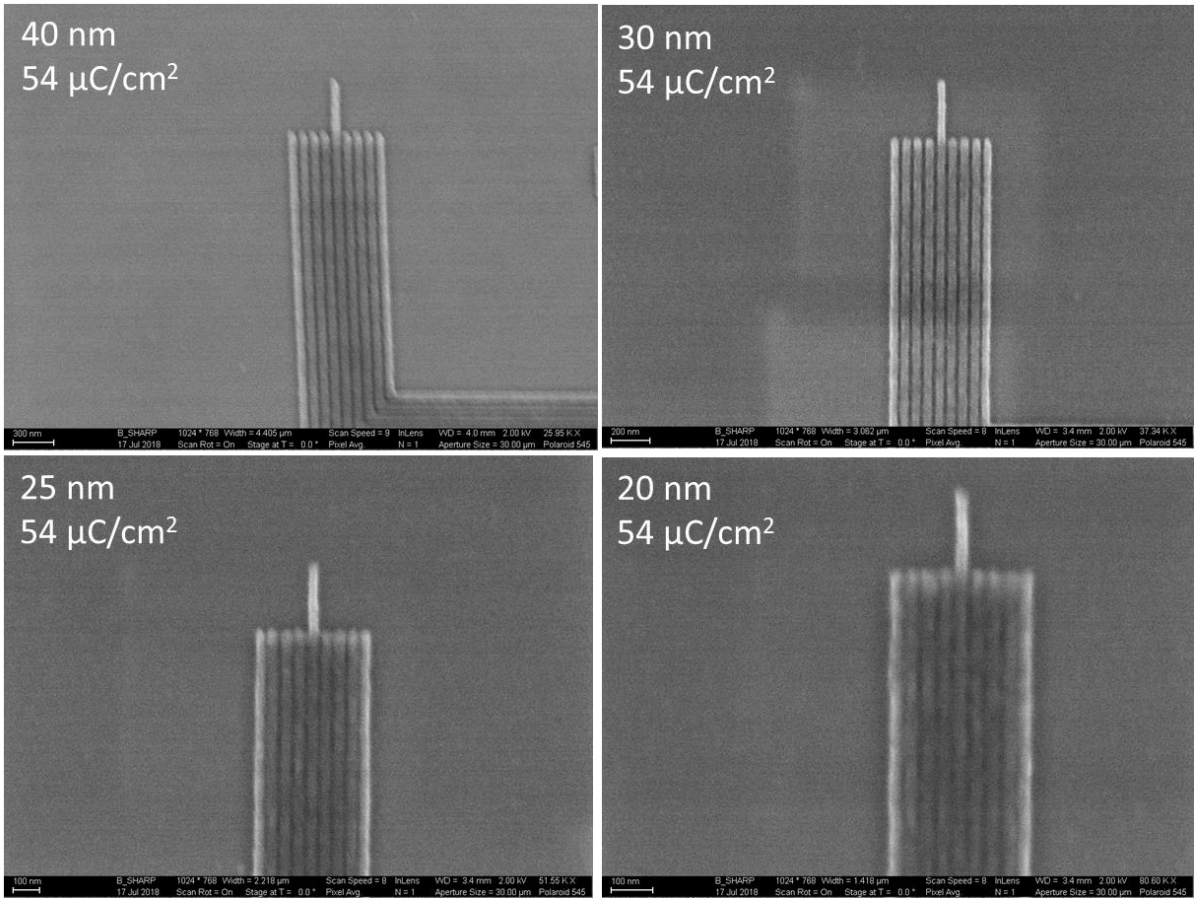

Figure 3.51 E-Beam pattern of THPE-2Ep, demonstrating the material can resolve 30nm patterns when developed in 0.26N TMAH.

The current resolution of this material at the doses and PEB temperature used appears to be approximately 30 nm, as shown in Figure 3.52, which is comparable to the previously-reported TPOE-3Ep, which achieved a resolution of 26 nm lines. The resist did not resolve lines below 30 nm at the conditions used in this study, as the material appears to blur and bridge significantly at sub-30nm features using these processing conditions.

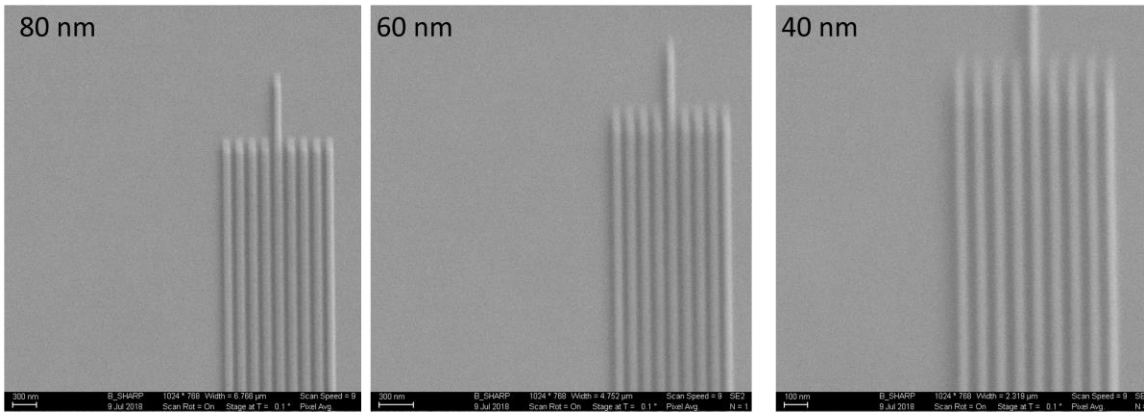

Figure 3.52 Lines resolved of THPE-2Ep from 80nm to 40nm at a dose of 56 μC/cm^2.

At a PEB of 50^{o}C, the material resolves much narrower lines that aren't blurred, as shown in Figure 3.53. However, as expected, the material requires slightly higher doses in order to resolve patterns. At this PEB, the minimum resolution appears to be 30 nm 1:1 (line:space) patterns, as shown in Figure 3.54.

63 µC/cm²

60°C PEB

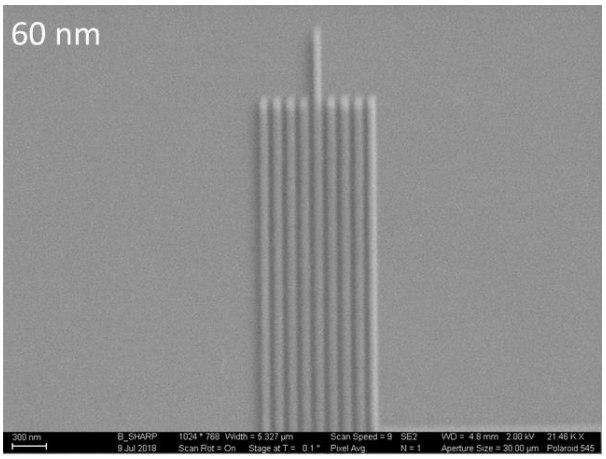

50°C PEB

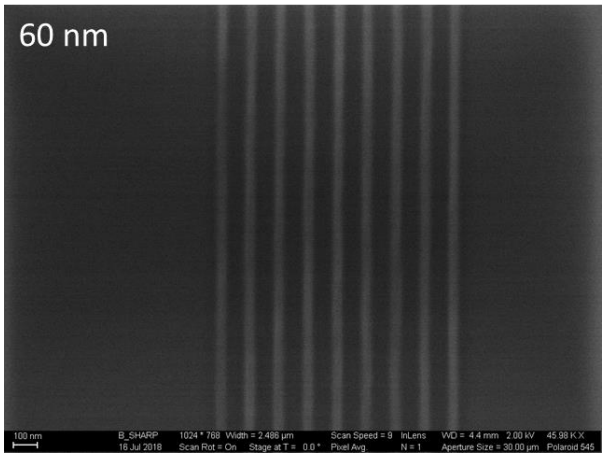

Figure 3.53 Comparison of 60 nm lines at a dose of 63 µC/cm^2.

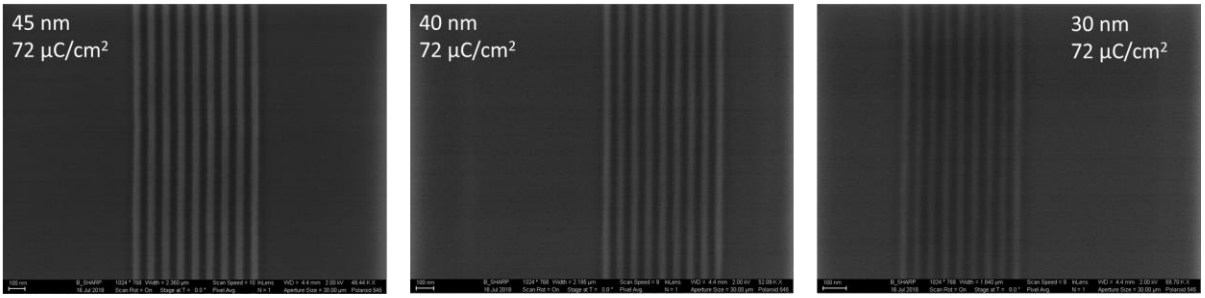

Figure 3.54 E-beam patterns of THPE-2Ep at a PEB of 50°C using a dose of 72 μC/cm^2.

3.5 Conclusion

This study has shed light on the various structural features that affect the crosslinking behavior of epoxide-based molecular resists by using 248nm DUV contrast curves. It has been shown that by increasing the number of phenols, the T_g of the resists is increased to a point that necessitates using very high PEB temperatures. This results in crosslinking in both exposed and unexposed regions. Methyl groups were introduced adjacent to the hydroxy groups in an attempt to reduce the T_g of these compounds, but only a slight reduction in T_g was observed, and the resulting TMPOE resists had a much lower NRT than the previous TPOE resists. By designing a molecule that has a low T_g, it is possible to achieve a high NRT at modest PEB temperatures. Such a molecule, called THPE-2Ep has been identified as a candidate for further e-beam evaluation studies. Presently, it can resolve roughly 30nm lines and spaces when developed in both MIBK and 0.26N TMAH. Future work will involve optimizing the processing conditions of this new resist to identify its resolution limit and develop other low-T_g base-soluble epoxide molecular resists.

3.6 References

1. Yang, D.; Chang, S. W.; Ober, C. K., Molecular glass photoresists for advanced lithography. *J Mater Chem* **2006,** *16* (18), 1693-1696.

2. Yeh, W. M.; Noga, D. E.; Lawson, R. A.; Tolbert, L. M.; Henderson, C. L., Comparison of positive tone versus negative tone resist pattern collapse bahavior*. *J Vac Sci Technol B* **2010,** *28* (6), C6s6-C6s11.

3. Dusek, K., Diffusion control in the kinetics of cross-linking. *Polym Gels Netw* **1996,** *4* (5-6), 383-404.

4. Lawson, R. A.; Lee, C. T.; Tolbert, L. M.; Younkin, T. R.; Henderson, C. L., High resolution negative tone molecular resist based on di-functional epoxide polymerization. *Microelectron Eng* **2009,** *86* (4-6), 734-737.

5. Lawson, R. A.; Lee, C. T.; Yueh, W.; Tolbert, L.; Henderson, C. L., Epoxide functionalized molecular resists for high resolution electron-beam lithography. *Microelectron Eng* **2008,** *85* (5-6), 959-962.

6. Lawson, R. A.; Noga, D. E.; Younkin, T. R.; Tolbert, L. M.; Henderson, C. L., Negative tone molecular resists using cationic polymerization: Comparison of epoxide and oxetane functional groups. *J Vac Sci Technol B* **2009,** *27* (6), 2998-3003.

7. Sharp, B.; Lawson, R. A.; Fralick, A.; Narcross, H.; Chun, J. S.; Neisser, M.; Tolbert, L. M.; Henderson, C. L., Base developable negative-tone molecular resist based on epoxide cross-linking. *Advances in Patterning Materials and Processes Xxxii* **2015,** *9425*.

8. Gutsche, C. D.; Bauer, L. J., Calixarenes .13. The Conformational Properties of Calix[4]Arenes, Calix[6]Arenes, Calix[8]Arenes, and Oxacalixarenes. *J Am Chem Soc* **1985,** *107* (21), 6052-6059.

9. Lawson, R., Molecular Resists for Advanced Lithography. **2011**.

10. Thakuria, R.; Sarma, B.; Nangia, A., Supramolecular networks of a H-shaped aromatic phenol host. *New J Chem* **2010,** *34* (4), 623-636.

11. Narcross, H.; Lawson, R. A.; Sharp, B.; Chun, J. S.; Neisser, M.; Tolbert, L. M.; Henderson, C. L., Effect of Molecular Resist Structure on Glass Transition Temperature and Lithographic Performance in Epoxide Functionalized Negative Tone Resists. *Advances in Patterning Materials and Processes Xxxii* **2015,** *9425*.

12. Kim, J. H.; Jang, J.; Zin, W. C., Thickness dependence of the glass transition temperature in thin polymer films. *Langmuir* **2001,** *17* (9), 2703-2710.

13. Inoue, R.; Nakamura, M.; Matsui, K.; Kanaya, T.; Nishida, K.; Hino, M., Distribution of glass transition temperature in multilayered poly(methyl methacrylate) thin film supported on a Si substrate as studied by neutron reflectivity. *Phys Rev E* **2013,** *88* (3).

14. Kwei, T. K., The Effect of Hydrogen-Bonding on the Glass-Transition Temperatures of Polymer Mixtures. *J Polym Sci Pol Lett* **1984,** *22* (6), 307-313.

15. Zhou, Q. H.; Li, M.; Yang, P.; Gu, Y., Effect of Hydrogen Bonds on Structures and Glass Transition Temperatures of MaleimideIsobutene Alternating Copolymers: Molecular Dynamics Simulation Study. *Macromol Theor Simul* **2013,** *22* (2), 107-114.

16. Griffiths, V. S.; Socrates, G., An Nmr Study of Hydrogen-Bonding in Substituted Phenols. *J Mol Spectrosc* **1966,** *21* (3), 302-+.

17. Kim, Y. S.; Kim, J. H.; Kim, J. S.; No, K. T., Prediction of glass transition temperature (T-g) of some compounds in organic electrolumineseent devices with their molecular properties. *J Chem Inf Comp Sci* **2002,** *42* (1), 75-81.

CHAPTER 4. POSITIVE-TONE CROSSLINKED MOLECULAR RESIST BASED ON ACID-CATALYZED DEPOLYMERIZATION

4.1 Introduction

One of the key driving forces towards obtaining a higher density of transistors on integrated circuits has been advancements in photolithography, through innovations in both the light sources and the photoresists used to generate useful relief patterns. Polymeric chemically-amplified resists (CARs) have traditionally filled the role of the photoresist in the lithography process, but as feature sizes decrease, issues such as photoacid diffusion into unexposed regions of the photoresist, line edge roughness (LER), and pattern collapse become increasingly problematic.

Molecular resists have been proposed to solve some of these challenges and offer several potential advantages when compared to polymeric resists. In contrast to polymers, which have an inherent molecular weight distribution, molecular resists are small molecules that can be made monodisperse such that every molecule in the resist composition has identical elemental composition and molecular weight through post-synthesis purification, which has been shown to lead to a reduction in LER.[1] Molecular glass resists have been shown to have a smaller photoacid diffusion length than similar polymeric materials, which can reduce blur caused by migration of photoacid into nominally unexposed regions of the resist.[2] The argument has also been made that molecular resists offer better mixing compatibility between the resist and any additives, such a photoacid generators (PAGs), which can further lead to a reduction in LER.[3]

A major resolution-limiting factor in sub-100nm lithography is pattern collapse caused by unbalanced capillary forces generated during post-development drying, which only becomes worse as the width between patterned features is decreased.[4] Several methods have been explored to combat this, including reactive rinses, supercritical CO_2 development, and surfactant-treated water, but each of these methods involves adding additional processing steps, equipment, or materials to an already costly process.[5,6] One method that has shown promise in preventing pattern collapse has been to crosslink resists to form insoluble networks to provide a negative-tone material, potentially eliminating the need for additional processing steps. These resists, based on acid-catalyzed homopolymerization, have been utilized by our group and have demonstrated the ability to withstand approximately twice the capillary force during post-development drying than a polymeric positive-tone resist through typical photoresist processing without any additional post-development processing.[7] The fundamental chemistry behind such negative tone crosslinked resists was studied in detail due to the early promising results of these materials, resulting in the development of several new resists that resolved sub-20 nm features.[8,9]

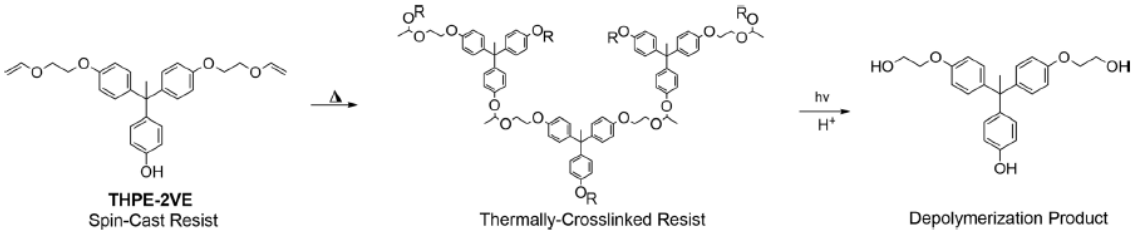

Figure 4.1 Structure and proposed imaging mechanism of THPE-2VE, illustrating the reactions required to first insolubilize the molecule and then catalytically render it soluble after exposure.

As lithographic processes continue to push the limit of modern imaging tools, the need for having access to both positive and negative tone resist materials has grown significantly. Given the promising imaging and pattern collapse results obtained for the crosslinked negative-tone materials, our group sought to incorporate a crosslinking scheme into a positive-tone resist design. Such a design requires two separate solubility-switching reactions to occur: (1) a first reaction must transform the initially solvent-soluble resist insoluble through crosslinking, and (2) a second reaction must induce solubility only in exposed regions to give the material positive-tone imaging behavior. In the resists discussed in this paper, the insolubilization reaction is accomplished through a PAB-induced thermal crosslinking reaction between vinyl ethers and either a phenol or a carboxylic acid, depending on the specific molecule used, as shown in Figure 4.1 for THPE-2VE. This reaction generates acetals in the final network, which are sensitive to cleavage by the photo-generated acids typically used in chemically amplified resists. These acetals are cleaved by a catalytic amount of photoacid to generate phenols and aliphatic alcohols in the exposed portion of the resist, thus rendering those exposed

regions soluble in developers.[10] This design scheme takes advantage of the benefits of both crosslinked resists, which provide a mechanically-robust material, and the low activation energy of acetals, which result in a highly sensitive material.[11,12] Our initial attempts on this front involved blending two different molecules together to form an insoluble network, but this approach suffered from a variety of shortcomings and was abandoned.[13] The next design incorporated thermally crosslinkable groups on the same resist core, and the molecule DPA-2VE (shown in Figure 4.2) was synthesized, which managed to resolve sub-40nm features, but suffered from significant dark loss and poor contrast.[14]

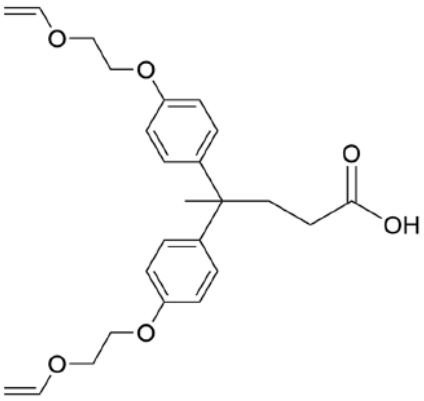

Figure 4.2 Structure of previously-reported resist, DPA-2VE.

To improve upon this design, a new, phenol-containing resist was designed because literature reports show that phenol-containing resists have a larger shift in E_1 away from zero dose when developed in aqueous alkaline developer, potentially reducing concerns from flare.[10] Other results have shown that switching from a carboxylic acid to a phenol resulted in increased shelf stability in depolymerization resists.[15] Although not

observed at the feature sizes resolved with DPA- 2VE, using a phenol may also help reduce concerns from swelling during development as smaller feature sizes are pursued with these materials.[16] THPE-2VE, shown in Figure 4.1, was designed to use a phenol while maintaining a 2:1 ratio of vinyl ethers to phenol in order to make a more direct comparison between DPA-2VE to determine the effect of switching from a carboxylic acid to a phenol. In this paper, we report on processing variables that affect the performance of THPE-2VE, including the deep ultraviolet (DUV) sensitivity and contrast as well as the 100 keV e-beam lithographic line:space patterns obtained using this material.

4.2 Synthesis

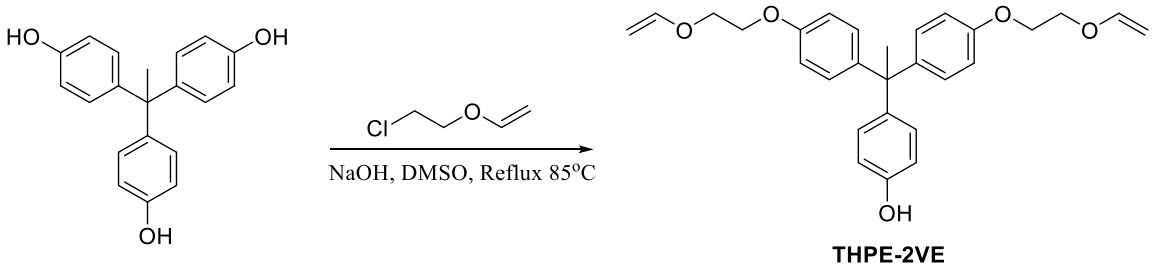

Figure 4.3 Synthesis of THPE-2VE.

1,1,1-tris(4-hydroxyphenyl) ethane (THPE), and 2-chloroethyl vinyl ether (CEVE) were ordered from TCI America and used as received. All other reagents and casting solvents were ordered from Sigma-Aldrich and used as received. THPE-2VE was synthesized via the reaction between THPE and CEVE in the presence of potassium hydroxide (KOH) in dimethyl sulfoxide (DMSO). 2 grams of THPE (1 equivalent) and 0.78g NaOH (6 eq.)

were added to 30 mL DMSO and stirred in a 100-mL round-bottom flask in an oil bath at 80^{o}C for 30 minutes. Afterwards, 1.04g of 2-chloroethyl vinyl ether (2 eq.) was added dropwise to the mixture, which was then stirred at 80 ^{o}C for 5 hours. After 5 hours, the solution was cooled to room temperature and washed once with deionized water and extracted with ethyl acetate. The organic layer was washed twice more with deionized water before filtering and drying over magnesium sulfate. Solvents were evaporated via rotary evaporator, and the resulting crude product was purified via silica gel column chromatography using ethyl acetate and hexanes (2:5) to isolate THPE-2VE as a colorless oil. ^{1}H NMR (300 MHz, CDCl3, δ): 7.00 ppm (d,4H), 6.93 ppm (d,2H), 6.82 ppm (d,4H), 6.73 ppm (d,2H), 6.54 ppm (q,2H), 5.67 ppm (s,1H), 4.12 ppm (m,12H), 2.10 ppm (s,3H). MS (EI) m/z: [M]+: 431.52. Calculated (HR MS (EI): 446.2093. Found: 446.2089. Anal. Calcd for $C_{28}H_{30}O_5$: C, 75.31; H, 6.77. Found: C, 73.62; H, 7.35. Yield: 0.63g.

4.3 Lithographic Evaluation

To create resist solutions for both DUV and e-beam lithographic evaluation, 3 wt% solutions (with respect to total solids) of THPE-2VE in cyclohexanone were formulated with 5 mol% (relative to moles of THPE-2VE) TPS-SbF_6 and filtered through a 0.2 μm Teflon membrane filter. Films of approximately 50 nm thickness were spin cast using a speed of 2000 rpm onto unprimed silicon wafers ordered from University Wafer. For the post-apply bake (PAB) study, approximately 50 nm films of THPE-2VE were spin cast from a 3 wt% solution in cyclohexanone with 5 mol% triphenyl sulfonium hexafluoroantimonate (TPS-SbF_6, Midori Kagaku, Ltd.) and baked for 10 minutes in ambient atmosphere at various temperatures to crosslink films. An

initial film thickness was measured after the 10-minute bake using ellipsometry, and then development in either aqueous 0.26 N tetra methyl ammonium hydroxide (TMAH) or methyl isobutyl ketone (MIBK) was performed and the thickness was measured again to obtain normalized remaining thickness (NRT) values, which is the ratio of the film thickness measured after development to the film thickness measured after the PAB. The procedure for the PAG loading study was very similar, with only the PAG mol% changing from 3 mol% to 5 mol% (with respect to moles of THPE-2VE). Comparison of choice of PAG between TPS-SbF_6 to TPS-Tf also followed a similar procedure, with 5 mol% of either TPS-SbF_6 or TPS-Tf added. Aside from these noted changes, all other processing variables were consistent with what was performed for all other DUV lithographic experiments.

Films were crosslinked at 200 ^{o}C and then exposed to either 100 keV e-beam or 248 nm DUV radiation, followed by a post-exposure bake (PEB) at 90 ^{o}C for 60 seconds in ambient atmosphere. The films were then developed in either MIBK for 30 seconds, followed by an isopropyl alcohol (IPA) rinse, or 0.26 N aqueous TMAH solution for 30 seconds, followed by a deionized water rinse. DUV contrast curves were obtained by exposing resist films with an Oriel Instruments 500W Hg-Xe arc lamp with a 248 nm bandpass filter, followed by solvent development, and then film thickness measurements using a J.A. Woolam M-2000 Ellipsometer. E-beam lithography evaluation was performed using a JEOL JBX-9300FS electron-beam lithography system with a 100-keV acceleration voltage and a 100-pA current. Resulting e-beam patterns were imaged using a Carl Zeiss Ultra 60 SEM with 2 keV acceleration voltage. E-beam contrast

curves were obtained by exposing crosslinked resist films to 100 keV e-beam radiation, followed by solvent development and then film thickness measurements were obtained using a Tencor P15 profilometer.

4.4 Results and Discussion

4.4.1 Contrast Curves

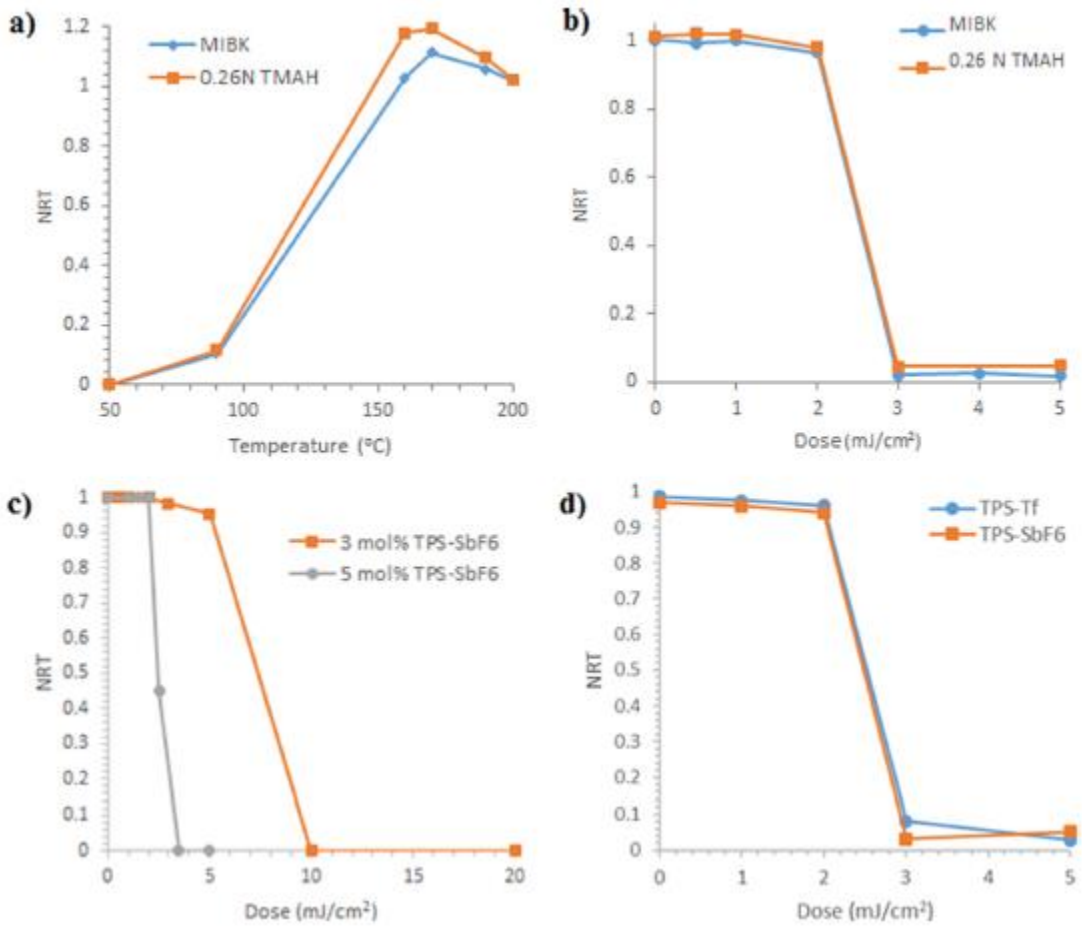

Figure 4.4 (a) PAB study of THPE-2VE, (b) 248 nm DUV contrast curve comparing organic solvent and aqueous base TMAH development, (c) PAG loading study for 0.26N

TMAH development, and (d) a comparison of two different PAGs in 0.26N TMAH development.

THPE-2VE was designed to have a 2:1 ratio of vinyl ethers to phenols in order to directly compare its performance to DPA-2VE and to investigate if using a phenol is a viable alternative to using a carboxylic acid. The material was first subjected to a post-apply bake (PAB) study to determine at what temperature the material should be crosslinked at, as shown in Figure 4.4a. The material largely shows similar normalized remaining thickness (NRT) values for each developer at the same temperature. At a PAB of 90^{o}C, the material begins to become insoluble, and then increases to an NRT >1 presumably due to swelling at a temperature of 170^{o}C because at this temperature, there is likely only a loosely-crosslinked network formed, which imbibes developer solution. The NRT value returns to 1 at a PAB temperature of 200^{o}C, and so this temperature was chosen as the standard PAB temperature.

The DUV contrast curve in Figure 4.4b, which plots the NRT vs. dose, shows that THPE-2VE has an increase in contrast ratio (7.2) as well as a much lower dose-to-clear of 3 mJ/cm^2, compared to a contrast ratio of 5.2 and a DUV dose-to-clear of 7 mJ/cm^2 for DPA-2VE.[14] THPE-2VE is more than twice as sensitive to DUV exposure than DPA-2VE, which was surprising because reported carboxylic-acid containing resists have a lower dose-to-clear than their phenolic counterparts.[10] This increase in sensitivity could arise from the different processing conditions used for the two resists. DPA-2VE was evaluated using a PAB of 160 ^{o}C due to concerns from thermal degradation at higher temperatures, while THPE-2VE was processed using a PAB of 200 ^{o}C, so it

makes a direct comparison between the two materials somewhat difficult. Carboxylic acid-containing resists have been shown to have a higher crosslinking rate than phenol-containing polymers, so even at a lower PAB, the DPA-2VE could have formed a more densely-crosslinked network versus THPE-2VE.[10] The more densely-crosslinked network would reduce the mobility of the photoacid, thus requiring slightly higher doses in order to generate enough photoacid to cleave the network to render it soluble in developer at equivalent PEB conditions.

Interestingly, the contrast curves between the two development conditions in Figure 4.4b are almost identical, which differs from our epoxy-based negative-tone resists, which show marked differences between 0.26 N TMAH and MIBK development curves.[8] In those materials, the two development conditions differed because the solubility transition for the two solvents occurred at different doses due to the different requirements to insolubilize the material. For any material to be rendered soluble in either developer in the current material, it needs to completely detach from the network. Due to the nature of the depolymerization chemistries, one phenol and one aliphatic alcohol are unmasked for each acid-catalyzed acetal cleavage, resulting in highly polar fragments (depolymerization product shown in Figure 4.1) that are soluble in 0.26 N TMAH developer.

Figure 4.4c shows that increasing the PAG loading from 3 mol% to 5 mol% results in a lower dose-to-clear while maintaining a shift in E_1 away from zero dose in 0.26 N TMAH developer. Due to the high PAB temperature used for this material, the PAG TPS-SbF_6 was used, which shows excellent thermal stability at elevated temperatures.

The DUV contrast curve in Figure 4.4d shows that the PAG triphenyl sulfonium triflate (TPS-Tf), which was used for DPA-2VE, shows nearly-identical performance to TPS-SbF_6 at 5 mol% loading with THPE-2VE when developed in TMAH.

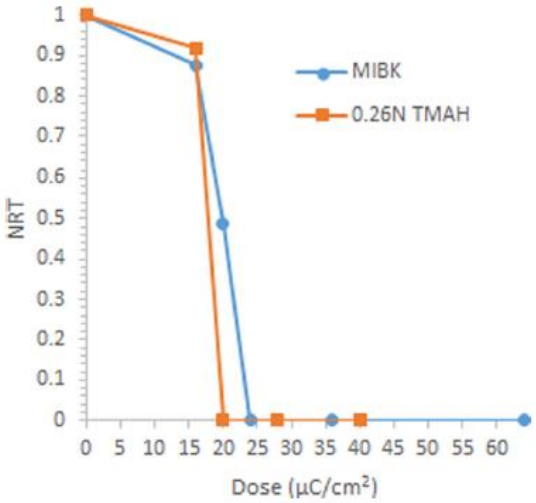

Figure 4.5 One hundred kilo-electron volt e-beam contrast curve of THPE-2VE, developed in MIBK and 0.26N TMAH.

The 100 keV e-beam contrast curve of THPE-2VE (**Figure 4.5**) shows similar sensitivity in both 0.26 N TMAH with a dose-to-clear (E_0) of 20 μC/cm^2 and an E_0 of 24 μC/cm^2 in MIBK development. Development in 0.26 N TMAH appears to result in a slightly more sensitive material, with an E_0 of 20 μC/cm^2. At this dose, MIBK development still shows an NRT of approximately 0.5, so a crosslinked network is still present, but this network is likely heavily fragmented, with a reduced crosslink density, which could result in swelling in 0.26 N TMAH developer, leading to swelling-induced delamination.[17] If delamination is occurring, this could result in

the NRT difference observed for TMAH and MIBK development at a dose of 20 μC/cm^2.

4.4.2 E-beam lithographic patterns

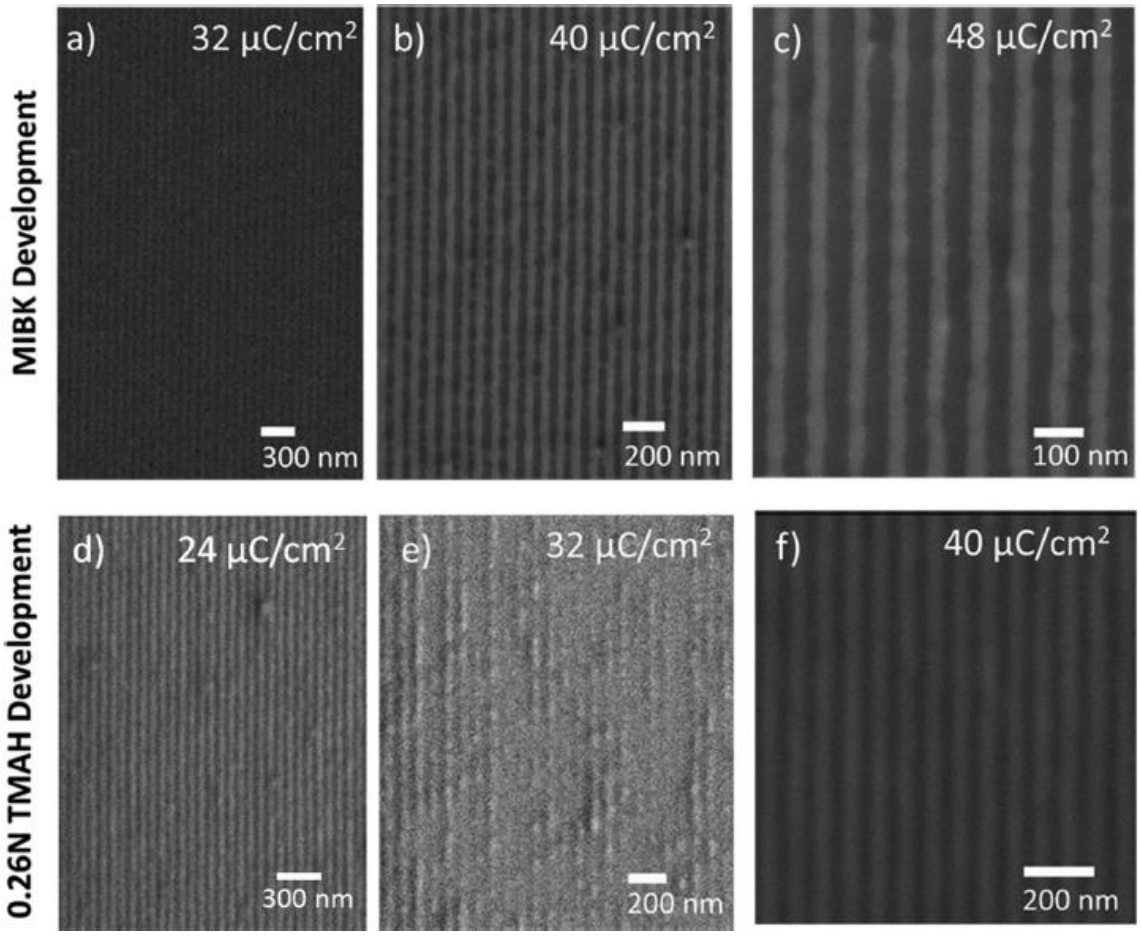

Figure 4.6 100 keV e-beam images of THPE-2VE comparing development in MIBK (a)–(c) and 0.26N TMAH (d)–(f) at various exposure doses, formulated with 5 mol. % TPS-SbF_6.

In MIBK development (**Figure 4.6**a-c), THPE-2VE suffers from bridging at e-beam doses of 32 μC/cm^2 and 40 μC/cm^2, but manages to resolve isolated lines at a dose

of 48 μC/cm^2, with a calculated 3σ LER value of 8.4 nm, and a minimum feature size of approximately 35 nm. This LER value is somewhat high compared to other molecular resists reported in the literature.[18] There are several side reactions that can compete with the acetal cleavage responsible for depolymerization that may be responsible for this poor LER. Due to excess vinyl ethers on THPE-2VE compared to phenols, one possible side reaction is the acid-catalyzed homopolymerization of vinyl ethers, which would result in insoluble material being formed.[19] It is possible that as the dose is increased, more acid is available to catalyze this undesired reaction, which results in a poor line edge profile. A study that probes the effect of these side reactions on patterning performance of these materials will be discussed in the next chapter.

Development of THPE-2VE in 0.26 N TMAH (**Figure 4.6**d-f) showed a slightly lower dose to pattern observable features compared to MIBK development, which is in agreement with the e-beam contrast curve. At lower doses, such as the 24 μC/cm^2 shown in **Figure 4.6**d, patterned lines do not appear to be fully formed. Increasing the dose to 32 μC/cm^2 does not appear to improve performance, possibly because of the delamination concerns raised earlier with the e-beam contrast curve. Increasing the dose to 40 μC/cm^2 allows the material to resolve sub-40nm features with a calculated LER value of 8.2 nm, which is somewhat lower than MIBK development. Despite the high LER values reported here, there is no evidence of pattern collapse at any of the feature sizes probed thus far in either developer, which is a promising early result as the processing conditions are optimized to determine the ultimate resolution limit of this material. To the best of our knowledge, these

lines are some of the smallest features ever resolved using acetal-containing depolymerization resists.[12,20,21]

4.4.3 Time-dependent properties of resist solutions

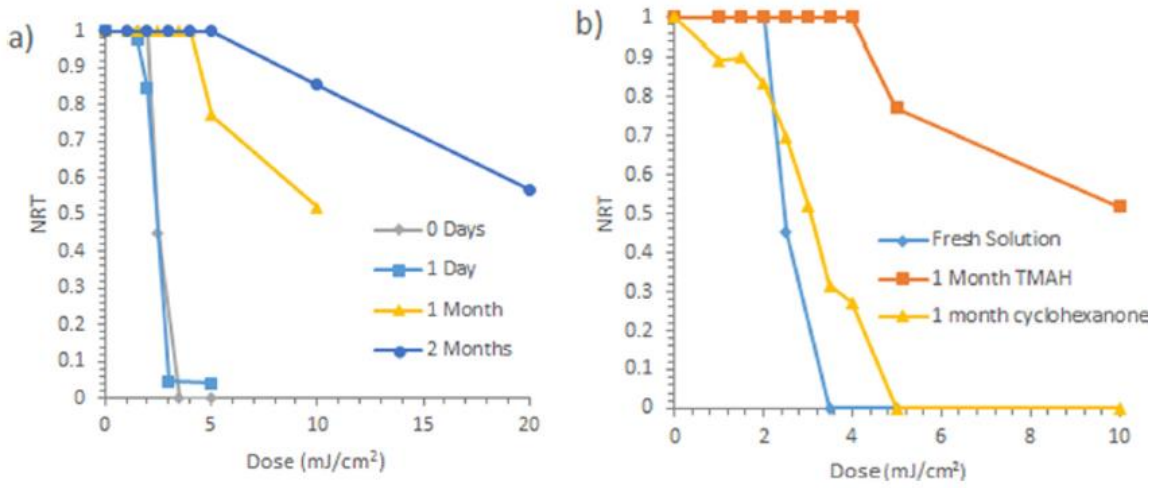

Figure 4.7 (a) DUV contrast curves for 0.26N TMAH development for the same nominal THPE-2VE (3 wt. % solids in cyclohexanone, 5 mol. % TPS-SbF6) solution after different periods of storage. (b) DUV contrast curve comparing development in an organic solvent to development in 0.26N TMAH.

In Figure 4.7a, THPE-2VE shows slightly improved shelf stability and is stable up to one day after solution creation, which is an improvement upon DPA-2VE, which began to show inconsistent contrast curves after 1 hour solution aging.[14] Similar improvements have been reported by the Willson group when switching from a carboxylic acid to a phenol-based design in similar materials, which suggests that the acidic functional group of the resist participates in the reactions responsible for the

limited shelf life.[15] Even with the improvement, THPE-2VE still appears prone to a dark reaction that slowly degrades its patterning performance over time.

To gain some insight into how this dark reaction affects development, a comparison was made between organic solvent and TMAH development, and the results are shown in Figure 4.7b. In this study, a distinct difference was shown between the two development methods, with TMAH showing severely degraded patterning behavior, while development in organic solvent looks comparatively similar to the original curve at 0 days solution age. While the mechanism responsible for this issue is currently unknown, it does appear that phenols are being consumed in the resist solution at some point prior to lithographic processing, since the presence of a phenol is a requirement for the resist to be soluble in 0.26 N TMAH. A potential reaction that could explain this behavior involves oxidation of vinyl ethers via atmospheric oxygen in solution, which would produce radicals that can potentially consume phenols, which are known to act as radical scavengers.[22,23] Assuming radicals are involved, phenols are reported to be better radical scavengers than carboxylic acids, which may be why the THPE-2VE shows a slightly extended shelf life compared to DPA-2VE.[24]

4.5 Summary and conclusions

A phenol-containing molecular resist based on acid-catalyzed depolymerization has been synthesized and patterned using 100 keV e-beam lithography. The first molecule in this family, THPE-2VE, was designed in order to

provide a direct comparison between a previous resist in order to examine the effect of changing the carboxylic acid to a phenol.

The initial DUV experiments shed light on the variables that affect the performance of this resist, including PAB temperature, choice of development solvent, PAG loading, and PAG type. The optimal PAB temperature was deemed to be 200 ^{o}C since this was the lowest temperature where no swelling was observed in either development solvent. PAG loading showed that increasing the percentage of TPS-SbF_6 from 3 to 5 mol% resulted in increased sensitivity while maintaining a shift in E_1 away from zero dose. Neither the choice of development solvents nor PAGs used here appears to markedly affect the DUV sensitivity or contrast of this material.

THPE-2VE showed both an increase in sensitivity and contrast compared to DPA-2VE, and initial 35 nm features were obtained using 100 keV e-beam lithography, showing a dose-to-size of 48 μC/cm^2 in MIBK development and 40 μC/cm^2 in 0.26 N TMAH development for 35 nm lines. An improvement in shelf life was observed upon switching to a phenol in the THPE-2VE design, though the material still showed gradual loss of sensitivity over time. Although 3σ LER values were high for THPE-2VE, the excellent resolution (with one of the smallest features ever reported for similar materials) and sensitivity make it an attractive candidate for future optimization towards smaller features. The results presented here lay the foundation for future studies that will probe the fundamental patterning performance of this family of materials.

4.6 References

1. Shiono, D.; Hada, H.; Yukawa, H.; Oizumi, H.; Nishiyama, I.; Kojima, K.; Fukuda, H., LER evaluation of molecular resist for EUV lithography. *Microelectron Eng* **2007,** *84* (5-8), 1084-1087.

2. Kang, S. H.; Wu, W. L.; Choi, K. W.; De Silva, A.; Ober, C. K.; Prabhu, V. M., Characterization of the Photoacid Diffusion Length and Reaction Kinetics in EUV Photoresists with IR Spectroscopy. *Macromolecules* **2010,** *43* (9), 4275-4286.

3. VanderHart, D. L.; Prabhu, V. M.; De Silva, A.; Felix, N. M.; Ober, C. K., Solid state NMR investigation of photoresist molecular glasses including blend behavior with a photoacid generator. *J Mater Chem* **2009,** *19* (18), 2683-2694.

4. Noga, D. E.; Lawson, R. A.; Lee, C. T.; Tolbert, L. M.; Henderson, C. L., Understanding Pattern Collapse in High-Resolution Lithography: Impact of Feature Width on Critical Stress. *Proc Spie* **2009,** *7273*.

5. Noga, D. E.; Yeh, W. M.; Lawson, R. A.; Tolbert, L. M.; Henderson, C. L., Methods to Explore and Prevent Pattern Collapse in Thin Film Lithography. *Advances in Resist Materials and Processing Technology Xxvii, Pts 1 and 2* **2010,** *7639*.

6. Sundararajan, N.; Yang, S.; Ogino, K.; Valiyaveettil, S.; Wang, J. G.; Zhou, X. Y.; Ober, C. K.; Obendorf, S. K.; Allen, R. D., Supercritical CO2 processing for submicron imaging of fluouropolymers. *Chem Mater* **2000,** *12* (1), 41-48.

7. Yeh, W. M.; Noga, D. E.; Lawson, R. A.; Tolbert, L. M.; Henderson, C. L., Comparison of positive tone versus negative tone resist pattern collapse bahavior*. *J Vac Sci Technol B* **2010,** *28* (6), C6s6-C6s11.

8. Sharp, B.; Lawson, R. A.; Fralick, A.; Narcross, H.; Chun, J. S.; Neisser, M.; Tolbert, L. M.; Henderson, C. L., Base developable negative-tone molecular resist based on epoxide cross-linking. *Advances in Patterning Materials and Processes Xxxii* **2015,** *9425*.

9. Lawson, R. A.; Narcross, H.; Sharp, B.; Chun, J. S.; Neisser, M.; Tolbert, L. M.; Henderson, C. L., Optimizing performance in cross-linking negative-tone molecular resists. *Advances in Patterning Materials and Processes Xxxii* **2015,** *9425*.

10. Moon, S.; Yamaoka, T., 3-Component Photopolymers Based on Thermal Cross-Linking and Acidolytic De-Cross-Linking of Vinyl Ether Groups .2. Effects of Acid Components on Photopolymer Characteristics. *Polym Advan Technol* **1995,** *6* (8), 566-572.

11. M. Bowden, S. M., Ferreira, *J Photopolym Sci Tec 13*.

12. Felix, N.; Ober, C. K., Acid-labile, chain-scission polymer systems used as positive-tone photoresists developable in supercritical CO2. *Chem Mater* **2008,** *20* (9), 2932-2936.

13. Lawson, R. A.; Noga, D. E.; Cheng, J.; Tolbert, L. M.; Henderson, C. L., Non-Traditional Resist Designs Using Molecular Resists: Positive Tone Cross-linked and Non-Chemically Amplified Molecular Resists. *Advances in Resist Materials and Processing Technology Xxvii, Pts 1 and 2* **2010,** *7639*.

14. Lawson, R. A.; Cheng, J.; Cheshmehkani, A.; Tolbert, L. M.; Henderson, C. L., Positive Tone Resists Based On Network Depolymerization of Molecular Resists. *Advances in Resist Materials and Processing Technology Xxx* **2013,** *8682*.

15. Yamada, S.; Medeiros, D. R.; Patterson, K.; Jen, W. L. K.; Rager, T.; Lin, Q. H.; Lenci, C.; Byers, J. D.; Havard, J. M.; Pasini, D.; Frechet, J. M. J.; Willson, C. G., Positive and negative tone water processable photoresists: A progress report. *Advances in Resist Technology and Processing Xv, Pts 1 and 2* **1998,** *3333*, 245-253.

16. Ito, H., Rise of chemical amplification resists from laboratory curiosity to paradigm enabling Moore's law - art. no. 692302. *Advances in Resist Materials and Processing Technology Xxv, Pts 1 and 2* **2008,** *6923*, 92302-92302.

17. Velankar, S. S.; Lai, V.; Vaia, R. A., Swelling-Induced Delamination Causes Folding of Surface-Tethered Polymer Gels. *Acs Appl Mater Inter* **2012,** *4* (1), 24-29.

18. Lawson, R. A.; Lee, C. T.; Tolbert, L. M.; Younkin, T. R.; Henderson, C. L., High resolution negative tone molecular resist based on di-functional epoxide polymerization. *Microelectron Eng* **2009,** *86* (4-6), 734-737.

19. Moon, S. G.; Naitoh, K.; Yamaoka, T., Novel Dual-Mode Photoresist Based on Cationic Polymerization and Acidolysis. *Chem Mater* **1993,** *5* (9), 1315-1320.

20. Kasai, T.; Higashihara, T.; Ueda, M., Synthesis of Calixresorcinarene Derivatives with Cross-linking units and Evaluation of Lithographic Performance. *J Photopolym Sci Tec* **2011,** *24* (6), 631-635.

21. Manouras, T.; Olziersky, A.; Argitis, P., New resist materials based on polyacetal main chain scission. *Advances in Patterning Materials and Processes Xxxiii* **2016,** *9779*.

22. Peirone, S. A.; Abrate, J. P. A.; Taccone, R. A.; Cometto, P. M.; Lane, S. I., Kinetic study of the OH-initiated photo-oxidation of four unsaturated (allyl and vinyl) ethers under simulated atmospheric conditions. *Atmos Environ* **2011,** *45* (30), 5325-5331.

23. Zhou, S. M.; Barnes, I.; Zhu, T.; Bejan, I.; Benter, T., Kinetic study of the gas-phase reactions of OH and NO3 radicals and O-3 with selected vinyl ethers. *J Phys Chem A* **2006,** *110* (23), 7386-7392.

24. Cai, Y. Z.; Sun, M.; Xing, J.; Luo, Q.; Corke, H., Structure-radical scavenging activity relationships of phenolic compounds from traditional Chinese medicinal plants. *Life Sci* **2006,** *78* (25), 2872-2888.

CHAPTER 5. STRUCTURAL EFFECTS ON THE PATTERNING PERFORMANCE OF CROSSLINKED DEPOLYMERIZATION MOLECULAR RESISTS

5.1 Introduction

In order to accommodate more transistors on integrated circuits, the size of the transistors must continually decrease, and this has traditionally been achieved through advancements in photolithographic materials and processes. In this process, a photoresist is used to generate a relief image which is then transferred to the underlying substrate through etching, and this litho-etch process is then repeated until the desired features are built. Historically, the development of new light sources for photolithography brought with it the need for new photoresist designs to meet the requirements for new processes. Polyphenolic chemically-amplified resists have been the dominant form of photoresists for many years in the semiconductor industry, but as feature sizes of transistors continue decrease well below 50nm, issues with these photoresists, such as photoacid diffusion into unexposed regions, line edge roughness (LER), and pattern collapse have become worse. New materials are needed to meet these increasing performance demands, and molecular resists have been proposed as a candidate to potentially overcome some of these resolution-limiting factors. Polymeric resists have a molecular weight distribution, so precise compositional control is difficult to achieve because very complex, and expensive synthetic methods are often employed to produce low-polydispersity materials. In contrast, molecular resists can be made truly monodisperse, which can eliminate batch-to-batch

variations, offering precise control over the molecular composition of resists. Compared to traditional polymeric resists, molecular resists have been shown to have a smaller acid diffusion length than similar polymeric materials, which can help reduce photoacid blur and offer potentially better mixing additives such as photoacid generators (PAGs).[1]

Pattern collapse in sub-100nm features is a major resolution-limiting issue, and so our group has pursued negative-tone crosslinked resists that have been demonstrated to withstand approximately twice the capillary forces compared to a polymeric, positive-tone, non-crosslinked resist before collapsing.[2] Encouraged by early results with these materials, the fundamental chemistry behind the class of molecules was studied, resulting in the development of several new materials that, through formulation and processing optimization, were capable of resolving sub-20nm features under extreme ultraviolet (EUV) exposure.[3,4]

Certain lithographic features produce better results depending on development tone, so it's important to have both positive and negative tone photoresists.[5,6] This led our group to pursue a positive-tone crosslinked molecular resist that could leverage the benefits of both crosslinked resists and highly-sensitive acetals throughout the network, which result in a highly sensitive material.[7,8] Both carboxylic acid and phenol-based designs of these materials were developed, and each demonstrated sub-50nm resolution and excellent sensitivity in both 248nm DUV and 100 keV e-beam exposures.[9] The phenol-containing design, THPE-2VE, showed improved contrast and shelf life compared to the carboxylic acid design and was capable of resolving sub-40nm lines using 100 keV e-beam patterning

with a dose-to-size (E_{size}) of 40 μC/cm^2 in 0.26N TMAH developer and 48 μC/cm^2 in organic solvent development.[10]

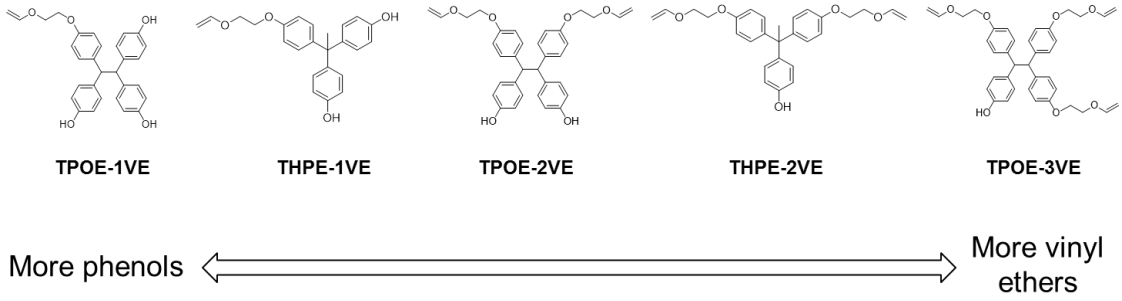

Figure 5.1 Structures of the resists used in this study, where the number of vinyl ethers attached to the phenolic core is varied.

The presence of vinyl ethers in these resists can result in various side reactions beyond the phenol/vinyl ether crosslinking and the acid-catalyzed acetal cleavage reactions that are responsible for the imaging chemistry of these resists.[11,12] In order for the depolymerization resists to provide good contrast and produce high-resolution features, an understanding of these side reactions and their effects on patterning performance is critical. Several molecules, whose structures are shown in Figure 5.1, were synthesized to have different ratios of phenols and vinyl ethers on their core. By systematically varying this ratio, we can investigate the effects that the relative content of the two functional groups have on the patterning performance of these materials, enabling optimization of future designs and formulations. 248nm DUV curves are used to quickly and cheaply study the effect of various formulation and processing variables to optimize the performance of the resists before obtaining high-resolution e-beam patterns. Here, we report the 248nm DUV contrast

curves and the 100keV e-beam patterns and discuss the impact of structural variations on the patterning performance of these materials.

5.2 Experimental

5.2.1 Synthesis

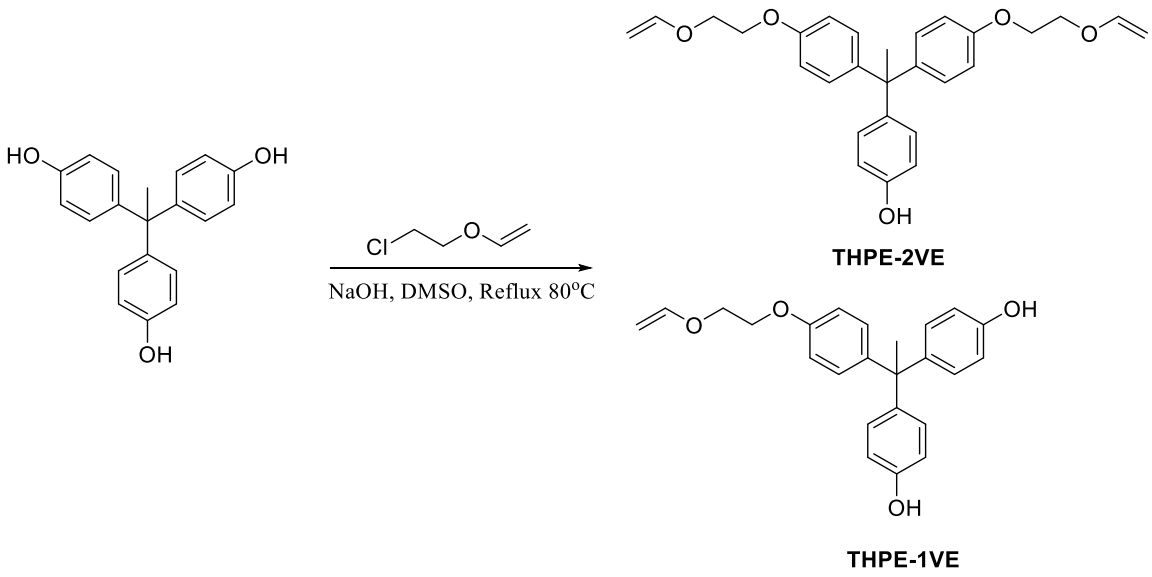

Figure 5.2 Synthesis of THPE-2VE and THPE-1VE. Products are isolated from a one-pot reaction via silica gel chromatography.

Reagents were ordered from TCI America and Sigma Aldrich, unless otherwise noted. The single-batch reaction between 5 grams of 1,1,1-tris(4-hydroxyphenyl) ethane (THPE) and 2-chloroethyl vinyl ether (VE) in the presence of potassium hydroxide (KOH) in dimethyl sulfoxide (DMSO) was used to synthesize both THPE-2VE and THPE-1VE. THPE (1 molar equivalent) and KOH (6 eq.) were added to 30 mL DMSO and stirred in a 100-mL round-bottom flask in an oil bath at 80°C for 30 minutes. Afterwards, 2-

chloroethyl vinyl ether (2 eq.) was added dropwise to the mixture, which was then stirred at 80°C for 5 hours. After 5 hours, the solution was cooled to room temperature and washed once with deionized water and extracted with ethyl acetate. The organic layer was washed twice more with deionized water before filtering and drying over magnesium sulfate ($MgSO_4$). Solvents were evaporated via rotary evaporator, and the resulting crude product was purified via silica gel column chromatography using ethyl acetate and hexanes (2:5) to isolate THPE-2VE and THPE-1VE. ^{1}H NMR (300 MHz, CDCl3, δ): THPE-2VE: 7.00 ppm (d,4H), 6.93 ppm (d,2H), 6.82 ppm (d,4H), 6.73 ppm (d,2H), 6.54 ppm (q,2H), 5.67 ppm (s,1H), 4.12 ppm (m,12H), 2.10 ppm (s,3H); Yield: 43% THPE-1VE: 7.00 ppm (d,2H), 6.93 ppm (d,4H), 6.82 ppm (d,2H), 6.73 ppm (d,4H), 6.55 ppm (q,1H), 5.18 ppm (s,2H), 4.12 ppm (m,6H), 2.12 ppm (s,3H); Anal. Calcd for $C_{24}H_{24}O_4$: C, 66.36; H, 7.28. Found: C, 72.34; H, 6.97; Yield: 37%.

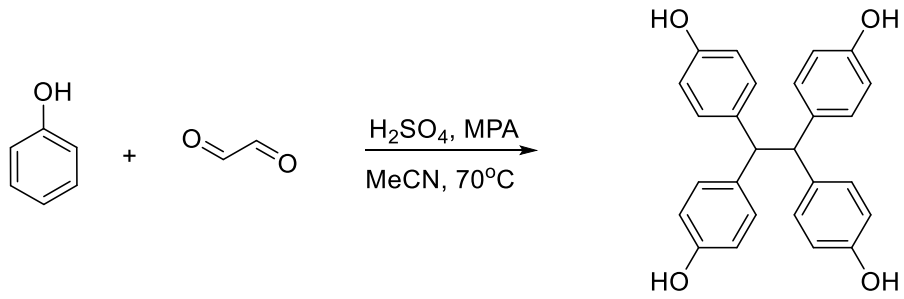

Figure 5.3 Synthesis of TPOE.

TPOE: 1,1,2,2-tetrakis(p-hydroxyphenyl)ethane (TPOE) was synthesized via the acid-catalyzed reaction between phenol and glyoxal, where 4 molar equivalents of phenol (60 g), 1 eq glyoxal (40% solution in water), and 0.05 eq. 2-mercaptopriopionic acid were added to acetonitrile with stirring. Concentrated sulfuric acid was added dropwise to the

solution. After addition, the flask was placed in an oil bath at 70°C and stirred for 48 hours, during which time the solution turned a dark brown. After 48 hours, the solution was cooled to room temperature and precipitated into acetone. A solid formed, which was vacuum filtered and washed with water and acetone to produce a white solid. ^{1}H NMR (300MHz, methanol-d4, δ): 6.99 ppm (d,8H), 6.65 ppm (d, 8H), 4.55 ppm (s, 2H). Anal. Calcd for $C_{26}H_{22}O_4$: C, 78.37; H, 5.57. Found: C, 73.89; H, 6.30. Yield: 57%.

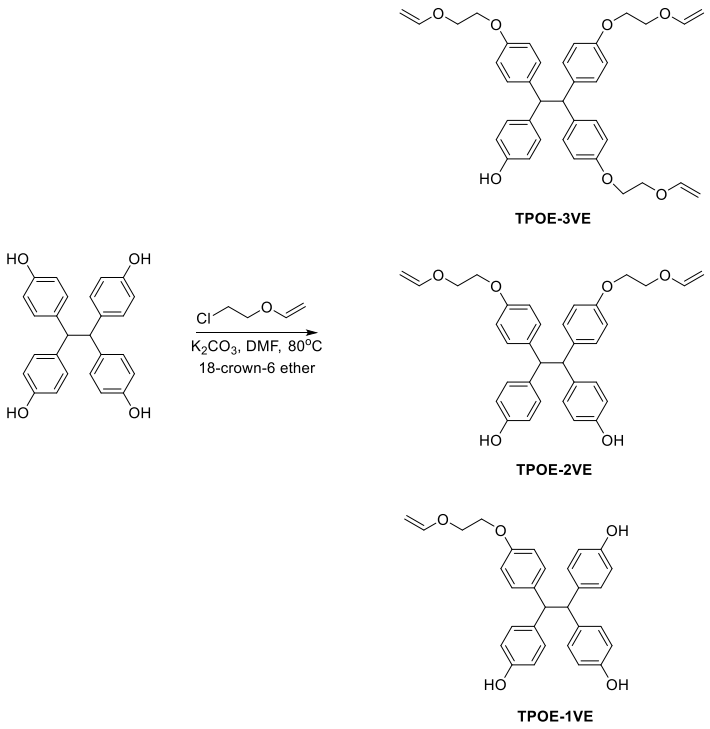

Figure 5.4 Synthesis of TPOE-3VE, TPOE-2VE, and TPOE-1VE. Each individual molecule is isolated from the same reaction via silica gel chromatography.

TPOE-1VE, TPOE-2VE, and TPOE-3VE were synthesized via a slightly different procedure from THPE-1VE and THPE-2VE. Potassium carbonate (K_2CO_3) is used as the base in this reaction since NaOH will deprotonate the ethyl bridge protons, forming a

carbanion which then attacks the 2-chloroethyl vinyl ether, forming unwanted side products. 3.181 g of TPOE (1 molar equivalent) was dissolved in dimethylformamide, followed by the addition of 8.61g (6 eq.) of potassium carbonate and 2.21g (2 eq.) of 2-chloroethyl vinyl ether (VE). The mixture was heated to 80^{o}C and stirred for 48 hours, after which the solution was cooled to room temperature, and deionized water and ethyl acetate were added. The aqueous layer was washed with dilute hydrochloric acid solution and extracted once with additional ethyl acetate. The organic layers were then combined, washed twice with additional deionized water, and then dried over $MgSO_4$, after which solvents were evaporated using a rotary evaporator. The resulting crude residue was then purified via silica gel chromatography using hexanes and ethyl acetate in a ratio of 5:3 to yield TPOE-3VE, TPOE-2VE, and TPOE-1VE as oils. ^{1}H NMR spectral data are as follows:

TPOE-1VE (300MHz, acetone-d_6, δ): 7.25 ppm (d, 2H), 7.11 ppm (d, 6H), 6.69 ppm (d, 2H), 6.58 ppm (d, 6H), 6.50 ppm (dd, 1H), 4.75 ppm (s, 2H), 4.11 ppm (m, 6H). Yield: 0.47g.

TPOE-2VE (300MHz, $CDCl_3$, δ): 7.00 ppm (d, 4H), 6.98 ppm (d, 4H), 6.65 ppm (d, 4H), 6.55 ppm (d, 4H), 6.49 ppm (dd, 2H), 4.85 ppm (s, 2H), 4.51 ppm (s, 2H), 4.15 ppm (m, 12H). Yield: 0.689g. Anal. Calcd for $C_{34}H_{34}O_6$: C, 75.82; H, 6.36. Found: C, 74.13; H, 6.93.

TPOE-3VE (300MHz, $CDCl_3$, δ): 7.01 ppm (d, 6H), 6.98 ppm (d, 2H), 6.65 ppm (d, 6H), 6.54 ppm (d, 2H), 6.50 ppm (dd, 3H), 4.85 ppm (s, 1H), 4.55 ppm (m, 18H). Yield: 0.83g. Anal. Calcd for $C_{38}H_{40}O_7$: C, 74.98; H, 6.62. Found: C, 73.89; H, 6.94.

5.2.2 Lithographic Evaluation

3 wt% resist solutions were created by dissolving the resist in cyclohexanone, containing 5 mol% (with respect to resist) triphenyl sulfonium hexafluoro antimonate (TPS-SbF_6) (Midori Kagaku, Ltd.) and filtering through a 0.2 μm Teflon membrane filter. Resist solutions were then spin-coated onto unprimed silicon wafers ordered from University Wafer to form films approximated 40nm thick. The films were then subjected to a post-apply bake (PAB) for 10 minutes in ambient atmosphere to crosslink and insolubilize the film in developers. Crosslinked films were then exposed to either 100 keV e-beam or 248nm DUV radiation, followed by a post-exposure bake (PEB) for 60 seconds. For organic solvent development, the exposed films were then developed in either methyl isobutyl ketone (MIBK) for 60 seconds, followed by an IPA rinse and nitrogen gun drying. For aqueous base development, the films were developed in 0.26 N aqueous tetramethyl ammonium hydroxide (TMAH) solution for 60 seconds, followed by a deionized water rinse and nitrogen gun drying. 248nm deep ultraviolet (DUV) contrast curves were obtained using an Oriel Instruments 500W Hg-Xe arc lamp with a 248 nm bandpass filter, using a M-2000 Woolam Ellipsometer for film thickness measurements. Normalized remaining thickness (NRT) measurements were obtained by measuring the thickness of the film after the PAB versus the thickness remaining after development. E-beam lithography evaluation was performed using a JEOL JBX-9300FS electron-beam lithography system with a 100-keV acceleration voltage and a 100-pA current. Resulting e-beam patterns were imaged using a Carl Zeiss Ultra 60 SEM with 1-5 keV acceleration voltage.

5.3 Results

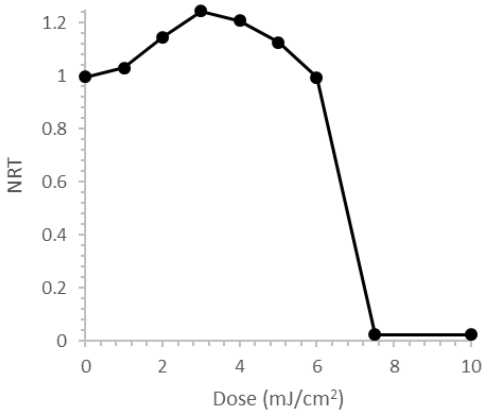

Figure 5.5 248nm DUV contrast curve of TPOE-1VE, using a PAB of 200 ^{o}C and a PEB of 90 ^{o}C in 0.26N TMAH development.

248nm DUV contrast curves offer a quick, inexpensive way for resist formulation and processing conditions to be optimized before obtaining high-resolution patterns. Beginning with TPOE-1VE, which has a threefold excess of phenols compared to vinyl ethers, the 248nm DUV contrast curve of the material in Figure 5.5 shows a dose-to-clear (E_0) of 7 mJ/cm^2. The material exhibits severe swelling in 0.26N TMAH developer at low doses, with the NRT first increasing with dose and then gradually decreasing to a thickness of 0, giving the material a contrast ratio of 6.6.

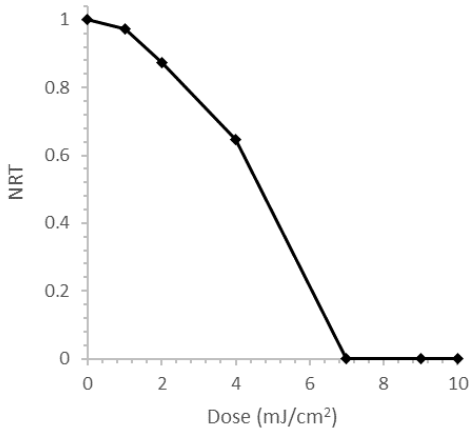

Figure 5.6 DUV contrast curve of THPE-1VE with a PAB of 200ºC and 90ºC PEB

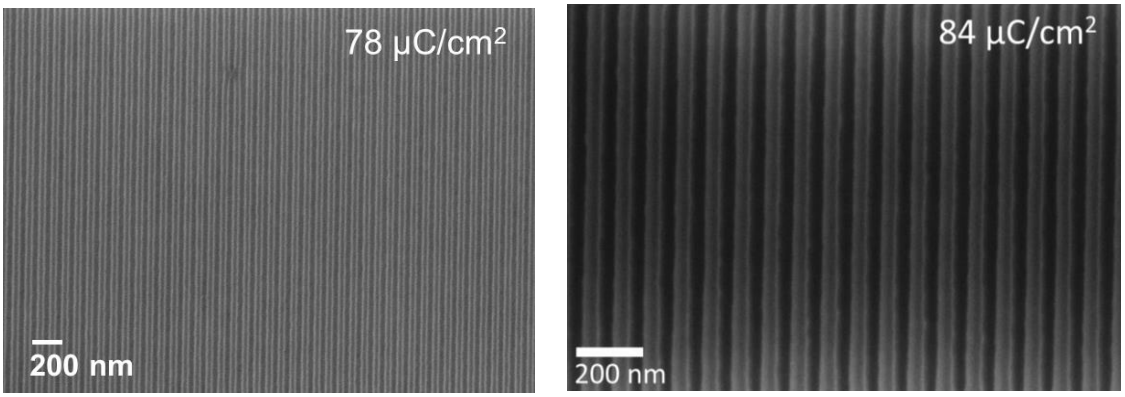

Figure 5.7 100 keV e-beam patterns of THPE-1VE in 0.26N TMAH development, when formulated with 5 mol% TPS-SbF_6 as PAG.

In the DUV contrast curve of THPE-1VE (Figure 5.6), no swelling is observed, and the material begins to show thickness loss at a dose of 1 mJ/cm^2, with an E_0 of 7 mJ/cm^2 when developed in 0.26N TMAH at a PAB of 200ºC and a PEB of 90ºC. The material has a contrast value of 3.2. Under 100keV e-beam patterning (Figure 5.7), the material demonstrates a sub-40nm resolution of 1:1 line:space patterns with no noticeable swelling

at a dose of 84 μC/cm^2 with a 3σ LER value of 4.98 nm. The lines appear under-dosed at 78 μC/cm^2.

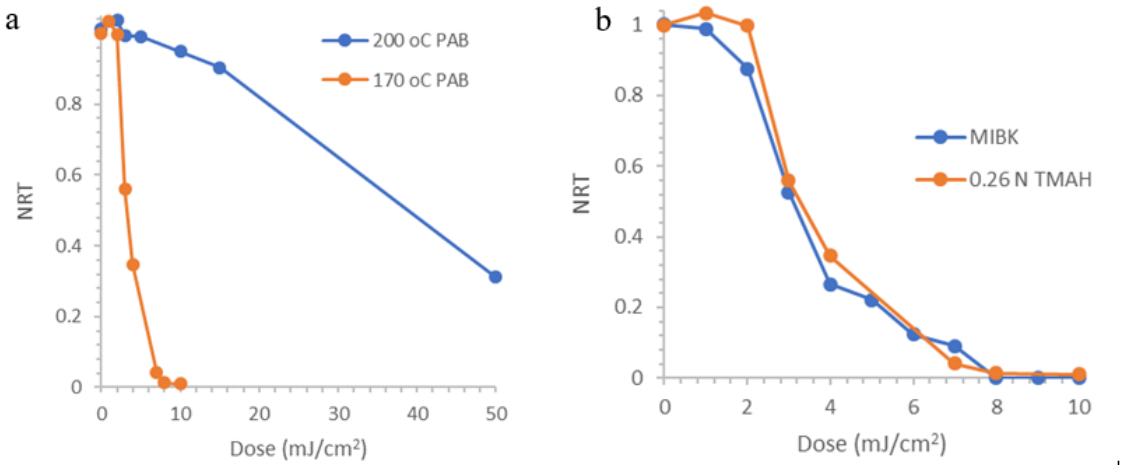

Figure 5.8 248 nm contrast curve of TPOE-2VE comparing (a) two different PAB temperatures at a PEB of 90°C in 0.26N TMAH and (b) comparing MIBK and 0.26N TMAH development at a PAB of 170°C and PEB of 90°C.

TPOE-2VE was designed to have an equal number of phenols and vinyl ethers, such that all functional groups can in principle be incorporated into the final crosslinked network, potentially strengthening the network relative to the resists that have an unequal ratio of the two. When a PAB of 200°C is used to crosslink the material, TPOE-2VE does not completely depolymerize, even at a dose 50 mJ/cm^2, as shown in Figure 5.8a. Lowering the PAB by 30 degrees to 170°C allows the material to completely depolymerize at a dose of 8 mJ/cm^2. The differences between MIBK and 0.26N TMAH development on the DUV performance of TPOE-2VE are shown in Figure 5.8b, when a PAB of 170°C and a PEB of 90°C were used. The curves are largely similar, with the TPOE-2VE having an E_0 of 8

mJ/cm^2 in both solvents and contrast ratio of 2.2 in TMAH development and 1.6 in MIBK development. Figure 5.9 demonstrates that the material is capable of resolving roughly 45nm lines at a dose of 78 μC/cm^2 with a 3σ LER of 5.5nm in TMAH development with no signs of pattern collapse at this feature size.

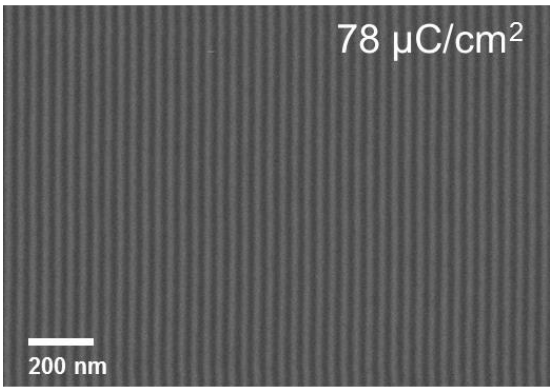

Figure 5.9 100 keV e-beam patterns of TPOE-2VE for 0.26N TMAH development, with a PAB of 170^{o}C and PEB of 90^{o}C.

The patterning performance of THPE-2VE has been reported previously, but it is still useful to include the data here for a full comparison to the other materials. The 248nm DUV contrast curve of THPE-2VE in Figure 5.10 shows that, when subjected to a PAB of 200^{o}C and PEB of 90^{o}C, the resist shows an E_0 of 3 mJ/cm^2 and a contrast value of 10.3. Figure 5.11 shows the 100keV e-beam images, which demonstrate that the material is capable of resolving lines down to approximately 40nm with a dose of 40 μC/cm^2 with an LER (3σ) of 8.2 nm in TMAH development.

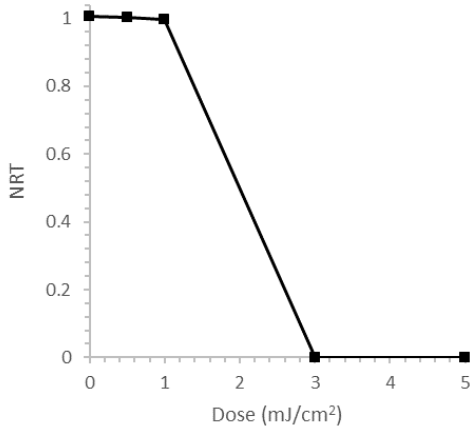

Figure 5.10 248nm DUV curve of THPE-2VE in 0.26N TMAH development. Processing conditions: 200ºC PAB, 90ºC PEB.

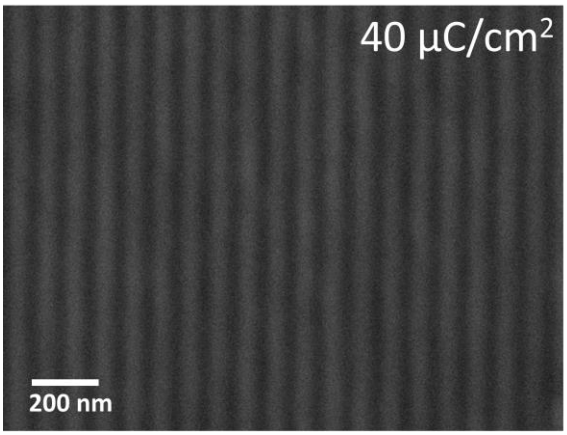

Figure 5.11 100 keV e-beam patterns of THPE-2VE in 0.26N TMAH development. Processing conditions: 200ºC PAB, 90ºC PEB.

TPOE-3VE, which has a threefold excess of vinyl ethers, does not completely depolymerize when a PAB of 170ºC is used, regardless of how high of a PEB was used, as shown in Figure 5.12a. In fact, the NRT even begins to increase with dose as the PEB is

raised to 170°C. In order to attempt to reduce the amount of remaining thickness at higher doses, even lower PAB temperatures of 160°C and 150°C were used, but as Figure 5.12b shows, the NRT never quite reaches a value of 0.

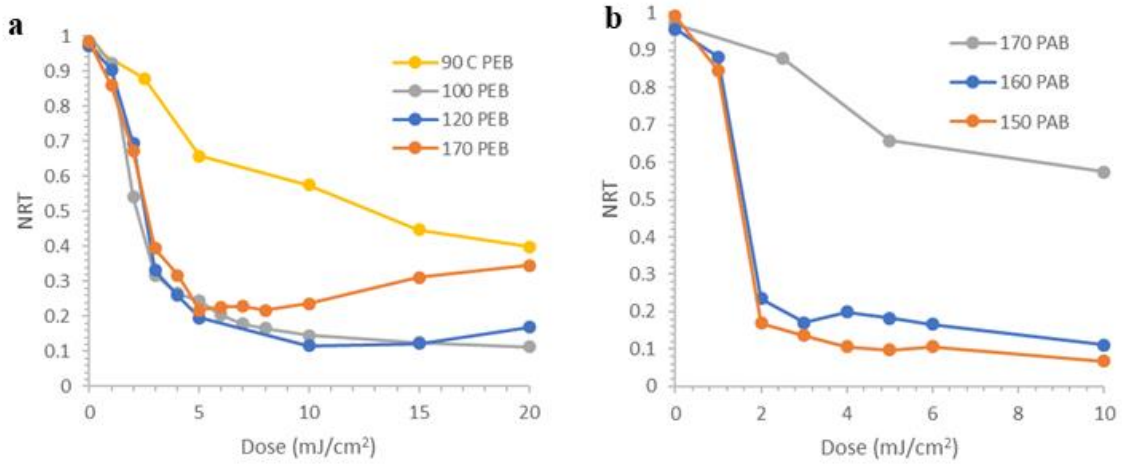

Figure 5.12 DUV contrast curves of TPOE-3VE, processed (a) at various PEB and (b) PAB temperatures in an attempt to reduce NRT.

Figure 5.13 compares the DUV contrast curves of THPE-1VE, THPE-2VE, and TPOE-2VE, when the materials are processed at identical conditions. The sensitivity of TPOE-2VE is significantly lower than that of the other two materials, even failing to depolymerize completely and return to an NRT of 0. THPE-1VE and THPE-2VE both show E_0 values below 10 mJ/cm^2.

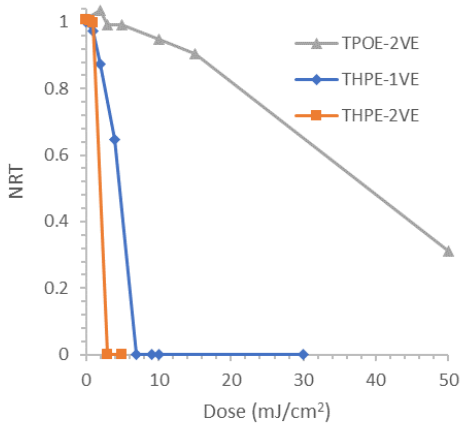

Figure 5.13 Comparison of THPE-1VE, THPE-2VE, and TPOE-2VE when processed at identical conditions (PAB = 200°C and PEB = 90°C).

5.4 Discussion

At lower doses, the network in TPOE-1VE is likely just beginning to fragment, but sufficient fragmentation has not yet occurred in order to solubilize the material in the developer, and so the network instead swells, up to an NRT value of approximately 1.2 in Figure 5.5.[13] Beyond some critical number of de-crosslinking reactions, the network has sufficiently fragmented to begin rendering the material soluble in developer, and the NRT decreases accordingly, eventually reaching an NRT of 0 at a dose of 7 mJ/cm^2. In this resist, by virtue of stoichiometry only one phenol per resist molecule is consumed during the crosslinking reaction with the single vinyl ether to form an acetal, resulting in a network that has many unreacted phenols present. The acidic phenols likely imbibe the basic developer, forming phenolate salts, which results in the high NRT observed in TMAH development at lower doses. Due to the extreme swelling of this material, the resist is

unlikely to yield quality high resolution patterns, and so e-beam imaging of this resist has not been pursued.

The lack of swelling in THPE-1VE in Figure 5.6, even though there is one unreacted phenol on the resist core would suggest that either a single unreacted phenol is not sufficient to result in swelling of the network or that depolymerization occurs rapidly enough to avoid any noticeable swelling, compared to TPOE-1VE. The material requires roughly twice the dose required to image compared to THPE-2VE at identical processing conditions and formulations.[10] Since THPE-1VE has one more phenol than vinyl ethers on the core, the unreacted phenol could result in a higher dose required to image if the photoacid mobility is sufficiently limited. Phenols have been reported to slow photoacid diffusion through films of photoresists due to both increases in glass transition temperature (T_g) and hydrogen-bonding interactions with the photoacid.[14] At a dose of 84 μC/cm^2, the material exhibits an LER of 4.98 nm, which is considerably lower than the 8.2 nm LER reported for THPE-2VE. The source of improved LER is unclear, but the presence of more hydroxyls in THPE-1VE may lead to better acid generation efficiency, which could lead to a more homogeneous distribution of acid, reducing LER.[15]

In Figure 5.8a, we show that the sensitivity of these materials can be modulated simply by crosslinking at different temperatures. TPOE-2VE fails to completely depolymerize when a PAB of 200^{o}C and PEB of 90^{o}C are used. This resist was designed to have an equal number of phenols and vinyl ethers so that all functional groups could theoretically be incorporated into the final network. Having such a densely-crosslinked network is likely to impede the diffusion of photoacid throughout the network, preventing the material from

depolymerizing completely. By lowering the PAB to 170°C, the density of crosslinks is reduced enough for the material to depolymerize completely by a dose of 8 mJ/cm^2. When processed at identical condition, TPOE-2VE is significantly less-sensitive than THPE-1VE and THPE-2VE in Figure 5.13, likely forming a more densely-crosslinked network than the other materials, resulting in its reduced sensitivity. The NRT of the 0.26N TMAH development curve of TPOE-2VE in Figure 5.8b increases slightly to 1.03 at a dose of 1 mJ/cm^2, which could suggest that small amounts of swelling are occurring. At this low dose, the network is likely just starting to fragment, but enough photoacid has not been generated to break enough crosslinks to render the material fully-soluble in the developer. This fragmentation would result in both phenols and aliphatic alcohols being unmasked during the depolymerization reaction, which could imbibe the basic TMAH developer, thus accounting for the observed swelling, similar to that seen in TPOE-1VE, though not as extreme.[16]

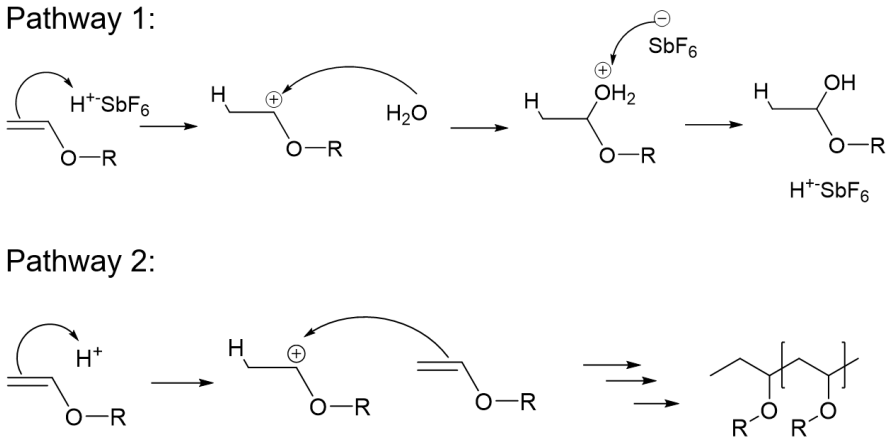

Figure 5.14 Mechanism showing the acid-catalyzed side reactions of vinyl ethers that are possible in the current materials.

THPE-2VE has the highest sensitivity and contrast of any of the materials in this study, with a DUV E_0 of 3 mJ/cm^2 and a contrast value of 10.3 in TMAH development. It manages to resolve roughly 40nm features in TMAH development with a rather high LER (3σ) of 8.2 nm. This high LER could arise from unwanted side reactions, such as acid-catalyzed homopolymerization, shown in Figure 5.14, which would result in insoluble material at the line edge, and increase the LER for this resist, compared to THPE-1VE and TPOE-2VE, which both show 3σ LER values of 4.98nm and 5.5nm, respectively.

TPOE-3VE was the resist with the least favorable patterning behavior and never completely depolymerized at any processing conditions attempted, as shown in Figure 5.12a and Figure 5.12b. In an effort to decrease the final NRT of the material at a PAB of 170^{o}C in Figure 5.12a, the PEB of the material was raised, but there was still remaining thickness even at the highest PEB of 170^{o}C. Surprisingly, at a PEB of 170^{o}C, we observed

an increase in NRT as the dose increased. In this curve, complete depolymerization has likely occurred between doses of 5 and 10 mJ/cm^2, where the contrast curve at 170^{o}C reaches its minimum. As the dose is increased, there are no more acetals to be consumed, and so the photoacid is consumed by available vinyl ethers, which then polymerize to form a product that is insoluble in 0.26N TMAH. Since TPOE-3VE contains only a single phenol with three vinyl ethers, only a single vinyl ether on each resist molecule can be consumed during the thermal crosslinking step to form the acid-cleavable acetals. Because of this, each resist molecule in the crosslinked network will have two unreacted vinyl ethers that are not incorporated into the final network during the PAB. These vinyl ethers can undergo two acid-catalyzed side reactions, outlined in Figure 5.14, and each of these reactions can contribute to the lowered sensitivity of TPOE-3VE. In Pathway 1, which is acid-catalyzed hydrolysis of vinyl ethers, the photoacid first protonates the vinyl ether, which is then attacked by an equivalent of water, eventually regenerating the photoacid. It is possible that this reaction can impede the progress of depolymerization, since several steps must occur before the photoacid is regenerated once it reacts with the vinyl ether. Pathway 2, which shows acid-catalyzed homopolymerization of the vinyl ethers, represents a much worse scenario. In this reaction, the photoacid would be completely consumed by the vinyl ethers, with would then react with themselves, forming carbon-carbon bonds which cannot be de-crosslinked by photoacid, resulting in the non-zero NRT values in Figure 5.12a and Figure 5.12b.[12] Similar to TPOE-2VE, the PAB temperature was lowered, which should reduce the number of crosslinks in the network to allow the material to be imaged at lower doses, since fewer acetal crosslinks would need to be cleaved by photoacid to render the

material soluble in developer. However, as shown in Figure 5.12b, the material still retained roughly 10% of its original thickness even at the lowest PAB of 150^{o}C. No PAB temperatures below 150^{o}C were attempted due to reduction of film quality and network swelling as the materials likely produced less densely-crosslinked networks at those temperatures. Assuming that lowering the PAB results in fewer crosslinks in the final film, this would also mean that even more vinyl ethers are not to incorporated into the network, potentially further compounding the remaining thickness issue. Additionally, as the concentration of acid in the film increases with increasing dose, the NRT does gradually decrease, which suggests that a competing reaction is occurring. Literature reports for these materials show that as the acid concentration increases, acid-catalyzed hydrolysis of the vinyl ethers begins to occur, reducing the number of vinyl ethers available for homopolymerization, but the NRT never returns to zero at the doses probed, and so no high-resolution patterns of TPOE-3VE were obtained.

5.4.1 Resist blends

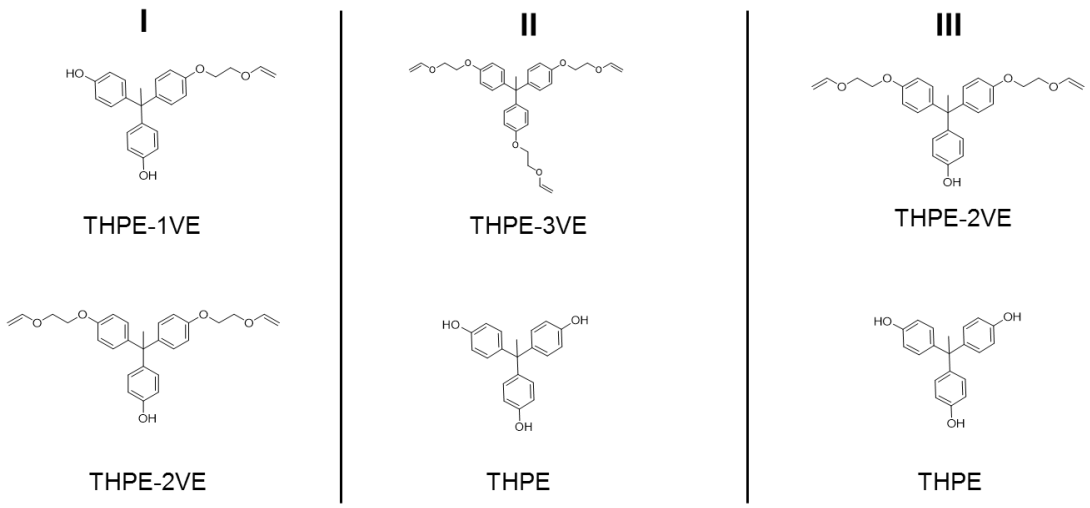

Figure 5.15 Composition of blends used in the blending study.

One option for modifying the patterning behavior of these resists is to blend different resists together to make a formulation that can be imaged. The potential benefits of doing this is that each functional group has an equimolar amount of the other functional group, such that each can be incorporated into the final network, which may minimize the side-reactions seen in the individual resists. As a starting point, blends of the THPE-VE resist family were created such that there was an equimolar amount of vinyl ethers and phenols in the blend, shown in Figure 5.15.

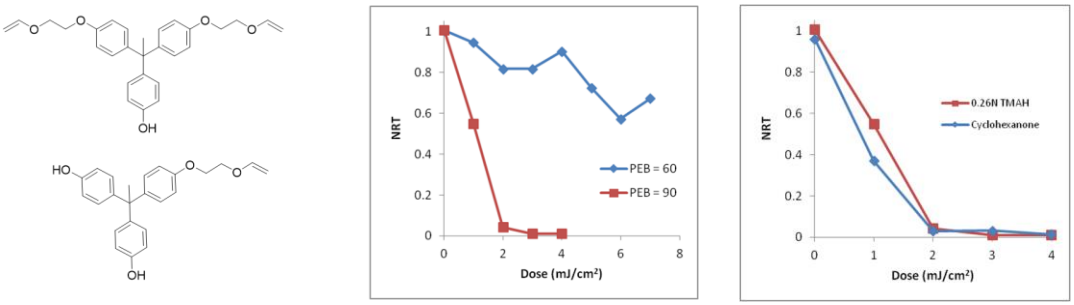

Figure 5.16 Imaging behavior of THPE-2VE and THPE-1VE blend comparing PEB temperatures (left) and cyclohexanone and 0.26N TMAH development solvents (right) (PAB = 200°C; 5 mol% TPS-SbF_6).

Figure 5.16 shows the 248nm DUV curve of a blend of THPE-2VE and THPE-1VE that is formulated to have an equimolar amount of phenols and vinyl ethers. The curve shows that the blend is more sensitive than either of the individual resists shown in Figure 4.4 and Figure 5.6. In the right contrast curve, the TMAH and cyclohexanone contrast curves are quite similar, with the resist film clearing completely by a dose of 2 mJ/cm^2. While this increase in sensitivity is attractive, the resist does lose the shift in E1 away from zero dose seen in THPE-2VE, which is desired to reduce pattern degradation from flare during exposure.

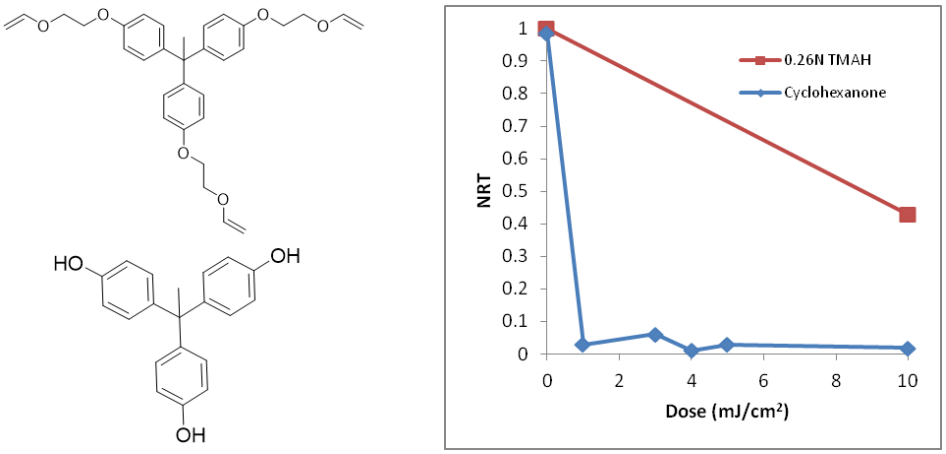

Figure 5.17 248 nm DUV contrast curve of a blend of THPE-3VE and THPE (PAB = 200ºC; 5 mol% TPS-SbF_6).

THPE-3VE is a by-product of the reaction that produces THPE-2VE and THPE-1VE. While the molecule itself is not a depolymerization resist, it can be blended with other resist molecules to produce a formulation that is capable of acting like a depolymerization resist. As an initial study, shown in Figure 5.17, THPE-3VE is blended with an equimolar amount of THPE core to produce a solution that can be thermally crosslinked during a PAB and then depolymerized in the presence of a photoacid during the PEB. The 248 nm DUV curve in Figure 5.17 shows that this blend can dissolve completely by a dose of only 1 mJ/cm^2 when developed in cyclohexanone. However, the material does not completely dissolve when using 0.26 N TMAH as the developer, and roughly 50% of the film remains after a 30s development time. This is because THPE-3VE does not contain a phenol which is necessary to be soluble in the basic TMAH developer.

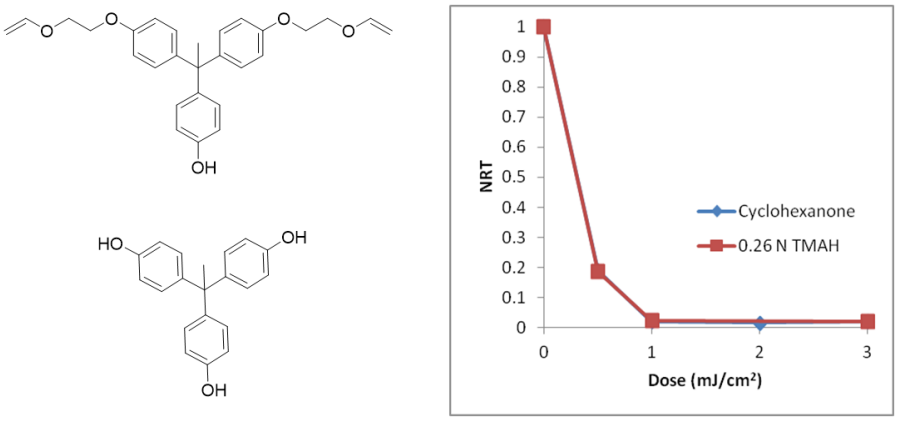

Figure 5.18 DUV contrast curves of a blend of THPE-2VE and THPE core (PAB = 200°C, 5 mol% TPS-SbF_6).

When THPE-2VE is blended with the THPE core, the material becomes more sensitive than THPE-2VE (Figure 4.4), with the resist film clearing by a dose of only 1 mJ/cm^2 in each development solvent. However, similar to the blend of THPE-2VE and THPE-1VE, the shift in E1 is again lost when THPE-2VE is blended with another material. Blended systems have higher sensitivities than their single-resist counterparts, but suffer from no shift in E1 away from zero dose, which is useful in mitigating flare, which can potentially cause depolymerization reactions in nominally unexposed regions.

5.5 Summary

A series of molecular resists was synthesized in which the number of vinyl ethers and phenols on the molecular core was systematically varied in order to provide insight into how varying the composition of these two groups affects the patterning behavior of this class of materials. The results showed that an extreme excess of either of the two functional groups leads to undesirable contrast curves, with an excess of phenols in TPOE-

1VE leading to network swelling. An excess of vinyl ethers in TPOE-3VE leads to residual material that is not cleaved by acid due to secondary acid-catalyzed reactions of vinyl ethers. A very slight imbalance of the two functional groups led to much more sensitive materials compared to TPOE-2VE, which had an equal number of phenols and vinyl ethers. Due to this imbalance, THPE-1VE and THPE-2VE likely formed a less-crosslinked network, which required fewer acid-catalyzed de-crosslinking reactions to occur before becoming soluble in developer versus TPOE-2VE. Comparing THPE-1VE and THPE-2VE, the resist with more phenols, THPE-1VE, showed a lower sensitivity, possibly because of reduced photoacid diffusion, due to either a higher T_g or photoacid interactions with phenols present in the network. The highest 3σ LER value was observed for THPE-2VE, with a value of 8.2 nm, compared to 4.98 nm for THPE-1VE and 5.5 nm for TPOE-2VE. This extremely high LER value is likely a result of acid-catalyzed homopolymerization, which would result in insoluble material forming at the line edge. The materials presented here are very sensitive to 248nm DUV lithography, with the ability to modulate their sensitivity through changes in the PAB temperature used. 100keV e-beam imaging of THPE-1VE, THPE-2VE, and TPOE-2VE show that the resists are all easily capable of resolving sub-50nm features in 0.26N TMAH development.

5.6 References

1. Kang, S. H.; Wu, W. L.; Choi, K. W.; De Silva, A.; Ober, C. K.; Prabhu, V. M., Characterization of the Photoacid Diffusion Length and Reaction Kinetics in EUV Photoresists with IR Spectroscopy. *Macromolecules* **2010,** *43* (9), 4275-4286.

2. Yeh, W. M.; Noga, D. E.; Lawson, R. A.; Tolbert, L. M.; Henderson, C. L., Comparison of positive tone versus negative tone resist pattern collapse bahavior*. *J Vac Sci Technol B* **2010,** *28* (6), C6s6-C6s11.

3. Sharp, B.; Lawson, R. A.; Fralick, A.; Narcross, H.; Chun, J. S.; Neisser, M.; Tolbert, L. M.; Henderson, C. L., Base developable negative-tone molecular resist based on epoxide cross-linking. *Advances in Patterning Materials and Processes Xxxii* **2015,** *9425*.

4. Lawson, R. A.; Lee, C. T.; Yueh, W.; Tolbert, L.; Henderson, C. L., Epoxide functionalized molecular resists for high resolution electron-beam lithography. *Microelectron Eng* **2008,** *85* (5-6), 959-962.

5. Brunner, T. A.; Fonseca, C., Optimum tone for various feature types: positive versus negative. *Advances in Resist Technology and Processing Xviii, Pts 1 and 2* **2001,** *4345*, 30-36.

6. Mack, C. A.; Connors, J. E., Fundamental Differences between Positive and Negative Tone Imaging. *Optical/Laser Microlithography V, Pts 1 and 2* **1992,** *1674*, 328-338.

7. Bowden, M., Outgassing Issues in Acetal Resist Design. *J Photopolym Sci Tec* **2000,** *13* (4), 507-512.

8. Felix, N.; Ober, C. K., Acid-labile, chain-scission polymer systems used as positive-tone photoresists developable in supercritical CO2. *Chem Mater* **2008,** *20* (9), 2932-2936.

9. Lawson, R. A.; Cheng, J.; Cheshmehkani, A.; Tolbert, L. M.; Henderson, C. L., Positive Tone Resists Based On Network Depolymerization of Molecular Resists. *Advances in Resist Materials and Processing Technology Xxx* **2013,** *8682*.

10. Sharp, B. L.; Narcross, H. L.; Tolbert, L. M.; Henderson, C. L., Positive-tone crosslinked molecular resist based on acid-catalyzed depolymerization. *J Vac Sci Technol B* **2017,** *35* (6).

11. Moon, S.; Yamaoka, T., 3-Component Photopolymers Based on Thermal Cross-Linking and Acidolytic De-Cross-Linking of Vinyl Ether Groups .2. Effects of Acid Components on Photopolymer Characteristics. *Polym Advan Technol* **1995,** *6* (8), 566-572.

12. Moon, S. G.; Naitoh, K.; Yamaoka, T., Novel Dual-Mode Photoresist Based on Cationic Polymerization and Acidolysis. *Chem Mater* **1993,** *5* (9), 1315-1320.

13. Xue, C. Y.; Wong, D. Y.; Kasko, A. M., Complex Dynamic Substrate Control: Dual-Tone Hydrogel Photoresists Allow Double-Dissociation of Topography and Modulus. *Adv Mater* **2014,** *26* (10), 1577-1583.

14. Houle, F. A.; Hinsberg, W. D.; Morrison, M.; Sanchez, M. I.; Wallraff, G.; Larson, C.; Hoffnagle, J., Determination of coupled acid catalysis-diffusion processes in a positive-tone chemically amplified photoresist. *J Vac Sci Technol B* **2000,** *18* (4), 1874-1885.

15. Yamamoto, H.; Kozawa, T.; Nakano, A.; Okamoto, K.; Tagawa, S.; Ando, T.; Sato, M.; Komano, H., Dependence of acid generation efficiency on the protection ratio of hydroxyl groups in chemically amplified electron beam, x-ray and EUV resists. *J Vac Sci Technol B* **2004,** *22* (6), 3522-3524.

16. De Silva, A.; Sundberg, L. K.; Ito, H.; Sooriyakumaran, R.; Allen, R. D.; Ober, C. K., A Fundamental Study on Dissolution Behavior of High-Resolution Molecular Glass Photoresists. *Chem Mater* **2008,** *20* (23), 7292-7300.

CHAPTER 6. DIRECTLY PHOTO-PATTERNABLE UNDERLAYERS FOR DIRECTED SELF-ASSEMBLY OF BLOCK COPOLYMERS

6.1 Introduction

Block copolymers (BCPs) have been proposed to extend the use of older lithography systems, such as 193nm immersion lithography due to their ability to self-assemble into a variety of potentially useful morphologies. However, in order for block copolymers to be lithographically useful, their assembly needs to be directed such that they can achieve long-range order over a large area with minimal defects. Currently, two main techniques are used to achieve the DSA of BCPs: graphoepitaxy and chemoepitaxy.[1,2] In graphoepitaxy, a lithographic guiding pattern is generated on top of a neutral underlayer using a photoresist with conventional photolithography at a pitch larger than the size BCP domains. Often, the side walls of this guiding pattern are preferential to one of the two blocks, allowing one of the two blocks to preferentially wet the wall and enhancing the strength of the guidance. In chemoepitaxy, whose process flow is shown in Figure 6.1a, a neutral underlayer is coated on top of a substrate. A lithographic relief pattern is formed using photolithography. An etch step is then performed, which generates hydrophilic groups in the portions of the underlayer that aren't covered by photoresist. The photoresist is then removed, leaving a chemical guiding pattern which preferentially wets the more hydrophilic of the two blocks. This process is long and complicated, which will only increase the cost of the devices

fabricated using this technique, thus there is motivation to reduce the number of steps used to direct the self-assembly of BCPs using a chemical guiding pattern.

One such option to reduce process time is to directly "write" a chemical pattern onto a neutral substrate using lithography, eliminating the need for the etch step (Figure 6.1b). Such a design has already been reported that is based on the acid-catalyzed deprotection of a poly(4-hydroxystyrene) (PHOST) polymer protected with isopropyloxycarbonyl (iPOC) groups, shown in Figure 6.2.[3] The design includes a methacrylate (MA) group as the crosslinking group, which is necessary to ensure that the underlayer does not dissolve once the BCP is coated atop the underlayer. The PHOST portion of the underlayer is protected with an isopropyloxycarbonyl (iPOC) protecting group, which deprotects in the presence of photogenerated acid and a PEB to generate hydrophilic phenols, which the more polar block of the BCP preferentially wets.

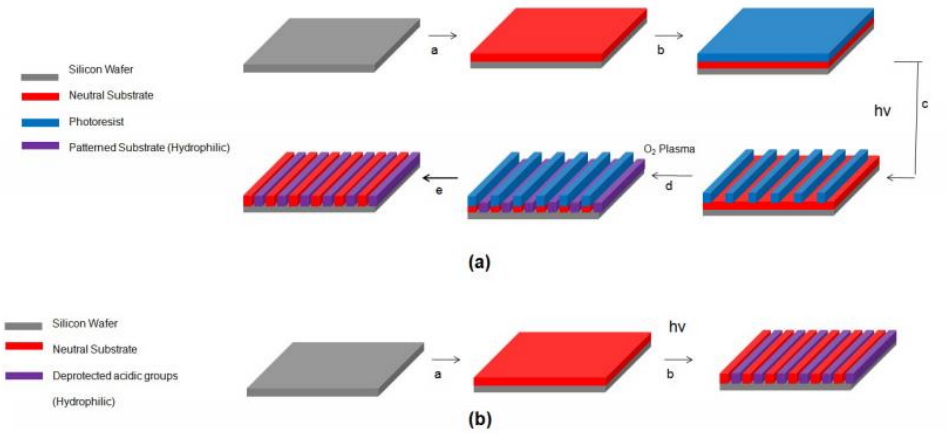

Figure 6.1: Comparison between typical chemoepitaxy process (a) and the directly-photodefinable underlayer (b).

This design showed good acid-catalyzed deprotection (as measured via contact angle change with increasing DUV dose), but it didn't crosslink as efficiently as expected. In order to verify that the underlayer would not wash away when the BCP was coated on top, the underlayer was sonicated in PGMEA for 10 minutes to remove crosslinked material. As much as 50% of the underlayer was lost after the crosslinking reaction was carried out, potentially because the methacrylate group was sensitive to oxygen, which resulted in chain termination as the crosslinking reaction was performed. Since the film was so thin, the underlayer had to be coated very thickly in order to direct the self-assembly of PS-*b*-PMMA.

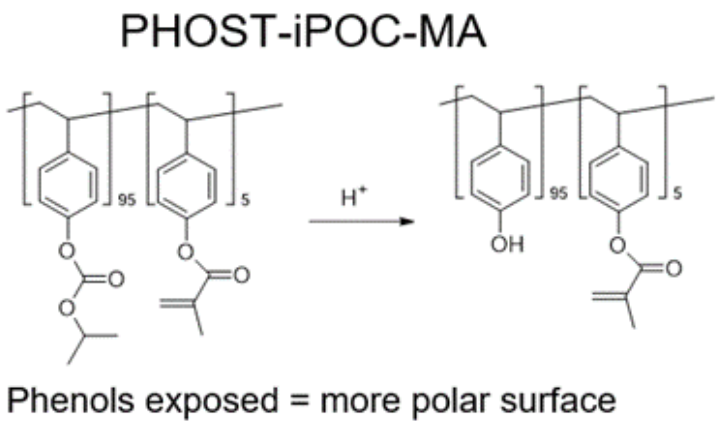

Figure 6.2: Structure (left) and chemistry of the acid-catalyzed deprotection of the PHOST-iPOC-*r*-MA underlayer.

Coating the underlayer so thickly results in wasted material and can also interfere with the etch steps to transfer the underlayer to the silicon substrate underneath. Thus, there is a need for a more efficient crosslinking chemistry which can achieve high NRT values during the crosslinking step without being washed away during subsequent coating steps. Two potential chemistries were investigated that have been demonstrated to achieve high NRT values in ambient conditions: epoxides and benzocyclobutene (BCB). These designs shown in Figure 6.3 are identical to the old design in Figure 6.2, but differ in the crosslinking group used.

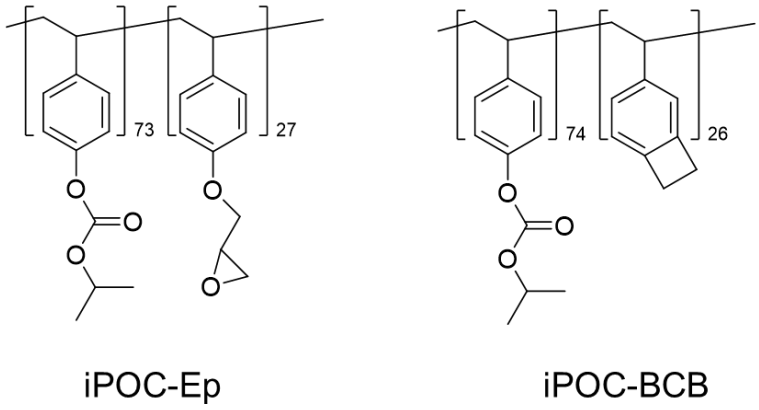

Figure 6.3 Structure of new underlayers designed with improved crosslinking groups.

The epoxide crosslinking group in iPOC-Ep has been shown to achieve high NRT values through thermal crosslinking, and the BCB group in iPOC-BCB by other groups.[4] The goal of this chapter is to evaluate whether either of these groups can be successfully integrated into the directly-photodefinable underlayer and increase the NRT of the film without affecting the deprotection chemistry needed to guide BCPs.

6.2 Experimental

6.2.1 Synthesis

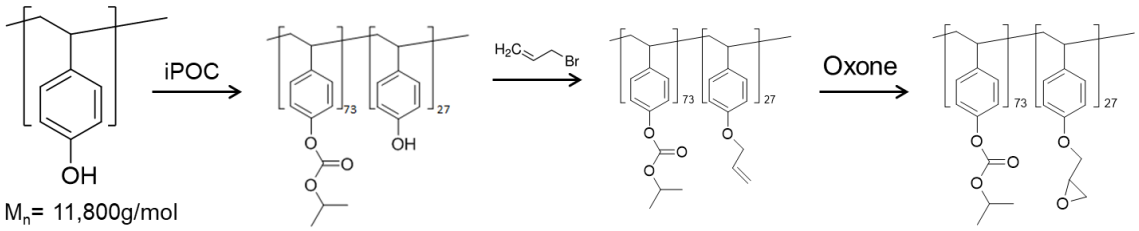

Figure 6.4 Synthesis scheme for iPOC-*r*-Ep underlayer.

PHOST-r-iPOC: Dissolve 2g *p*-poly(hydroxystyrene) (PHOST) (11,800 g/mol) in 50 mL THF, then add 17 mL isopropyl chloroformate (iPOC) (1.0 M in toluene). Add 6 mL triethylamine (TEA) and stir at room temperature for 24 hours. The reaction was quenched with dilute HCl solution, and ethyl acetate was added. The organic layer was washed twice with deionized water before it was filtered/dried over $MgSO_4$. Yield: 2.00 g.

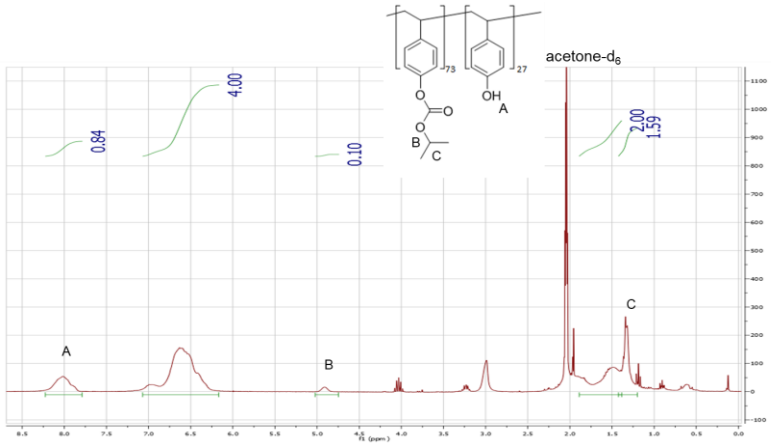

Figure 6.5 ^{1}H NMR spectrum of PHOST-*r*-iPOC in acetone-d_6.

iPOC-*r*-Allyl: Dissolve 1g (0.025 mol) PHOST-r-iPOC in 30 mL dimethylformamide (DMF), and add 0.1 g potassium carbonate and 2 g (1.5 mL, 0.13 mol) allyl bromide to the

solution, along with 0.1 g (0.3 mmol) 18-crown-6 ether. Place solution into oil bath set to 75°C and stir for 24 hours. Afterwards, cool solution to room temperature, add ethyl acetate, and wash once with dilute HCl solution and twice with deionized water. The organic layer was then filtered/dried over $MgSO_4$ before solvents were evaporated. Yield: 0.85g.

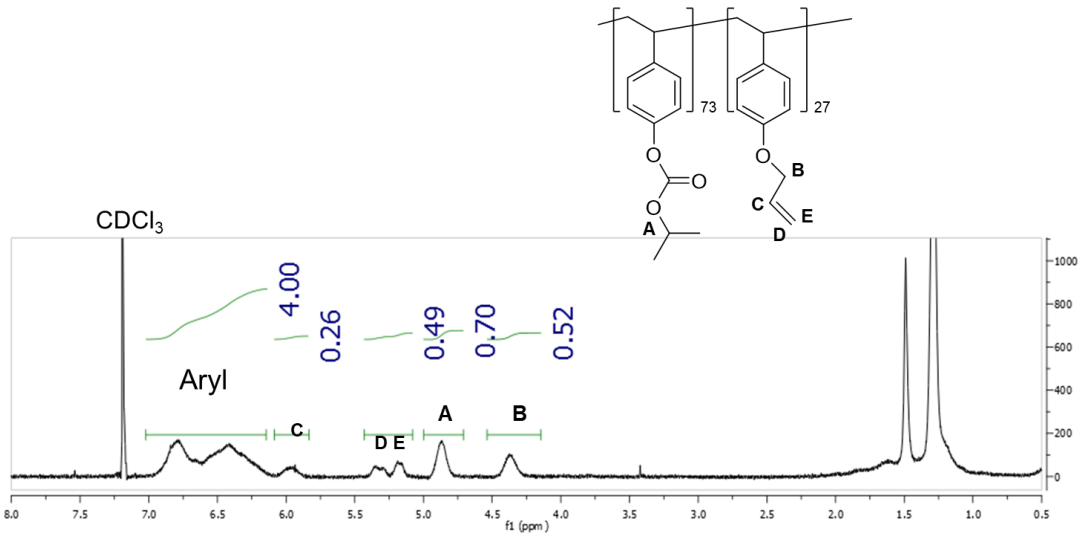

Figure 6.6 ^{1}H NMR spectrum of iPOC-*r*-Allyl in $CDCl_3$.

iPOC-*r*-Ep: Dissolve 1.61 g iPOC-*r*-Allyl in 40 mL of chloroform in an ice bath. Add 10 mL acetone along with 3.65 g sodium bicarbonate. Dissolve 4.45 g Oxone in 30 mL deionized water and add dropwise to the solution. Remove the solution from the ice bath and stir at room temperature for 24 hours. A small sample was extracted, washed with water and extracted with ethyl acetate in order to track conversion of alkenes to epoxides via ^{1}H NMR. The procedure was repeated until conversion to epoxides was complete. Once conversion was complete, the solution was washed with water and extracted with ethyl

acetate. The organic layer was washed twice more with water before being filtered/dried over $MgSO_4$ and solvents evaporated. Yield: 1.20 g.

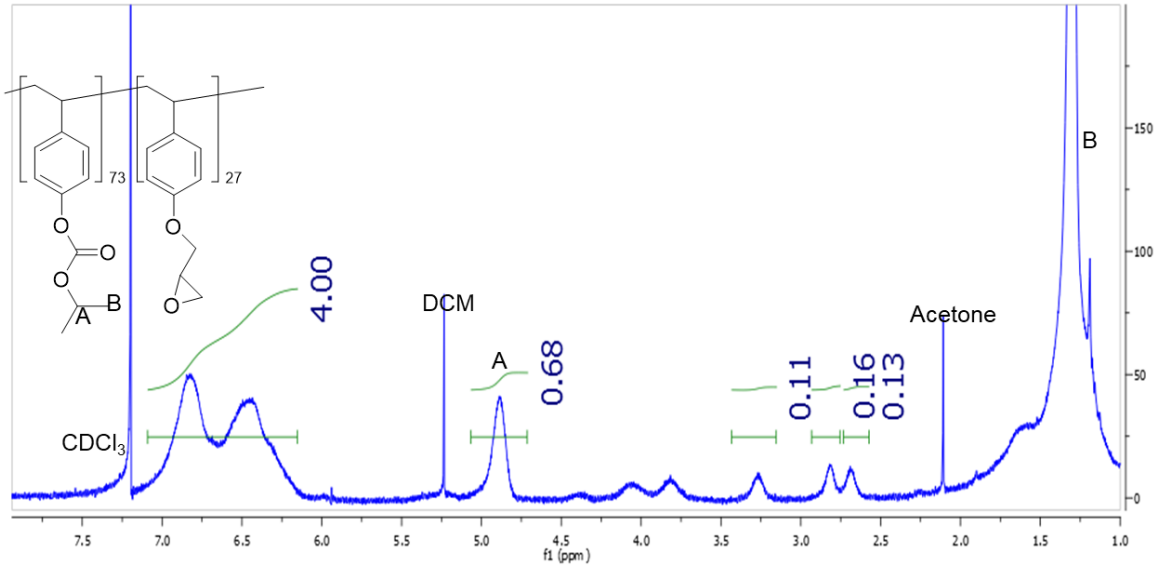

Figure 6.7 ^{1}H NMR spectrum of iPOC-*r*-Ep in $CDCl_3$.

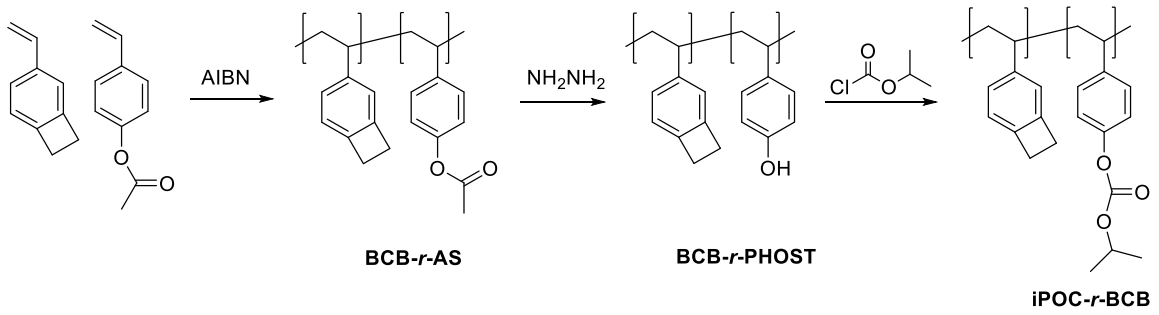

Figure 6.8 Synthesis scheme for iPOC-*r*-BCB underlayer.

BCB-*r*-AS: To a 10-mL Schlenk flask, add 0.022 g vinyl-benzocyclobutene (BCB), 0.9927 g acetoxy styrene, and 0.0531 g AIBN in 2 mL dry toluene. Perform three freeze-pump-thaw-backfill (N_2) cycles. Allow flask to warm to room temperature and then place in an oil bath set to 75^{o}C and stir for 24 hours. The reaction vessel was then opened to air to quench the reaction and allowed to cool to room temperature. The solution was then diluted slightly with dichloromethane (DCM) and then precipitated into cold methanol, where a white powder formed, which was vacuum filtered and dried in a vacuum oven overnight. Yield: 0.5032 g. M_w (7,300 g/mol).

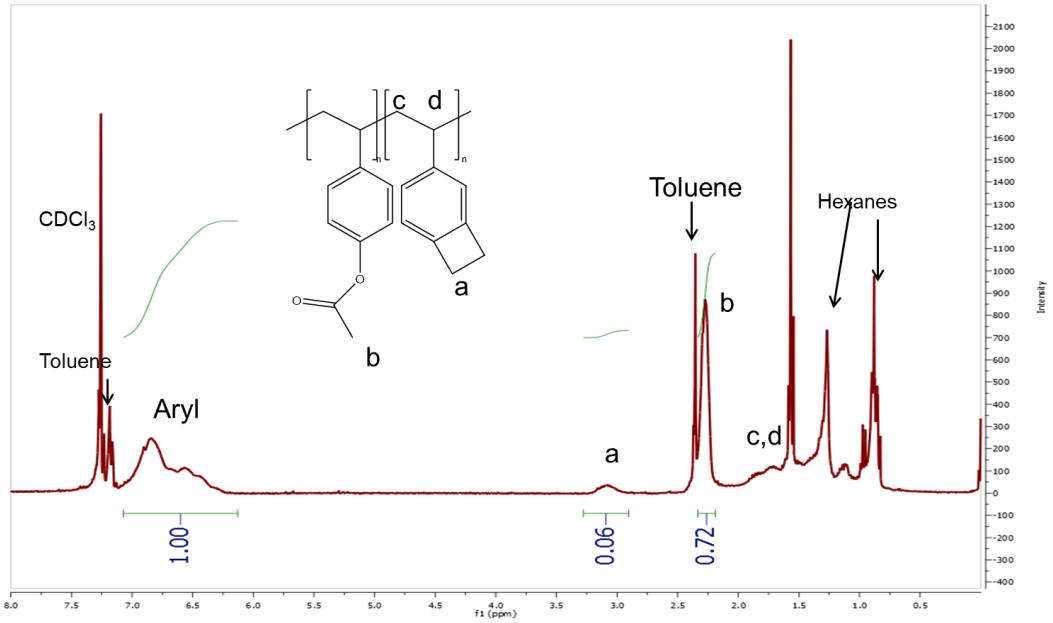

Figure 6.9 ^{1}H NMR (300 MHz) spectrum of BCB-*r*-PAS in $CDCl_3$.

BCB-*r*-PHOST: BCB-*r*-AS (1 g) was dissolved in 20 mL *p*-dioxane and then flushed with N_2. Hydrazine hydrate (NH_2NH_2) was added dropwise and the reaction stirred at room temperature for 6 hours. After this time, the reaction was quenched via addition of deionized water and then extracted with ethyl acetate. The organic layer was dried over $MgSO_4$ and solvent evaporated via rotary evaporator. Yield: 0.64g.

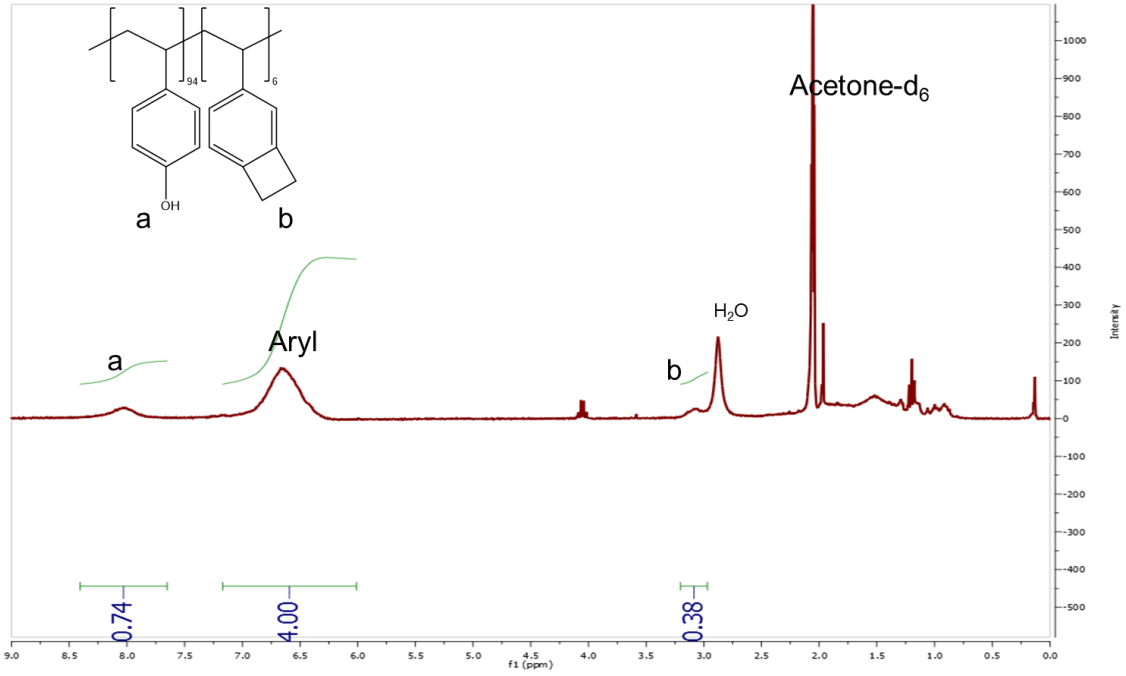

Figure 6.10 ^{1}H NMR (300 MHz) spectrum of BCB-*r*-PHOST in acetone-d_6.

BCB-*r*-iPOC: BCB-*r*-AS (1.2 g) was dissolved in 60 mL of ethyl acetate and 1.55 mL triethylamine and 13 mL isopropyl chloroformate (1.0 M solution in toluene) were added. The reaction was then sealed with a rubber septum and allowed to stir for two days at room temperature, after which time it was quenched via addition of dilute HCl solution and extracted with ethyl acetate. The organic layer was dried over $MgSO_4$ and solvents evaporated via rotary evaporator. Yield: 1.1g.

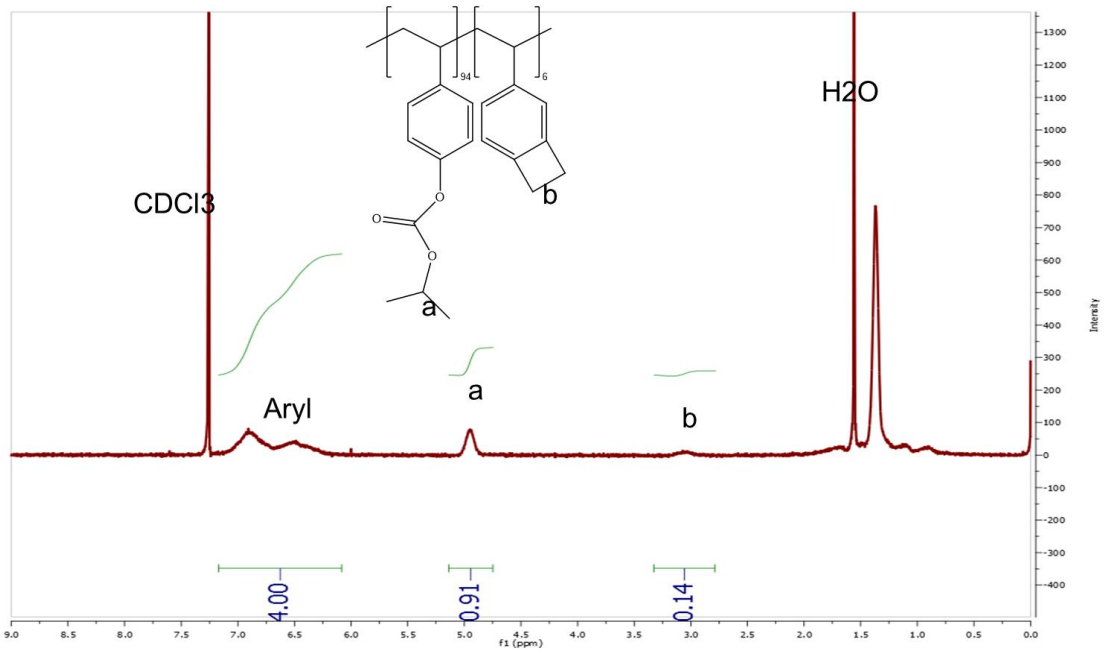

Figure 6.11 ^{1}H NMR (300 MHz) spectrum of BCB-*r*-iPOC in $CDCl_3$.

Figure 6.12 Synthesis of HEMA-THP monomer.

HEMA-THP: 2 g (1 molar equivalent) of hydroxyethyl methacrylate (HEMA) was dissolved in ethyl acetate in a 22mL glass vial. To this solution, 1.1 eq. dihydropyran (DHP) was added, along with a catalytic amount (0.2 eq.) of trifluoroacetic acid (TFA). This solution was stirred at room temperature for 2 hours. Afterwards, the solution was

washed with sodium bicarbonate solution and then twice with water. The organic layer was filtered/dried over $MgSO_4$ before solvents were removed via rotary evaporator. Yield: 2.26g.

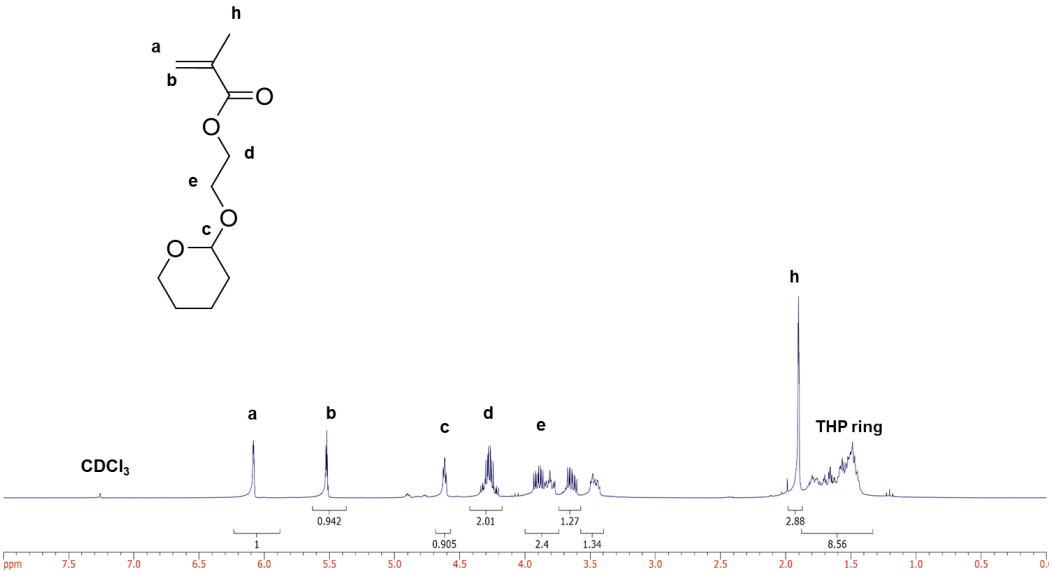

Figure 6.13 ^{1}H NMR spectrum of HEMA-THP in $CDCl_3$.

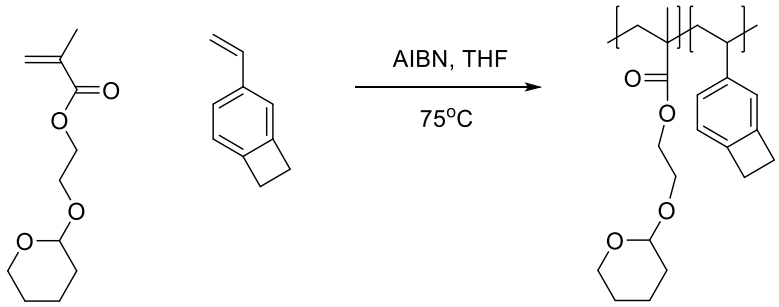

Figure 6.14 Synthesis scheme of PHEMA-*r*-BCB underlayer.

PHEMA-*r*-BCB: Dissolve 0.5 g (1 eq.) HEMA-THP, 0.05 eq. vinyl-benzocyclobutene (BCB), and 0.05 eq. AIBN in 1 mL THF and stir at room temperature until the AIBN is

dissolved. Three free-pump-thaw-backfill cycles were performed, and once completed, the solution was allowed to warm to room temperature before being placed in an oil bath set to 75°C to stir for 2 hours. Excess THF was removed via rotary evaporation, and the resulting crude material was re-dissolved in ethyl acetate and precipitated into cold methanol to obtain a white powder. Yield: 0.32 g.

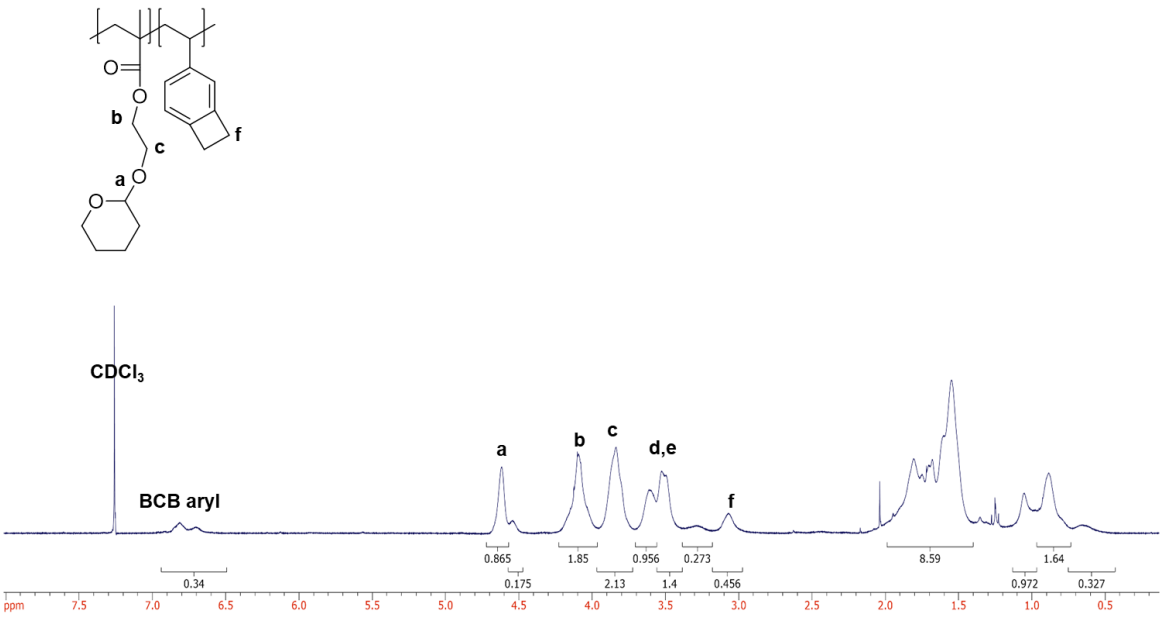

Figure 6.15 ^{1}H NMR (300 MHz) spectrum PHEMA-THP-*r*-BCB in $CDCl_3$.

6.2.2 Lithographic Evaluation

Films of the underlayers were coated onto freshly O_2-plasma cleaned wafers ordered from University Wafer. The films were then subjected to PABs for 10 minutes to determine the optimal temperature necessary to crosslink the films. After the PAB, the film thickness was measured, and the films were sonicated in PGMEA for 10 minutes, and the film thickness

was measured once again via spectroscopic ellipsometry. These two thicknesses were compared to generate an NRT value.

After the optimal crosslinking temperature was identified, solutions of the underlayers were formulated with TPS-SbF_6 as PAG. Films were cast from these solutions, crosslinked, and then exposed to 248nm DUV radiation, and baked during a PEB for 2 minutes. Thickness measurements were taken after the crosslinking temperature and after the PEB to generate NRT curves. After the thickness was obtained, water contact angle measurements were obtained using deionized water on a water contact angle measurement system.

6.3 Crosslinking studies

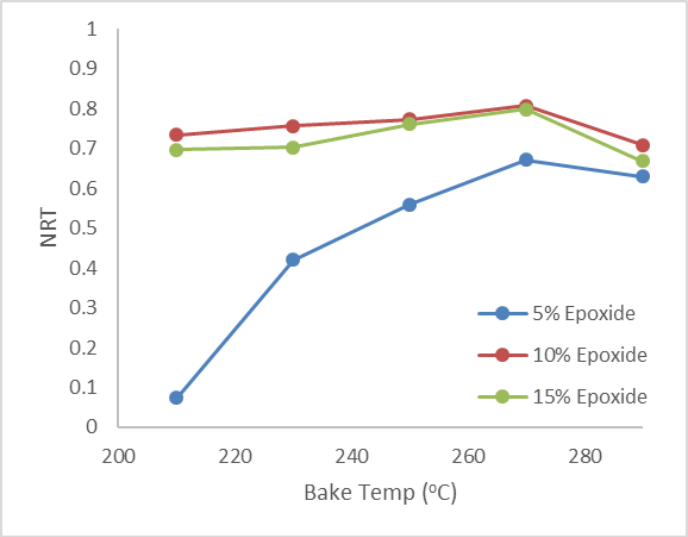

Figure 6.16 Crosslinking study of the iPOC-Ep underlayer with various percentages of epoxides.

In the first design, using an epoxide as the crosslinking group, a PAB study was performed to quantify the underlayer's ability to thermally crosslink. When using only 5% epoxide, extremely high PAB temperatures are required in order to achieve relatively high NRT values. By increasing the epoxide content to 10%, high NRT values can be achieved at much more reasonable PAB temperatures, but the NRT never quite reaches an NRT of 1 at its highest value. Increasing the content of epoxides to 15 mol% does little for the NRT. In each of the three designs, the NRT begins to decrease at a PAB temperature of 290°C, likely due to thermal decomposition reactions.

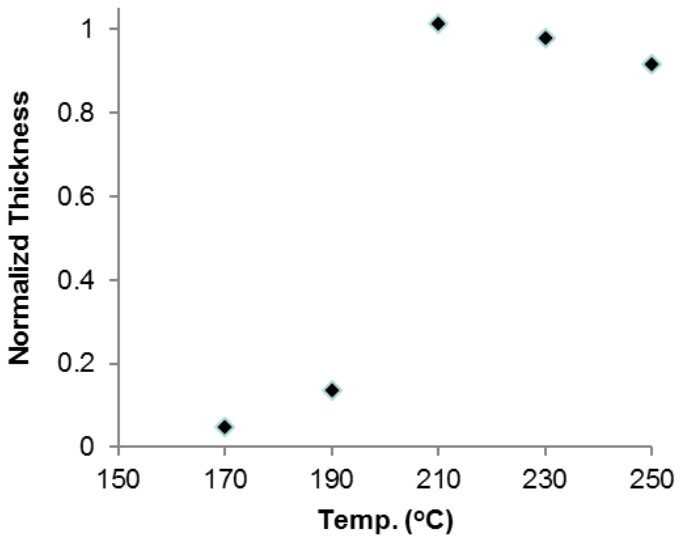

Figure 6.17: Crosslinking study for iPOC-*r*-BCB underlayer containing 5 mol% BCB.

For the iPOC-*r*-BCB design containing only 5 mol% BCB, Figure 6.17 shows that a maximum NRT of 1 is achieved at a PAB temperature of 210°C. Above this temperature, the thickness begins to decrease, which could potentially be due to thermal deprotection reactions of the iPOC group. Because the thickness decreases above 210°C, this temperature was chosen to crosslink the underlayers in future studies.

6.4 DUV contrast curves

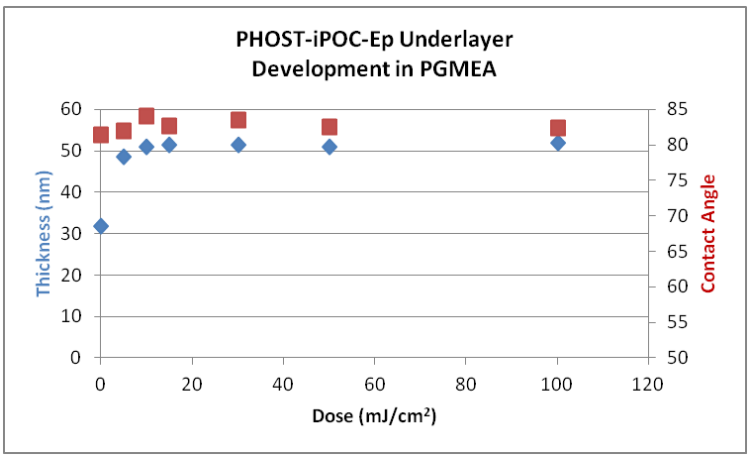

Figure 6.18: iPOC-Ep contact angle and thickness change versus dose using 248 nm lithography.

When PHOST-iPOC-*r*-Ep was formulated with 5 wt% TPS-SbF_6, no contact angle modulation was observed as with previous designs, even at incredibly high doses (Figure 6.18). Additionally, it was observed that the thickness actually began to increase with increasing dose. Since the deprotection reaction results in a large portion of mass loss, it would be expected that the thickness of the resist would decrease as more deprotection reactions occur with increasing dose. The most likely explanation for this phenomenon is that there are unreacted epoxides within the film that the photoacid encounters. These epoxides competitively and irreversibly react with the photoacid, preventing it from reacting with the iPOC protecting groups. Thus, the film essentially continues to cure as more photoacid is generated without any contact angle modulation.

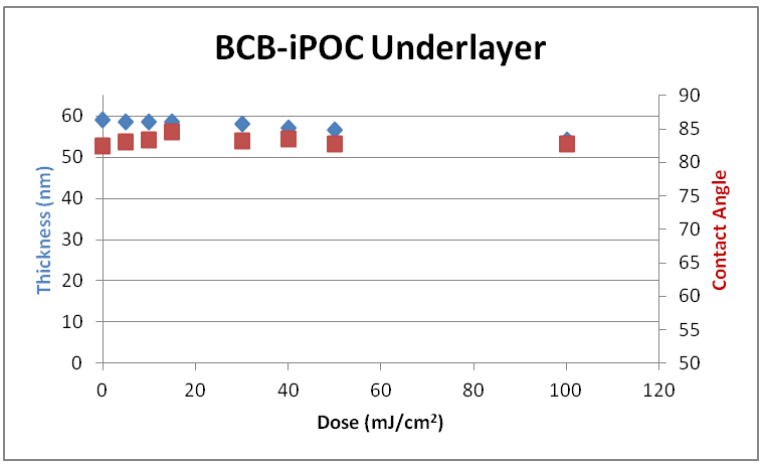

Figure 6.19 DUV study of thickness and contact angle versus exposure dose using 248 nm lithography with 25 mol% BCB group.

A design with 25 mol% BCB group (relative to iPOC groups) was formulated with 5 mol% TPS-SbF_6 and then exposed to 248nm DUV light to determine the dose required to achieve maximum deprotection of the PHOST group. Figure 6.19 shows this initial study, which shows that enough deprotection does not occur to change the water contact angle at the doses studied. Additionally, this deprotection reaction should also result in a slight thickness decrease, since the deprotection reaction outgasses CO_2 and 2-butene, but the thickness is constant. By simply lowering the BCB percentage to 5 mol%, a contact angle change is achieved by a dose as low as 30 mJ/cm^2 when using a PEB of 170^{o}C (Figure 6.20).

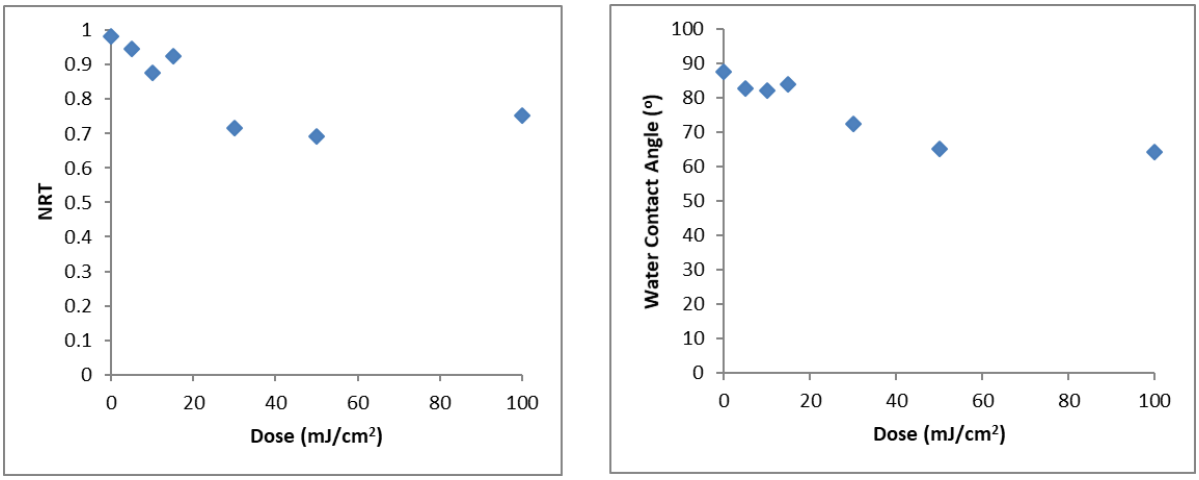

Figure 6.20: Contact angle change for the iPOC-BCB design using 5 mol% BCB group (relative to iPOC/PHOST portion).

6.5 PHEMA-THP-*r*-BCB

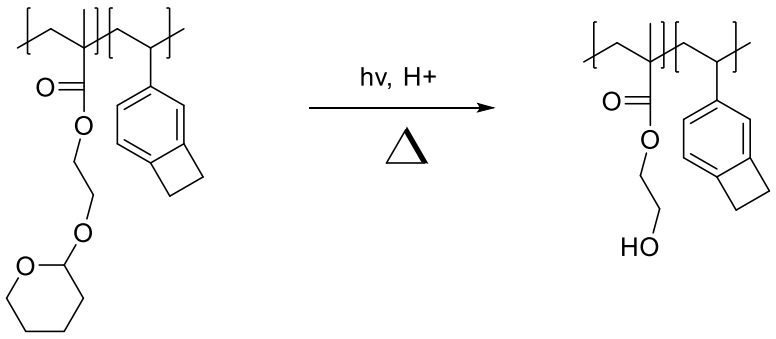

Figure 6.21 Photochemistry of PHEMA-THP-*r*-BCB underlayer.

Two BCPs developed in our group (PS-*b*-PHEMA and PtBS-*b*-PHEMA) use the PHEMA block as the more polar of the two blocks. In order to provide stronger guidance during DSA of this BCP, it may be better to design an underlayer that uses the HEMA monomer

itself, since it is more likely to preferentially wet itself versus another polar block. Thus, the more guidance the BCP is given during DSA, the less likely defects will be to form.[5,6]

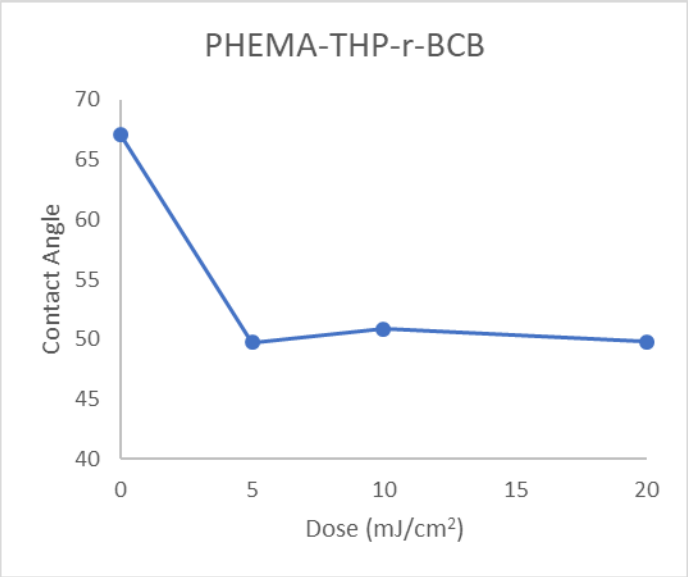

Figure 6.22 Contact angle change of the PHEMA-THP-*r*-BCB underlayer using 248 nm DUV lithography.

As seen in Figure 6.22, the contact angle begins to decrease at much lower doses (5 mJ/cm^2) versus the iPOC-protected designs. This is due to the THP group being a low-activation energy acetal-based protecting group.[7] Although the initial contact angle is much lower than the iPOC designs (68^o versus ~85^o), this initial angle can be modified by including a third monomer into the design. The most likely candidate would be the monomer that comprises the second block of the BCP that includes PHEMA, such as PS or PtBS. Doing so would allow the "neutral," un-patterned region of the underlayer to have a slight preference to the non-polar block, which has been shown to improve the DSA of block copolymers.[8,2]

6.6 Conclusion

The iPOC-Ep design showed a much lower ultimate NRT versus the iPOC-BCB design, even when the iPOC-Ep underlayer was formulated with three times the percentage of crosslinking group. iPOC-BCB showed excellent crosslinking at lower temperatures than the iPOC-Ep design and showed good contact angle modulation using 248 nm DUV exposures. PHEMA-THP-*r*-BCB has been designed and demonstrated as a PHEMA-containing underlayer that is capable of achieving much lower final contact angles than previous designs, which can help better guide the DSA of a PHEMA-containing BCP. It also demonstrates that, provided that the protecting group is thermally stable during the crosslinking step, the photo-definable underlayer designs are not restricted to iPOC-containing designs.

6.7 References

1. Bita, I.; Yang, J. K. W.; Jung, Y. S.; Ross, C. A.; Thomas, E. L.; Berggren, K. K., Graphoepitaxy of self-assembled block copolymers on two-dimensional periodic patterned templates. *Science* **2008,** *321* (5891), 939-943.

2. Liu, C. C.; Ramirez-Hernandez, A.; Han, E.; Craig, G. S. W.; Tada, Y.; Yoshida, H.; Kang, H. M.; Ji, S. X.; Gopalan, P.; de Pablo, J. J.; Nealey, P. F., Chemical Patterns for Directed Self-Assembly of Lamellae-Forming Block Copolymers with Density Multiplication of Features. *Macromolecules* **2013,** *46* (4), 1415-1424.

3. Cheng, J.; Lawson, R. A.; Yeh, W. M.; Tolbert, L. M.; Henderson, C. L., Developing Directly Photodefinable Substrate Guiding Layers for Block Copolymer Directed Self-Assembly (DSA) Patterning. *Advances in Resist Materials and Processing Technology Xxviii* **2011,** *7972*.

4. Ryu, D. Y.; Shin, K.; Drockenmuller, E.; Hawker, C. J.; Russell, T. P., A generalized approach to the modification of solid surfaces. *Science* **2005,** *308* (5719), 236-239.

5. Nation, B. D.; Breaux, C. L.; Ludovice, P. J.; Henderson, C. L., Free energy of defects in chemoepitaxial block copolymer directed self-assembly: effect of pattern density and defect position. *J Micro-Nanolith Mem* **2017,** *16* (4).

6. Williamson, L. D.; Seidel, R. N.; Chen, X. X.; Suh, H. S.; Delgadillo, P. R.; Gronheid, R.; Nealey, P. F., Three-Tone Chemical Patterns for Block Copolymer Directed Self Assembly. *Acs Appl Mater Inter* **2016,** *8* (4), 2704-2712.

7. Kim, J. H.; Lee, C. H.; Park, S. B.; Kim, W. A.; Moon, S. S.; Kim, K. M.; Lee, S. Y.; Yoon, S.; Kim, Y. H.; Chon, S. M., Influence of activation energy on LER in chemically amplified KrF photoresists. *Advances in Resist Technology and Processing Xxi, Pts 1 and 2* **2004,** *5376*, 790-800.

8. Detcheverry, F. A.; Liu, G. L.; Nealey, P. F.; de Pablo, J. J., Interpolation in the Directed Assembly of Block Copolymers on Nanopatterned Substrates: Simulation and Experiments. *Macromolecules* **2010,** *43* (7), 3446-3454.

CHAPTER 7. SUMMARY AND RECOMMENDATIONS FOR FUTURE WORK

7.1 Summary

This thesis details the efforts to design new materials to enable the adoption of next-generation lithographic techniques.

In Chapter 1, a new, molecular resist called TPOE-3Ep was developed in order to provide an example of an epoxide-based resist that is soluble in the industry standard developer, 0.26N TMAH. The material showed very promising results and managed to resolve 26 nm lines and spaces in MIBK development when using EUVL. Several problems were observed when patterning in TMAH, however, including delamination and microbridging. An underlayer corrected the delamination issue, but microbridging persisted.

Chapter 2 details a study where numerous base-soluble molecular resists were synthesized and evaluated in order to gain insight into how various structural features affect the lithographic performance of these materials. It was shown that increasing the number of phenols on the resist core increased the T_g of the materials, which then required a high bake temperature to achieve high NRT values. In order to achieve NRT values of 1, high bake temperatures were required, which caused crosslinking to occur outside exposed regions. Thus, a low T_g 0.26N TMAH-developable molecular resist was developed, called THPE-2Ep that shows 30nm resolution using e-beam lithography in both MIBK and 0.26N TMAH.

Chapter 3 provides an example of a positive-tone crosslinked molecular resist, named THPE-2VE. The motivation is to develop a positive-tone crosslinked material to exploit the pattern-collapse resistance shown in the negative-tone crosslinked materials. The resulting material was highly-sensitive to both DUV and e-beam lithography and resist was able to resolve roughly 35nm lines in both MIBK and 0.26N TMAH using e-beam lithography.

Chapter 4 delves deeper into positive-tone depolymerization resists and examines the effect of varying the ratio of phenols to vinyl ethers using five different resists. Results from this study showed that resists with more vinyl ethers had a slightly higher sensitivity than those with phenols. Resists with more phenols had a lower sensitivity but a lower LER value and higher resolution. As a whole, the depolymerization resists appear to be a highly-sensitive family of resists worthy of future studies.

Chapter 5 details the design of new photodefinable underlayers with improved crosslinking chemistries to achieve a higher NRT than previous designs. Two crosslinking groups, epoxides and benzocyclobutene, were investigated. The epoxide designs showed much lower ultimate NRT values than the BCB design. The BCB design showed that it was capable of achieving an NRT of 1 at both a lower mole percentage of BCB and a lower crosslinking temperature. iPOC-*r*-BCB was demonstrated to show good acid-catalyzed deprotection, as evidenced by the change in water contact angle observed.

7.2 Recommendations for future work

THPE-2Ep has demonstrated promising initial patterning using e-beam lithography, but its processing needs to be optimized. The material appears to fail by blurring of exposed lines, and reducing the PEB temperature is likely the most straightforward way to counteract this problem. In addition, the influence of methyl groups on the T_g and patterning behavior of the TMAH-soluble resists could be further explored by synthesizing resists which contain methoxy groups adjacent to the phenol, as this has been shown to drastically reduce the T_g of phenolic polymers.[1] An additional route would be to explore different substitution patterns of the phenols, as this has also been shown to lead to a reduction in T_g.[2]

The poor shelf life of the depolymerization resists will limit their ultimate usefulness as a resist material, so identifying the cause of this instability would be an excellent place to begin optimizing their performance. Furthermore, the outgassing observed during their PEB is a potential problem since acetaldehyde is a toxic compound. Thus, a mass-persistent design, such as the one shown in Figure 7.1, may be desirable. In this resist, called THPE-2DHP, the aldehyde which would normally outgas during the PEB is tethered to the resist, such that only a ring-opening reaction occurs.

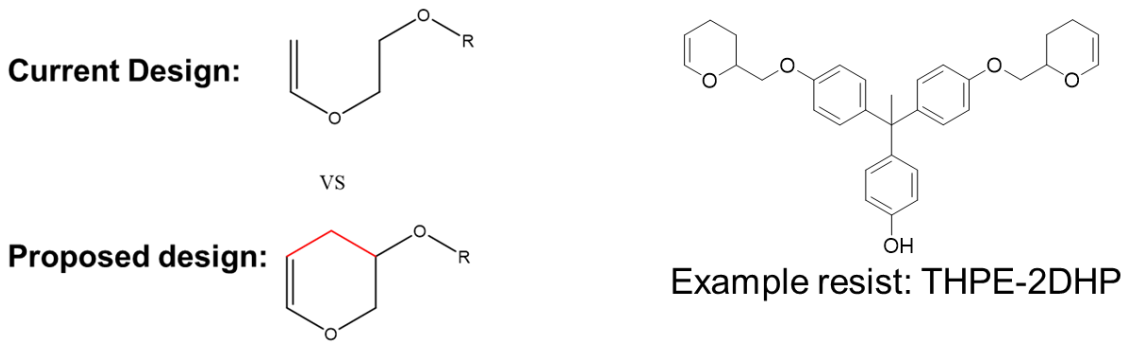

Figure 7.1 Example of a mass-persistent depolymerization resist, THPE-2DHP.

The iPOC-*r*-BCB designs should be patterned using e-beam lithography in order to demonstrate that they can direct the self-assembly of a block copolymer. Various other photodefinable underlayers can be designed to tailor their chemistry to the need of the user. Different protecting groups, such as ring-opening chemistries, can be utilized in order to create a totally mass-persistent system.

The photo-definable underlayers that have been previously reported, both here and in the literature, have relied upon acid-catalyzed deprotection reactions to effect a change in contact angle.[3] While such designs have the benefit of typically requiring lower exposure doses compared to non-catalytic processes, there are several potential advantages to designing an underlayer that does not need photoacid to cause a contact angle change. A directly photo-cleavable protecting group would eliminate the need for a PEB, eliminating one processing step. In addition, since no PAG is needed, there are no concerns from PAG aggregation.

One such chemistry that has been demonstrated for use in both 248nm and 193nm lithography is the nitrobenzyl (NBn) group.[4,5] This protecting group can be directly cleaved using ultraviolet light and has been used in organic chemistry as a photo-cleavable protecting group.[6] A prototypical design using a nitrobenzyl protecting group on a PHOST backbone is shown in Figure 7.2. The design uses the previously-developed BCB crosslinking group due to its high NRT.

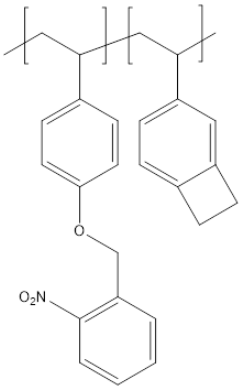

Figure 7.2: Structure of PHOST-Nbn-*r*-BCB directly photodefinable underlayer.

7.3 References

1. Nakamura, K.; Hatakeyama, T.; Hatakeyama, H., Dsc Studies on Hydrogen-Bonding of Poly(4-Hydroxy-3, 5-Dimethoxystyrene) and Related Derivatives. *Polym J* **1986,** *18* (3), 219-225.

2. Nakamura, K.; Hatakeyama, T.; Hatakeyama, H., Effect of Substituent Groups on Hydrogen-Bonding of Polyhydroxystyrene Derivatives. *Polym J* **1983,** *15* (5), 361-366.

3. Maher, M. J.; Bates, C. M.; Blachut, G.; Carlson, M. C.; Self, J. L.; Janes, D. W.; Durand, W. J.; Lane, A. P.; Ellison, C. J.; Willson, C. G., Photopatternable Interfaces for Block Copolymer Lithography. *Acs Macro Lett* **2014,** *3* (8), 824-828.

4. Lawson, R., Molecular Resists for Advanced Lithography. **2011**.

5. Guo, L. X.; Guan, J.; Lin, B. P.; Yang, H., Synthesis and characterization of methacrylate matrix resin bearing o-nitrobenzyl group. *J Cent South Univ* **2015,** *22* (9), 3296-3301.

6. Bochet, C. G., Photolabile protecting groups and linkers. *J Chem Soc Perk T 1* **2002,** (2), 125-142.

CHAPTER 8. APPENDIX: CHARACTERIZATION DATA

8.1 ^{1}H NMR Spectra of Selected Compounds

All spectra were collected using a 300 MHZ spectrometer, using $CDCl_3$ as the solvent, unless otherwise noted.

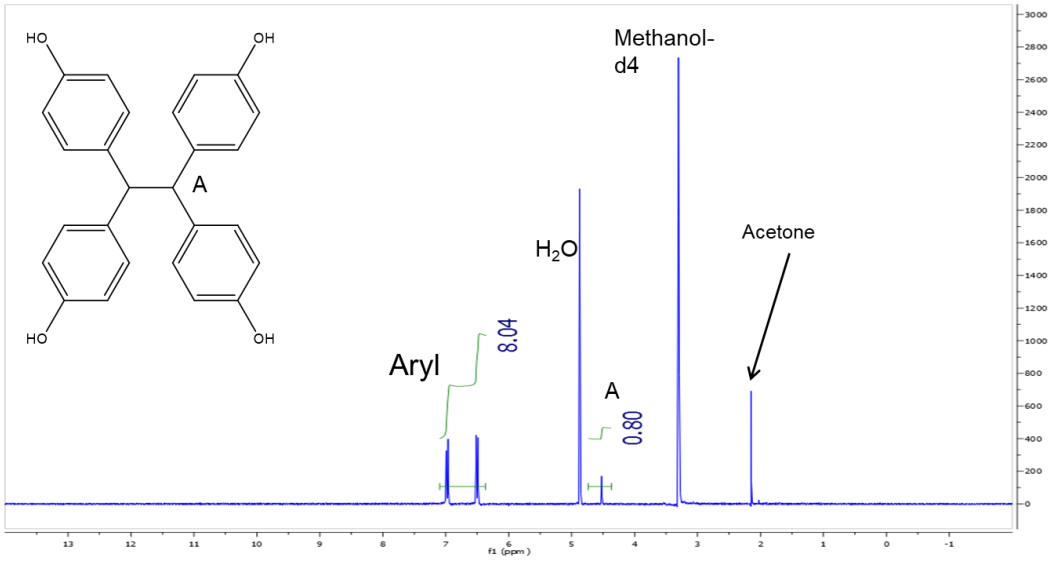

Figure 8.1. ^{1}H NMR spectrum of TPOE in methanol-d_4.

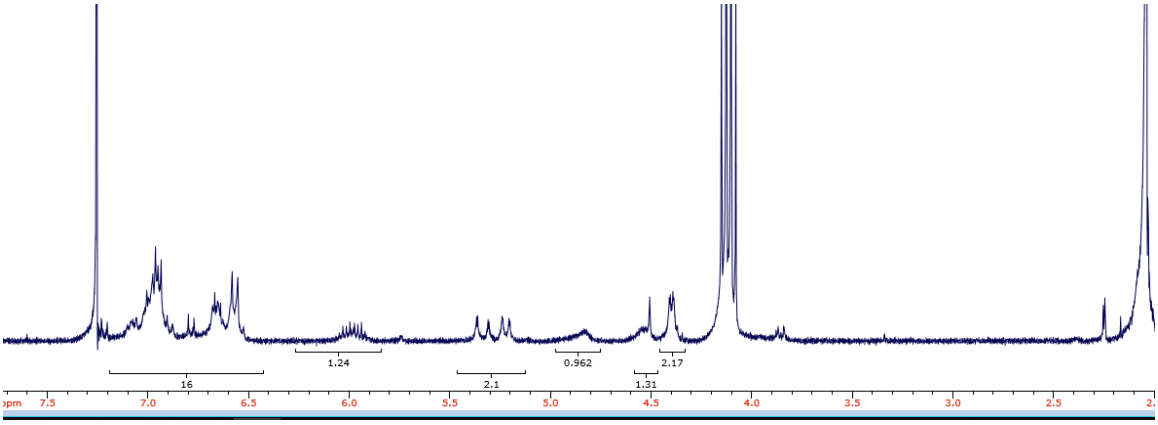

Figure 8.2 TPOE-1OAllyl.

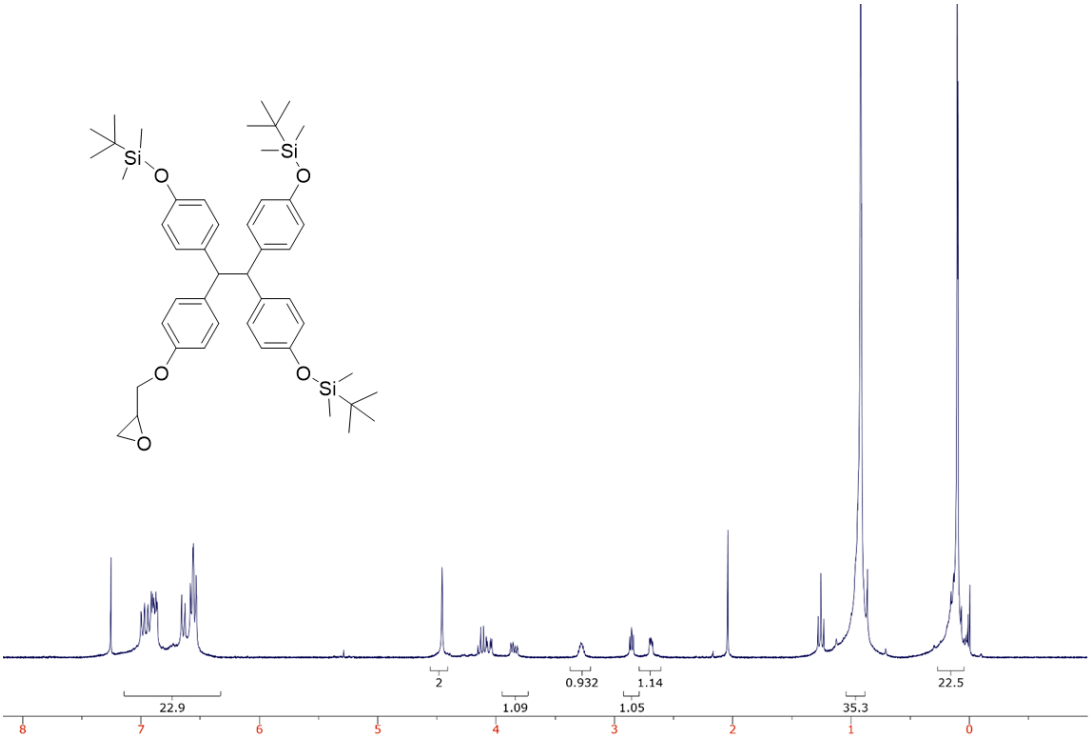

Figure 8.3. TPOE-1Ep-3TBS.

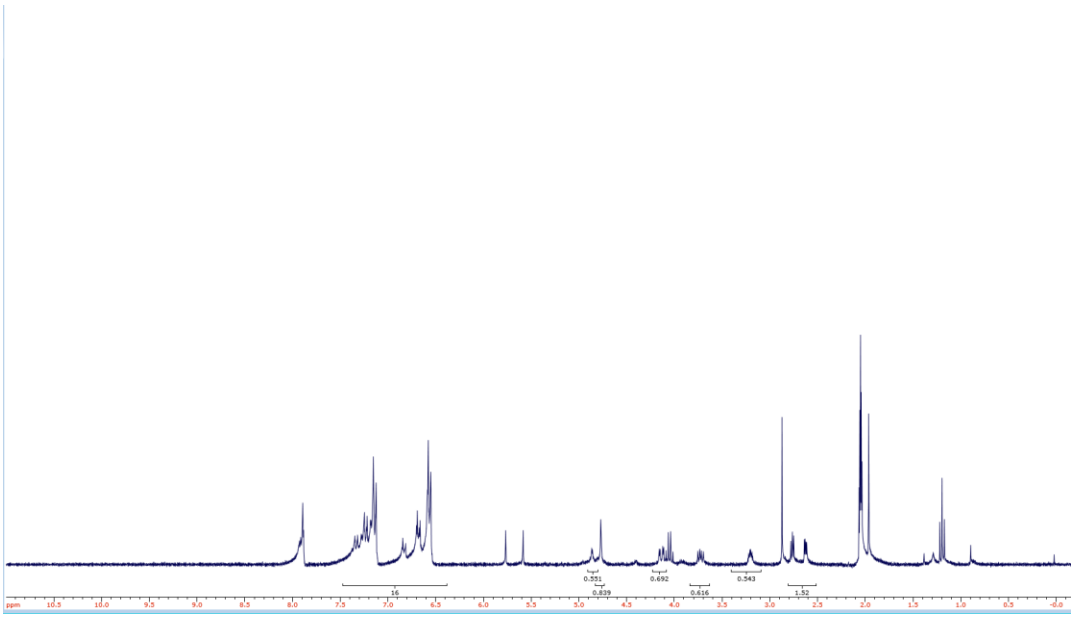

Figure 8.4 TPOE-1Ep.

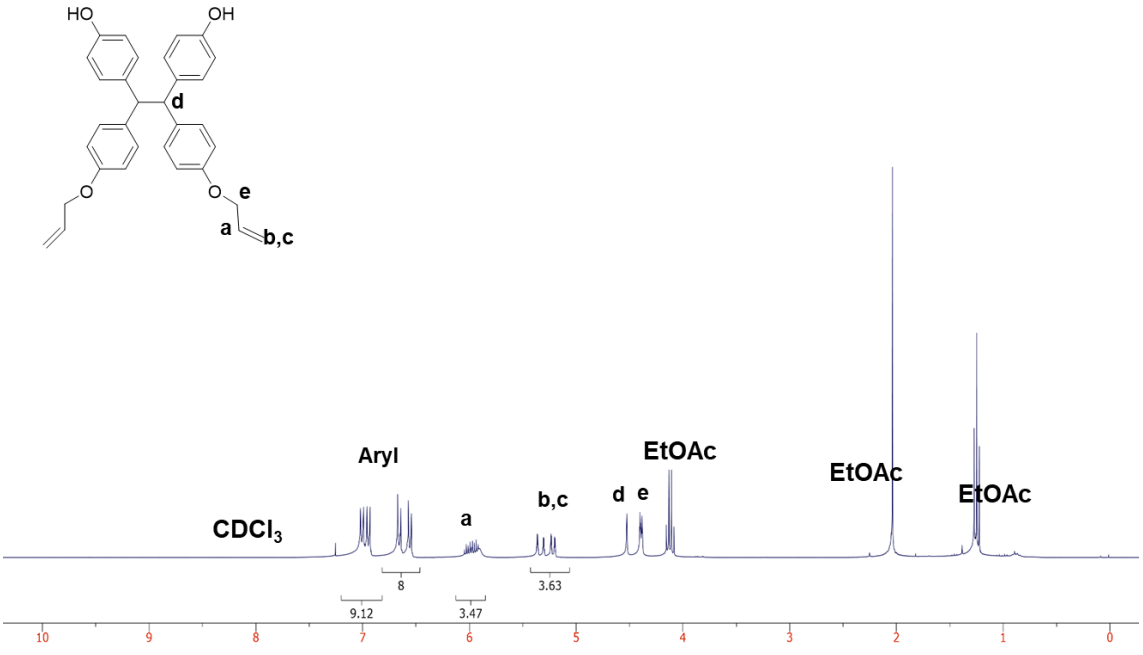

Figure 8.5 TPOE-2OAllyl.

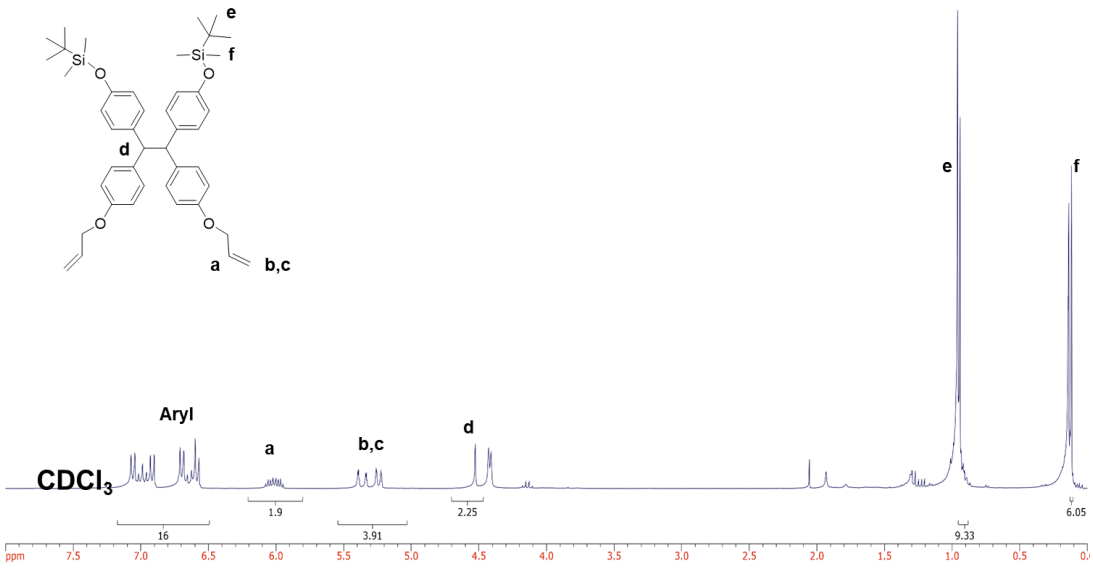

Figure 8.6 TPOE-2OAllyl-2TBS.

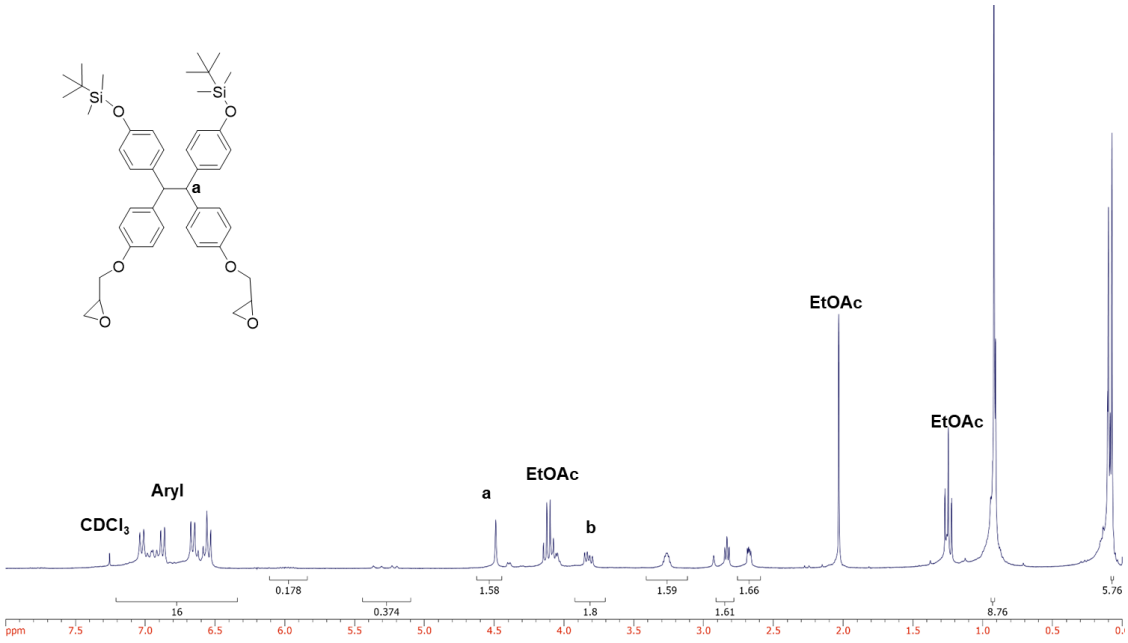

Figure 8.7 TPOE-2Ep-2TBS.

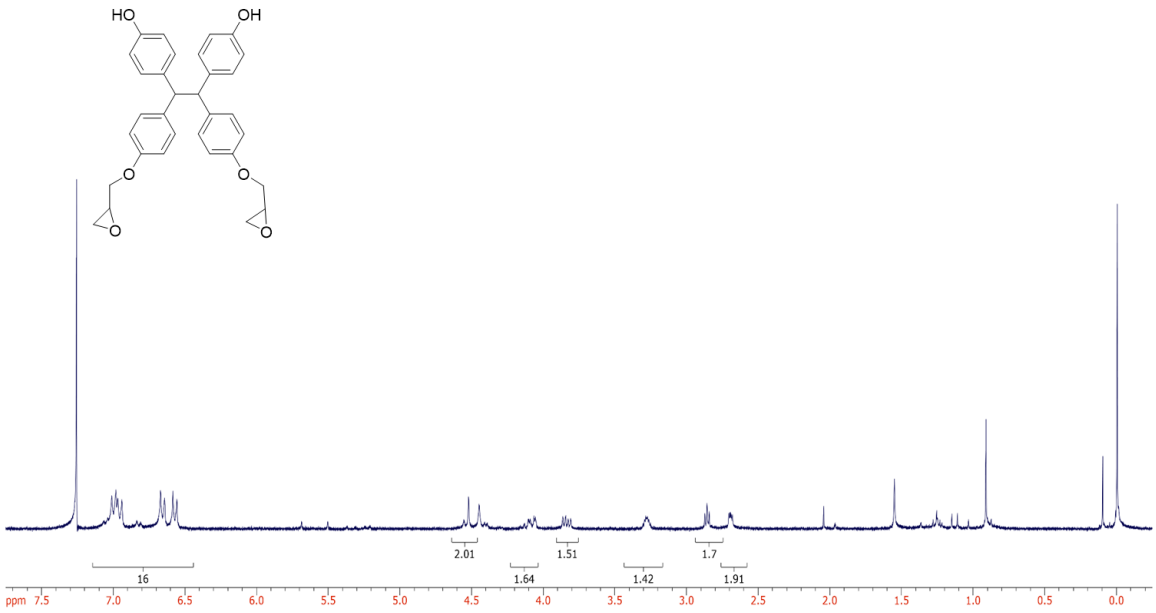

Figure 8.8 TPOE-2Ep.

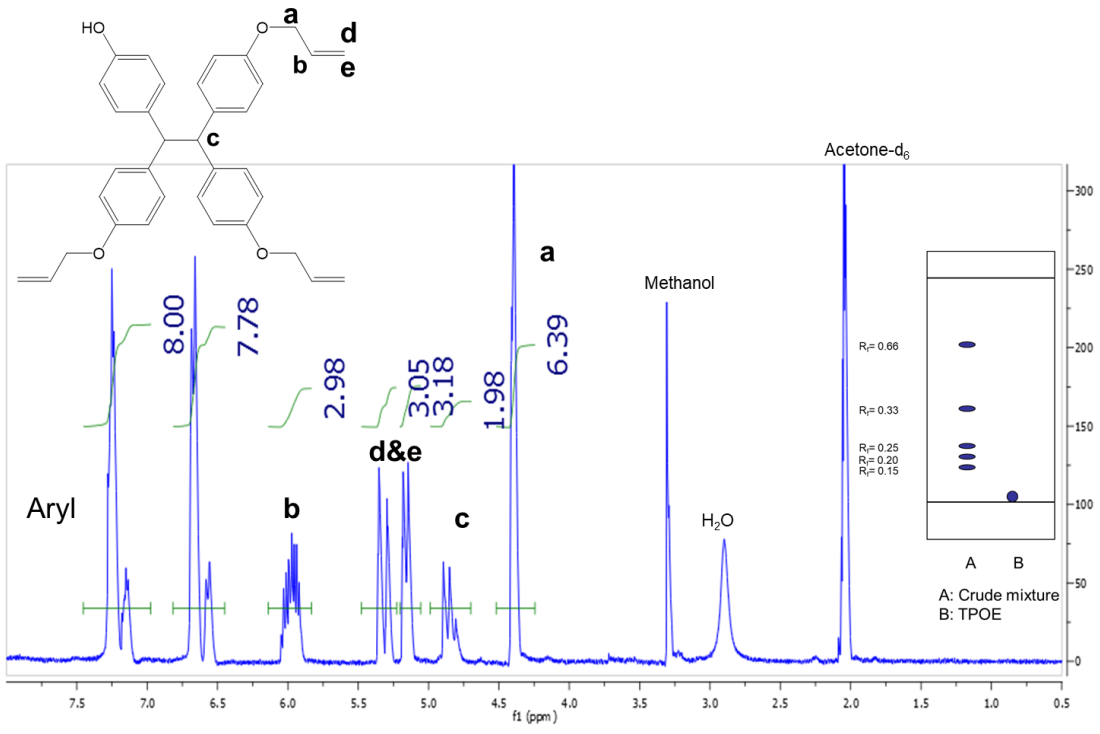

Figure 8.9 TPOE-3OAllyl, along with the TLC plate taken of the crude TPOE-OAllyl product prior to TPOE-3OAllyl separation using hexanes:ethyl acetate (3:2).

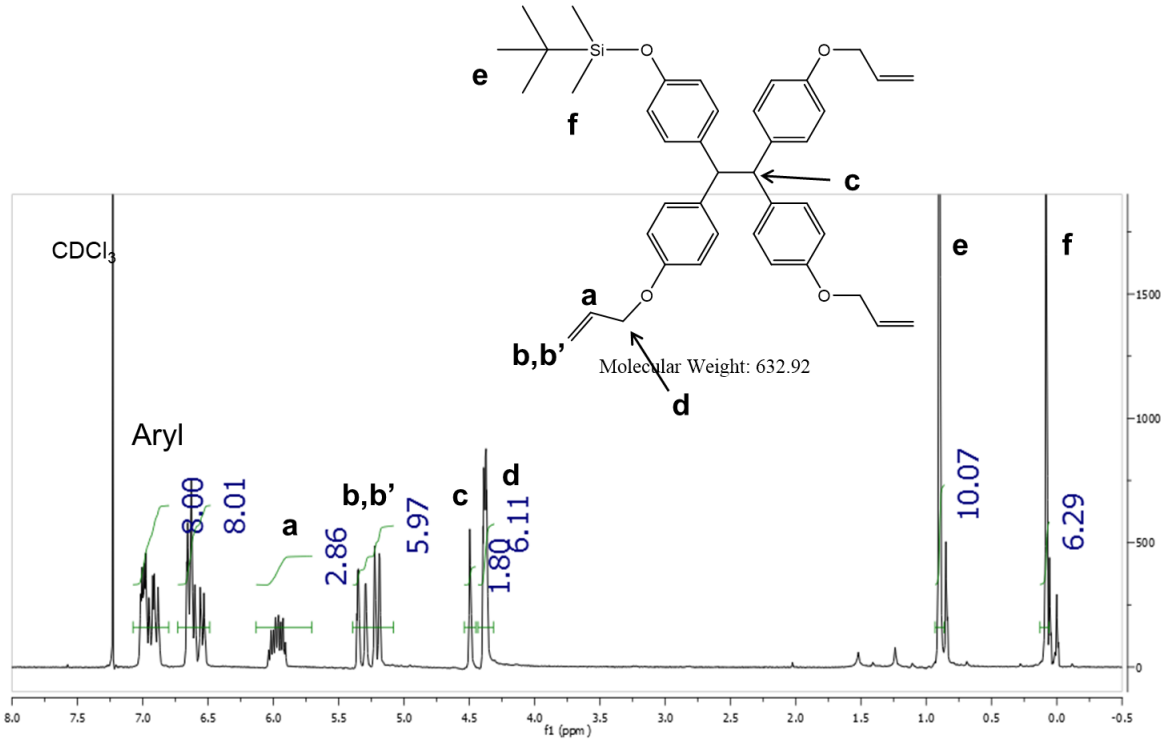

Figure 8.10 TPOE-3OAllyl-TBS.

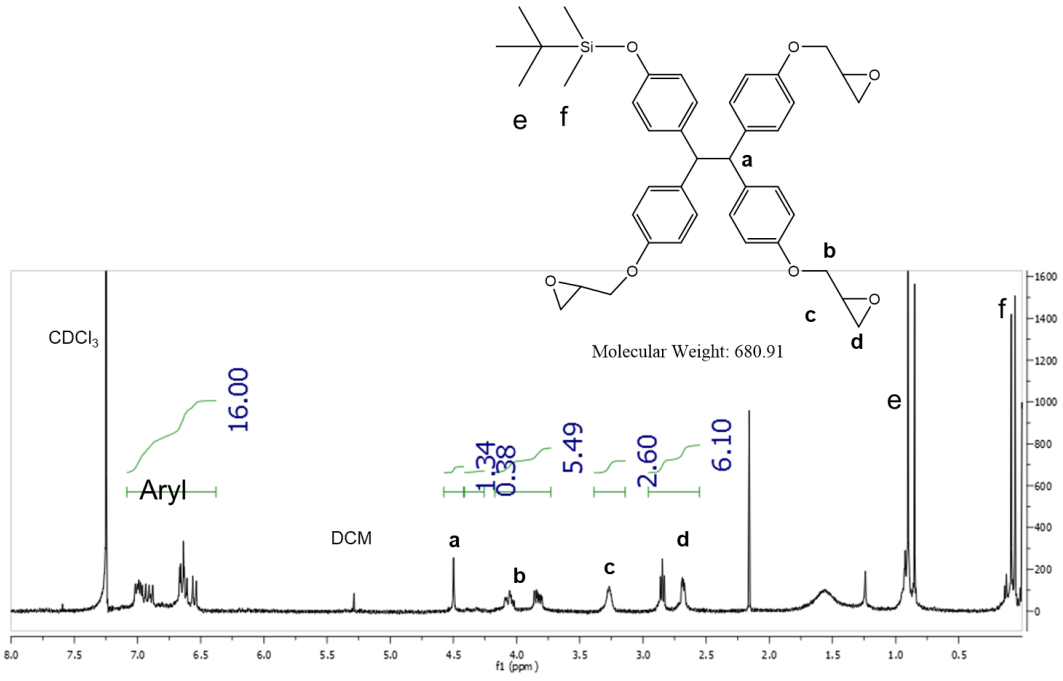

Figure 8.11 TPOE-3Ep-TBS.

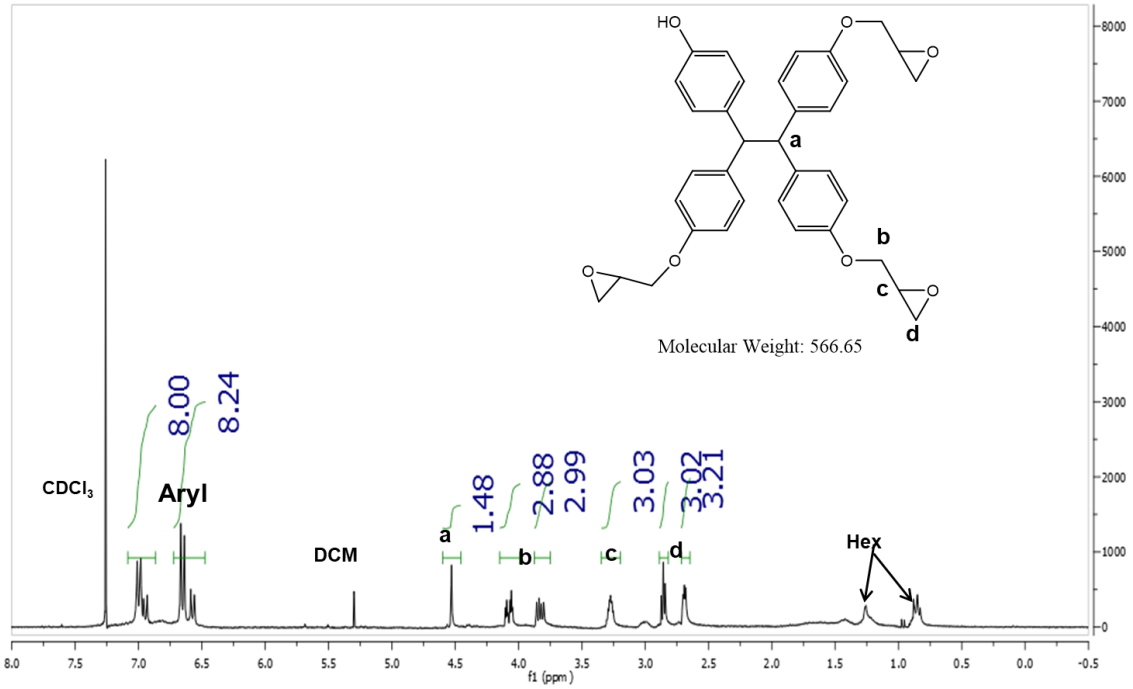

Figure 8.12 TPOE-3Ep.

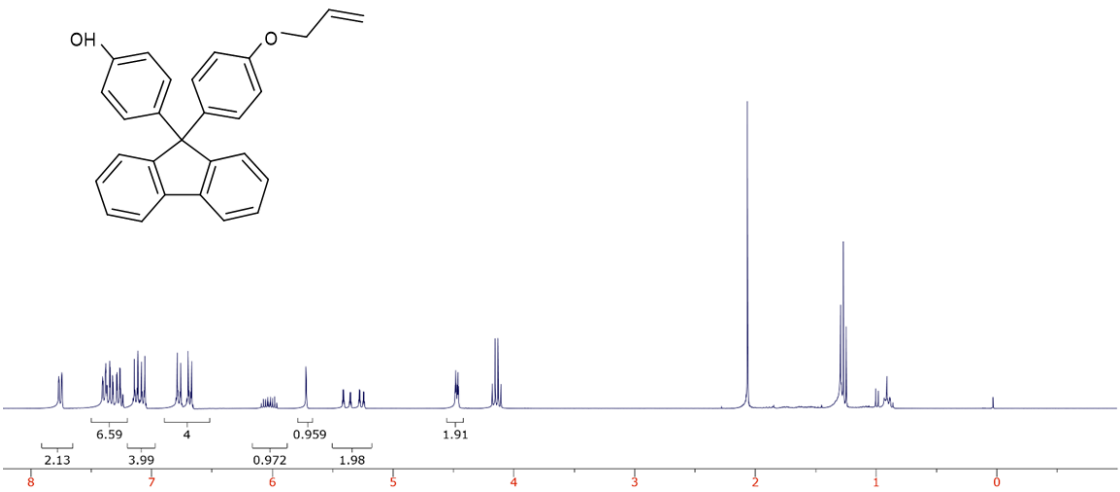

Figure 8.13 BHPF-1OAllyl.

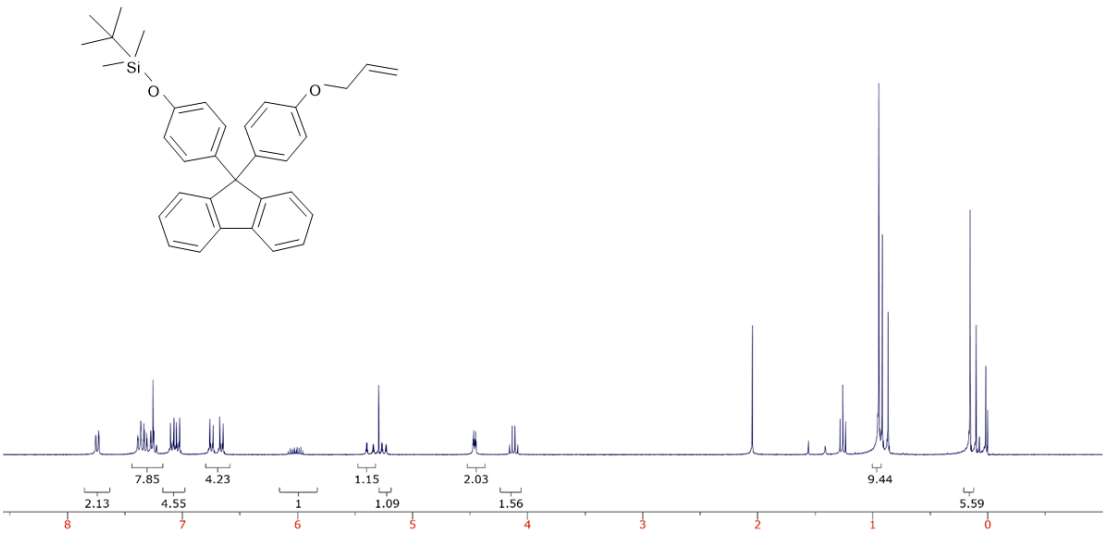

Figure 8.14 BHPF-1OAllyl-TBS.

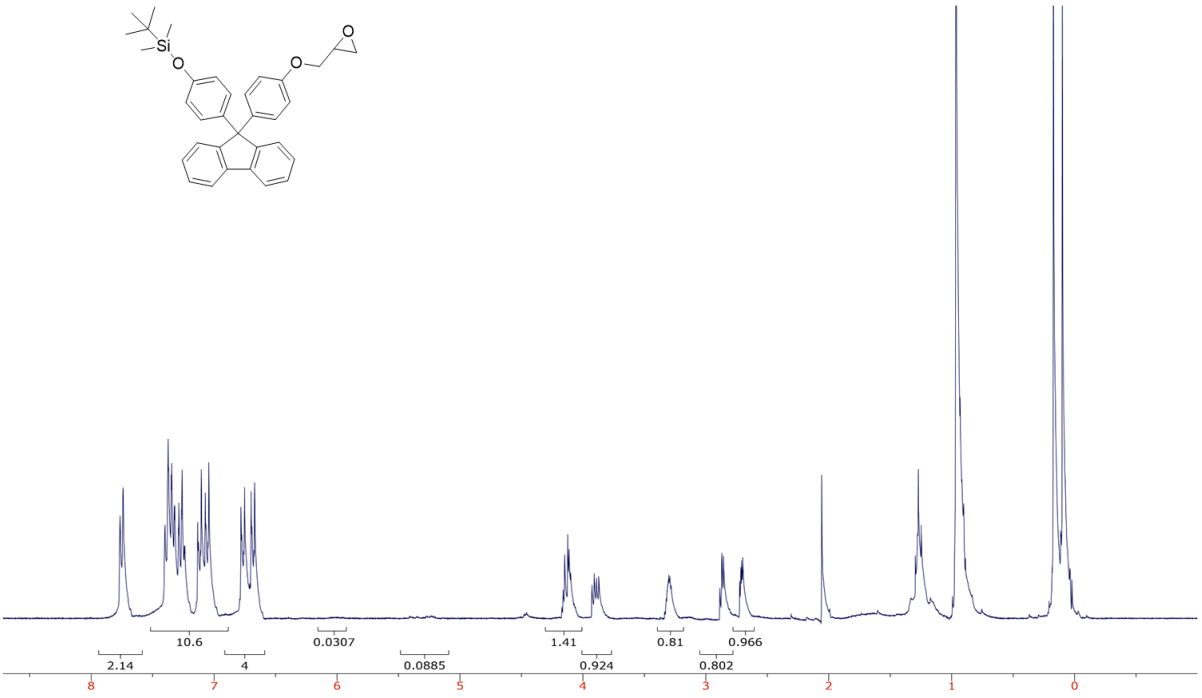

Figure 8.15 BHPF-1Ep-TBS.

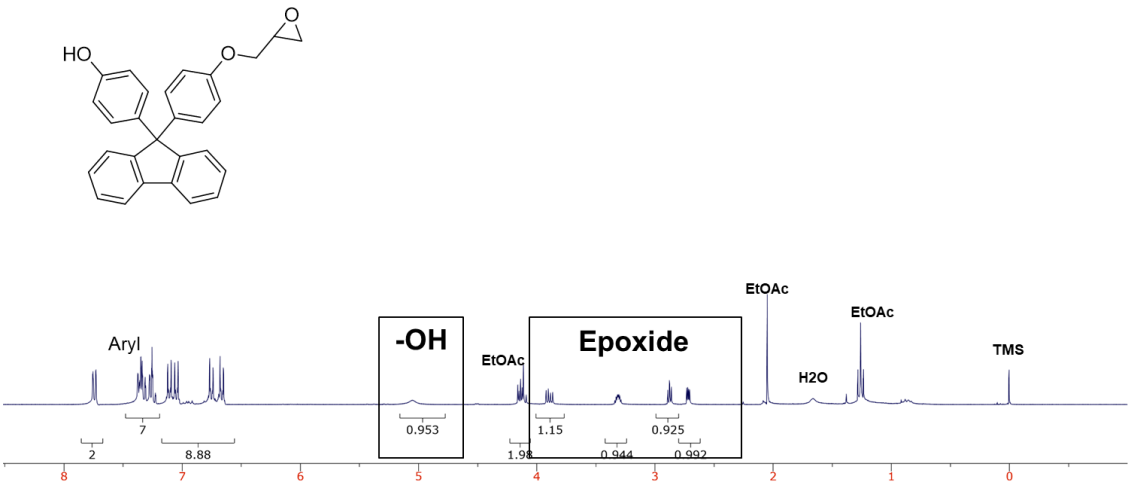

Figure 8.16 BHPF-1Ep.

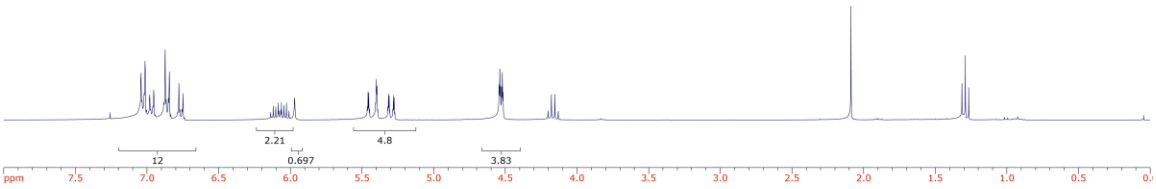

Figure 8.17 THPE-2OAllyl.

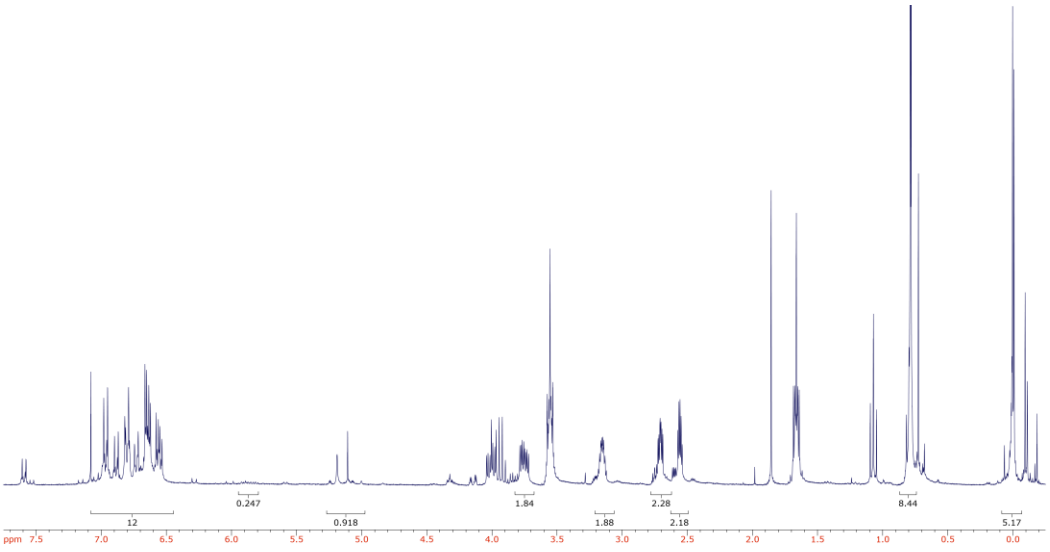

Figure 8.18 THPE-2Ep-TBS.

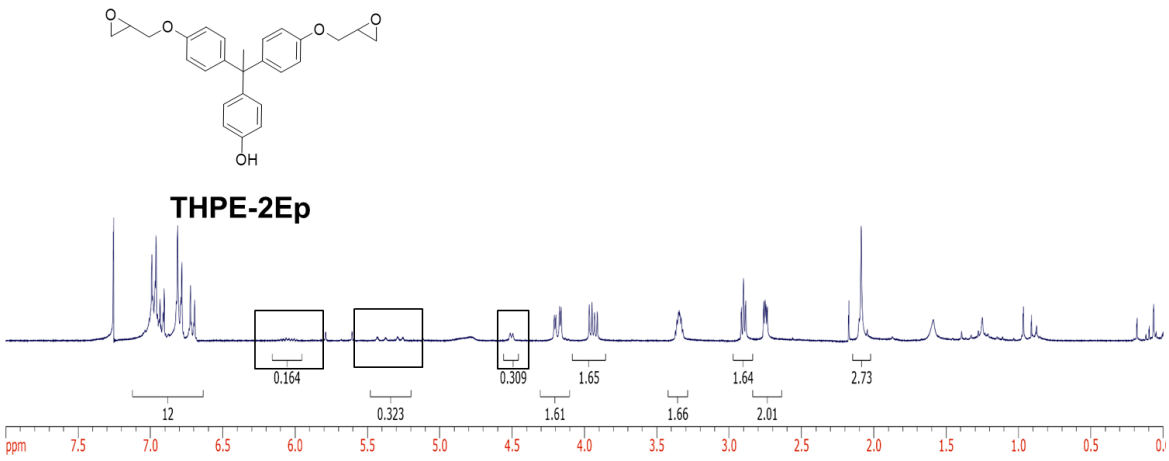

Figure 8.19 THPE-2Ep. A small amount of alkenes is still present.

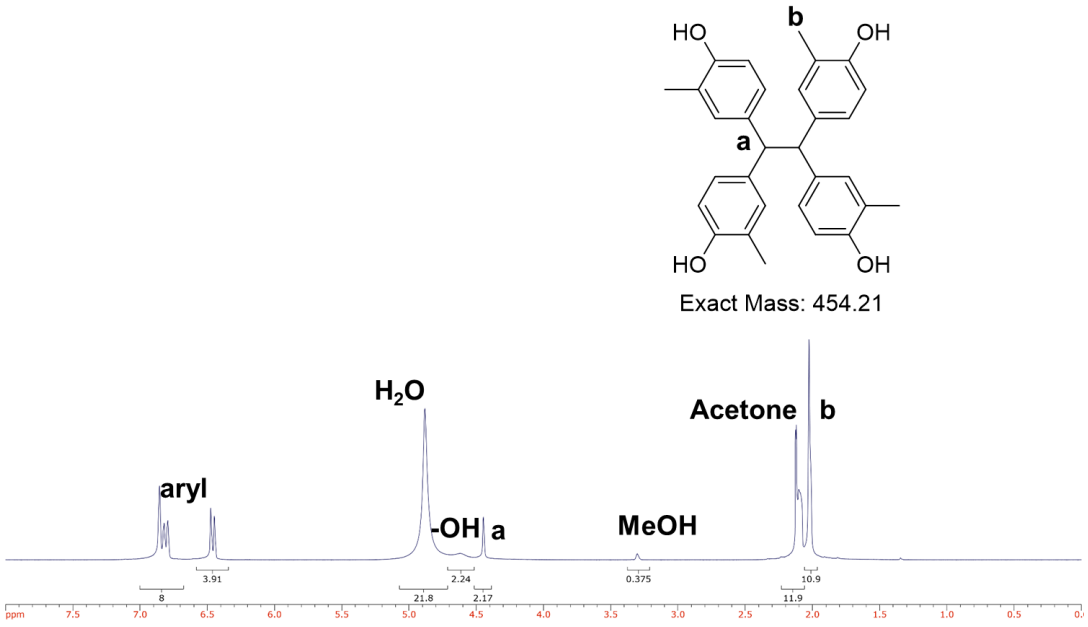

Figure 8.20 TMPOE in methanol-d_4.

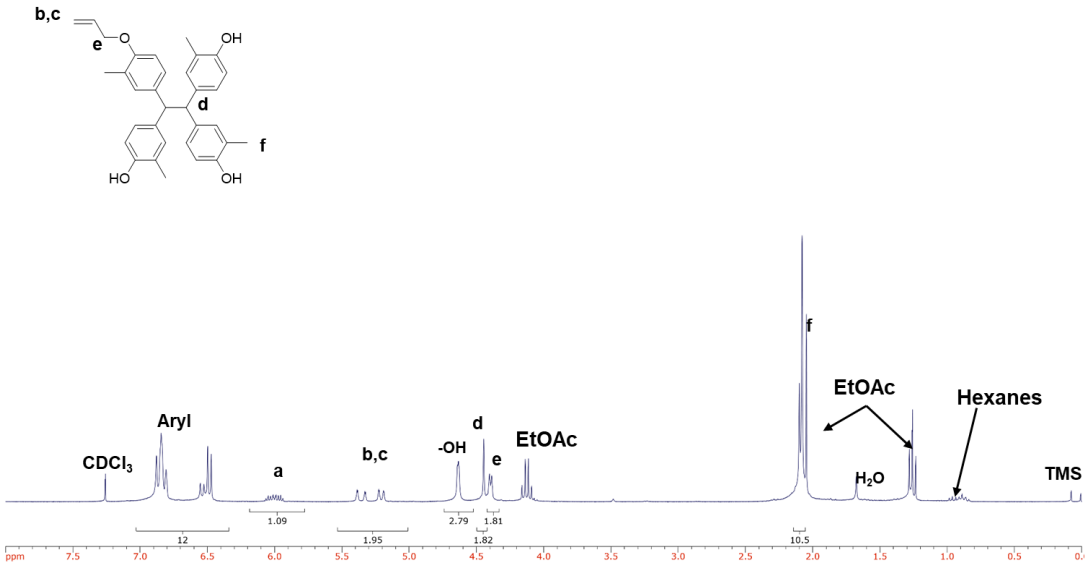

Figure 8.21 TMPOE-1OAllyl.

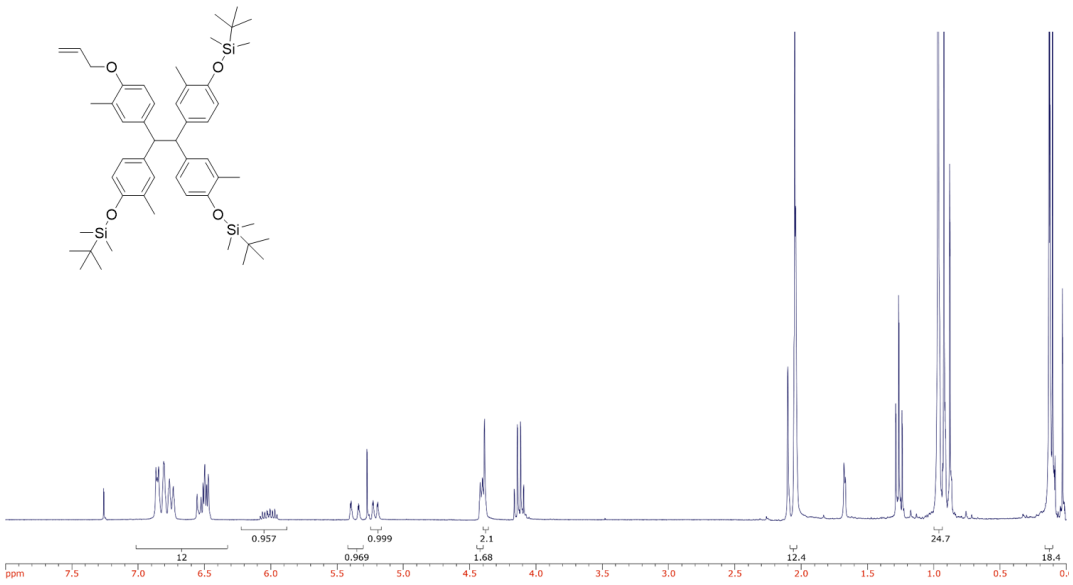

Figure 8.22 TMPOE-1OAllyl-3TBS.

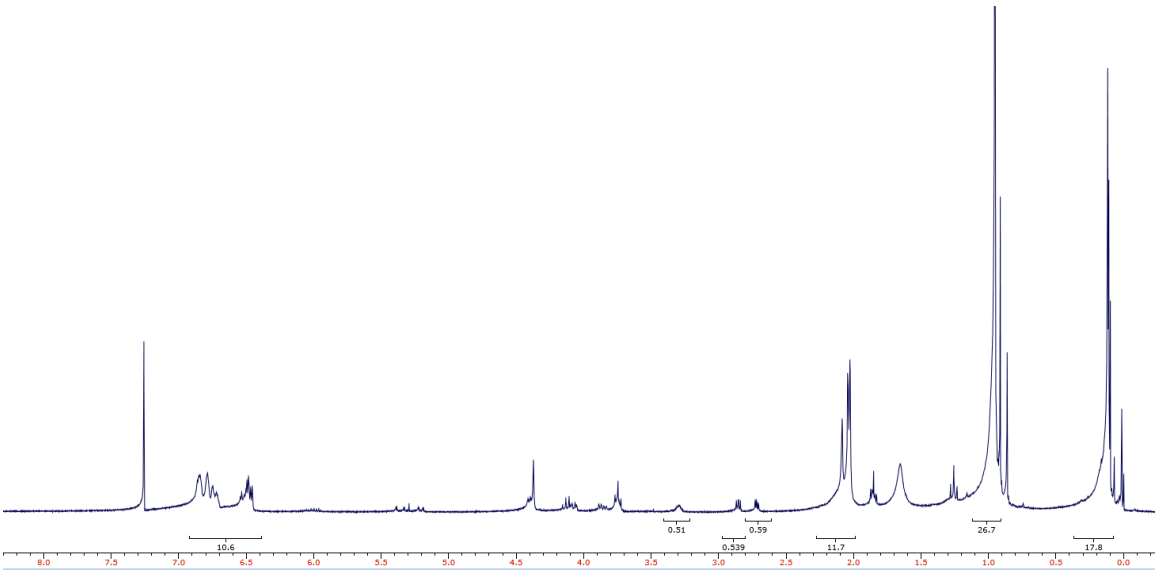

Figure 8.23 TMPOE-1Ep-3TBS.

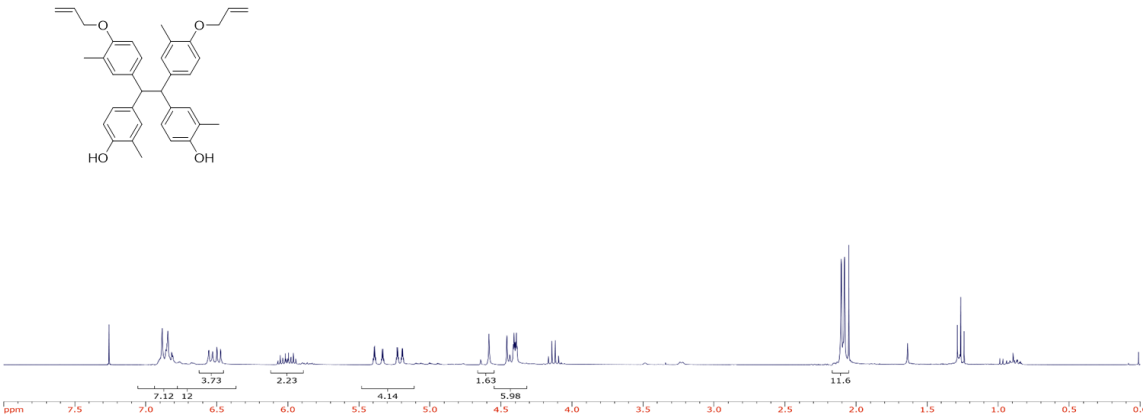

Figure 8.24 TMPOE-2OAllyl.

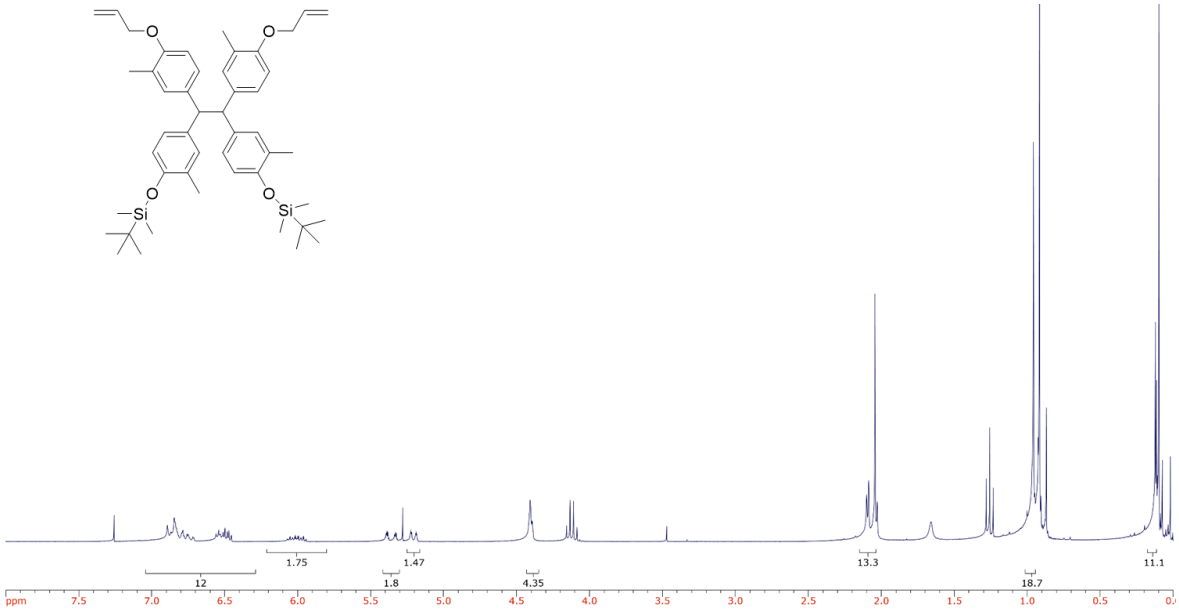

Figure 8.25 TMPOE-2OAllyl-2TBS.

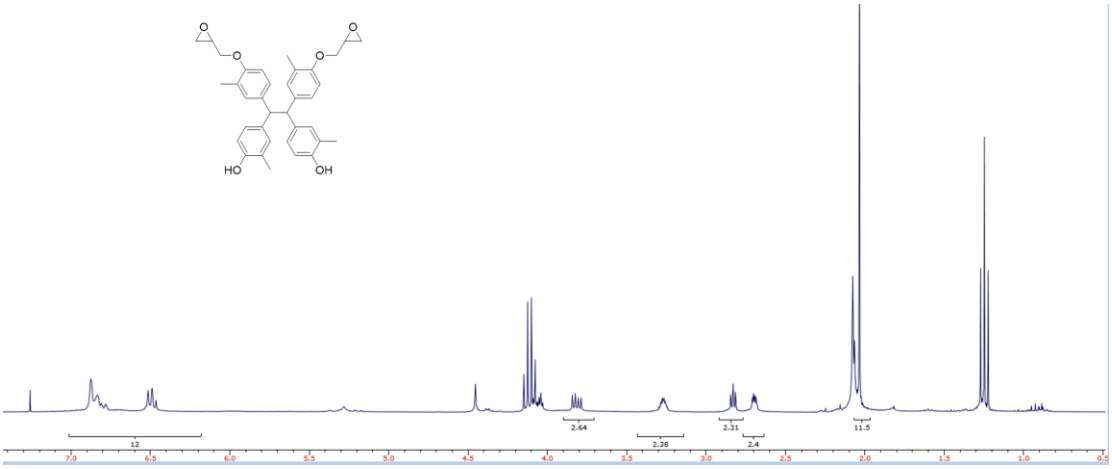

Figure 8.26 TMPOE-2Ep.

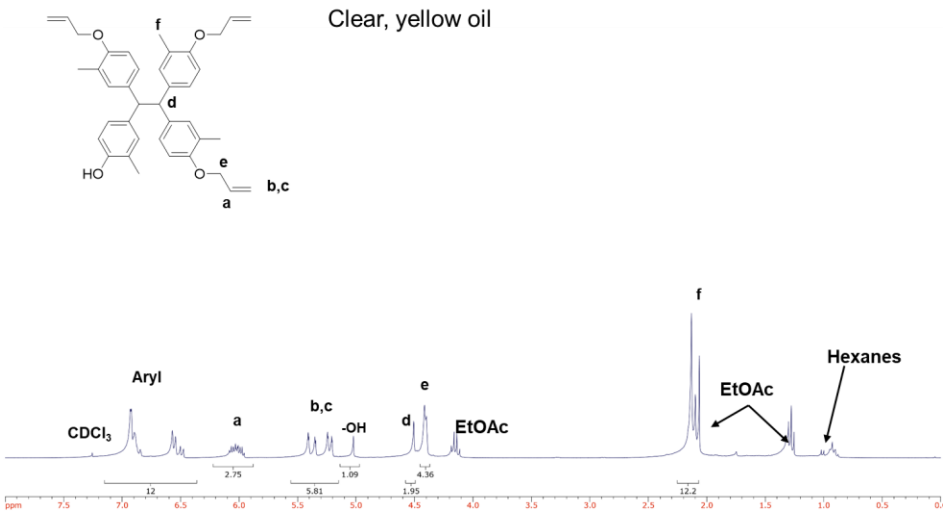

Figure 8.27 TMPOE-3OAllyl.

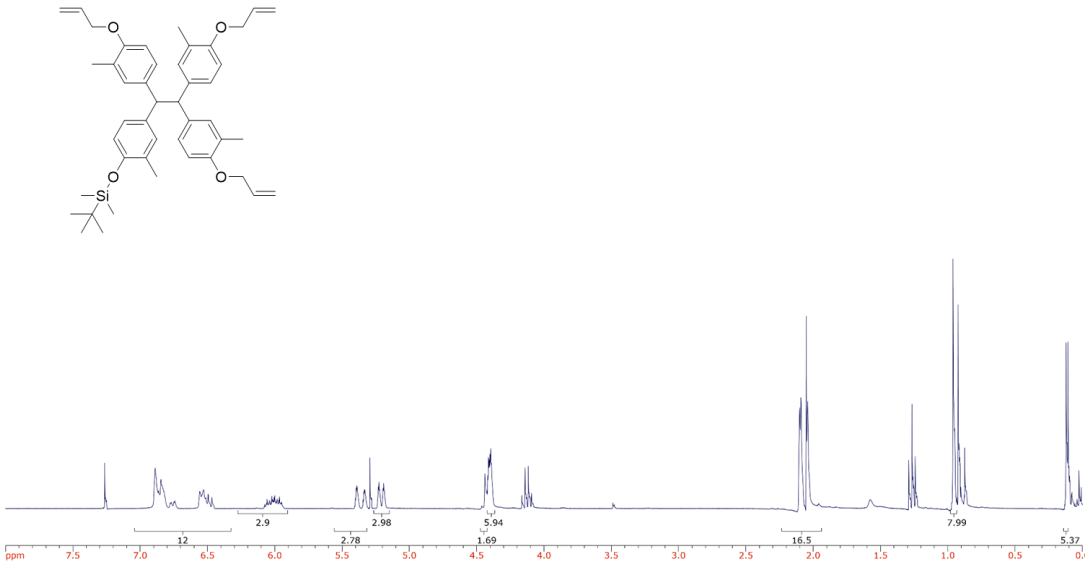

Figure 8.28 TMPOE-3OAllyl-TBS.

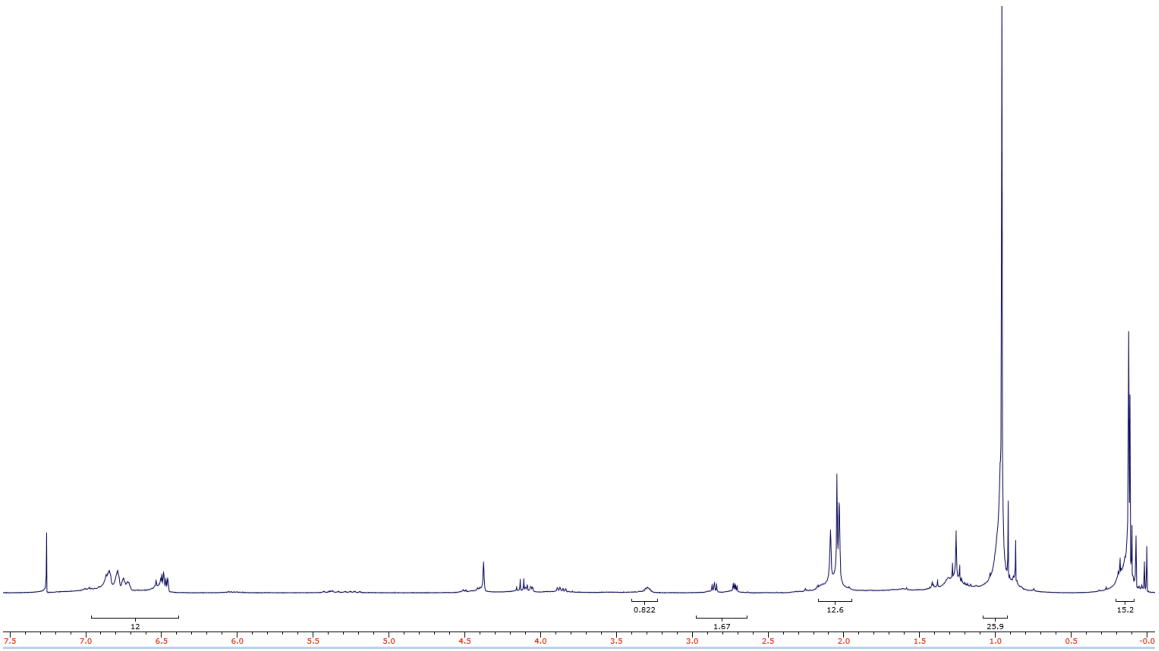

Figure 8.29 TMPOE-1Ep-3TBS.

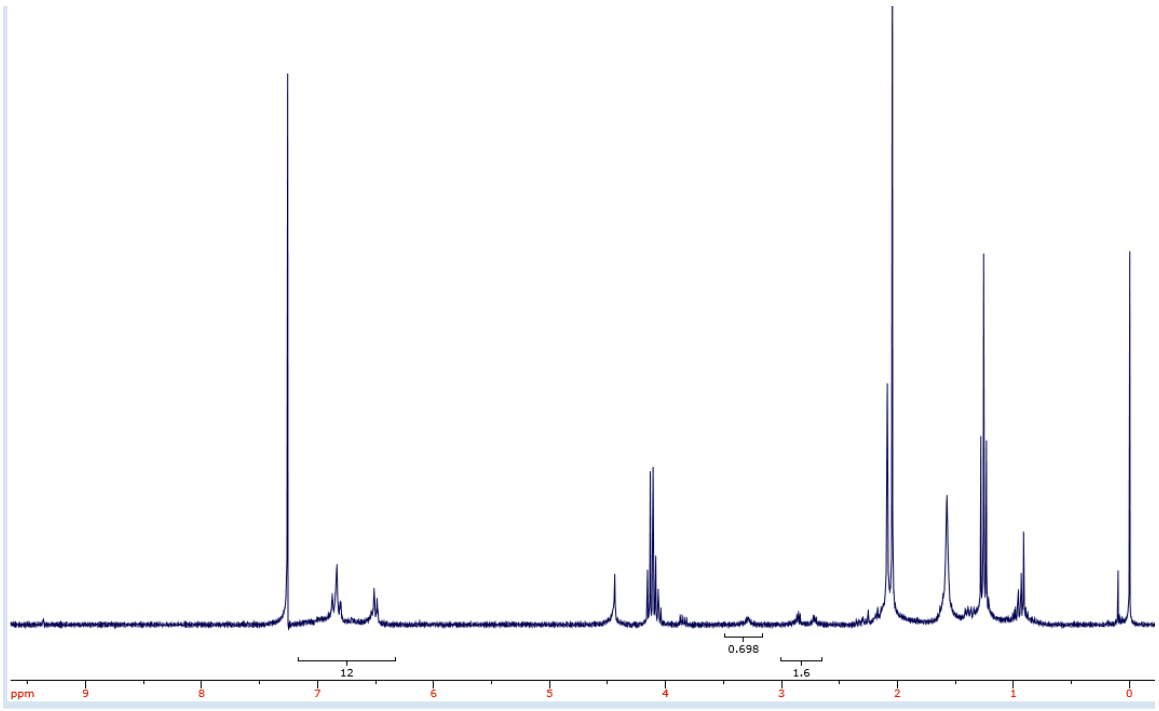

Figure 8.30 TMPOE-1Ep in $CDCl_3$.

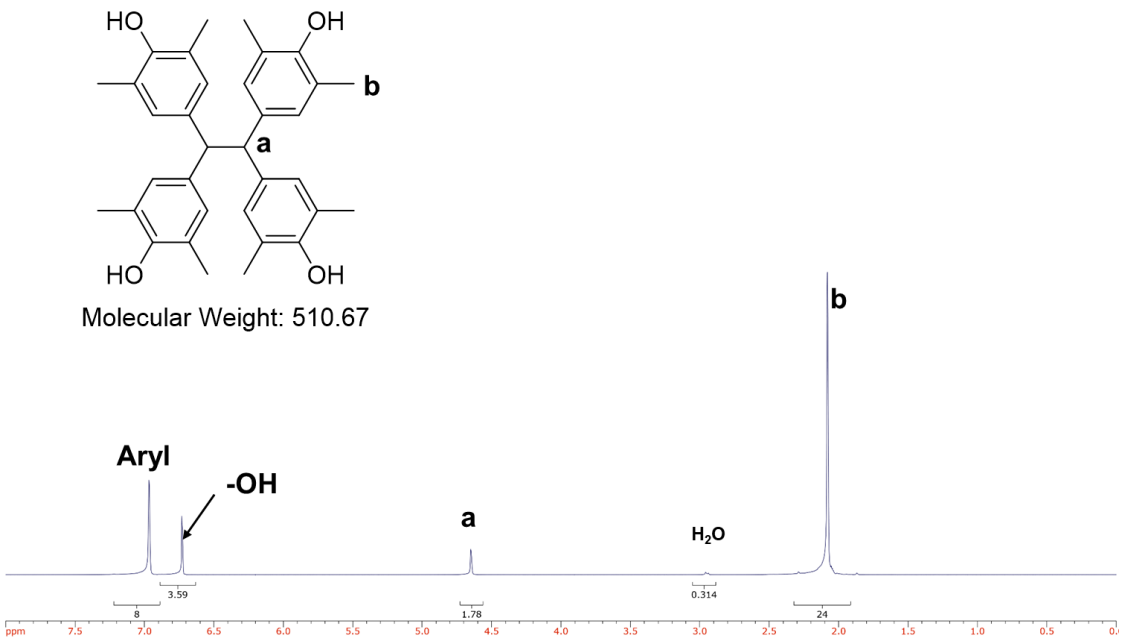

Figure 8.31 TDMPOE in acetone-d_6. Anal. Calcd for $C_{34}H_{38}O_4$: C, 79.97; H, 7.50. Found: C, 79.95; H, 7.36.

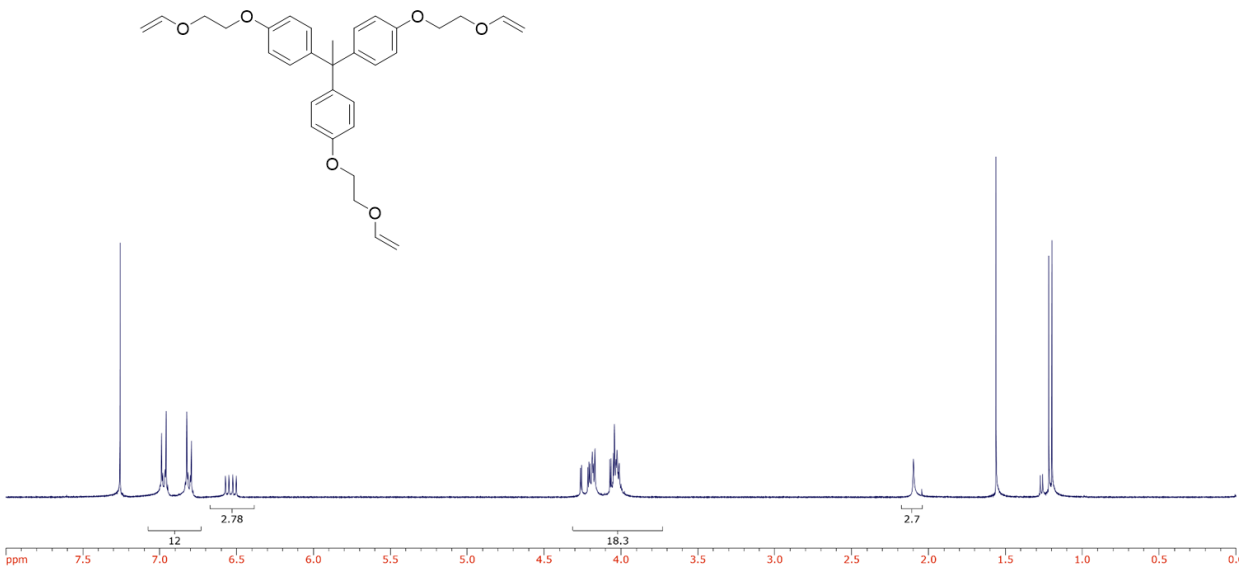

Figure 8.32 THPE-3VE.

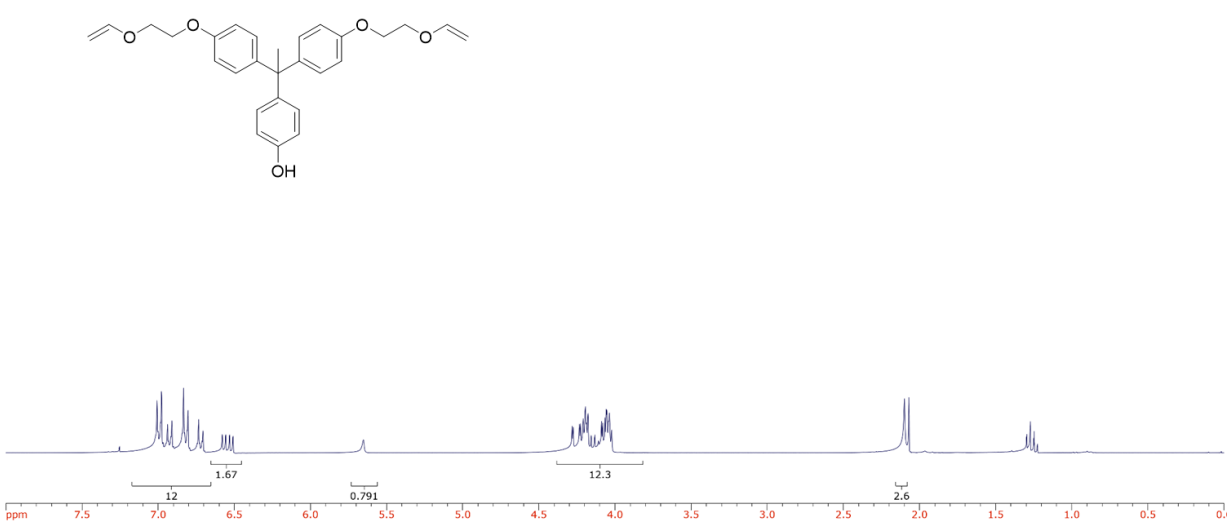

Figure 8.33 THPE-2VE.

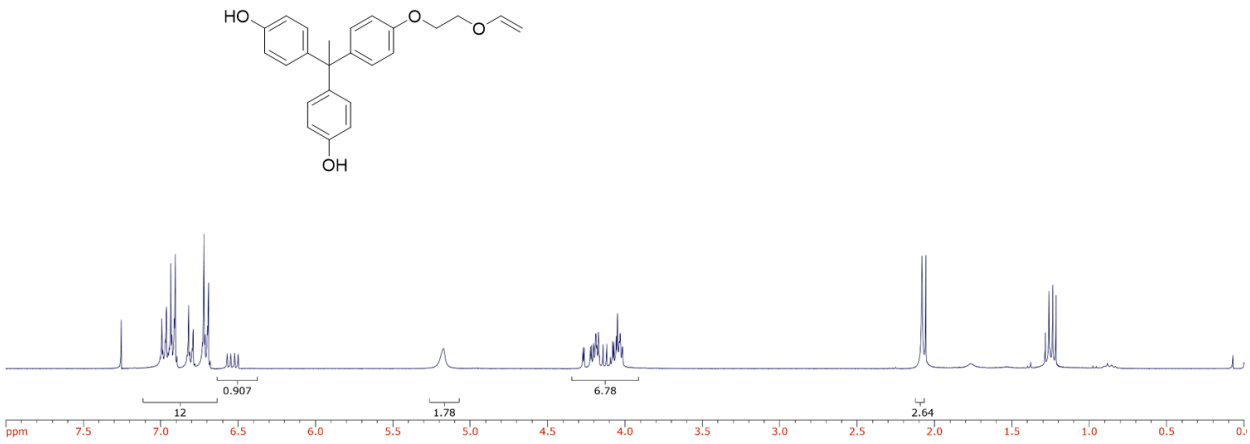

Figure 8.34 THPE-1VE.

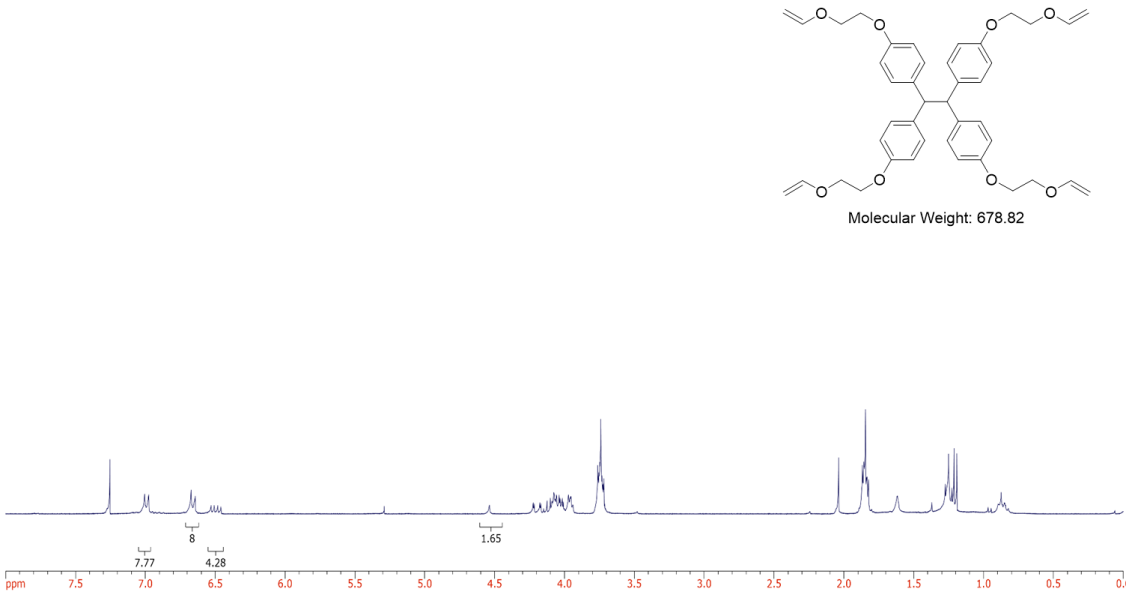

Figure 8.35 TPOE-4VE.

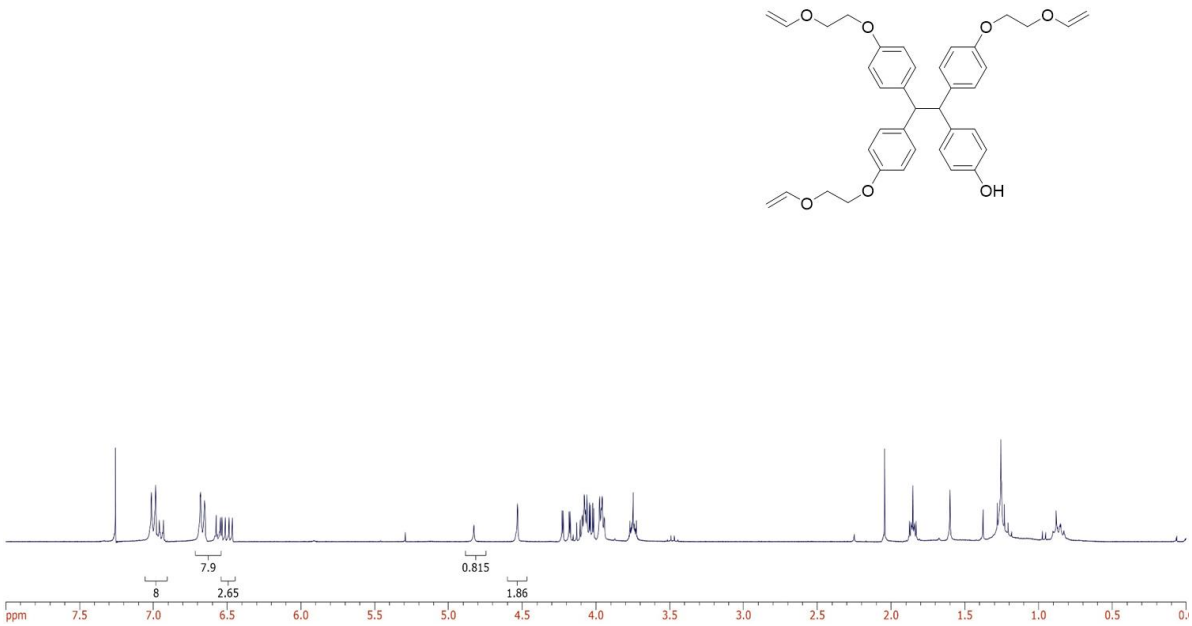

Figure 8.36 TPOE-3VE.

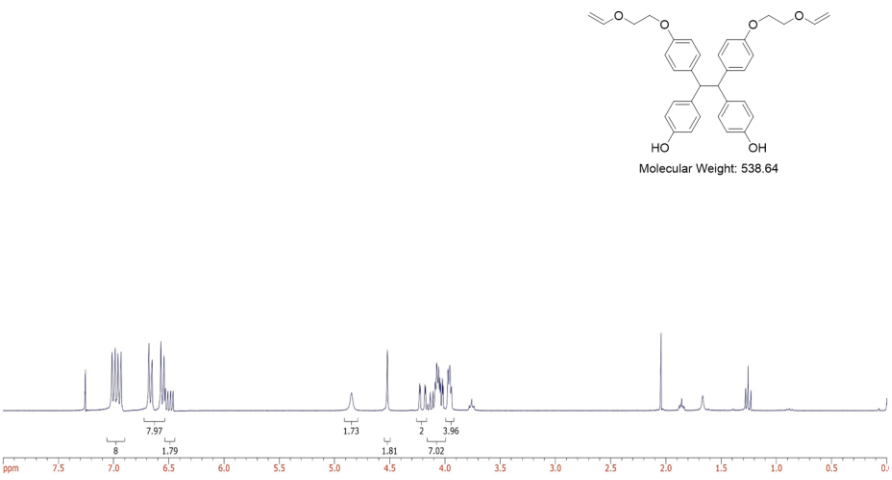

Figure 8.37 TPOE-2VE.

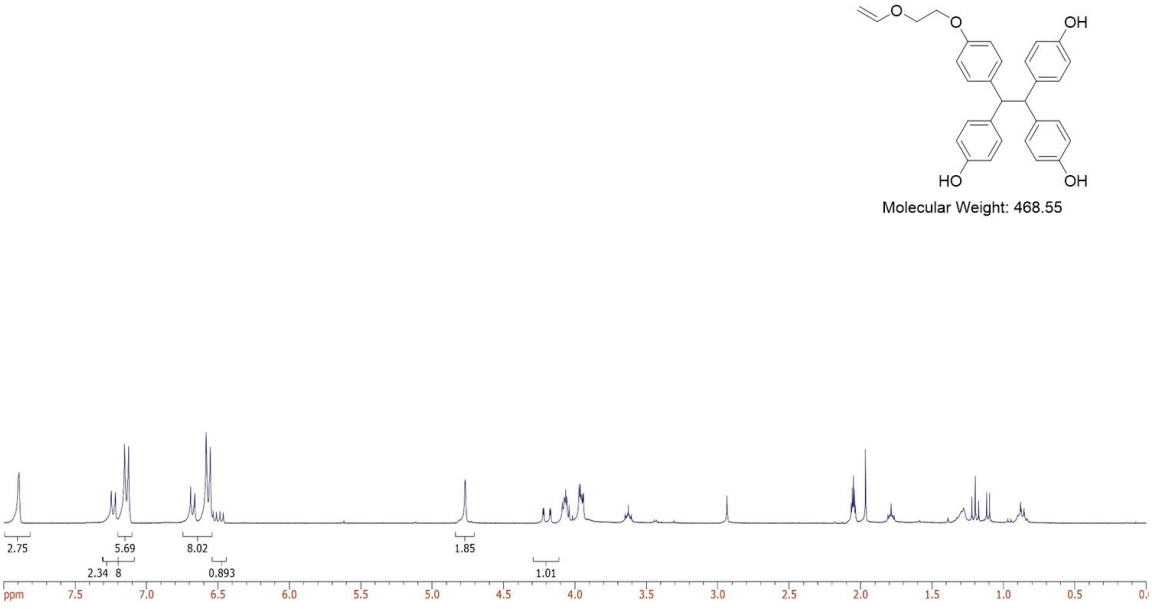

Figure 8.38 TPOE-1VE in acetone-d_6.

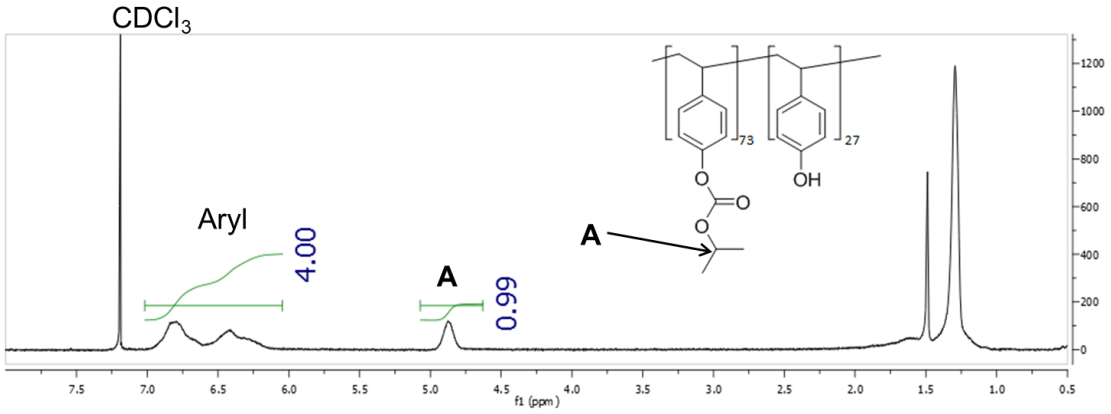

Figure 8.39 PHOST-*r*-iPOC.

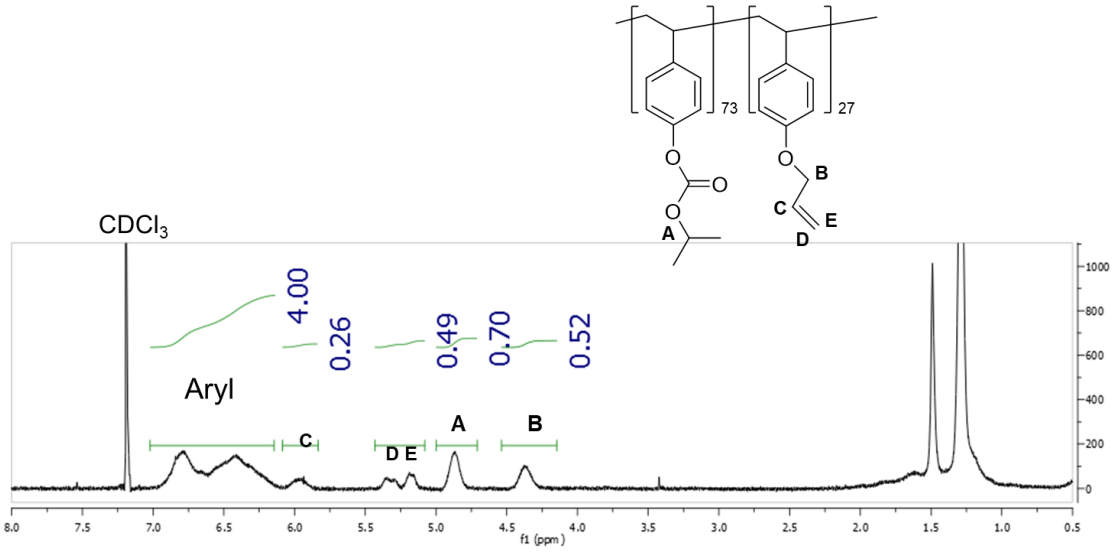

Figure 8.40 iPOC-*r*-Allyl.

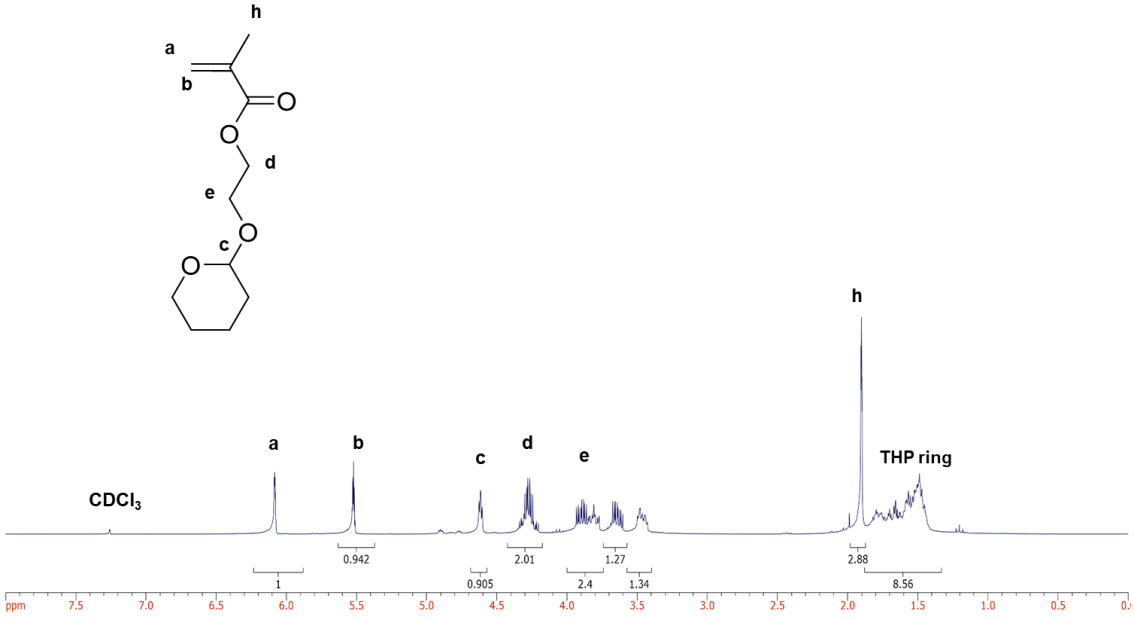

Figure 8.41 HEMA-THP.

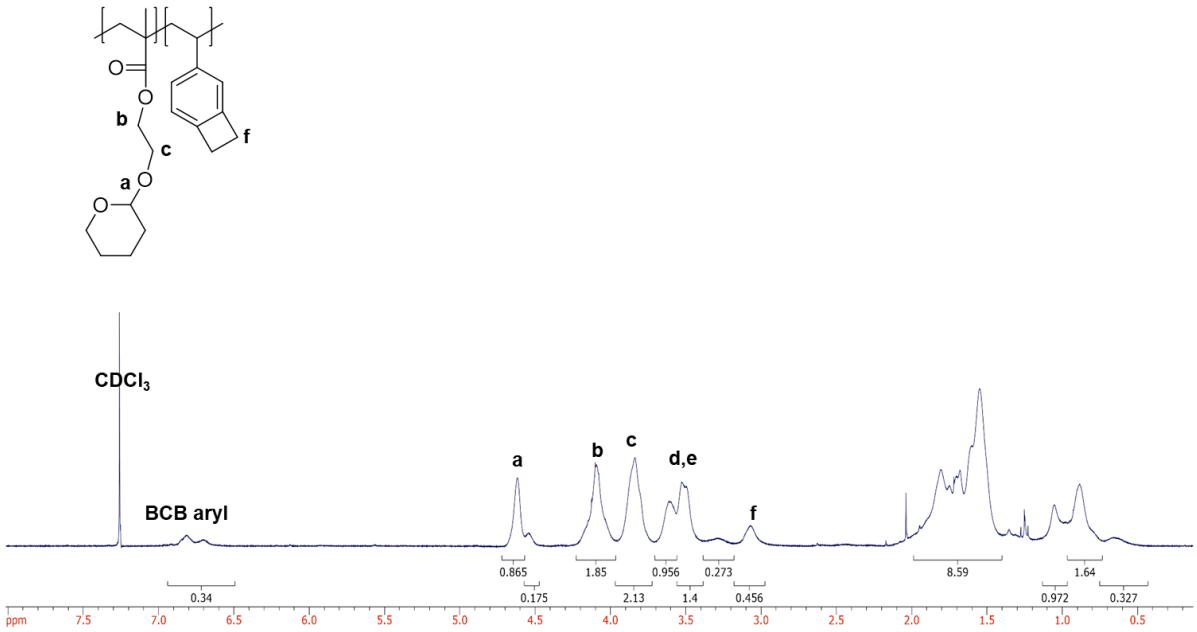

Figure 8.42 PHEMA-*r*-BCB.

8.2 Mass Spectra

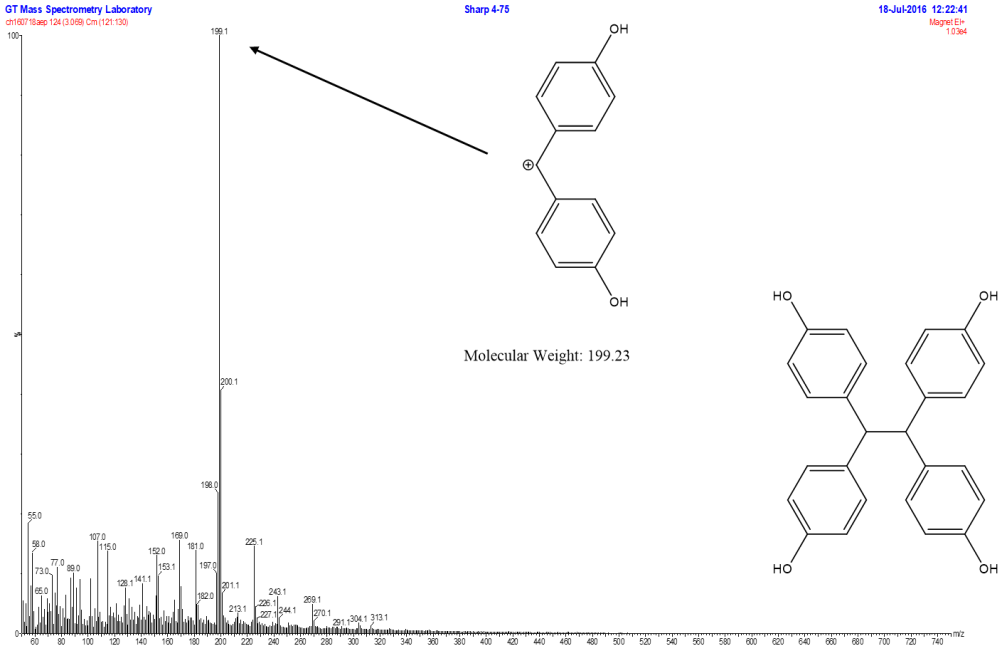

Figure 8.43 TPOE EI mass spectrum.

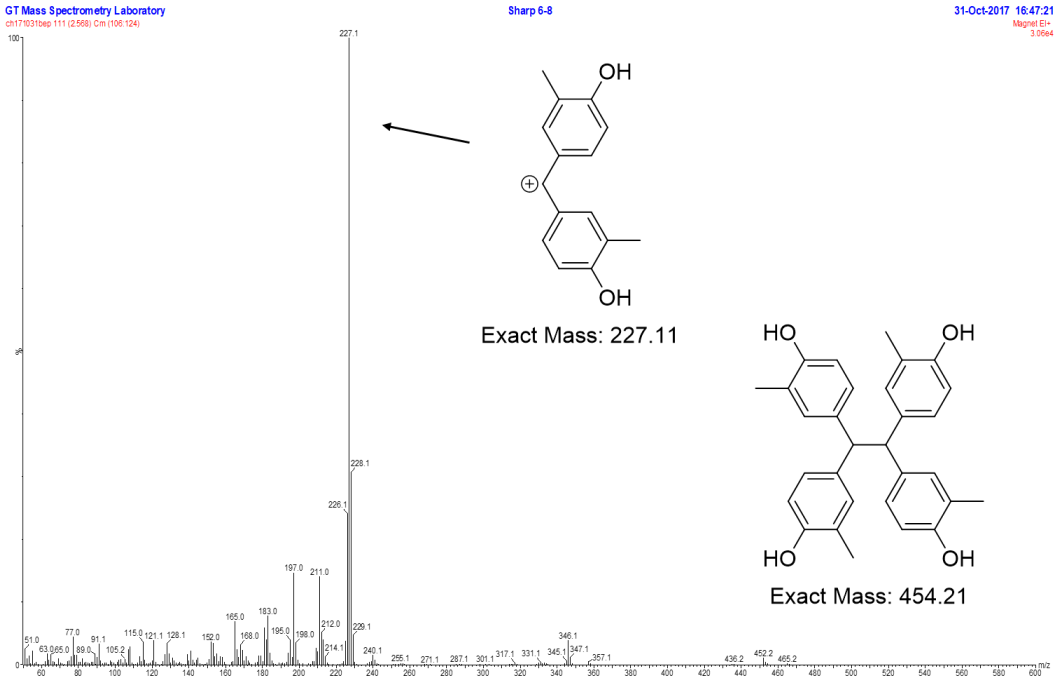

Figure 8.44 TMPOE EI mass spectrum.

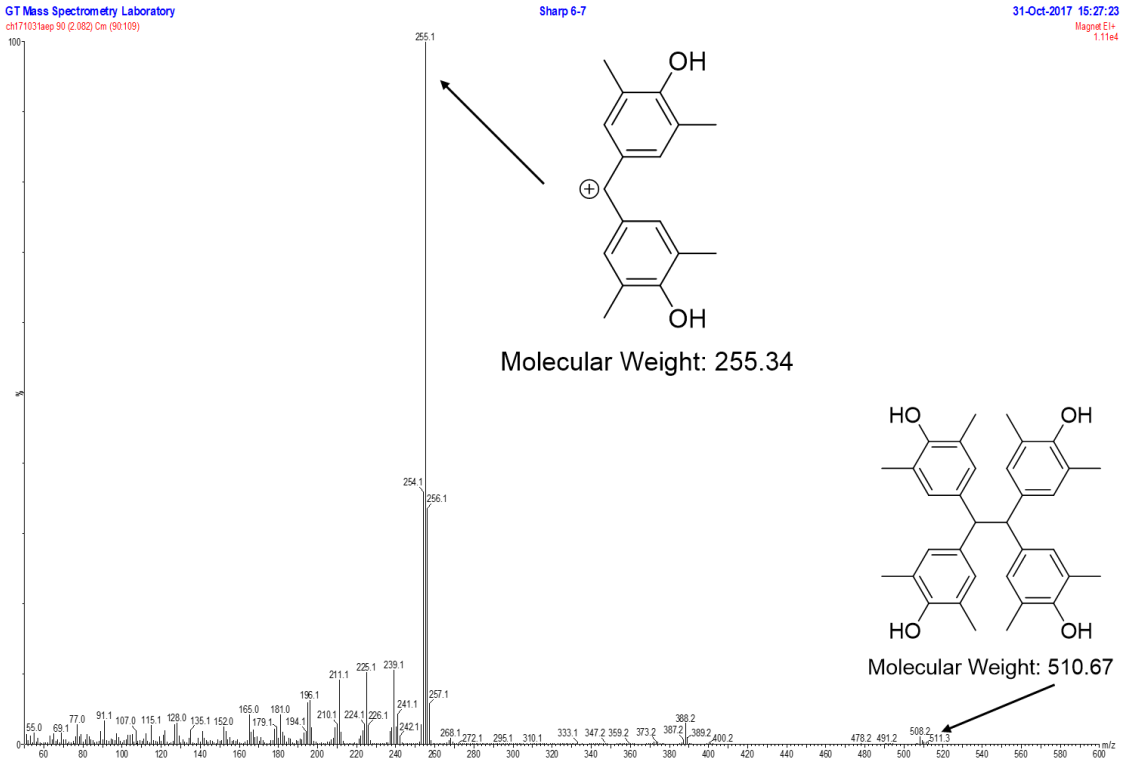

Figure 8.45 EI Mass spectrum of TDMPOE.

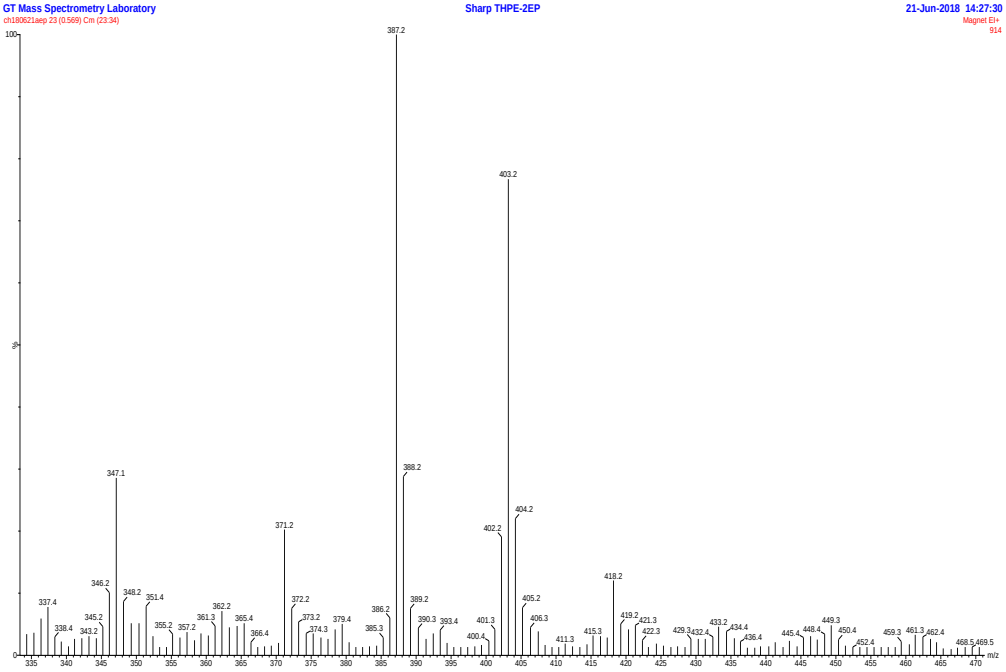

Figure 8.46 EI Mass spectrum of THPE-2Ep.

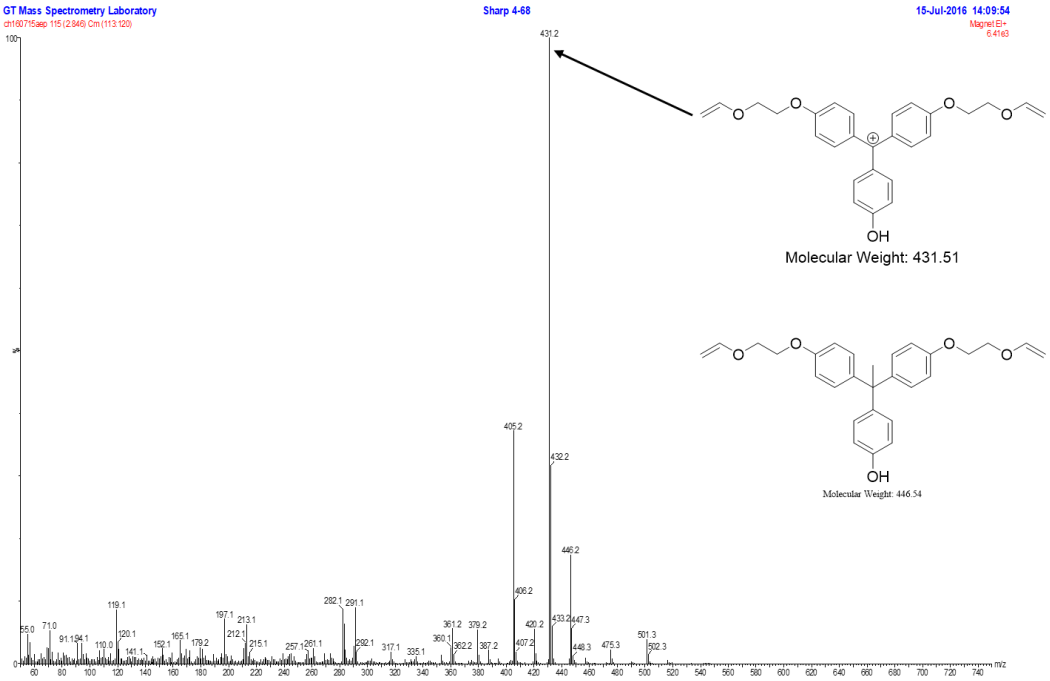

Elemental Composition Report

Single Mass Analysis

Tolerance = 5.0 PPM / DBE: min = -5.5, max = 300.0

Selected filters: None

Monoisotopic Mass, Odd and Even Electron Ions

30 formula(e) evaluated with 1 results within limits (all results (up to 1000) for each mass)

Elements Used:

C: 0-500 H: 0-1000 O: 3-7

Minimum:				-5.5	
Maximum:		5.0	5.0	300.0	
Mass	Calc. Mass	mDa	PPM	DBE	Formula
446.2089	446.2093	-0.4	-0.9	14.0	C28 H30 O5

Figure 8.47 (top) EI mass spectrum of THPE-2VE and (bottom) its exact mass from EI MS.

8.3 TGA Traces

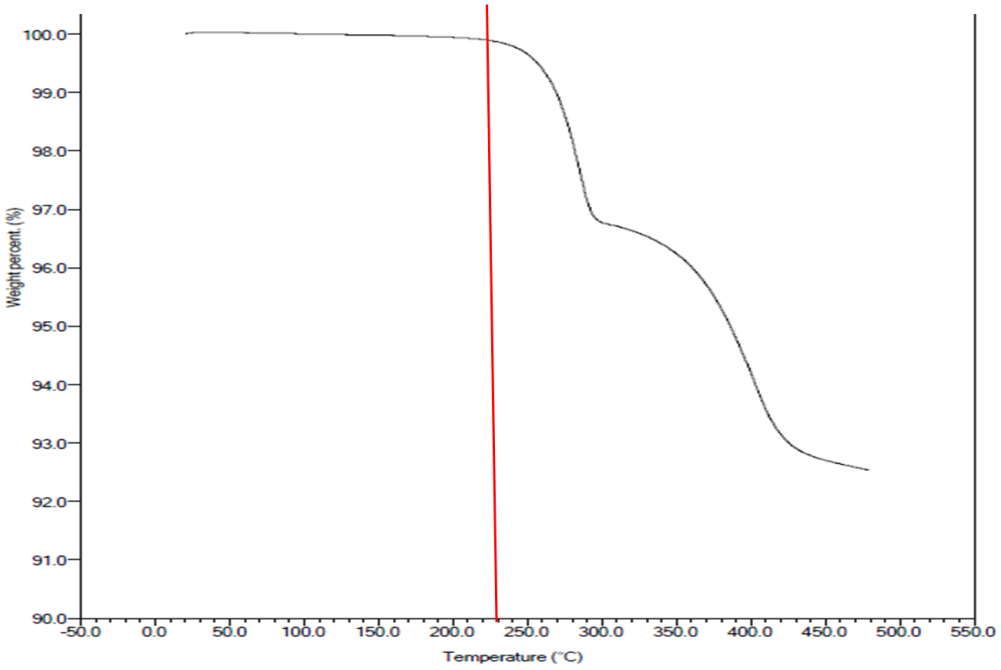

Figure 8.48 TGA trace of iPOC-*r*-Ep. Heating rate: 10°C/min.

8.4 GPC traces

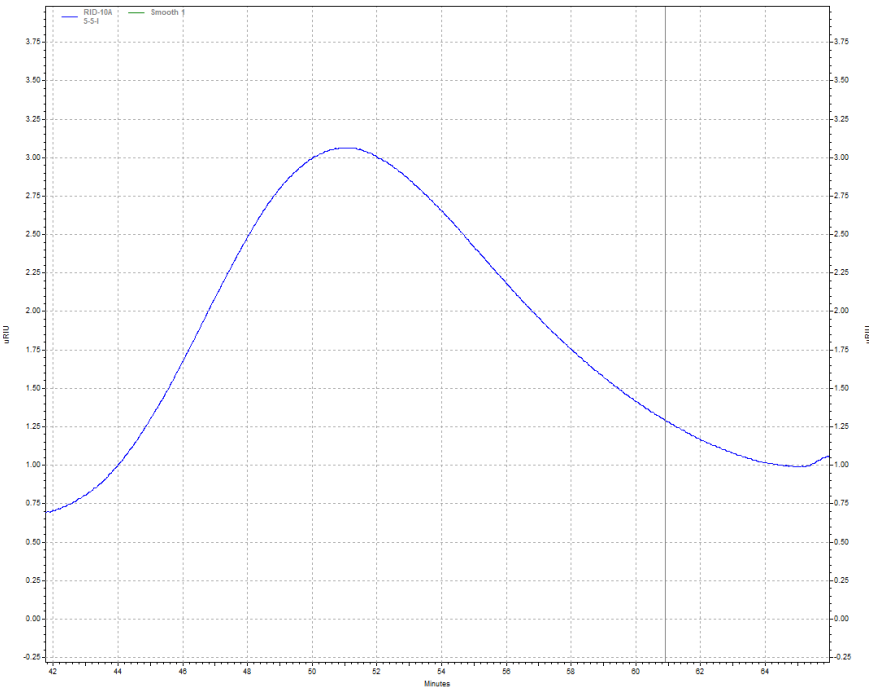

Figure 8.49 GPC trace of BCB-*r*-AS M_w = 7,300 g/mol; PDI = 2.3.